Synthesis, electrochemistry, phase studies and computational chemistry of gamma-substituted beta-diketonato-carbonyl complexes of rhodium(I).

N.F. Stuurman-Molefe

Synthesis, electrochemistry, phase studies and computational chemistry gamma-substituted betadiketonato-carbonyl complexes of rhodium(I).

A dissertation submitted in accordance with the requirements of the degree

Philosophiae Doctor

Department of Chemistry

Faculty of Natural and Agricultural Sciences

University of the Free State

Promoter

Prof. J Conradie

Nomampondomise Faurette Stuurman-Molefe

July 2014

Acknowledgements

I thank the Lord Almighty for giving me grace to be the best I can, a wife, mother, lecturer, student, daughter, sister and a friend among many, all at once. Great is your faithfulness Oh! Lord and your mercies are new every morning.

I thank my dear husband Phaladi for his unfailing and amazing support. Love, you are a gift and a testimony, for this you are blessed in your spirit and soul. Thank you for the un-measurable sacrifice you have done throughout the period of my study. I love you.

I thank my two boys Tshepo who is five years and Botle who is one year. Thank you boys for the times you missed Mama so much but with no complaint. You will always be my pride and Mama's little boys.

I thank my promoter Prof. Jeanet Conradie for her valuable support and guidance throughout this study. Prof. you are my true mentor and role model. I am and will continue to look up to you. Thank you very much.

I thank Prof Jannie Swarts for his support and willingness to share his expertise. Prof. thank you for everything, starting from the lifts in the blue bakkie up to the Friday afternoon business meetings as you named them. Thank you

I thank my colleagues from both Qwaqwa and Bloemfontein campuses, my friends and family for undying support and help when I most needed. Your willingness to run around helping when I asked is highly appreciated.

I wish to acknowledge Dr. A.J. Muller for the data collection and refinement of the crystal structures, Katherin Hopmann for the Gaussian calculations, Prof. Jeanet Conradie for the ADF calculation.

I thank NRF and Chemistry Department for their financial support without which this study would not have been possible.

Thank you.

Mpondi

Contents

List of abbreviations.

β-diketones

Hacac	2,4-pentanedione (acetylacetone)
Hba	1-phenyl-1,3-butanedione (benzoylacetone)
Hdbm	1,3-diphenyl-1,3-propanedione (dibenzoylmethane)
Hdpm	2,2,6,6-tetramethyl-3,5-heptanedione (dipivaloylmethane)
Htfaa	1,1,1-trifluoro-2,4-pentanedione (trifluoroacetylacetone)
Htfth	4,4,4-trifluoro-1-(2-thenoyl)-1,3-butanedione (trifluorothenoylacetone)
Htffu	4,4,4-trifluoro-1-(2-furoyl)-1,3-butanedione (trifluorofuroylacetone)
Htfba	4,4,4-trifluoro-1-(phenyl)-1,3-butanedione (trifluorobenzoylacetone)
Hhfaa	1,1,1,5,5,5-hexafluoro-2,4-pentanedione (hexafluoroacetylacetone)

*The removal of H in the above abbreviations represents the anion (enolate) of the β-diketone.

Solvents

THF	tetrahydrofuran
CH_3CN	acetonitrile
DCM	dichloromethane
EtOH	ethanol

Cyclic Voltammetry

CV	cyclic voltammetry
$E^{0'}$	formal reduction potential
E_{pa}	anodic peak potential
E_{pc}	cathodic peak potential
ΔE_p	separation of anodic and cathodic peak potentials
i_{pa}	anodic peak current
i_{pc}	cathodic peak current
$TBAPF_6$	tetrabutylammonium hexafluorophosphate $[NBu_4][PF_6]$
$TEABF_4$	tetraethylammonium tetrafluoroborate

SCE	saturated calomel electrode

1

Introduction

1.1 Background

Homogeneous catalysts are commonly used in industry for the processing of organic raw material, and rhodium complexes are among the widely used catalysts. Few classic examples of effective catalytic rhodium complexes are $[Rh(CO)_2I_2]^-$ (Monsanto process)[1] for methanol carbonylation to give acetic acid, $[RhHCO(PPh_3)_2]$ catalyst[2] for hydroformylation of alkenes, $[RhCl(PPh_3)_3]$ (Wilkinson's catalyst)[3] for hydrogenation of olefins and hydroformylation of olefins by $[Rh(CH_3COCHCOCH_3)(CO)_2]$[4]. In the Monsanto process, one of the most well know processes of using a rhodium-catalyst in industry, the rate-determining step involves oxidative addition where the redox state of the catalytic metal centre changes from rhodium(I) to rhodium(III). The oxidation potential of the Rh(I) centre of a complex is related to the activity of the complex towards chemical oxidation.[5] The electron donating properties of ligand surroundings, that are among other things reflected by their ease of oxidation or reduction,[6] is a major contributor in the highly respected catalytic reactivity of the above mentioned rhodium systems.[7]

A study of the electronic and other properties of the ligands are thus of importance. Synthesis of a number of β-diketones containing groups with different electron donating properties, have been given a lot of attention recently, also due to their use in mesogenic coordination as organic ligands of many transition metal ions.[8,9] Specifically γ-substituted β-diketones showed to exhibit mesomorphic properties, it is where the melting process of the complex (γ-substituted β-diketones in this case) occurs by way of one or more intermediate phases as the temperature increases. The intermediate states are called the liquid-crystal state or the mesomorphic state. The compounds exhibiting mesophases are called mesogens. Mesophases

thus have properties that are intermediate between those of the fully ordered crystalline solid and the isotropic liquid.

Liquid crystalline complexes that contain transition metal atoms produce intermolecular interactions and molecular shapes that are rare in pure organic complexes. Properties like colour, electric conductivity and paramagnetism, can be more easily be obtained in metal-organic materials than in pure organic complexes.[10,11] γ-Substituted β-diketonates are important precursors for the synthesis of metallomesogenic derivatives. Complexes of many transition metals with γ-substituted β-diketonates, lead to[12] conjugate structures where the metallic component (e.g. $[M(CO)_2]$ or $[RhCl(CO)_2]$) acts as a polar terminal group at the one end while the other end is given by an electron donor decyloxy group on the γ-substituent. This fulfils the requirement for second harmonic generation which may be of importance in nonlinear optic studies.[11]

1.2 Aim of the study

With this background, the following goals were set for this study.

1. The synthesis and characterization of selected γ-substituted and β-substituted β-diketones, their rhodium(I)dicarbonyl complexes and their rhodium(I)monotriphenylphoshine complexes similar to classic examples of effective catalytic rhodium complexes mentioned above with emphasis on the nature of the ligand.
2. An electrochemical investigation by voltammetry into the redox properties of the γ-substituted β-diketones and their rhodium complexes. The formal reduction potential, ($E^{0\prime}$) as well as the electrochemical and chemical reversibility/irreversibility, will be evaluated for the redox-active rhodium centre as a measure of the activity of the complex towards oxidative addition.
3. Application of a computational method by means of Density Functional Theory (DFT) calculations to investigate redox properties of selected γ-substituted β-diketones.
4. A phase study utilizing a differential scanning calorimeter (DSC) and a polarizing optical microscope (POM) of the γ-substituted β-diketones, as well as the γ-substituted β-diketonato-carbonyl and -phosphine complexes of rhodium(I) with potential mesophase properties.

References

[1] Maitlis, P. M., Haynes, A., Sunley, G. J., Howard, M. J. *J. Chem. Soc. Dalton Trans.* **1996**, 2187.

[2] Atwood, J. D. *Coord. Chem. Rev.* **1988**, 83, 93.

[3] Masters, C. *Homogeneous Transition-Metal Catalysis*, A Gentle Art **1981** Chapman & Hall, London.

[4] Pedrós, M. G., Masdeu-Bultó, A. M., Bayardon, J., Sinou, D. *Catalyst Letters* **2006**, 107, 205.

[5] Conradie, J., Swarts, J. C. *Eur. J. Inorg. Chem*. **2011**, 13, 2439.

[6] du Plessis, W. C., Erasmus, J. C., Lamprecht, G. J., Cameron, T. S., Aquino, M. A. S., Swarts, J. C. *Can. J. Chem.* **1999**, **77**, 378.

[7] Shor, E. A., Shor, A. M., Nasluzov, V. A., Rubaylo, A. I. *J. Struct. Chem.* **2005**, 46, 220.

[8] Trzaska, S. T., Zheng, H., Swager, T. M. *Chem. Mater*. **1999**, 11, 130.

[9] Trzaska, S. T., Swager, T. M. *Chem. Mater.* **1998**, 10, 438.

[10] Espinet, P., Esteruelas, M. A., Oro, L. A., Serrano, J. L., Sola. E. *Coord. Chem. Rev.* **1992**, 117, 215.

[11] Barbera, J., Elduque, A., Gimenez, R., Lahoz, F. J., Lopez, J. A., Oro, L. A., Serano, J. L. , Vfillacampa, B., Villalba, J. *Inorg. Chem.* **1999**, 38, 3085.

[12] Cativiela, C., Serrano, J. L., Zurbano, M. M. *J. Org. Chem*. **1995**, 60, 3074.

2

Literature survey and fundamental aspects

2.1 Long chain γ-substituted β-diketones: synthesis and complexion to rhodium

2.1.1 Introduction

Investigations have been done for more than a century on β-diketones (1,3-substituted-propane-1,3-diones).[1] The following tautomeric forms of β-diketones are observed in solution: the keto (I) and two enol forms (IIa and IIb) (Scheme 2. 1). In various aprotic solvents, above 80% of the product observed is the enol form (II), which is maintained by the symbiotic strengthening of intra-molecular hydrogen bonding and O–C=C–C=O π-system delocalization.[2,1] Generally the keto-enol inter-conversion of β-diketones is fast[3] – although sometimes proved to be slow.[4,5]. However, by orders of magnitude there is a faster equilibrium between enol isomer IIa and IIb observed.[6] R^1, R^2 and R^3substituents of various combinations were selected due to their electron-donating and their electron-withdrawing character, leading to more possible known β-diketones.

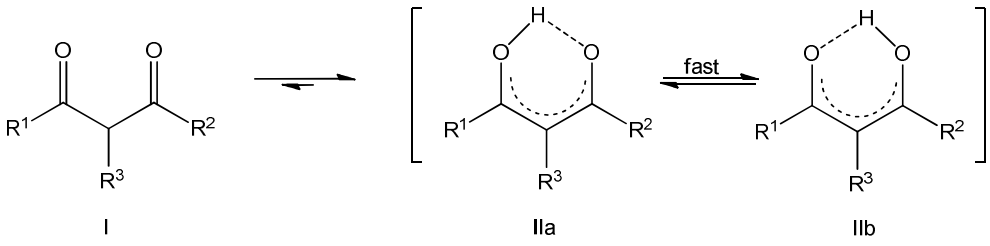

Scheme 2. 1. Keto-enol change with rapid enol isomerization of β-diketones.

Inorganic and organic chemistry use β-diketones as versatile reagents and ligands. Coordination of an enolate anion of β-diketones to metals provides a significant category of thermally resistant metal complexes. Shown in **Scheme 2. 2** is an anion of a β-diketonate ligand that acts as a bidentate chelating ligand which is a case commonly, observed in these complexes. When a methine group of a β-diketonate anion is replaced by a transition-metal a metalla-β-diketone is formed.[7] This is so when there is a direct integration of metal moieties into the σ- and π-bonding lattice of the β-diketonate functionality.[7]

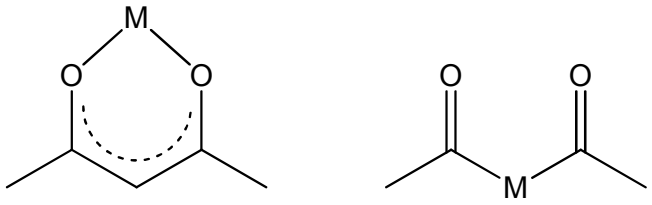

Scheme 2. 2. **Metal-β-diketonato complex (left) and metalla-β-diketone (right).**

Synthesis of various kinds of mesogenic compounds, i.e. complexes exhibiting liquid crystal properties, has proved β-diketones to be very efficient precursors. β-diketones can form mesogenic complexes with nearly all metals.[8, 9, 10]

Several aryl and aryloxy gamma (γ)-substituted β-diketones where the β-diketone with an alkyl chain of six to eight carbon atoms separating it from a substituted benzene ring exhibits a broad scale of antiviral action *in vitro* prevention of both RNA and DNA viruses.[11]

2.1.2 Synthesis of γ-substituted β-diketones

The syntheses of β-diketones with different γ-substituents will be described in this section (see **Scheme 2. 3** to **Scheme 2. 9** for a summary of the γ-substituted β-diketones that will be discussed). β-diketone **1** was prepared by Hauser,[12] β-diketone **2** by Diana *et al.*[11(a)] and the β-diketone series **2 - 8** by Serrano *et al.*[13] The β-diketone series **9 – 13** was prepared by Wan *et al.*[14]

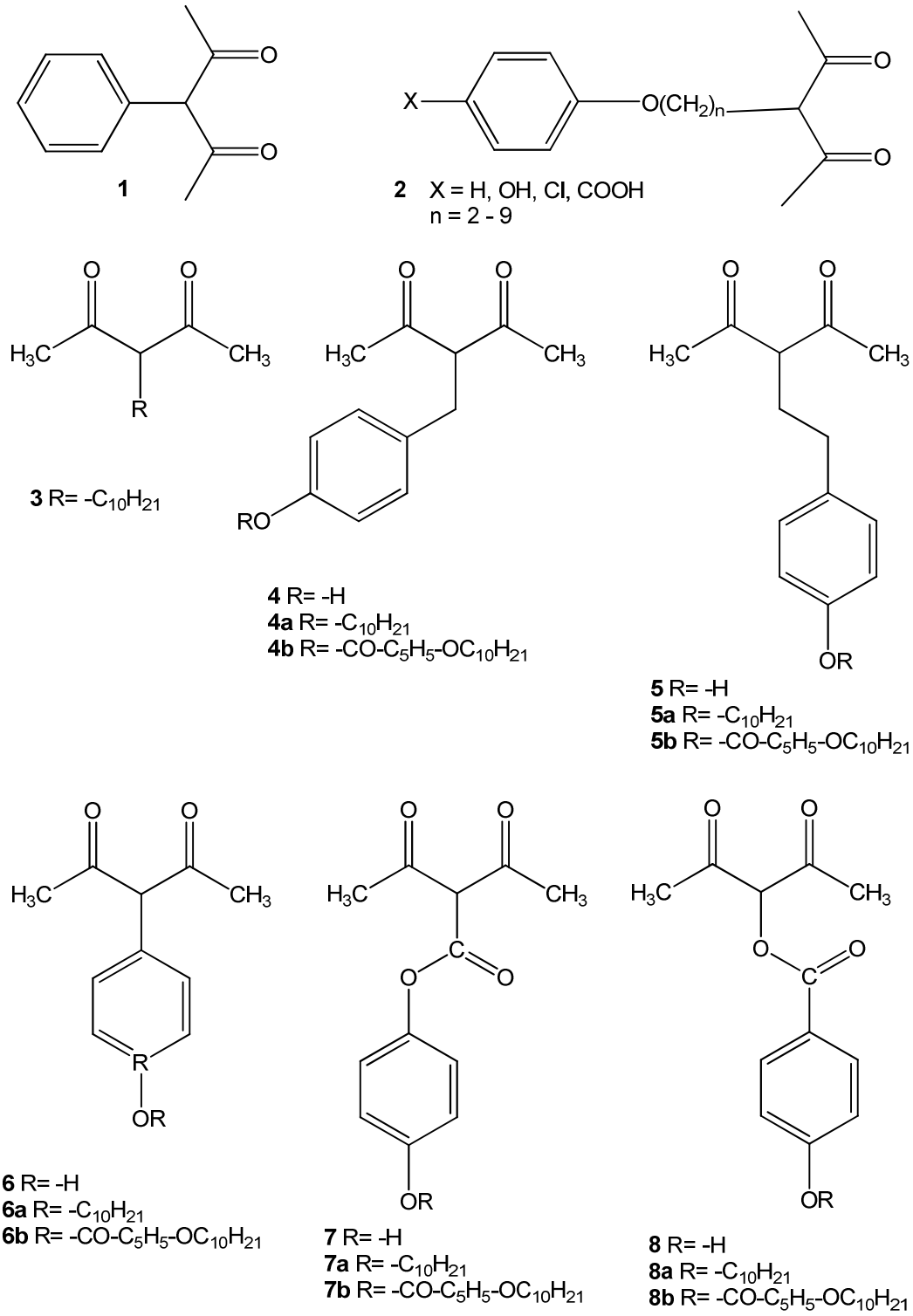

Scheme 2. 3. Summary of selected γ-Substituted β-diketones.

(i) *Synthesis of β-diketone 1*

β-diketone **1** (**Scheme 2. 3**) with a phenyl group at the γ position was prepared by Hauser *et al.*[12] where the acetylation of phenylacetone with acetic anhydride with the help of boron trifluoride was used. The yield was improved by purification and the presence of *p*-toluenesulfonic acid as a catalyst. A solution of phenylacetone, acetic anhydride and *p*-toluenesulfonic acid (0.4 : 0.8 : 0.12 mol) was stirred for 5 minutes, followed by the saturation at 0–10^{o}C with boron trifluoride for 3 to 4 hours. A very viscous mixture resulted and a decrease in the rate of addition of the reagent keept the temperature below 10 ^{o}C. After the reaction was saturated with boron trifluoride, the flow of boron trifluoride went on further for 15 minutes and room temperature was reached when three hours lapsed. The reaction mixture was then decomposed by further refluxing for one hour with sodium acetate trihydrate in water, after which it was cooled to room temperature and then extracted several times with ligroin. Saturated sodium bicarbonate solution was used to wash combined ligroin extracts removing the acid, dried over calcium sulphate, and the solvent distilled. Recrystallization using ligroin (b.p. range 60-90°) gave on cooling, in dry ice-acetone, 63% of 3-phenyl-2,4-pentanedione.[12]

(ii) *Synthesis of β-diketone 2*

β-diketones **2** in **Scheme 2. 3** where between the diketone moiety and the aryl group there are modified alkyl bridges, were prepared by two different pathways, as proposed by **Scheme 2. 4** (a) and (b) below.[11] The potassium carbonate-acetone mixture served as a base-solvent system since it was found that under these conditions C-alkylation will be predominant.[15] Purification of the β-diketones was done by column chromatography, distillation or, in some cases, recrystallization.[11]

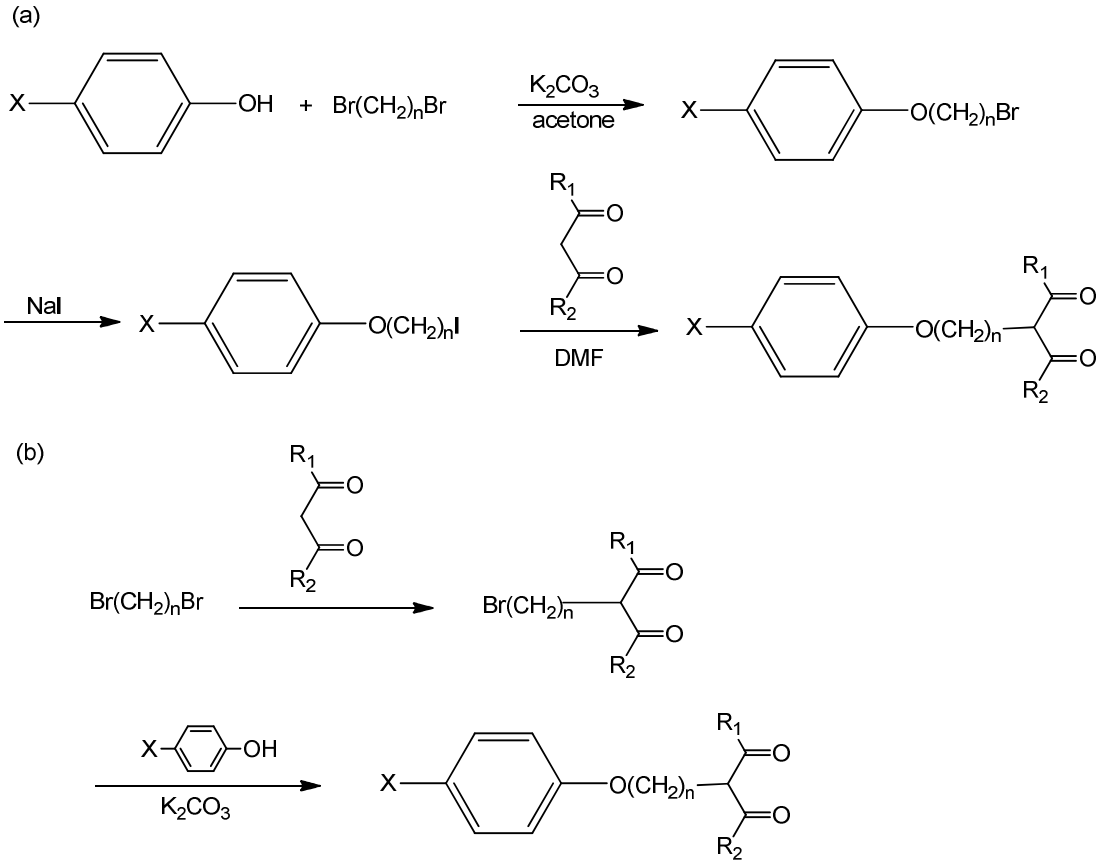

Scheme 2. 4. **Two different pathways (a) and (b) for the synthesis of β-diketone 2 (n = 2 – 9, X = H, OH, Cl, COOH etc, see reference 11).**

(iii) *Synthesis of the β-diketone 3 series*

Synthesis of β-diketone **3** (3-decylpentane-2,4-dione) in **Scheme 2. 3** was achieved by the Carbon-alkylation of the acetylacetone (pentane-2,4-dione).[13] **Scheme 2. 5** outline synthesis of β-diketone **3**.

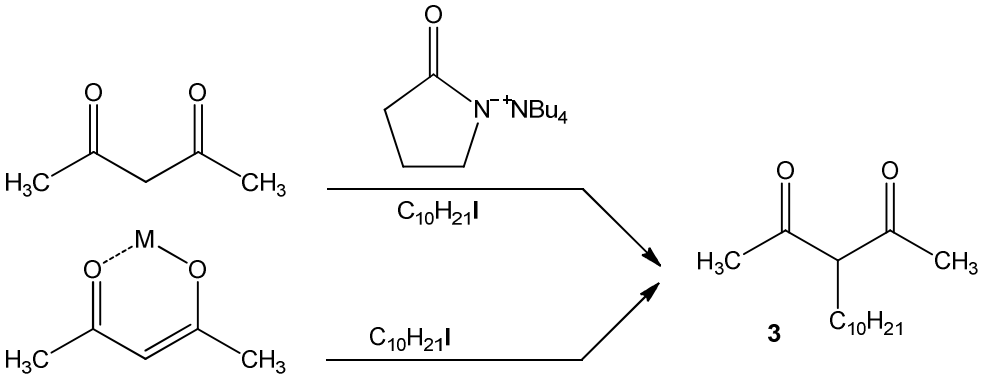

Scheme 2. 5. **Synthesis of β-diketone 3.**

The alkylating agent decyliodide and a solvent dimethylformamide (DMF) were used in one route of synthesis; tetrabutylammonium 2-pyrrolidonate gave a discriminative C-alkylation of acetylacetone. The other route used β-diketone metal enolates of to get discriminative C-alkylation. C-alkylation products were achieved only by thallium and sodium enolates when decyliodide was used as the alkylating agent while other metals failed to give the product in moderate yields. There are three procedures reported for the synthesis of β-diketone **3**.[13]

Procedure 1 for the synthesis of β-diketone 3[13]

A blend of 1-decyl iodide and sodium acetyl acetonate in methyl ethyl ketone is refluxed for 72 h. Water is added to the residue after the solvent is distilled off, and then it is extracted with ether and dried. Dichloromethane is used as an eluent during the purification of the product on a silica gel column after the evaporation of the solvent. This gives about a 51% yield.[13]

Procedure 2 for the synthesis of β-diketone 3[13]

A solvent 1,4-dioxane is heated and used to mix thallium(1) acetylacetonate and for 48 h 1-decyliodide was refluxed in N_2 atmosphere. Cooling and filtering the mixture to room temperature followed. Following dispersal of the solvent, the raw produce is refined using silica gel column, employing DCM (dichloromethane) as the eluent, to afford a yield of about 37%.[13]

Procedure 3 for the synthesis of β-diketone 3[13]

At room temperature (RT) the reaction mixture of a solution of acetylacetone in dry DMF, and tetrabutylammonium 2-pyrrolidonate is stirred for 15 minutes. At RT the mixture is then stirred for 72 h after the addition of 1-decyl iodide. An aqueous solution of ammonium chloride is used to quench the reaction mixture, after which it is extracted with ether and dried. Dichloromethane is used as an eluent during the purification of the product on a silica gel column after the evaporation of the solvent. This gives about a 50% yield.[13]

(iv) *Synthesis of the β-diketone 4 series*

Synthesis of the 4 series β-diketones[13] (**4, 4a, 4b** in **Scheme 2. 3**) was achieved by making the formation of O-alkylation products impossible where sodium or thallium enolates were employed to do so. Careful control on the reaction conditions minimized di-C-alkylation products which enabled enolates to synthesise the desired products. **Scheme 2. 6 (a)** below show that at the end of the synthesis the desired groups are incorporated by suitably protecting the phenolic hydroxyl group, thus possible where sodium or thallium enolates involving the employment of an appropriate benzyl iodide are employed. According to Classen *et al.,*[16] 4-(Benzyloxy)-benzyl iodide as a starting material was better produced from the commercially available 4-(benzyloxy)benzyl alcohol employing chlorodiphenylphosphine with iodine. Typical hydrogenolysis reaction was used to deprotect the resulting product following discriminative C-alkylation by sodium or thallium enolates by hydrogen and Pd/C as catalysts to afford β-diketone **4,** afterwards alkylated to afford β-diketone **4a** employing 1-decanol; diethyl azodicarboxylate **(DEAD);** and Ph_3P or benzoylated resulting to β-diketone **4b,** employing 4-(n-decyloxy)benzoylchloride.[13]

(v) *Synthesis of the β-diketone 5 series*

The **5** series β-diketones[13] in **Scheme 2. 3** were synthesized following **Scheme 2. 6 (b),** outlined below. Use of metal enolates in this series gave very low yields except when a phase transfer catalyst, tetrabutylammonium 2-pyrrolidonate, was used, in which case the desired product **5** were obtained in moderate yields.[13]

(vi) *Synthesis of the β-diketone 6 series*[13]

Selective arylation with aryl iodides and addition of CuI on sodium enolates of β-dicarbonyl compounds was employed for the synthesis of β-diketones in the 6 series, as outlined in **Scheme 2. 7 (a)** below. After which, deprotection of the hydroxyl group of acetylacetone using hydrogen and Pd/C as a catalyst gave β-diketone **6,** which was easily O-alkylated using an appropriate alcohol in the existence of DEAD/Ph_3P giving β-diketone **6a.** Acylation with 4-(n-decyloxy)-benzoyl chloride gave β-diketone **6b.**[13]

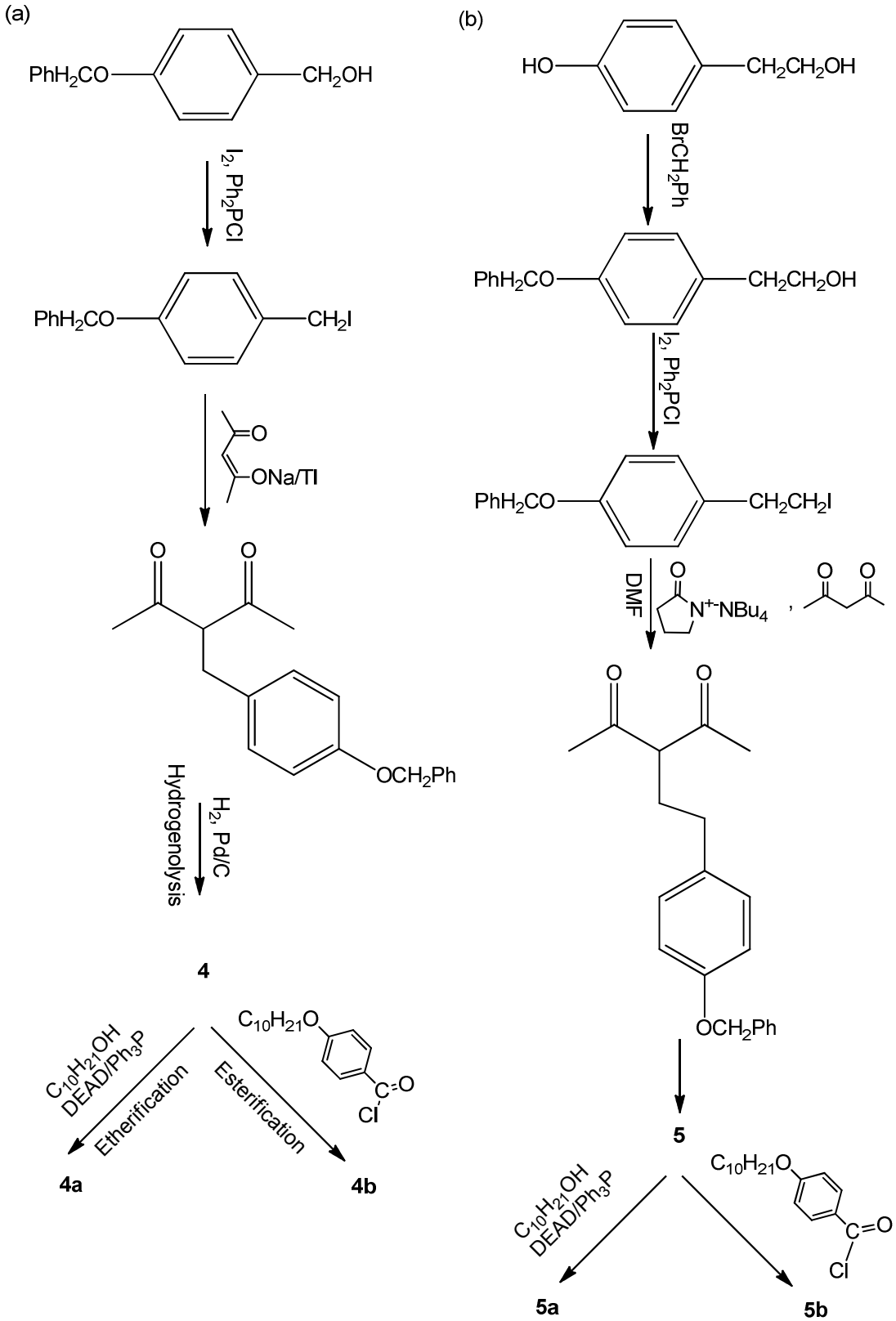

Scheme 2. 6. (a) Synthesis of the β-diketone 4 series and (b) synthesis of β-diketone 5 series.

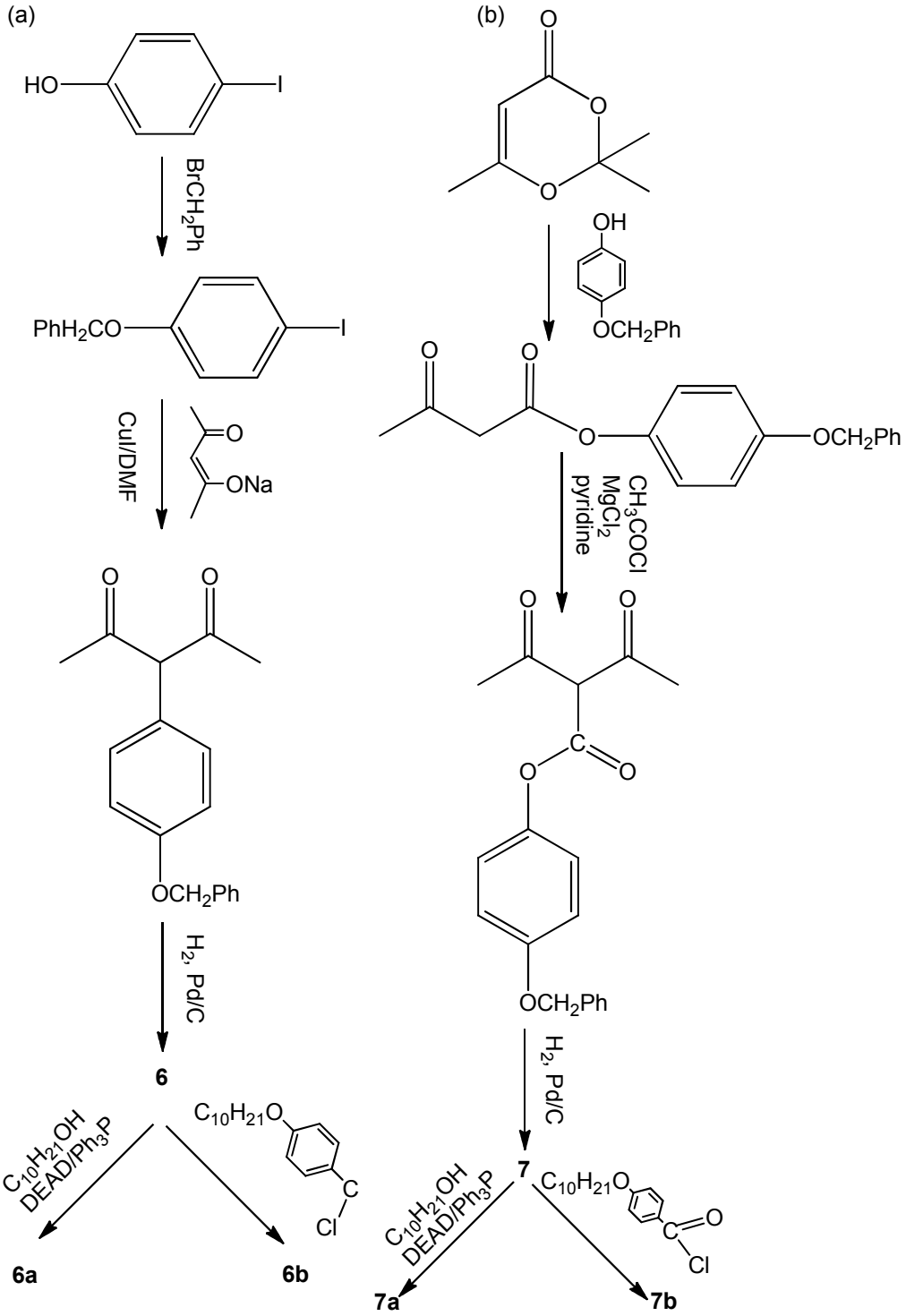

Scheme 2. 7. (a) Synthesis of the β-diketone 6 series and (b) synthesis of β-diketone 7 series.

(vii) *Synthesis of the β-diketone 7 series*

Clemens *et al.,*[17] reports incorporation of 2,2,6-trimethyl-4-H-l,3-dioxin-4-one (dioxinone) to be an appropriate precursor during a production of β-keto esters to reacted with nucleophiles, as the best method for the production of the target compounds in the **7** series β-diketones[13] in **Scheme 2. 3**, where 4-(benzy1oxy)phenol is used as the nucleophile (see Scheme 2. 7 **(b)**). An excellent yield of a β-diketone was produced when dioxinone reacted with 4-(benzyloxy)phenol, and subsequently in pyridine a reaction with acetyl chloride continued where $MgCl_2$ was added. Hydrogen Pd/C was used for deshielding, and lastly, O-alkylation was done with an appropriate alcohol in the company of DEAD/Ph_3P resulting on β-diketone **7a** being produced**.** Alternatively, it was acylated with 4-*(n*-decy1oxy)benzoyl chloride affording β-diketone **7b.**[17]

(viii) *Synthesis of the β-diketone 8 series*

The use of phase transfer catalyst was probably the better method for the production of compounds having a widespread form of the **8** series β-diketones[13] in **Scheme 2. 3**. The accessible 3-chloropentane-2,4-dione with the comparable carboxylate 4-(benzyloxy)benzoic acid were used in this synthesis, where quaternary ammonium salt tetrabutylammoniumhydrogen sulphate was a catalyst. Williamson reaction was used to obtain 4-(Benzyloxy)benzoic acid using 4-hydroxybenzoic acid, 3-chloropentane 2,4-dione resulted from sulfuryl chloride and acetylacetone. The product gave the desired β-diketones in good yields after it had been easily exposed by deshielding and O-alkylated or O-acylated, (see **Scheme 2. 8** below).[13]

At room temperature hydrogenolysis of series **4** to **8** β-diketones was done with a mixture of the appropriate benzyl ether and 10% palladium/carbon in dichloromethane at atmospheric pressure. The reaction took 8 h to come to completion. Filtering of the crude product was followed by solvent evaporation. Silica gel column was used to purify the product. Etherification was done by a solution of diethyl azodicarboxylate introduced slowly to a solution of triphenylphosphine; an appropriate β-diketone **(4, 5, 6, 7**or **8** respectively), and 1-decanol in ether at room temperature. Triphenylphosphine oxide and diethyl hydrazinedicarboxylate soon came out as white precipitate. The precipitate was removed by filtration after stirring the mixture at room temperature overnight. An *in vacuo* evaporation was performed and silica gel column was used to purify the crude product. Esterification by a

solution of 4-(n-decyloxy)benzoylchloride in dichloromethane was slowly added at 0 °C to a solution of β-diketone (**4, 5, 6, 7** or **8** respectively), 4-(dimethylamino)pyridine and triethylamine in drydichloromethane**.** At RT the reaction mixture was stirred overnight. Following the dispersal of the solvent by evaporation, the raw product was refined using silica gel column.[13]

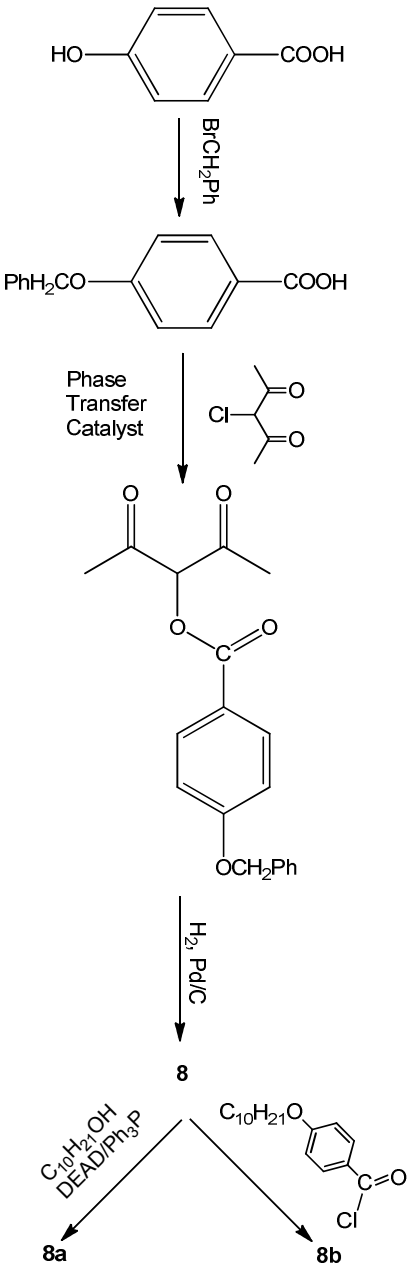

Scheme 2. 8. **Synthesis of the β-diketone 8 series.**

A reaction in dry DMF at a temperature of 40–50 °C between potassium 4-*n*-alkoxybenzoxybenzoate and 3-chloro-2,4-pentanedione synthesising β-diketone 8a[13] was reported by Wan *et al.,*[14] where after stirring overnight the reaction mixture afforded red solution. Cooling the reaction mixture followed then water was added after which extraction was done several times with chloroform. Sodium sulphate was used as the drying agent for the combined extracts and the solvent was distilled off. Silica gel column was used to purify the product employing a 1:2 mixture of ethyl acetate: petroleum ether (60–90 °C) as eluent. Recrystallization of the product with ethanol gave yields of 50–60%.[14]

(ix) *Synthesis of the β-diketone 9 - 13 series*

A 2,4-dioxo-3-pentyl 4-hydroxybenzoate compound was used as a major precursor for production of γ-substituted β-diketone by Han *et al.*[18] He reports that Serrano's method[13] of employing $BrCH_2Ph$ as a shielding reagent, a costly Pd/C catalyst used to deshield, and the phase transfer catalyst is generally complicated and affords low yields. He proposes a practical and facile method where 3-chloropentane-2,4-dione with solid sodium 4-hydroxybenzoate in dry DMF are stirred at 50 ^{0}C overnight to give 2,4-dioxo-3-pentyl 4-hydroxybenzoate. Cooling the reaction to room temperature mixture followed then water was added after which extraction was done with chloroform. Extracts were combined and were dried over sodium sulphate. Reduced pressure was used to evaporate the solvent and the crude product was refined on silica gel column (EtOAc-petrodeum ether 1:1) moreover a white product was afforded after recrystallization done in benzene. Aqueous solution of NaOH reacted with 4-hydroxybenzoic acid giving sodium 4-hydroxybenzoate almost stiochio-metrically.[18] According to Han's method[18] involving phase transfer catalyst and shielding reagent is not necessary. Simple and mild conditions used for all the reactions obtained a total yield of about 80%, almost twice the yield obtained by Serrano's method. β-diketones by Han *et al.*[18] are outlined below from β-diketone **9a** to **13a**.

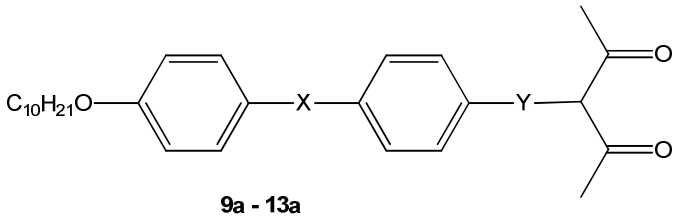

9a - 13a

Scheme 2. 9. A series of β-diketones by Han *et al.*[18] where:

Series 9a: X = -CH=CHCOO- and Y = -COO-

Series 10a: X = -CH=CHCOO- and Y = -CH=CHCOO-

Series 11a: X = -COO- and Y = -CH=CHCOO-

Series 12a: X = -CH_2O- and Y = -COO-

Series 13a: X = -N=N- and Y = -COO-.

Synthesis of 2,4-dioxo-3-pentyl 4-[[4-(ndecyloxy)cinnamoyl]oxy] benzoate **9a** was generally the same as in **10a** and **11a.**[18] To a solution of 4-(decyloxy)cinnamic acid in anhydrous benzene, $SOCl_2$ was added during stirring. Reflux of the resulting product was done overnight and reduced pressure was used to evaporate the solvent. Anhydrous benzene diluted the residue. To this solution was added an appropriate intermediate (2,4-dioxo-3-pentyl 4-hydroxybenzoate or 2,4-dioxo-3-pentyl 4-hydroxycinnate) and this was put under reflux for 16 h. Next, reduced pressure was used once more to remove the solvent; recrystallization was done in anhydrous ethanol affording a white precipitate with a yield of 82%.[18]

2.1.3 Synthesis of rhodium-β-diketonato complexes with γ-substituent

Wan's outline for the synthesis of rhodium β-diketonato complexes series **14** with a γ-substituent is outlined by **Scheme 2. 10** below. At room temperature acetone solutions of β-diketone and μ-dichlorotetracarbonyldirhodium $[Rh_2(\mu\text{-}Cl)_2(CO)_4]$ were stirred for 30 minutes under N_2 with an excess of solid barium carbonate.[14] Han[18] did the same but under argon for 2 h, also at room temperature. The remaining mixture when filtration and distillation was done went through chromatography on silica gel where chloroform was an eluent.[14] Recrystallization from ethanol was used to refine the crude product, and a yield of approximately 85% was obtained.[14] Barbera *et al*[19] obtained the rhodium complexes series **15** (see **Scheme 2. 11** below) by direct reaction of sodium diketonate salts and the

tetracarbonylrhodium complex $[Rh_2(\mu\text{-}Cl)_2(CO)_4]$. Complexes **15a** and **15c** were red in colour while **15b** gave a yellow colour.

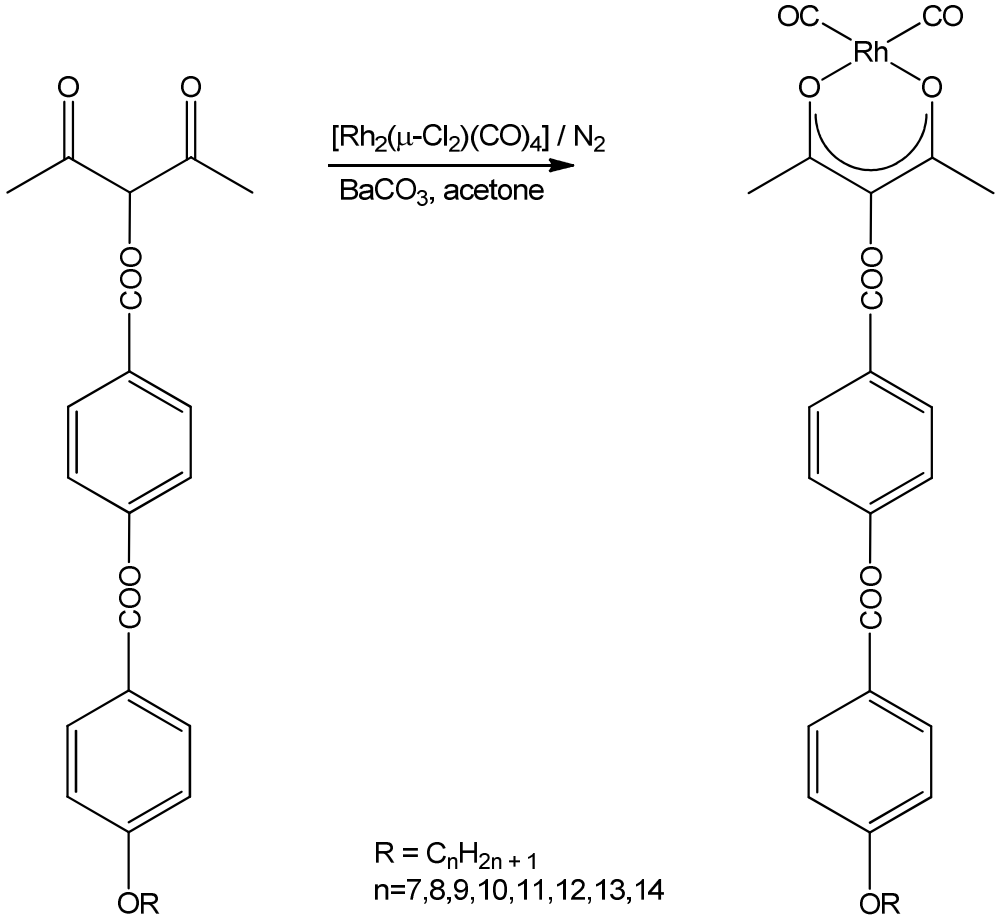

Scheme 2. 10. Synthesis of Rhodium complexes series 14.

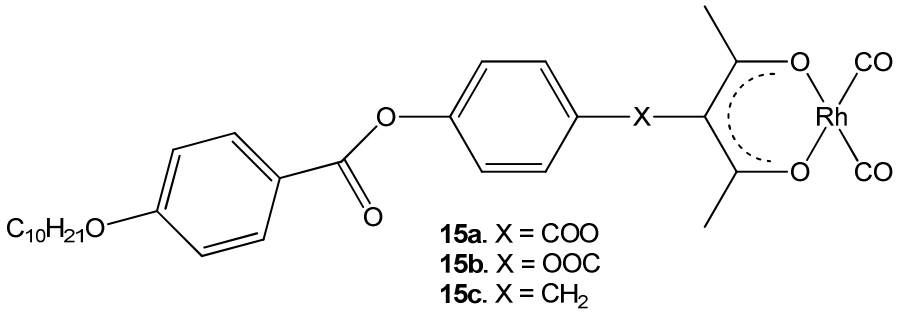

Scheme 2. 11. Rhodium complexes series 15.

2.2 Electrochemistry

2.2.1 Cyclic voltammetry (CV) aspects

Introduction

Cyclic voltammetry is an electro-analytical procedure to investigate electro-active species. Electrochemistry, inorganic chemistry, organic chemistry and biochemistry broadly utilise this technique. It has been used by organic chemists to study biosynthetic pathways and electrochemically produced free radicals. The effect of a ligand on the redox potential of the central metal ion in complexes has been evaluated by inorganic chemists using cyclic voltammetry.[20] Cyclic voltammetry (CV) is capable of quickly observe the redox behaviour on a broad potential range and is as such very effective.[21] It provides quick location of oxidation or reduction potentials of electro-active species.

Cyclic voltammetry

A basic CV experiment exists of a **three-electrode** cell connected to a potentiostat. Between a working electrode and a reference electrode the potentiostat puts in the expected potential. An electrode where the electrolysis of the species of interest occurs is called the working electrode. The current needed to keep up electrolysis at the working electrode is supplied by the auxiliary electrode, thus preventing a lot of current passing through the reference electrode resulting into its potential changing. A cyclic voltammogram (CV) is acquired by calculating the current between the working electrode and an auxiliary electrode during a potential scan. The response signal to the potential excitation signal is considered as the current. It is therefore an exhibit of current *versus* potential.[22] A triangular waveform found in linear potential scan results to the excitation signal (**Figure 2.1**). Control of this working electrode's potential is done against a reference electrode. A reference electrode is used to control the potential of this working electrode.[22]. A saturated calomel electrode (SCE) and silver chloride (Ag/AgCl) are examples of reference electrode.[21]

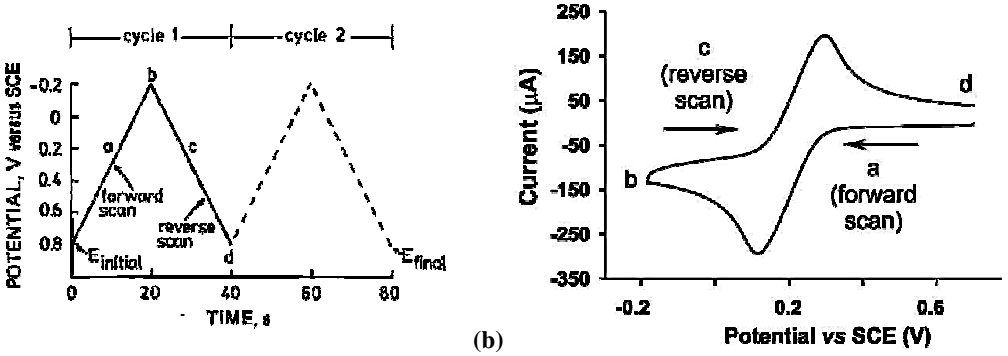

Figure 2.1 (a). Typical excitation signal for cyclic voltammetry: a triangular potential wave form with switching potentials at 0.7and -0.2 V versus SCE (from reference 21). "Reprinted with permission from Kissinger, P.T.; Heineman, W.R. *J. Chem. Ed*., 60, 702. Copyright, 1983, American Chemical Society." (b) Example of the resulting cyclic voltammogram, scan initiated at 0.7 V versus SCE in negative direction.

Triangular potential excitation signal occurring repetitively for cyclic voltammetry results on a back and forth sweep of the working electrode's potential between the two labelled values known as switching potentials.[21] Although the potential scan is frequently terminated at the end of the first cycle, it can be continued for a number of cycles; hence this technique is known as *cyclic voltammetry* (CV).[20] The resulting current-potential graph is called a cyclic voltammogram. There is often little difference between the first and the successive scans. If such differences occur, they are key indicators of reaction mechanisms.[20] The slope of the graph indicating volt *versus* time in **Figure 2.1** gives the scan rate and the dotted line denotes a second cycle. Mechanisms and rates of reactions studied by the cyclic voltammetry technique often reveal the presence of intermediates.

A typical CV, acquired by calculating the current at the working electrode in an unstirred solution throughout a potential scan, is displayed in **Figure 2.2**.[23] The magnitude of the anodic peak current (i_{pa}), the cathodic peak current (i_{pc}), the anodic peak potential (E_{pa}) and the cathodic peak potential (E_{pc}) are the important parameters of a cyclic voltammogram. The extrapolation of a baseline, as shown by the dotted lines in **Figure 2.2**, is one method of measuring i_{pa} and i_{pc}.[23] The setting up of a correct baseline is important for the correct calculation of peak currents though this is sometimes a challenge.[20]

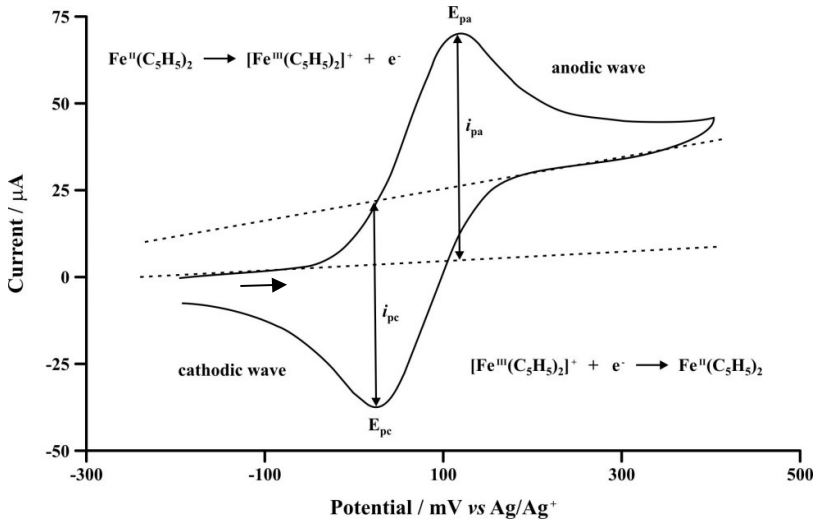

Figure 2.2. Cyclic voltammogram of a 3.0 mmol dm^{-3} ferrocene (ferrocene = [Fe(C_5H_5)$_2$]) measured in 0.1 mol dm^{-3} tetrabutylammonium hexafluorophosphate/acetonitrile on a glassy carbon electrode at 25˚C, scan rate 100mV s^{-1}.[23] The arrow designates the direction of the scan. "From ref 23, copyright (2003) University of the Free State, Bloemfontein, RSA."

A redox couple which is electrochemically reversible is when there is a rapid interchange of electrons between both species with the working electrode.[21] When the electron shift across the electrode and substrate is rapid adequately to keep the concentration of the oxidised and the reduced species in equilibrium – as stated by the Nernst equation, at the electrode surface at a certain scan rate – such a system is said to be reversible. This implies that a compound can be quantitatively oxidized and reduced to the original material.[24] Calculation of a potential difference between two peak potentials from a cyclic voltammogram identifies such a couple. Equation 1 applies to a system that is electrochemically reversible.

Equation 1: $\Delta E_p = E_{pa} - E_{pc} \approx 0.059V/n.$

In Equation 1, n is the number of electrons transferred, E_{pa} the anodic peak potential and E_{pc} the cathodic peak potential, both indicated in volts. This 0.059V/n separation peak potential is not subject to the scan rate of a reversible couple, but somewhat subjected to the switching potential and cycle number.[25] Thus, ΔE_p will have a value of 59 mV for a one-electron process such as the reduction of Fe^{3+} back to Fe^{2+}, for example.

The diagnostic ΔE = 59 mV for electrochemical reversible one-electron transfer activities is many times hard to attain without instrument reimbursement for cell resistance and over

potentials. Thus, frequently a potential difference of ΔE_p up to 90mV is often still considered electrochemically reversible.[24] An increase of the peak separation is caused by a slow electron transfer at the electrode surface and depends *inter alia* on the electrolyte and solvent system. A centre between the two peak potential of the redox couple is a formal electrode $E^{0'}$.[22]

Equation 2: $E^{0'} = (E_{pa} + E_{pc})/2$

This $E^{0'}$ is an estimate of the polarographic $E_{1/2}$ value which is the value that was given to the potential where the current is half the value of that on the current plateau.[26]

Equation 3: $E_{1/2} = E^{0'} + (RT/nF)\ln(D_R/D_O)$

D_R is the diffusion coefficient of the reduced species, and D_O the diffusion coefficient of the oxidized species. Randles-Sevcik equation expresses the peak current for a reversible system for the forward sweep of the first cycle.[21]

Equation 4: $i_p = (2.69 \text{ X } 10^5)n^{3/2}AD^{1/2}C\upsilon^{1/2}$

If i_p, the peak current is in amperes, n is the stoichiometry of the electrons, A the electrode area in cm^2, C the concentration in mol cm^{-3} and υ the scan rate in Vs^{-1}, then D, the diffusion coefficient, will be in cm^2s^{-1}. If plots of i_{pa} and i_{pc} *versus* $\upsilon^{1/2}$ are linear with intercepts at the origin and equal slopes, we have a reversible systems. A linear relationship between i_p and the square root of scan rate (υ in Vs^{-1}) means that the electro-active species is in solution preferably than surface bound.[24] For a straight forward chemically reversible swift couple, the values of i_{pa} and i_{pc} must be identical.

Thus

Equation 5: $i_{pa} / i_{pc} = 1$ (the denominator is from the 'forward' scan)

A slow transaction of redox species with the working electrode caused an electrochemical irreversible reaction. This implies that Equations 1, 4 and 5 will not be applicable. Theoretically electrochemical irreversibility is distinguished by a separation of peak potentials that are more than 59mV (or 90mV practically) and dependence of ΔE_p on the scan rate.[21] The

term quasi-reversible is often used for a system where the electrochemical kinetics is slow, but the redox process still takes place. A complete irreversible system is one in which only oxidation or only reduction is possible.[27]

Shape of CV	Chemical	Electrochemical
	reversible (i_{pa} / i_{pc} = 1)	reversible (ΔE_p< 90 mV)
	reversible (i_{pa} / i_{pc} = 1)	quasi reversible (90 mV < ΔE_p< 150 mV)
	reversible (i_{pa} / i_{pc} = 1)	irreversible (ΔE_p> 150 mV)
	irreversible	irreversible (no oxidation peak)

Figure 2.3. A schematic representation of the cyclic voltammogram expected for reversible/irreversible chemical/electrochemical behaviour.

Square wave voltammetry

Square Wave Voltammetry (SWV) is a very valuable and solid electrochemical technique in electro-analysis. It is a scanning voltammetric technique like is cyclic voltammetry (CV) with advantages to enable a rapid examination, less utilization of target species and lessened contamination of the electrode surface. SWV differentiate the charging and background currents to a certain extent, giving greater sensitivity and better definition of the response than CV.[28]

Kalousek commutator and Barker's square wave polarography derived the SWV technique. Three procedures for programming the voltages as types I, II, and III was designed, and these are displayed in **Figure 2. 4**. A peak to peak between the ranges of 20 to 50 mV type I polarograms were noted by superimposing a low-amplitude square wave on the ramp voltage of standard polarography. Larger potential half-cycles were used to note the current.[29]

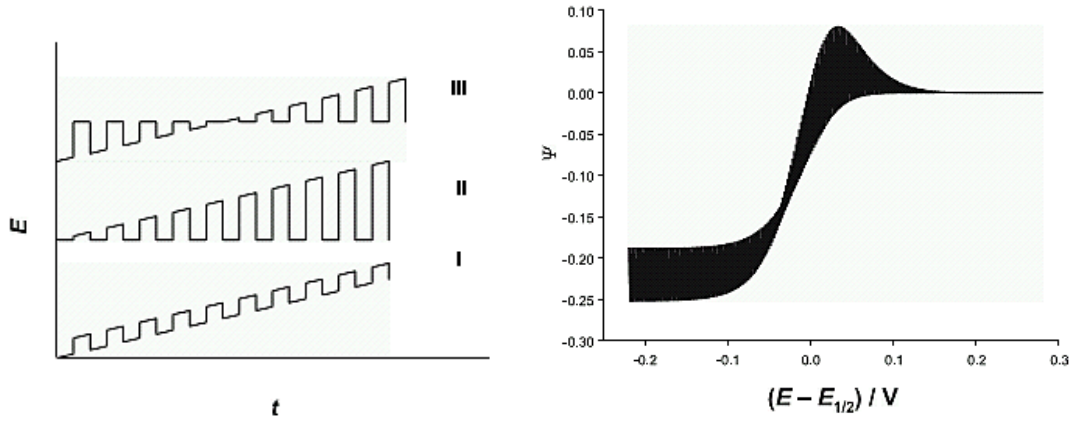

(a) **(b)**

Figure 2. 4. (a) Kalousek commutator showing potential versus time graph.

(b) Type I polarogram shown by Kalousek on a dropping mercury electrode also explained by the reaction $O^{m+} + ne^- \rightarrow R^{(m-n)+}$.[29] "Springer and *Monographs in Electrochemistry* (Square-Wave Voltammetry), 2007, 1-12, Introduction, V. Mirčeski, Š. Komorsky-Lovrić, M. Lovrić, figure 1.1 and 1.2, Copyright © 2008, Springer-Verlag Berlin Heidelberg; with kind permission from Springer Science and Business Media."

A straight forward and electrochemically reversible electrode reaction has been conceptually studied:

$$O^{m+} + ne^- \quad \rightarrow \quad R^{(m-n)+} \qquad (1.1)$$

Acquired by the type I programme is shown in **Figure 2. 4(b)** where O^{m+} and $R^{(m-n)+}$ are the oxidised and reduced species respectively. In the bulk solution, O^{m+} is the only species originally available. The outset potential is −0.25V vs. $E_{1/2}$, and the polarogram electrode reaction (1.1) indicates that $E_{1/2}$ is a half-wave potential.[29] An oxidation peak current which appears at 0.034V vs. $E_{1/2}$ distinguishes the feedback. At lower potential half cycle the reactant is reduced while at higher potential half cycle the product is oxidised all occurring in the region of the half-wave potential. Further developments were done by superimposing the square wave signal onto a staircase signal. **Figure 2.5(a)** show possible potential versus time waveforms.[29]

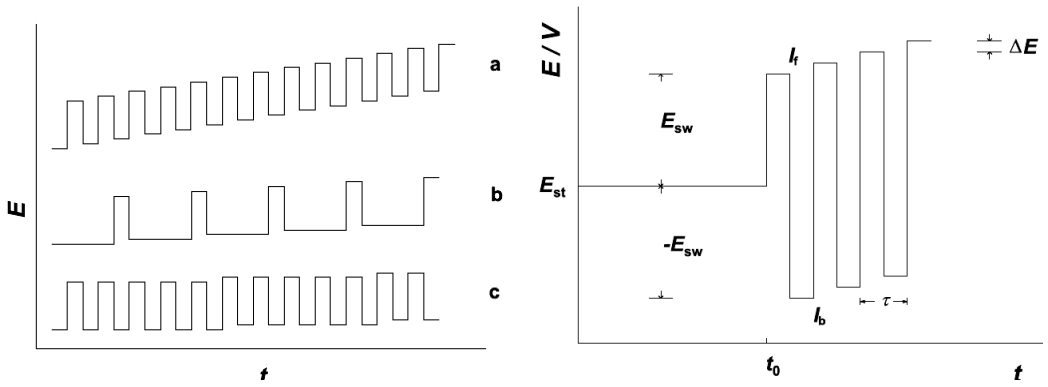

(a) **(b)**

Figure 2.5 (a). A superimposed square wave signal on a staircase signal giving potential versus time waveforms: a: square wave voltammetry, b: differential pulse voltammetry and c: multiple square wave voltammetry. (b) Square wave voltammetric scheme for excitation signal: starting potential (E_{st}), pulse height (E_{sw}), potential increment (ΔE), staircase period (τ), delay time (t_0), forward current (I_f) and backward currents (I_b).[29] "Springer and *Monographs in Electrochemistry*(Square-Wave Voltammetry), 2007, 1-12, Introduction, V. Mirčeski, Š. Komorsky-Lovrić, M. Lovrić, figure 1.7 and 1.8, Copyright © 2008, Springer-Verlag Berlin Heidelberg; with kind permission from Springer Science and Business Media."

Generally, at one staircase interval only one square wave cycle is happening, occasionally it is named Osteryoung SWV, but a one-step utilization of many cycles in several square wave voltammetry is employed. The asymmetric signal b in **Figure 2.5 (a)** is a common shape of differential pulse voltammetry.[29]

A potential versus time graph of the contemporary SWV is shown in **Figure 2.5 (b)**. Initial potential is an average of intense potentials of the square wave signal, as compared to a curve of **Figure 2.5 (a)**. One square wave cycle is superimposed on each step of the staircase signal – this implies that the graph can be studied as a series of vibrations close to upper and lesser potentials equal to the potential that adjusts in a step by step fashion. One half of the peak-to-peak amplitude of the square wave signal is proportionate to the magnitude of each vibration, E_{sw}. For classical logic, a vibration peak E_{sw} is named the square wave amplitude. One vibration span is equal to half of the staircase cycle: $t_p = \tau/2$.[29] Complementary to the staircase cycle: $f = 1/\tau$ is the signal frequency. The peak of the staircase wave shape is the potential increment ΔE. Analogous to the direction of the scan, ΔE, forward and backward vibrations can be separated. The currents are calculated in the final few split seconds of each vibration

and the contrast between the current calculated on two consecutive vibrations of the same step is noted as a total reaction ($\Delta I = I_f - I_b$).[29]

Linear sweep voltammetry

This is analytical technique is most useful in determining oxidisable organics with a glassy carbon electrode. A linear sweep voltammogram (LSV) is one half of that of a cyclic voltammogram. The peak height is in proportion with the concentration, and has an analytical sensitivity of 1 ppm.[30] Current is determined as the potential is changed at a constant rate. The electronic flow or the potential difference between two electrodes is measured instead of recording an entire calculation. The peak current is directly proportional to the square root of the scan rate. Positive and negative values are employed respectively for the identification of oxidation and reduction for both potential and current.[30]

Linear sweep can be done at a rotating disk electrode or at a dropping mercury electrode and this is sometimes known as hydrodynamic voltammetry or polarography. In hydrodynamic voltammetry, at a fixed rate the solution is blended by spinning the working electrode. [30] As the sweep accomplishes potential at which the reduction or oxidation starts, the background current is fixed. There is a strong escalation of current until the highest reaction rate is achieved; stirring of the solution continually, restores the analyte around the electrode so as to keep the current present.[30] An example of a linear sweep voltammogram is given in **Figure 2.6**.

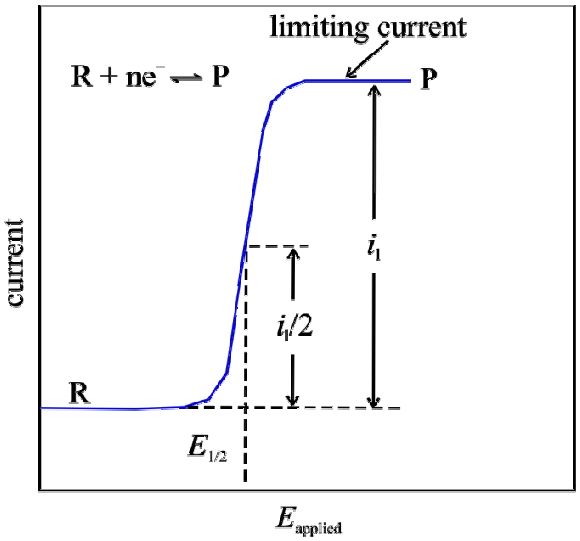

Figure 2.6. Linear-Sweep Voltammogram for the reduction of a hypothetical species R to give a product P.

The maximum current, also called the limiting current, $i_{p,}$ is comparable to the analyte concentration as stated in the Levich equation:[31,32]

$$i_1 = 0.620nFD^{2/3}\omega^{1/2}v^{-1/6}C^*$$

In the equation, i_1 = limiting current (A), n = number of electrons transferred (mole$^-$/mol analyte), F = Faraday's constant (96.484 C/mole$^-$), A = area of the electrode (cm^2), ω = rate of rotation of working electrode (s^{-1}), D = diffusion coefficient of analyte (cm^2/s), v = scan rate (V/s) and C* = bulk concentration of analyte (mol/cm^3).[31]

The half-wave potential $E_{½}$ is associated to the standard potential for the half-reaction and is frequently used for the qualitative recognition of species. The half-wave potential is the applied potential at which the current *i* is $i_{½}$. At a slow rotation rate only reactions or reaction steps which consider a longer period to occur will be observed. [31]

Solvent effect

A medium composed of a solvent carrying a supportive electrolyte is frequently employed to convey electrochemical measurements. Solubility of an analyte and its redox activity in the solvent window of interest are primary dictators of the choice of which solvent should be used. Solvent effects, such as the electrical conductivity, electrochemical activity and chemical activity, also play a role. The solvent used must never react with the analyte or products and must never experience an electrochemical reaction over the potential range of interest.[33] Water proved to be a suitable solvent. However, in the study of the chemistry of metal complexes, non-aqueous solvents such as acetonitrile, propylene carbonate, dimethylformamide (DMF), dimethylsulfoxide (DMSO), or methanol can be used.[33] Solvents which are dipolar aprotic are often used since they have a large dielectric constant (≥ 10) and have low proton availability. Acetonitrile is commonly used in anodic studies because it has a wide potential range, a high conductivity, but it is moderately nucleophilic.[34] Conradie *et al* show that CH_3CN sometimes coordinates with metal complexes to form a solvent-coordinated species.[35] If a strictly non-coordinating solvent is required, dichloromethane will be a good choice.[34] However, THF may be a beneficial solvent if there is a requirement for a solvent with a bigger potential window than CH_2Cl_2. THF has been thought to be not interacting with negatively charged species since it is nucleophilic and can react with electrophiles when conditions are oxidising.[24] Some preparations preferred blended solvents. For a majority of

experiments in aqueous media double-distilled water is sufficient. However, when trace analysis is needed, triple-distilled water is frequently needed.[36]

Supporting electrolytes

Controlled potential experiments require supporting electrolytes in order to minimise the resistance of the solution, cancel electro-migration effects and keep a consistent ionic strength.[37] Inorganic salts, mineral acids or buffers can be used as inert supporting electrolytes. When water is used as a solvent, potassium chloride or nitrate, ammonium chloride, sodium hydroxide or hydrochloric acid is extensively employed. In organic media, tetraalkylammonium salts are frequently used. Acetate, phosphate or citrate as buffer systems, are employed when pH control is of importance. The constitution of the electrolyte may influence discrimination of voltammetric calculations.[33] The concentration of the analyte must be at most 10% that of the electrolyte to prevent the analyte acting as an electrolyte. Tetrabutylammonium hexafluorophosphate, $[NBu_4]^+[PF_6]^-$ ($TBAPF_6$), or $[NBu_4]^+[ClO_4]^-$, is widely used as a supporting electrolyte and is soluble in CH_3CN. A solution of $[NBu_4]^+[B(C_6F_5)_4]^-$ in acetonitrile display a very commonly attainable potential range, having positive and negative decomposition potentials of 3.4 V and -2.9 V (*vs* SCE) respectively.[34] Electrolytes with PF_6^- or ClO_4^- anions are disadvantageous to use since they often form ion-pairs with oxidised species and, and since ClO_4^- salts are explosive; perchlorate-containing supporting electrolytes involvement are not favoured. Ion-pair development with positively charged, oxidized species may be lessened if the negative charge of the anion of the supporting electrolyte is dispersed over a large volume, as it is the case with the positive charge on the N atom of the $N(^nBu)_4^+$ cation, which is lessened by the four electron-donating butyl groups.[24] The non-coordinating supporting electrolyte, tetrabutylammonium tetrakis(pentafluorophenyl)borate, $[NBu_4]^+[B(C_6F_5)_4]^-$, improves the electrochemistry when compared to the weakly coordinating supporting electrolyte, tetrabutylammonium hexafluorophosphate, $[NBu_4]^+[PF_6]^-$, in solvents of low dielectric strength.[38] With the use of this new electrolyte, electrochemistry could be conducted in solvents of low dielectric strength, and reversible electrochemistry is obtained for compounds that are normally irreversible.[38] The peak separation between two very close oxidation peaks could also be better analysed with the use of this electrolyte.[39]

Reference electrode

In aqueous media, a saturated calomel electrode (SCE), a standard hydrogen electrode (SHE or NHE) or a silver/silver chloride electrode (Ag/AgCl) reference electrode is often used. When necessary, a salt bridge is used to separate the reference electrode from the solution so that if leakage from the reference electrode does occur contamination is prevented. When a complex is insoluble or instable in water, non-aqueous solvents can be used. Because the non-aqueous media leakage of water from an aqueous reference is a concern, a non-aqueous bridge or a Ag/Ag^+ electrode (0.01 M $AgNO_3$ in CH_3CN) or a Ag-wire placed directly into the solution can be used as reference electrodes.[40] The recommendation by IUPAC is that all electrochemical data are to be reported *vs* an internal standard. The oxidation and reduction of ferrocene (Fc^+/Fc couple where $E^{0'}$ = 0.400 V *vs* NHE) as an internal standard in non-aqueous solvents are commonly used.[40,41,42]

The ideal Fc/Fc^+ couple have a ΔE_p value of 59 mV and reversible under ideal conditions. The use of the formal reduction potential of ferrocene as an internal standard, independent of the reference system is illustrated in **Figure 2.7.**

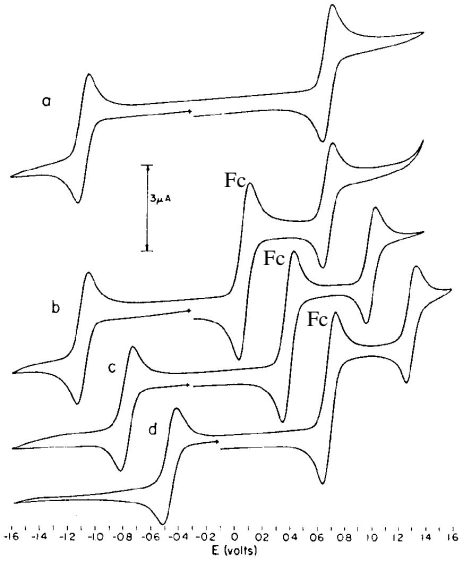

Figure 2.7. Platinum button cyclic voltammetry at 50 mV/s of 0.005 M $[Ru(acac)_3]$ in CH_3CN with tetrabutylammonium perchlorate (TBAP = 0.1M); (b), (c) and (d) ferrocene added; (a) and (b) *vs* $Ag/AgNO_3$ (0.01M), (c) *vs* SCE and (d) *vs* Cu wire. "Reprinted (adapted) with permission from R.R. Gagne, C.A. Koval, G. C. Lisensky *Inorg. Chem.*, *19* (9), Copyright (1980), American Chemical Society."

The cyclic voltammogram of *tris*(acetylacetonato)ruthenium(III) in acetonitrile is shown in **Figure 2.7**. The resulting cyclic voltammogram of *tris*(acetylacetonato)-ruthenium(III), after the addition of a small amount of ferrocene to give $E^{0'}$ values of 0.602 and -1.157 V *vs.* Fc^+/Fc, is shown in **Figure 2.7b**. SCE and copper-wire were used in **Figure 2.7c** and d as a reference electrode respectively, and conditions used were similar to those found in **Figure 2.7b**. The value of the formal potentials relative to Fc^+/Fc stayed the same even when the values on the potential axis seem to have shifted.[41]

2.2.2 Redox behaviour of β-diketones

The electrochemical oxidation of 1,3-diketones has been explored in the past by a several researchers[43]. Their investigation show that the conduct of an enol and keto forms vary electrochemically,[44] and is conditional on the identity of substituent groups,[45] also greatly affected by whether the solvent is aprotic or protic.

(i) *Dibenzoylmethane (Hdbm)*

An intense study has been done on electrochemistry by polarography on a β-diketone dibenzoylmethane (Hdbm).[46,47,48] In a 50% ethanol-water mixture, it was found that Hdbm could be reduced to three possible products, depending on the electrode potential and the pH of the solution. The first one-electron reduction product at first polarographic wave, was interpreted to be the pinacol known as 1,4-dibenzoyl-2,3-diphenyl-2,3-butanediol.[47] A neutral enol form of Hdbm has been studies with dimethylsulfoxide (DMSO) as a solvent.[48] A complex electrochemical behaviour resulted due to the acidity of this species. A number of reactions after the initial charge transfer resulted to the formation of radicals from the starting material. The data obtained indicated that processes other than diffusion limited the current, suggesting an involvement of coupled chemical reactions. It was further suggested that Hdbm is reduced to a product which may give Hdbm pinacol and enolate by following chemical reactions. Though Evans *et al.*[47] are not certain of the mechanism of this process; they propose that it is most probable that the first reduction of Hdbm produces an anionic radical which is protonated by another Hdbm molecule. The resulting neutral radical dimerised to a pinacol and an enolate (see **Reaction 1**).

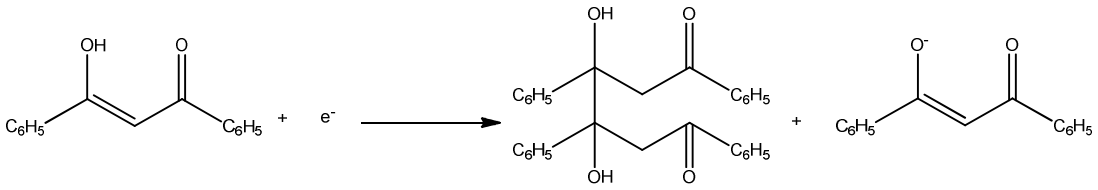

Reaction 1

The pinacol decomposes into a diketone and two molecules of acetophenone, especially with the addition of 2% of sodium hydroxide at room temperature, which is otherwise stable in dimethylsulfoxide (DMSO). This was followed by the reduction of the diketone (see **Reaction 2**).

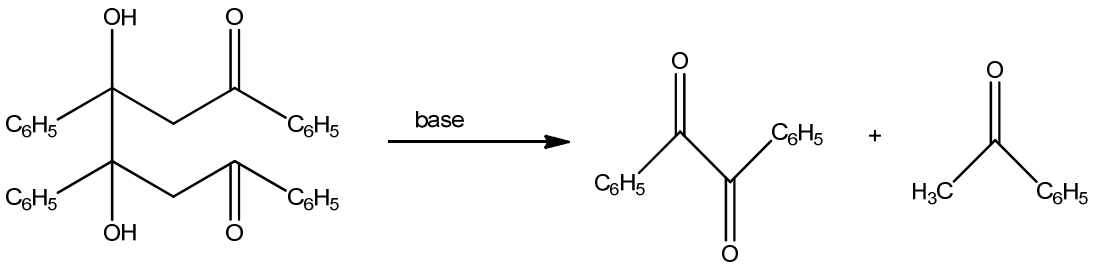

Reaction 2

(ii) *Acetylacetone (Hacac)*

Reduction waves for aliphatic Hacac have been reported in aqueous media.[49] Neal and Murray find that the reduction of acetylacetone in acetonitrile is completely irreversible with the reduction wave at E_{pc} = -2200 mV (*vs* SCE). In acetonitrile, acetylacetone exists as a 56:44 enol-keto mixture, and the reduction action happens via an enol form, having a keto-enol tautomeric change allows complete transformation. The reduction of acetyacetone is kinetically administered by a foregoing chemical reaction hypothesized as keto-Hacac ↔ enol- Hacac.[50]

(iii) *Series of enolized β-diketones, $R^1COCHC(OH)R^2$*

The first comprehensive study of the reduction on a series of ten enolized 1,3-substituted β-diketones accommodating either or both aromatic and aliphatic side groups was done by Kuhn *et al.*[51] The cyclic voltammograms of β-diketones $R^1COCHC(OH)R^2$(R^1, R^2 = CF_3,$PhNO_2$ (**1**), CF_3, CF_3 (**2**), CF_3,Th (**3**), CF_3,Ph (**4**), CF_3,CH_3 (**5**), CF_3,CMe_3 (**6**), Th, Th (**7**), Ph, Th (**8**),

Ph, Ph (**9**) and Ph, CH_3 (**10**), where $PhNO_2$ = (pNO_2-C_6H_4), Th = (C_4H_3S), Ph = phenyl (C_6H_5) and Me = methyl (CH_3)), comprising electron-withdrawing and/or electron-donating species, display a one-electron reduction process as suggested in **Scheme 2. 12**:[51]

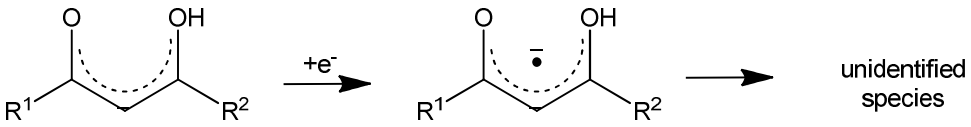

Scheme 2. 12. Reduction of enolized β-diketones.

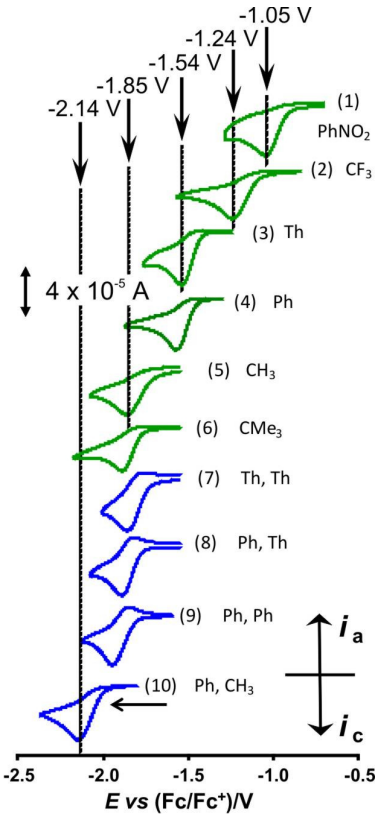

Figure 2.8. Comparative CVs (*vs* Fc/Fc$^+$) at a scan rate of 0.100 V s^{-1} for the β-diketone series $R^1COCHC(OH)R^2$ (0.003 mol dm^{-3}), studied in 0.1 mol dm^{-3} [NBu_4][PF_6]/CH_3CN on a glassy carbon working electrode at 25 °C. Vertical dashed lines indicate a few E_{pc}. Colour coding (online version): green graphs stand for CVs of β-diketones (1) - (6) $CF_3COCHC(OH)R^2$ (R^2 shown on the graph), and the blue graphs stand for CVs of β-diketones (7) - (10) $R^1COCHC(OH)R^2$ (R^1 and R^2 shown on the graph). Scans commenced in the direction as shown by the horizontal arrow. "Reprinted from *Electrochim. Acta*, 56, Kuhn, A.; von Eschwege, K.; Conradie, J., Electrochemical and density functional theory modelled reduction of enolized 1,3-diketones, 6211, Copyright (2011), with permission from Elsevier."

It was found that, generally, reduction potentials increase or become more anodic with an increase in the electron-withdrawing capacity of the substituents R^1 and R^2, and its possible conjugation extension in the following order: CMe_3<CH_3<Ph<Th<CF_3<$PhNO_2$ (see **Figure 2.8**).[51] The pseudo-aromatic β-diketone reduces more readily when an electron density is removed from its backbone. An excellent electronic communication *via* conjugation in the middle of the electro-active centre and the side R group prevail, as postulated by the notable effect on reduction potentials by electronic behaviour of the R substituent group.[51]

A DFT study[51] (see (v) below) shows the reduced species to be a radical anion, in agreement with electron spin resonance spectroscopy.[52] It was, however, found that for β-diketones in which R^1 and R^2 are aromatic groups, reduction to become reversible or quasi-reversible during higher scan rates is permitted by an extensive preservation of the radical anion.[51] Therefore, β-diketones containing both two (i.e. both R^1 and R^2) aromatic groups with a fast enough scan rate to prevent follow-up reactions, the tallying oxidation of the reduced species materializes.[51] The cyclic voltammograms have scan rates of between 0.1 and 1.0 Vs^{-1} of β-diketones having two aromatic R groups: one has an aromatic R group and one doesn't have an aromatic R group. These illustrate the redox reversibility or irreversibility of the β-diketones. They are displayed in **Figure 2.9**.[51]

Relative stability of the radical anion can thus be achieved: first by delocalizing the negative charge in the pseudo-aromatic β-diketone moiety, and moreover by an electron density decrease in the pseudo-aromatic moiety by conjugating aromatic substituent groups.[51] A reduction in electron density in the pseudo-aromatic moiety can happen by inductive consequence where an σ-system has an electron-withdrawing group as a substituent and by resonance influence in a π-system where there is a straight resonance found at the electro-active centre and the substituent group in the radical anion. The strength of the radical is observed in β-diketones composed of two aromatic R groups. Hence a drop in the vitality of the radical anion appears to be through resonance instead of inductive effects of the R groups.[51]

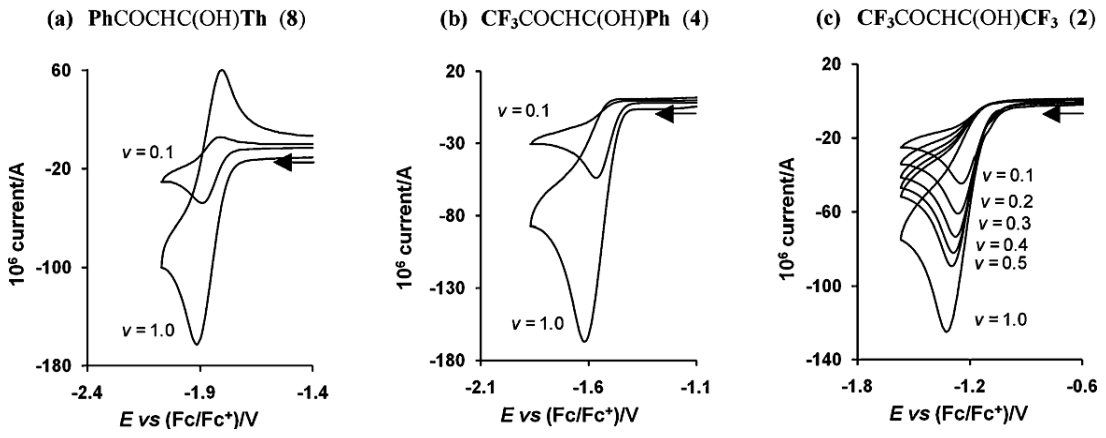

Figure 2.9. Cyclic voltammograms (vs Fc/Fc^+) at scan rates of between 0.100 and 1.000 V s^{-1} for β-diketones with (a) two aromatic side groups, (b) one aromatic (and one aliphatic) side group and (c) without aromatic (two aliphatic) side groups. Scans began in the direction of the arrow. Measurements performed in 0.1 M $[NBu_4][PF_6]/CH_3CN$ on a glassy carbon working electrode at 25 °C. [β-Diketone] = 0.003 mol dm^{-3}. "Reprinted from *Electrochim. Acta*, 56, Kuhn, A.; von Eschwege, K.; Conradie, J., Electrochemical and density functional theory modelled reduction of enolized 1,3-diketones, 6211, Copyright (2011), with permission from Elsevier."

(iv) *Tetrathiafulvalene (TTF)*

Redox behaviour of a γ-substituted β-diketone with tetrathiafulvalene (TTF) being substituted in the γ position of the β-diketone has been investigated.[53] The TTF group was chosen as a β-diketone substituent due to the high electron-donating ability of its reduced form and because it can experience two electrochemically reversible one-electron oxidations. Electrochemistry of this β-diketone was investigated in CH_2Cl_2/0.1 $moldm^{-3}$ as a solvent and with $[N^nBu_4][B(C_6F_5)_4]$ as the supporting electrolyte. The TTF core relates to two one electron-transfer redox couples exhibited by cyclic voltammograms.[53] They are labelled 1 and 2 in **Figure 2.10**.

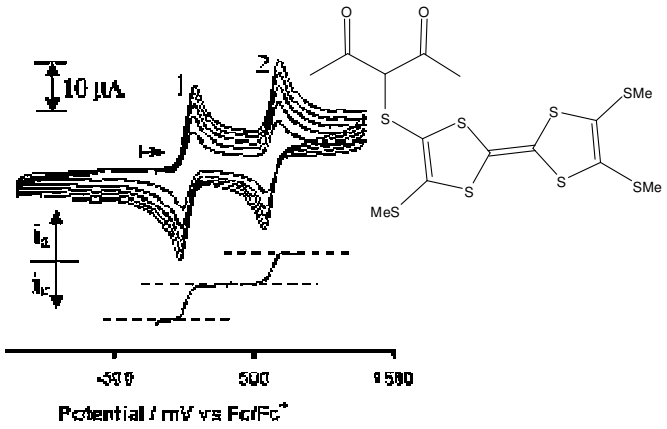

Figure 2.10. The structure and cyclic voltammograms of a γ-substituted β-diketone with tetrathiafulvalene (TTF) at scan rates of 100 (smallest peak current), 200, 300, 400, and 500 mVs^{-1} and LSV at 2 mV^{-2} in CH_2Cl_2/0.1 $moldm^{-3}$ [N^nBu_3][$B(C_6F_5)$], T = 25^0C, on a glassy carbon working electrode. "Reprinted (adapted) with permission from Fourie, E.; Swarts, J. C.; Lorcy, D.; Bellec, N. *Inorg. Chem.* 2010, 49, 952, Copyright (2010) American Chemical Society."

(v) *Density functional theory*

Density functional theory using the ADF software (Amsterdam Density Functional),[54] utilizing OLYP and hybrid B3LYP functional in gaseous medium and in acetonitrile solution, was used by Kuhn *et al.*[51] to calculate geometries and relative energies for a series of β-diketones. Calculations were done to determine the relationships between determined LUMO energies (E_{LUMO}), electron affinity (EA), worldwide electrophilicity index (ω), determined Mulliken electronegativities ($\chi_{calc.}$) and exploratory specifications that are comparable to the electron density on the β-diketone. These parameters are pK_a of the β-diketones, the Gordy scale group electronegativities of R^1 and R^2 side groups on $R^1COHC(OH)R^2$ and the reduction potential E_{pc} of the β-diketone. A prototype of β-diketonato ligands with distinct redox potentials is feasible due to the pre-eminent association established, for instance:[51]

$E_{pc} = -0.623\ E_{LUMO} - 3.6065$ ($R^2 = 0.99$)

$E_{pc} = 0.9415\ \omega - 3.1761$ ($R^2 = 0.94$)

$E_{pc} = 0.6169\ EA - 2.3928$ ($R^2 = 0.84$)

The agreement between E_{pc} and the theoretical descriptor E_{LUMO} is expected because the generated electrochemical reduction bring along the movement of electrons into the lowest

unoccupied molecular orbital of the neutral molecule.[51] Thus, the essence and make-up of the LUMO command the redox chemistry. The LUMO has π-character which involves the conjugated β-diketone backbone and aryl substituents (see **Figure 2.11**).[51] A general conclusion is that an increase in the electron-withdrawing capacity of the substituent and a subsequent decrease in the electron density in the *pseudo*-aromatic moiety result in an increase of anodic reduction potentials which show increased reduction possibility, lowering of the LUMO energies. This indicates a ready addition of electrons and larger calculated electron affinity values, which signifies more energy being liberated after an addition of an electron to a neutral β-diketone derivative.[51]

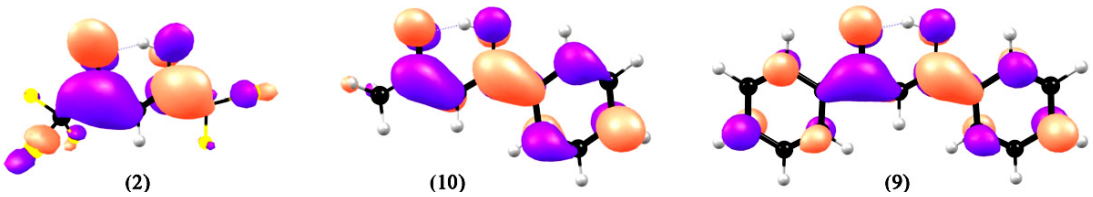

Figure 2.11. LUMOs (lowest unoccupied molecular orbitals) of $R^1COCHC(OH)R^2$, for R^1, R^2 = CF_3, CF_3 (2), CH_3, Ph (10) and Ph, Ph (9) as labelled and numbered in Figure 2.8. "Reprinted from *Electrochim. Acta*, 56, Kuhn, A.; von Eschwege, K.; Conradie, J., Electrochemical and density functional theory modeled reduction of enolized 1,3-diketones, 6211, Copyright (2011), with permission from Elsevier."

The charge dispensation in the radical anion of the aromatic centre of the reduced β-diketone can be indicated by the calculated Mulliken unpaired spin density. As the β-diketone substituents become more aromatic, spin density in the *pseudo*-aromatic β-diketone core decreases.[51] The decrease in spin density on the β-diketone backbone from about 85% to 55% and to 50% is calculated for β-diketones containing two aliphatic groups, one of which is aromatic and the other an aliphatic group, and two aromatic groups respectively, see **Figure 2.12**.[51] The inductive ability of acyclic substituents with electron-withdrawing properties does not affect the dispensation of the unpaired electron in the reduced species but electronegativity of the aromatic group has a noticeable outcome. According to Kuhn *et al*., chemical reversibility was observed only on β-diketones in which the unpaired electron was delocalised uniformly over the conjugated system including both R^1 and R^2 groups.

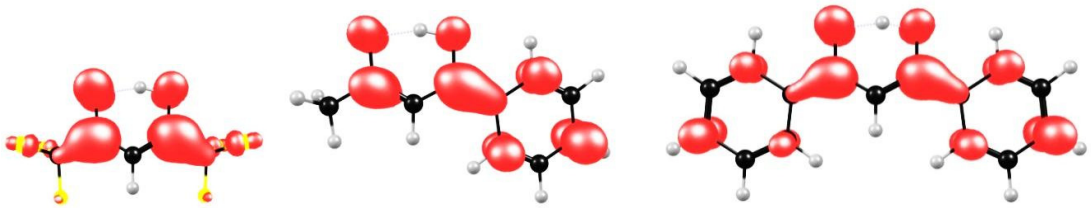

(**2**) $^{\bullet-}$ (5:87:8) (**10**) $^{\bullet-}$ (1:55:44) (**9**) $^{\bullet-}$ (22:50:28)

Figure 2.12. Spin density plots for the reduced species, $R^1COCHC(OH)R^{2\,\bullet-}$, with R^1, R^2 = CF_3,CF_3 (2), Ph, Ph (9) and Ph, CH_3 (10) as labelled and numbered in Figure 2.8. Molecules are depicted in black with H = grey, F = yellow and majority electron spin density indicated in red. The spin density percentages are indicated for (R^1:COCHC(OH):R^2). "Reprinted from *Electrochim. Acta*, 56, Kuhn, A.; von Eschwege, K.; Conradie, J., Electrochemical and density functional theory modeled reduction of enolized 1,3-diketones, 6211, Copyright (2011), with permission from Elsevier."

2.2.3 Redox behaviour of Rh-β-diketonato complexes

In the fields of both pure and applied chemistry, attention is given to metal complexes with β-diketones.[55] Rhodium-containing complexes are very relevant in homogeneous catalysis; especially knowledge of the changes in the metal oxidation state is important. This depends on the bonding of the molecule. Changes in the number of electrons of the rhodium complexes may induce changes in structure and reactivity. The electron density on the rhodium centre is affected by the nature of ligands around it.[56] These ligands, together with their physical properties, may be of use to project the oxidation potential of a rhodium centre.[57] Electron density of the rhodium(I) centre is removed if there is a more electronegative ligand in the rhodium complex, causing the complex to be less favourable for oxidative addition since it becomes a stronger Lewis acid. Thus a weaker electrophile is created from the rhodium atom.[58] During oxidation an electron that is taken away from the metal ion is from the highest occupied molecular orbital (HOMO). More energy is needed for electron displacement on metal complexes with lower lying HOMOs and have higher potentials for oxidation, i.e. more positive potentials.[59] Werner *et al.* suggest that the comparable energy of the LUMO rely predominantly on the π-acceptor capability of the ligands. The π-acceptor capability frequently lowers the HOMO energy by reducing inter-electron repulsion in the metal ion.[60]

A projection of oxidation potentials which enable a model of organometallic molecules having distinct oxidation potential, a correlation of electrochemical specifications as peak oxidation potentials, specifications on kinetic properties as oxidative addition rate constants affecting electron density of the Rh(I) centre (electron donating or withdrawing ligands) is vital.[61] Electrochemical studies can therefore provide innumerable up to date techniques to probe *i.e.* the reactivity on rhodium complexes.[62]

(i) *[Rh(β-diketonato)(CO)L] and [RhH(CO)L_3] complexes*

Electrochemical studies by cyclic voltammetry in 0.2 mol dm^{-3} $[N(^nBu_4)][BF_4]/CH_2Cl_2$ at a Pt-disc electrode were conducted by Guedes da Silva *et al.*[63] for a series of twelve tetracoordinate [Rh(β-diketonato)(CO)L] and six pentacoordinate $[RhH(CO)L_3]$ complexes with L = CO, PPh_3, PCy_3, $P(OPh)_3$ and other phosphines and β-diketonato = $(CH_3COCHCOCH_3)^-$ (acac), $(CH_3COCHCOC_6H_5)^-$ (ba) and $(CF_3COCHCOC_6H_5)^-$ (tfba).[63]

An irreversible one-electron oxidation process is obtained for the oxidation of the tetracoordinate rhodium complexes at scan rates up to of 500 Vs^{-1} (faster scan rates produced a loss of wave definition) and low temperatures of as low as -40 °C. The CV of the tetracoordinate rhodium complexes at 200 mV s^{-1} exhibit an irreversible oxidation wave (I) at $E^{oxI}_{p/2}$ in the 0.20–2.44 V versus NHE range, which, in a few instances, is pursued (at a higher potential ($E^{oxII}_{p/2}$ in the range 0.57–2.77 V)) by a second irreversible oxidation wave II, (see **Figure 2.13**) for $[Rh(CH_3C(O)CHC(O)CH_3)(CO)PCy_3]$.[63] The electrode process at wave I is interpreted to comprise an individual electron, i.e. the Rh(I)-Rh(II) oxidation. This is supported in a few instances by anodic regulated potential electrolysis.[63] The utilization of CH_2Cl_2 as the solvent and $[N(^nBu_4)][BF_4]$ as the supporting electrolyte most probably made the detection of the unstable Rh(II) species possible.[63]

The oxidation waves of the dicarbonyl complexes $[Rh(CH_3C(O)CHC(O)CH_3)(CO)_2]$ and $[Rh(PhC(O)CHC(O)CH_3)(CO)_2]$ were detected only in acetonitrile (CH_3CN), which is a solvent with a wider anodic potential window relative to dichloromethane (CH_2Cl_2) at 2.14 and 2.44 V *vs* NHE respectively. For $[Rh(CH_3C(O)CHC(O)CH_3)(CO)_2]$, two not often resolved irreversible oxidation waves, were observed at lesser potentials of 1.2 and 1.5 V (than those of wave I, 2.14 V) with an irreproducible and lower peak current, but only in the first anodic scan.[63] Conceivably they are associated with adsorption effects.

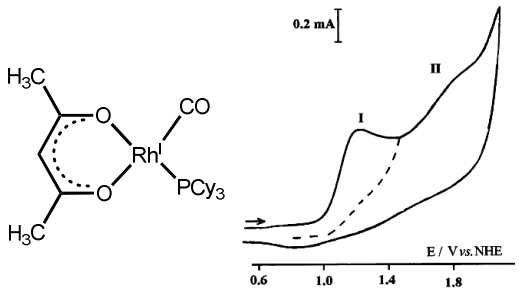

Figure 2.13. Structure and cyclic voltammogram of the tetracoordinate complex [Rh($CH_3C(O)CHC(O)CH_3$)(CO)PCy_3] (1.1 mmol.dm^{-3} in CH_2Cl_2 with 0.2 mol.dm^{-3} [NBu_4][BF_4]) at a platinum disc (d = 0.5 mm) working electrode and at a scan rate of 0.2 Vs^{-1}.[63]"Reprinted from Guedes da Silva, M. F. C.; Trzeciak, A. M.; Ziólkowski, J. J.; Pomberiro, A. J. L. *J. Organomet. Chem.* 2001, 620, 174, Copyright (2001), with permission from Elsevier."

Lever[64] proposes a factual relation where oxidation potential measured in volts versus SHE of the redox couple M(q)/M(q+1) of a complex is linked to electrochemical properties related to both the ligands and the metal centre:

$$E_{redox}\ (vs.\ \text{SHE}) = S_M X\ \Sigma E_L + I_M$$

in which ΣE_L is the total of the values of the ligand E_L parameter for all the ligands (additive effects) and S_M and I_M symbolise the slope and intercept determined by the redox couple, metal, stereochemistry and spin state . The values for the initial oxidation potential for a series of rhodium(I) complexes fits Lever's electrochemical parameterization, reflecting the comparative electron donor-acceptor capabilities of the β-diketonato, CO and phosphine or phosphite ligands.[61]

(i) *[Rh(β-diketonato)$(CO)_2$] complexes*

Dicarbonyl complexes of the form [Rh(FcC(O)CHC(O)R)$(CO)_2$] where R = CF_3, CH_3, Ph, and Fc where measured by Conradie *et al.*[35] These complexes contain two (or three for R = Fc) metal redox centres. The CV of these complexes was complicated by overlapping peaks for the Rh and Fc oxidation, as well as by the formation of a solvent coordinated species ([Rh(FcC(O)CHC(O)R)$(CO)_2(CD_3CN)$]), which is in slow equilibrium with [Rh(FcC(O)CHC(O)R)$(CO)_2$] in acetonitrile as solvent. The [Rh(FcC(O)CHC(O)R)$(CO)_2$] +

$CD_3CN \rightleftharpoons$ [Rh(FcC(O)CHC(O)R)$(CO)_2$(CD_3CN)]) equilibrium was confirmed by ^{1}H NMR with deuterated acetonitrile as solvent, see **Figure 2.14** right.[35]

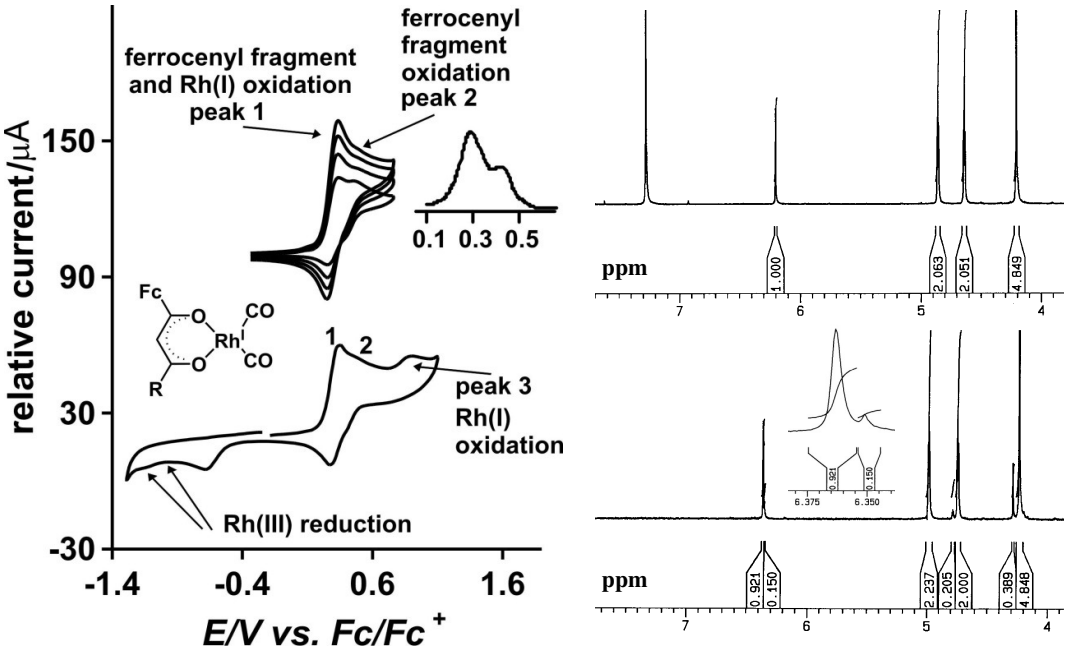

Figure 2.14. Left: Structure and CVs of solutions of [Rh(FcC(O)CHC(O)CF_3)$(CO)_2$] at scan rates of 50, 100, 150 and 200 mV s^{-1}, showing two ferrocenyl waves (top) at 100and 200 mV $s^{-1}$and also showing rhodium oxidation and reduction peaks (bottom). Peak 1 represents the ferrocenyl-based redox process associated with [Rh(FcCOCHCOCF_3)$(CO)_2$(CH_3CN)] while peak 2 is associated with the ferrocenyl group of [$Rh^{oxidised}$(FcCOCHCOCF_3)$(CO)_2$(solvent)$_x$].

Inset: OSWV analysis confirmed the presence of peaks 1 and 2 at 0.289 and 0.419 V, respectively. Scan rate = 4 mV s^{-1}.

Right: The ^{1}H NMR spectrum in the region 4–6.5 ppm of [Rh(FcC(O)CHC(O)CF_3)$(CO)_2$] in CD_3CN (bottom) clearly shows the existence of the adduct [Rh(FcCOCHCOCF_3)$(CO)_2$(CD_3CN)] alongside that of the parent compound [Rh(FcC(O)CHC(O)CF_3)$(CO)_2$]. In weakly coordinating $CDCl_3$ (top), only one species, free [Rh(FcC(O)CHC(O)CF_3)$(CO)_2$], is observable. "Reprinted from *Inorganica Chimica Acta*, 358, Jeanet Conradie, T. Stanley Cameron, Manuel A. S. Aquino, Gert J. Lamprecht, Jannie C. Swarts, Synthetic, electrochemical and structural aspects of a series of ferrocene-containing dicarbonyl β-diketonato rhodium(I) complexes, 2530–2542., Copyright (2005), with permission from Elsevier."

The electrochemical results obtained from CV, OSWV, bulk electrolysis and IR are summarized **Figure 2.14** and are harmonious with the below normal electrochemical scheme (acetonitrile = solvent, Rh^{ox} = products of electrochemically irreversible Rh^{I} oxidation):[35]

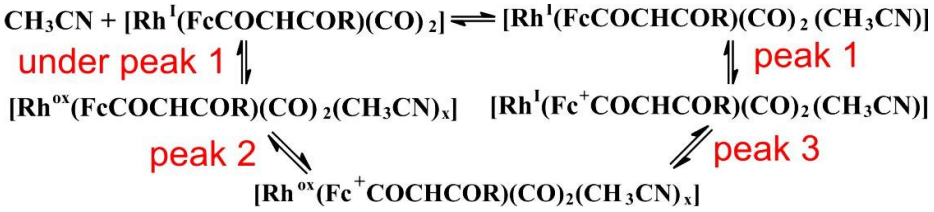

Rhodium(II) intermediate could not be identified from studies done by Conradie *et al*[35] in contrast to studies by Guedes da Silva *et al.*[63] A solvent used by Pombeiro gave very different results from the one used by Conradie. Pombeiro uses CH_2Cl_2, while in Conradie's investigation CH_3CN is favoured. Geiger[65]and others[24,66] have displayed that the utilization of CH_2Cl_2 over CH_3CN likewise $[N(^nBu_4][B(C_6F_5)_4]$ instead of $[N(^nBu_4)][PF_6]$ as the supporting electrolyte many times direct to the discovery of volatile compound, as ruthenocenium radical cations.

An electrochemical study by Fourie[67] on $[Rh(FcC(O)CHC(O)R)(CO)_2]$ where R = CF_3, Fc, Rc and Oc (Rc = ruthenocenyl and Oc = osmocenyl) in the non-coordinating solvent CH_2Cl_2 using $[N(^nBu_4][B(C_6F_5)_4]$ as electrolyte, does detect the Rh(II) intermediate. The CV obtained for $[Rh(FcC(O)CHC(O)CF_3)(CO)_2]$ showed only one oxidation peak representing the oxidation of the ferrocenyl and rhodium to overlap (**Figure 2.15**), consistent with the following scheme:[67]

$$[Rh^{I}(FcCOCHCOCF_3)(CO)_2] \underset{+2 \times (1e^-)}{\overset{-2 \times (1e^-)}{\rightleftharpoons}} [Rh^{II}(Fc^{+}COCHCOCF_3)(CO)_2]$$

peaks unresolved

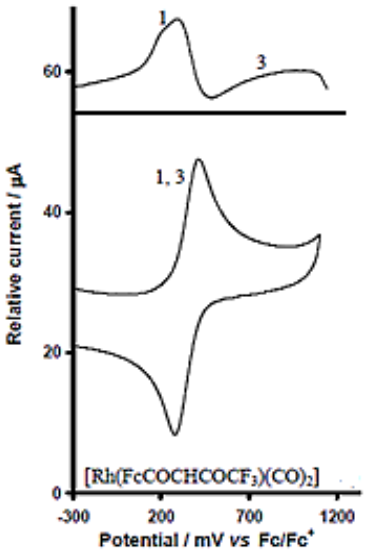

Figure 2.15. CV (bottom part of diagram) and SWV (top) of rhodium(I) dicarbonyl complex [Rh(FcC(O)CHC(O)CF_3)$(CO)_2$] in CH_2Cl_2/0.1 mol dm^{-3} [N($^nBu_4$)][B(C_6F_6)], T = 25°C on a glassy carbon working electrode measured at a CV scan rate of 100 mVs^{-1}, and SW measured at a frequency of 50 Hz. The Fc/Fc^+ couple is labelled peak 1 and the rhodium(II/I) couple is labelled peak 3. "From reference 67, copyright (2003) University of the Free State, Bloemfontein, RSA."

(ii) *[Rh(β-diketonato)(CO)(PPh_3)]*

The CV of a set of four [Rh(I)(β-diketonato)(CO)(PPh_3)] complexes was done by Lamprecht *et al.*[62] The β-diketones were chosen to have different electronegativities and steric hindrances: dibenzoylmethane (Hdbm), benzoylacetone (Hba), benzoyltrifluoroacetone (Hbtfa) and trifluoroacetone (Htfaa).[62] The CVs each showed an oxidation wave at *ca* 0.4 V *vs* Fc/Fc^+ and a small reduction wave, more than 1 V to the left (negative) of the oxidation wave. The oxidation wave is set as the oxidation of Rh(I) to Rh(III). To prove the oxidation of Rh(I) to Rh(III) during the electrochemically irreversible two-electron transfer process bulk electrolysis was carried out at peak anodic potentials 0.308-0.491 *vs.* Fc/Fc^+. To prove that the observed reduction peaks were coupled to the Rh(III) oxidation, negative scans were run, see **Figure 2.17** left. The absence of a reduction peak was due to the absence of Rh(III) when scanning negative, since the production of Rh(III) is possible electrochemically when Rh(I) is oxidised. An increase in scan rate increases the cathodic peak height, **Figure 2.17** right. At higher scan rates, less Rh(III) had time to diffuse off from the working electrode surface, generating additional Rh(III) which is reduced to Rh(I). Additional clarification is that, at

higher scan rates, less Rh(III) had time to decompose. The anodic peak current was in direct proportion to $\upsilon^{1/2}$, according to the Randles-Sevcik equation, $i_p = (2.69 \text{ X } 10^5)n^{3/2}AD^{1/2}C\upsilon^{1/2}$.[62]

The cyclic voltammograms of four [Rh(I)(β-diketonato)(CO)(PPh_3)] complexes, disclose a straightforward connection at Rh(I) to Rh(III) species of irreversible oxidation potentials and the pK_a-values of the independent β-diketones dibenzoylmethane (Hdbm), benzoylacetone (Hba), benzoyltrifluoroacetone (Hbtfa) and trifluoroacetone (Htfaa), see **Figure 2.16**.[62] The extra electron-rich Rh(I) centre is a consequence of a β-diketone substituents with high pK_a values which cause less positive oxidation potentials showing simple oxidation of Rh(I) to Rh(III) and extra negative reduction potentials that indicate difficulty in the reduction of Rh(III) species. The fact that the peak oxidation potentials of [Rh(btfa)(CO)(PPh_3)] and [Rh(tfaa)(CO)(PPh_3)] are similar, were interpreted within experimental error that steric parameters had no influence during electrochemical oxidation. The expertise of electrochemical oxidation may hence be utilised to compute steric effects throughout chemical oxidation.[62]

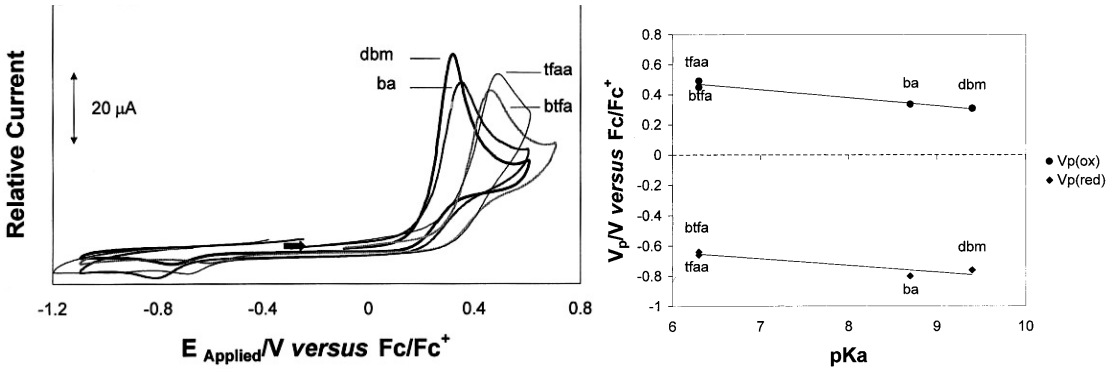

Figure 2.16. Left: Cyclic voltammograms of [Rh(β-diketonato)(CO)(PPh_3)] complexes on a glassy carbon working electrode in 0.1 mol dm^{-3} TBAHFP: where CH_3CN was used as solvent-supporting electrolyte. The scan rate was 0.1 V s^{-1}. Right: Connection of the peak oxidation and peak reduction potentials of the different [Rh(β-diketonato)(CO)(PPh3)] complexes and the pK_a values of appropriate β-diketones. "Reprinted from *Inorganica Chimica Acta*, 309, Delanie Lamprecht, Gert J. Lamprecht, Electrochemical oxidation of Rh(I) to Rh(III) in rhodium(I) β-diketonato carbonyl phosphine complexes, 72–76, Copyright (2000), with permission from Elsevier."

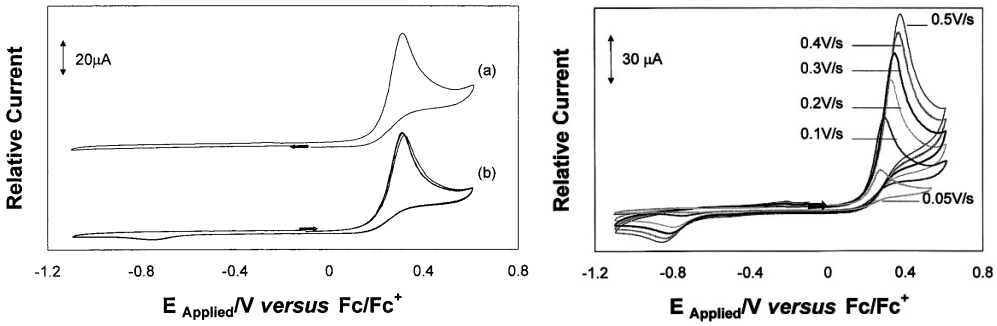

Figure 2.17. Left: (a) Negative scan CVs and (b) consecutive positive scan CVs of [Rh(dbm)(CO)(PPh_3)] on a glassy carbon working electrode in 0.1 mol dm^{-3}. [N($^nBu_4$)][PF_6]/CH_3CN solvent-supporting electrolyte. The scan rate was 0. 1 V s^{-1}.

Right: CVs of [Rh(dbm)(CO)(PPh_3)] on a glassy carbon working electrode in 0.1 mol dm^{-3} [N($^nBu_4$)][PF_6]/CH_3CN solvent-supporting electrolyte. The scan rate was varied between 0.05 and 0.5 V s^{-1}. "Reprinted from *Inorganica Chimica Acta*, 309, Delanie Lamprecht, Gert J. Lamprecht, Electrochemical oxidation of Rh(I) to Rh(III) in rhodium(I) β-diketonato carbonyl phosphine complexes, 72–76, Copyright (2000), with permission from Elsevier."

Rhodium(I) complexes with a form [Rh(FcCOCHCOR)(CO)(PPh_3)] where ferrocene is one of the substituents, R = Fc (ferrocenyl), Ph (phenyl), CH_3, and CF_3, have two (or three for R = Fc) metal redox centres. The complexes with R ≠ Fc (thus an unsymmetrical backbone) have two isomers in solution (**Figure 2.18**).[57] The CV results of the ferrocene-containing [Rh(FcCOCHCOR)(CO)(PPh_3)] complexes are comparable with Rh^I being oxidised initially at electrochemically irreversible process of two-electron transfer at peak anodic potentials: E_{pa}(Rh) = 108 mV for R = Fc**,** 123 and 273 mV for R = Ph, 154 and 253 mV for R = CH_3 and 196 and 327 mV *vs* Fc/Fc^+ for R = CF_3 at scan rate 100 mV s^{-1}. This was followed with oxidation of each ferrocenyl group which was considered electrochemical reversible in a single-electron transfer activity at moderately high potentials. Two discrete waves resolved only E_{pa}(Rh) CV peaks, each affiliated with an isomer.[57] Moderate isomerisation kinetics enabled the observation of both isomers of each of **2**–**4** (see **Figure 2.18**, right for **3**). Rhodium(III) reduction of oxidised **1**, **2**, **3** and **4** was noticed at higher negative potentials: -0.69, -0.75, -0.86 and -0.70 V respectively, while for the Rh(III) complex [Rh(FcCOCHCOCF_3)(CH_3)(I)(CO)(PPh_3)], it was noticed at -1.492 V *vs* Fc/Fc^+ (see **Figure 2.19**).[57] The structure of [Rh(FcCOCHCOCF_3)(CH_3)(I)(CO)(PPh_3)] was established by X-ray crystallography.[68] The electrochemical scheme that outlines the outcome for the ferrocene-containing [Rh(FcCOCHCOR)(CO)(PPh_3)] complexes are shown in **Scheme 2. 13.**[57]

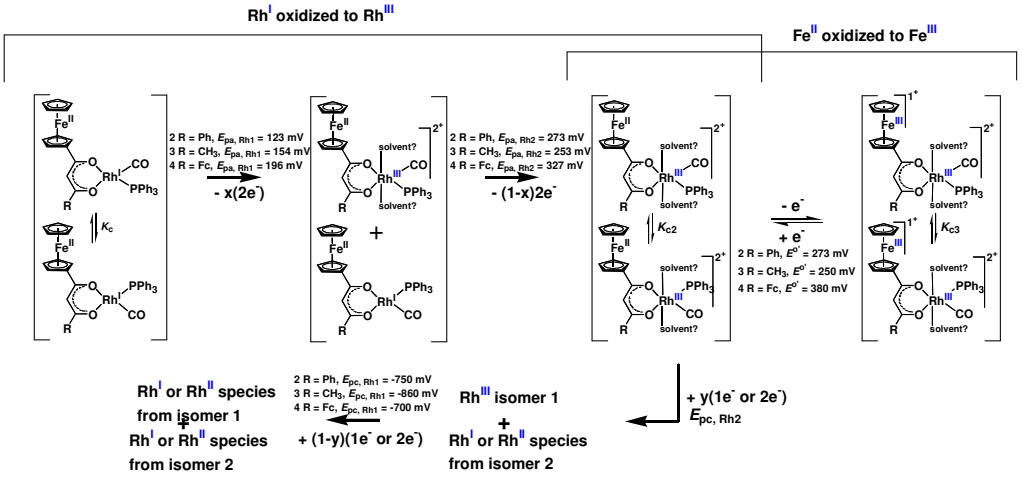

Scheme 2. 13. Electrochemical oxidation of [Rh(FcCOCHCOR)(CO)(PPh$_3$)] complexes 1–4 in Figure 2.18. Isomers in scheme may exchange. The fragment of reduced rhodium(I) complexes prevailing as isomer that oxidizes first is indicated by x, while y indicates the fragment of oxidized compound prevailing as isomer 2 that is reduced on the reverse cycle. It is eminent that x and y are not certainly the same. Rhodium(III) reduction is in the above scheme suggested to produce either rhodium(I) or rhodium(II) because it was not possible to decide the oxidation state of the reduced species explicitly. However, the reduction results of the rhodium(III) complex, [Rh^{III}(FcCOCHCOCF$_3$)(CH$_3$)(I)(CO)(PPh$_3$)], was displayed to be a rhodium(II) species. "Reprinted from *European Journal of Inorganic Chemistry*, Jeanet Conradie, Jannie C. Swarts, The Relationship between the Electrochemical and Chemical Oxidation of Ferrocene-Containing Carbonyl-Phosphane-β-Diketonato-Rhodium(I) Complexes – Cytotoxicity of [Rh(FcCOCHCOPh)(CO)(PPh$_3$)], 2439–2449, DOI: 10.1002/ejic.201100007, Copyright (2011) WILEY-VCH Verlag GmbH & Co. KGaA, Weinheim."

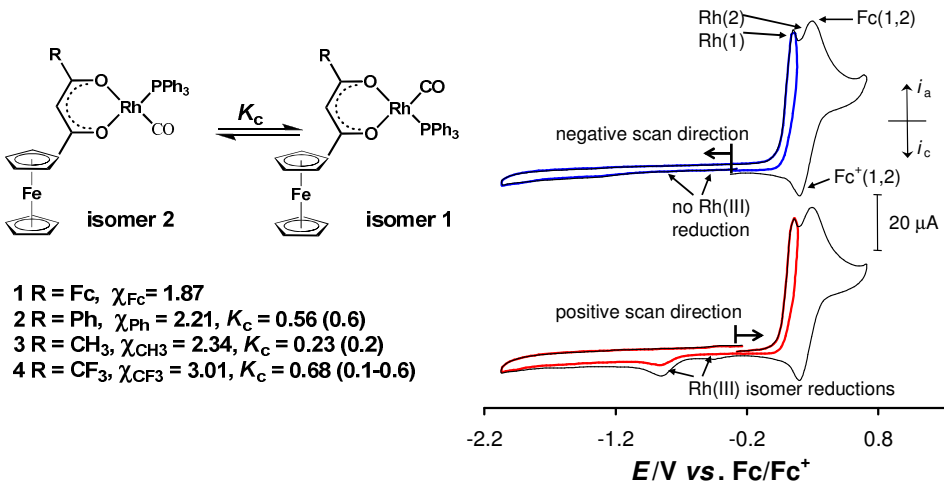

Figure 2.18. Left: Rhodium complexes with three (in 1) or two (in 2, 3 and 4) metal redox centres. An equilibrium occurs between the two isomers of [Rh(FcCOCHCOR)(CO)(PPh$_3$)], permitting K$_c$= [isomer 1]/[isomer 2] at 298K in CDCl$_3$ (value in brackets is for CD$_3$CN) when R ≠ Fc.

Right: Cyclic voltammogram of 2 mmol dm^{-3} [Rh(FcCOCHCOCH$_3$)(CO)(PPh$_3$)], computed in 0.1 mol dm^{-3}[N(^{n}Bu$_4$)][PF$_6$]/CH$_3$CN at a scan rate of 100 mV s^{-1} on a glassy carbon working electrode at 25.0(1) °C. The arrows show initial scan directions. "Reprinted from *European Journal of Inorganic Chemistry*, Jeanet Conradie, Jannie C. Swarts, The Relationship between the Electrochemical and Chemical Oxidation of Ferrocene-Containing Carbonyl-Phosphane-β-Diketonato-Rhodium(I) Complexes – Cytotoxicity of [Rh(FcCOCHCOPh)(CO)(PPh$_3$)], 2439–2449, DOI: 10.1002/ejic.201100007, Copyright (2011) WILEY-VCH Verlag GmbH & Co. KGaA, Weinheim."

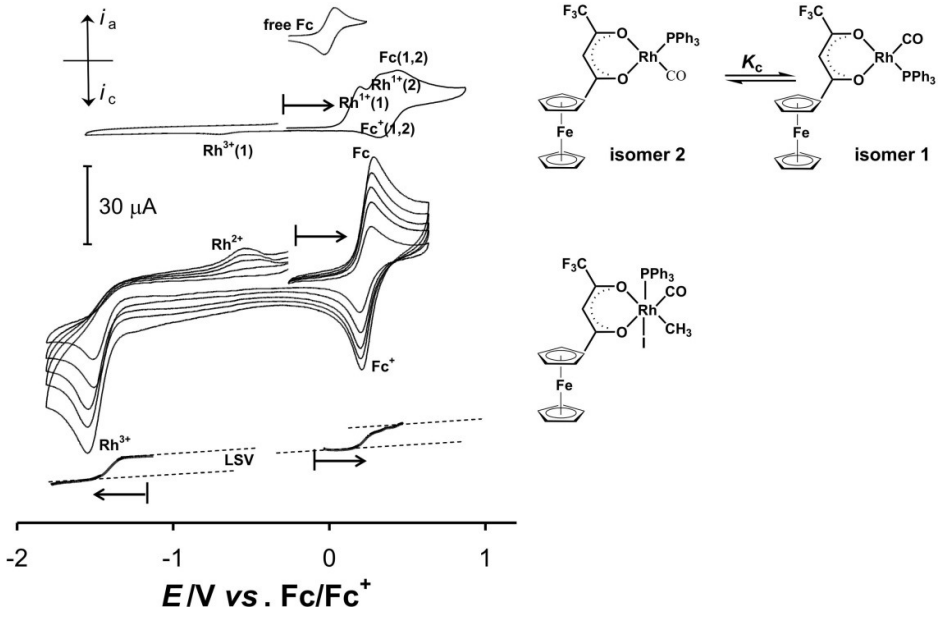

Figure 2.19. Cyclic voltammograms of 0.7 mmol dm^{-3} [Rh^{I}(FcCOCHCOCF$_3$)(CO)(PPh$_3$)], (top at 100 mV s^{-1}) and 1.5 mmol dm^{-3} [Rh^{III}(FcCOCHCOCF$_3$)(CH$_3$)(I)(CO)(PPh$_3$)], (middle at scan rates of 50, 100, 150, 200 and 250 (largest i_{pa}) mV s^{-1}) computed in 0.1 mol dm^{-3} [N(^{n}Bu$_4$)][PF$_6$]/CH$_3$CN at a glassy carbon working electrode at 25.0(1) °C. The CV of [Rh^{III}(FcCOCHCOCF$_3$)(CH$_3$)(I)(CO)(PPh$_3$)] display an electrochemically reversible Fc/Fc$^+$ couple which equates to the formal reduction potential of the ferrocenyl group of the (FcCOCHCOCF$_3$)$^-$ ligand coordinated to [Rh^{III}(FcCOCHCOCF$_3$)(CH$_3$)(I)(CO)(PPh$_3$)] and an electrochemically irreversible one-electron transfer process corresponding to the reduction of the rhodium(III) centre. The linear sweep voltammogram (LSV) of [Rh^{III}(FcCOCHCOCF$_3$)(CH$_3$)(I)(CO)(PPh$_3$)] (bottom) at a scan rate of 2 mV s^{-1} indicates a one-electron transfer process for both the oxidation of the ferrocenyl group and the reduction of rhodium of complex [Rh^{III}(FcCOCHCOCF$_3$)(CH$_3$)(I)(CO)(PPh$_3$)]. "Reprinted from *European Journal of Inorganic Chemistry*, Jeanet Conradie, Jannie C. Swarts, The Relationship between the Electrochemical and Chemical Oxidation of Ferrocene-Containing Carbonyl-Phosphane-β-Diketonato-Rhodium(I) Complexes – Cytotoxicity of [Rh(FcCOCHCOPh)(CO)(PPh$_3$)], 2439–2449, DOI: 10.1002/ejic.201100007, Copyright (2011) WILEY-VCH Verlag GmbH & Co. KGaA, Weinheim."

(iii) *[Rh(β-diketonato)(P(OPh)$_3$)$_2$]*

A set of ten [Rh(RCOCHCOR')(P(OPh)$_3$)$_2$] complexes with R, R' = CF_3, CF_3 (**1**), CF_3, CH_3 (**2**), CF_3, Ph (C_6H_5) (**3**), CF_3, Fc (ferrocenyl = $(C_5H_5)Fe(C_5H_4)$) (**4**), CH_3, Ph (**5**), CH_3, CH_3 (**6**), Ph, Ph (**7**), Fc, CH_3 (**8**), Fc, Ph (**9**) and Fc, Fc (**10**) with electrochemical conduct was investigated in acetonitrile carrying 0.100 mol dm^{-3} of a supporting electrolyte tetra-*n*-butylammonium hexafluorophosphate , employing a glassy carbon working electrode.[61] Oxidation of Rh(I) is initially observed in an electrochemical irreversible two-electron transfer activity giving compatible outcomes at peak anodic potentials ranging from E_{pa}(Rh) = 0.124 - 0.881 V *vs* Fc/Fc$^+$. For complexes with ferrocene as one of the substituents (**4**), (**8**), (**9**) and (**10**), oxidation on rhodium was pursued where a single electron transfer activity on the ferrocenyl group at a moderately larger positive potential was observed to be reversibly oxidized electrochemically (see **Figure 2.20**).[61]

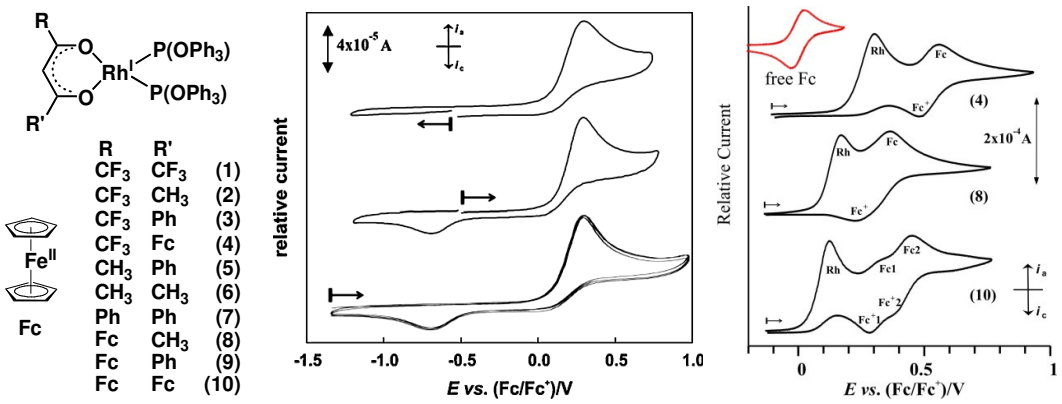

Figure 2.20. Left: Composition and identification of [Rh(RCOCHCOR')(P(OPh)$_3$)$_2$] complexes.

Middle: Cyclic voltammetric reaction of [Rh(PhCOCHCOPh)(P(OPh)$_3$)$_2$], in 0.1 mol dm^{-3} [N(^{n}Bu$_4$)][PF$_6$]/CH$_3$CN on a glassy carbon working electrode at υ = 0.100 V s^{-1}, T = 25.0(1) °C. Scans are resumed in the direction, as shown by the arrow.

Middle Bottom: Constant cyclic voltammetric sweeps noted for [Rh(PhCOCHCOPh)(P(OPh)$_3$)$_2$]. Right: Cyclic voltammograms of [Rh(FcCOCHCOR)(P(OPh)$_3$)$_2$], R = CF_3 (4), CH_3 (8) and Fc (10) at 0.100 V s^{-1}. Calculations performed in 0.1 M [N(^{n}Bu$_4$)][PF$_6$]/CH$_3$CN on a glassy carbon working electrode at 25.0(1) °C. Scans are started in the positive direction, as shown by the arrow. [Rh(β-diketonato)(P(OPh)$_3$)$_2$] = 0.003 mol dm^{-3}. "Reprinted from *Electrochimica Acta*, 56, Johannes J.C. Erasmus, Jeanet Conradie, Electrochemical study of β-diketonatobis(triphenylphosphite)rhodium(I) complexes, 9287– 9294, Copyright (2011), with permission from Elsevier."

The CV in different solvent systems revealed that an increase in solvent donicity cause more strain to reduce Rh(III) to Rh(I).[61,62] A coupled reduction peak is highly affected by the added acetonitrile, causing it to shift to more negative potentials as the solvated species formation increases. The essence of the addition of a solvent has no influence the potential of the oxidation peak, which affirms that addition of a solvent has no influence on the essence of the initial Rh(I) species (see

Figure 2.21). Working from dichloromethane to pyridine, the maintaining of continuously more of complexes with an octahedral geometry solvent-coordinated is stipulated by a stable rise in the peak reduction currents. E_{pc} shifts significantly to more negative potentials as the donicity of the added solvent increases, thus confirming an increase in the establishment of the Rh(III) intermediate possible by co-ordination of two solvent molecules chemically to it. In contrast to dichloromethane, pyridine as a vigorous coordinating solvent, does not only preserve the electro-generated species but as well generates a secure bond with the Rh(III) core; hence an increase of negative values for E_{pc} were observed.[61] An electrochemical scheme that outlines these outcomes have been suggested (**Scheme 2. 14**).

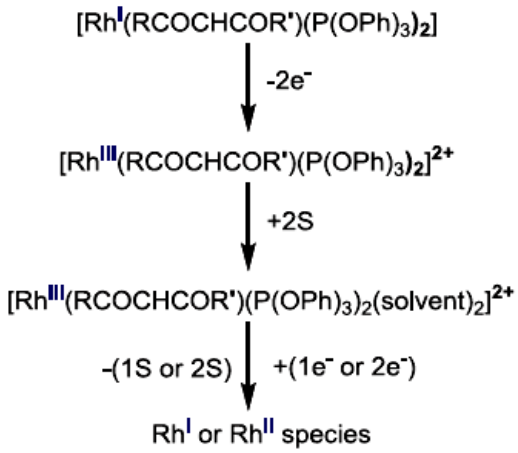

Scheme 2. 14. A recommended mechanism for the electrochemical oxidation of Rh(I) in [Rh(RCOCHCOR′)(P(OPh)$_3$)$_2$] to Rh(III). S = solvent molecule. "Reprinted from *Electrochimica Acta*, 56, Johannes J.C. Erasmus, Jeanet Conradie, Electrochemical study of β-diketonatobis(triphenylphosphite)rhodium(I) complexes, 9287– 9294, Copyright (2011), with permission from Elsevier."

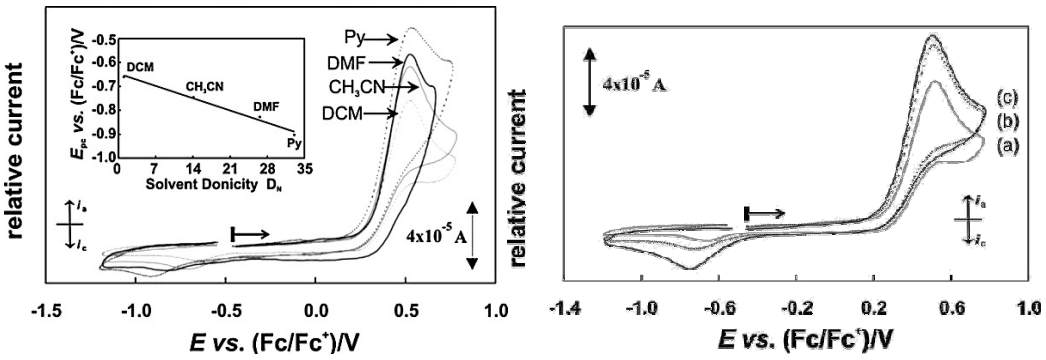

Figure 2.21. Left: Influence solvent addition (Rh:Solvent = 1:20) on the cyclic voltammetric reaction of [Rh(PhCOCHCOPh)(P(OPh)$_3$)$_2$], in 0.1 mol dm^{-3} [N(^{n}Bu$_4$)][PF$_6$]/CH$_2$Cl$_2$ on a glassy carbon working electrode at υ = 0.100 V s^{-1}, T = 25.0(1) °C. Solvent = dichloromethane (DCM), acetonitrile (CH$_3$CN), dimethylformamide (DMF) and pyridine (Py). Scans are resumed in the positive direction, as shown by the arrow.

Inset: linear relationship between E$_{pc}$(Rh) of [Rh(PhCOCHCOPh)(P(OPh)$_3$)$_2$] and the donicity of the added solvents.

Right: Influence of CH$_3$CN addition on the cyclic voltammetric reaction of [Rh(PhCOCHCOPh)(P(OPh)$_3$)$_2$], (7), in 0.1 mol dm^{-3}[N(^{n}Bu$_4$)][PF$_6$]/CH$_2$Cl$_2$ on a glassy carbon working electrode at ν = 0.100 V s^{-1}, T = 25.0(1) °C. (a) Rh: CH$_3$CN = 1: 0, (b) Rh: CH$_3$CN = 1: 2, (c) Rh: CH$_3$CN = 1: 20. Scans are resumed in the positive direction, as shown by the arrow. "Reprinted from *Electrochimica Acta*, 56, Johannes J.C. Erasmus, Jeanet Conradie, Electrochemical study of β-diketonatobis(triphenylphosphite)rhodium(I) complexes, 9287– 9294, Copyright (2011), with permission from Elsevier."

2.3 Mesomorphic properties

Differential scanning calorimetry and optical microscopy have been widely utilised in the study of mesogenic behaviour of compounds. Rigidity, rod shape and polarity are properties expected as the molecular structure criteria for liquid crystallinity.[69,70] Phenols and primary amines of *p*-phenylene dibenzoates have been reported as the first the examples of liquid crystals in their group.[71] Nonetheless, they are rare because the intermolecular hydrogen bonding elevates melting point higher than the mesomorphic-isotropic liquid transition temperature – which might motivate a nonlinear molecular pattern that discourages mesomorphic formation.[70]

2.3.1 Liquid crystals (LCs)

There are mainly three different physical states of matter: solid, liquid and gas. These phases vary largely according to how ordered and what kind of order the phase is. The design found in systems is not adequately identified by the three states of matter. Upon heating, it is commonly observed that texture move from a solid (usually crystalline, possessing high order) to an isotropic liquid (highly disordered). An increase in thermal energy increases the motion of the molecule until the motion are sufficient to break the forces of attraction which hold the crystalline solid together and the material melts into a liquid phase (see **Figure 2. 22**).[72]

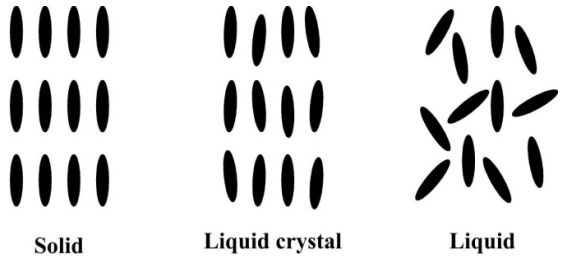

Figure 2. 22. Schematic representation of the liquid crystal intermediate between the traditional crystalline solid phases (with long-range order) and liquid phases (with no directional or long-range order).

Mesophase is a name given to liquid crystal which is a transition between the three-dimensionally ordered crystal phase and the disordered liquid phase; mesogens being a name given to its component molecules.[73] Phase transitions are a result of heating a liquid crystalline material, depending on the material's intrinsic properties where the arrangement of the molecules plays a role, i.e. the conformation of the molecules, and intermolecular interactions.[74] In the liquid phase, the constituent molecules are free to rotate, vibrate and flow; they no longer possess any positional or orientation order and thus are described as isotropic. Intermediate states without order are found in solids of some substances, but possess greater order as compared to liquids. These ordered fluids are called liquid crystals (LC) and they thus exhibit characteristics of both liquids and solids: they are fluid, but their molecules are arranged in a highly ordered way. Different optical properties can be used to differentiate a large variety of LC phases. Well defined textures for a variety of liquid crystal phases can be observed under a microscope that utilises a polarized source.[74] Andrienko[75]

suggests that there are certain structural traits observed in molecules of liquid crystals and summarises them as follows:

1. The molecules have anisotropic shape (e. g. are elongated). Liquid crystallinity is mostly possible when the molecules possess flat segments, e. g. in benzene rings.
2. Reasonably a good rigid backbone having double bonds explains the long axis of the molecule.
3. The presence of strong dipoles and simple polarisable groups in the molecule appear to be vital.
4. The groups joined to the ultimate end of the molecules are normally with no bigger influence.

Four main kinds of liquid crystals (see **Figure 2.25**) which are composed of rod-like or disk-like molecules, but differ in the kind of order that exists, are:

Nematic liquid crystals

Nematic liquid crystals are the least ordered and simplest of all mesophases. The rod-like molecules are arranged like loosely packed straws. They are distinguished by molecules that do not have positional order instead are likely to point in the same direction (along the director).[75]

Smectic liquid crystals

In smectic state, the molecules are likely to align themselves in layers but maintaining the normal orientation of nematics. The order is thus greater than the nematic liquid crystal (see **Figure 2. 23**)[76]. The parallel rod-like molecules are arranged in layers.[75] A breakdown of the ordered crystalline solid at definite temperatures results into transitions between crystalline-nematic-smectic phases; also the positional order of molecules is lost giving a smectic liquid crystal mesophase exhibiting an orientational order.[74] Generally when melting, there is a possibility of one or more smectic phases being observed. Smectic A, smectic B, and smectic C commonly differ with molecular packing order, see **Figure 2. 24**.[74]

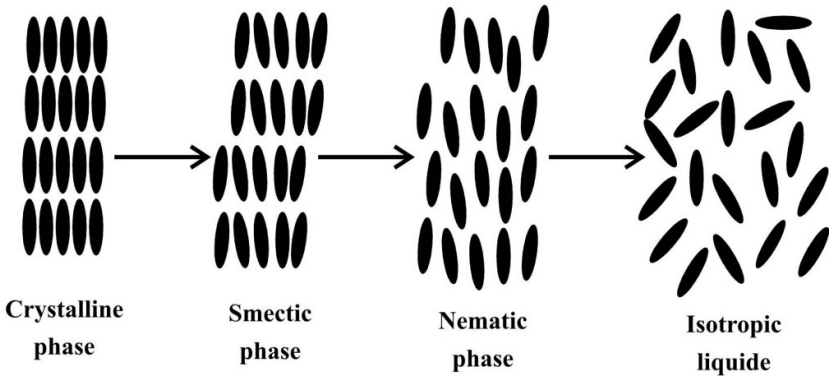

Figure 2. 23. Schematic representation of phase transition between crystaline, smectic, nematic and isotropic liquid as function of temperature.

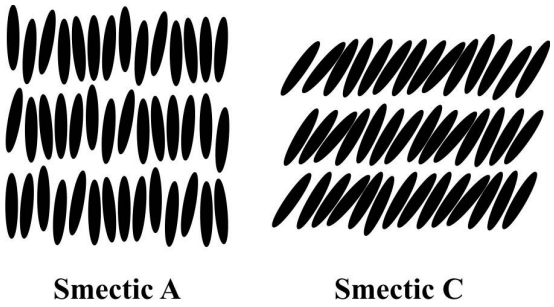

Figure 2. 24. Schematic representation of the alignment in the smectic phases. The smectic A phase (left) has molecules organized into layers along the layer normal. In the smectic C phase (right), the molecules are tilted inside the layers away from the along the layer normal. The smectic-B mesophase (not shown) are similar to A, but the molecules are arranged into a network of hexagons within the layer.

Cholesteric liquid crystals

The molecules are in layers, like the nematic crystals, but with a helical twist to the direction of orientation slightly different from one another.[75] This phase is also called twisted or chiral nematic.

Apart from the rod-like molecules, more advanced-shaped liquid crystals are possible such as disk-like or banana-shaped (bent-core molecules) liquid crystals which can give rise to other types of ordering, e.g. a columnar phase and various stacking possibilities for banana shaped liquid crystals, see Figure 2.25 and Figure 2.26. The banana phases are classified as B1–B8 on the basis of textural features and preliminary X-ray results, as they were discovered.[77]

Columnar liquid crystals

Columnar liquid crystals are disk shaped in comparison to the long rods previously discussed. This mesophase is distinguished by stacked columns of molecules. These stacked columns are arranged such that they form a two-dimensional crystalline pattern. The ordering of the molecules inside the columns and the one of columns themselves generate different mesophases.[75]

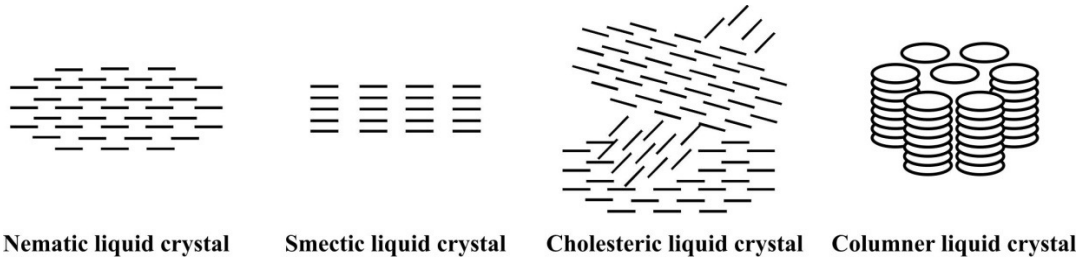

Figure 2.25. Schematic representation of four main classes of liquid crystals.

Figure 2.26. Schematic representation of stacking possibility for banana shaped liquid crystals.

2.3.2 Differential scanning calorimetry (DSC)

A difference in the amount of heat needed to rise the temperature of a sample and a reference is calculated as a function of temperature by a thermo-analytical technique called differential scanning calorimetry (DSC). Therefore, heat flow to and from a sample is measured relative to a reference. The same temperature in the sample and in the reference is closely maintained throughout the experiment. The temperature of the sample holder generally increases linearly as a function of time. A schematic illustration of a DSC instrument is shown in **Figure 2.27**.

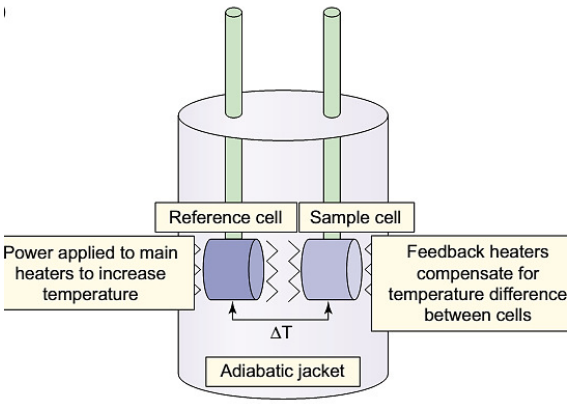

Figure 2.27. Schematic illustration of a typical DSC instrument.[78] "Reprinted from *Drug Discovery Today*, 10, Holgate, G. A.; Ward, W. H. J., Measurements of binding thermodynamics in drug discovery, 1543, Copyright (2005), with permission from Elsevier."

The energy involved in phase transitions (melting, glass transition, decomposition) are the important applications that can be measured by the DSC. With great sensitivity, DSC detects energy changes or heat capacities which are involved during transitions.[79]

Oxidation as well as other chemical reactions can be studied by DSC.[80] As the temperature of the amorphous solid increases and the mechanical properties change from being brittle to being elastomeric, glass transitions (Tg) may occur and these transitions come out like a stair in the baseline of the displayed DSC signal.[80,81] On molecular level, Tg is the temperature at which the molecules of the amorphous regions of the material gain enough thermal energy to begin sliding past one another at a noticeable rate.[82] The cold crystallization temperature (*T*c) is the temperature obtained as the increases in temperature further from the *T*g, molecules in the amorphous material get sufficient independence of motion to naturally organise themselves into a crystalline form. A rise in temperature causes the sample to ultimately attain its melting temperature (T_m). Melting produces an endothermic peak in the DSC curve. DSC is a vital mechanism with a potential to deduce transition temperatures and enthalpies by providing phase diagrams for diverse chemical systems.[80] Since all structural changes (transition) either absorbs or releases heat then DSC is the comprehensive detector for calculating these structural changes. The output of a DSC measurement is called a thermogram, which is a plot of the difference of heat delivered to the sample and to the reference as a function of the sample temperature (**Figure 2.28**). Rise in temperature at uniform rate is a result of power being supplied to the main heaters. DSC therefore calculates

the temperature difference between the sample and reference cells which is compensated by the feedback heaters.[78]

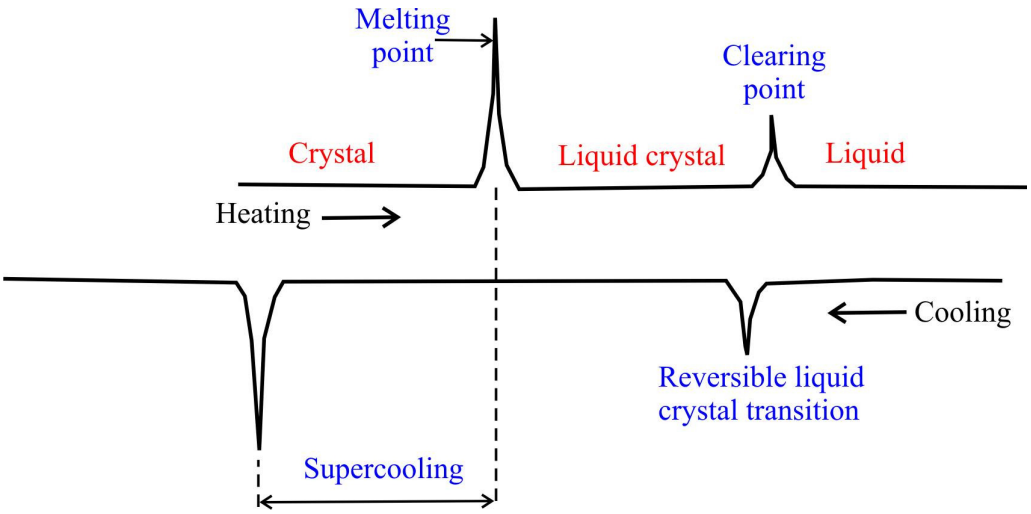

Figure 2.28. Schematic representation of a typical DSC taken of a complex with liquid crystalline properties.

Material characterisation has been widely done utilising DSC in diverse research areas including chemistry, physics, material science, pharmaceutics, food science, attributed to many of notable benefits, such as simplicity of sample preparation, easy to use on solid and liquid samples, quick analysis time, and a wide temperature range.[83]

2.3.3 Optical variable temperature polarised light microscopy

Existence of liquid crystal phases in solution is observed utilising conventional polarized optical microscopy. This technique is of importance because thermal analysis by DSC only does not completely show what sort of phase change formed. Polarized optical microscopy provides a determination of both the temperatures of the phase transition and the type of phase. This is possible by temperature-dependant texture investigations between crossed polarizers.[84] This corresponds to the polarization of light basically schematically represented in **Figure 2. 29**. A filter allowing only light aligned in a particular course with its polarizing direction to pass through is called a polarizer.[85]

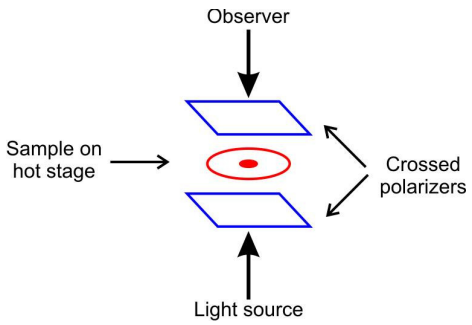

Figure 2. 29. Schematic representation of Polarised Optical Microscope (POM).

A practical use for POM is specifically thoroughly checking the structure of an anisotropic and birefringent material. Anisotropic material is a material possessing optical properties differing with the direction of incident light with the crystallographic axes, and that exhibit a variety of refractive indices, which depends on the propagation direction of light through the substance and on the vibrational plane coordinates. Two light rays are observed due to the ability of anisotropic materials acting as beam splitters. Utilisation of polarizing microscopy achieves the interference of the split light rays, because of their unity beside the same optical path to produce facts on these materials.[86] If light passes through a birefringent material, a nematic liquid crystal for example the light breaks up into a fast ordinary ray (o-ray) and a slow extraordinary ray (e-ray). Since these rays travel at different speed their waves get out of phase leading to a change in polarization state when the rays combine when leaving the birefringent material.[75] This means therefore that the mesophase has two different refractive indices, one parallel and one perpendicular to the liquid crystal's director.

A typical pattern under the microscope is given when a sample in its liquid crystalline state is struck by a polarized beam of light and two refracted rays form which interact with each other. Each mesophase will give a different pattern called a texture.[87]

Normally in a liquid crystal, the length of a sample and its birefringence are not always similar throughout the sample some regions in the sample will appear light while other appear dark where the dark areas are referred to as brushes. An example is a nematic liquid crystal put between crossed polarizers of a microscope exhibiting a schlieren texture with dark brushes(see **Figure 2. 30a**).[88] A number of selected liquid crystal textures and patterns are exhibited in Figure 2. 30 below:

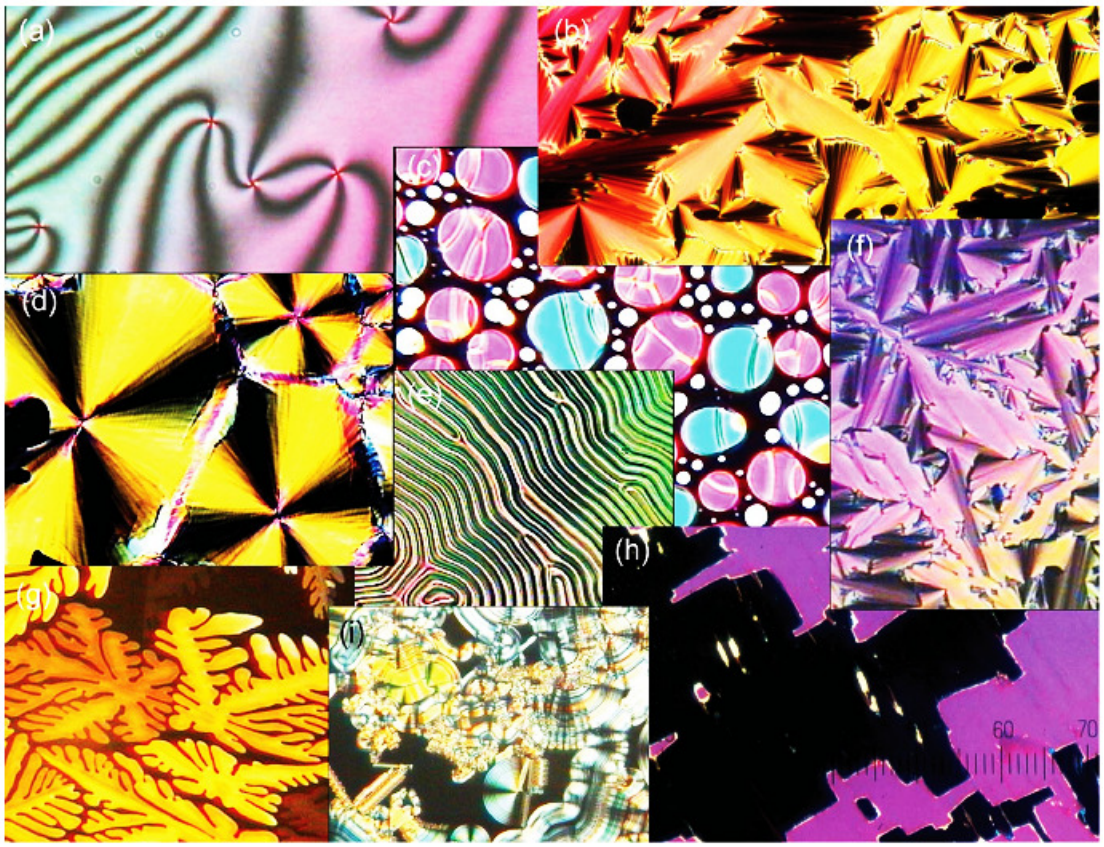

Figure 2. 30. (a) The schlieren texture of the nematic phase, (b) a smectic A fan-shaped texture, (c) the cholesteric phase separating from the isotropic liquid, (d) liquid crystal spherulites, (e) cholesteric fingerprints, (f) fan-shaped texture of a 'banana' B6 phase, (g) dendritic patterns of the 'banana' B1 phase, which at later times coarsen into a mosaic texture, (h) ferroelectric domains in the bookshelf geometry of a smectic C phase and (i) the intriguing structures of the 'banana' B7 phase observed when cooled from the isotropic melt. "Reprinted from *Liquid Crystals, Fractals and Art*, Dierking I. Liquid Crystals Today Vol.21:3, pp.64, Copyright (2012) with permission from Taylor and Francis."

Disclinations are locations where two or four brushes converge in correspondence with the director singularities in the structure. These disclinations are defined by their strength k, exhibiting the extent to which the director rotates in each point on the closed curve around the singularity point. The disclinations with $k = \pm½, \pm1$ exist in nematics. Locations where four brushes converge is in correspondence with disclinations of $k = \pm1$, and, locations where two brushes converge is in correspondence with disclinations of $k = \pm½$. These point defects and surface singular points are named boojums.[89] **Figure 2. 31** show boojums and disclinations observed in a schlieren texture.

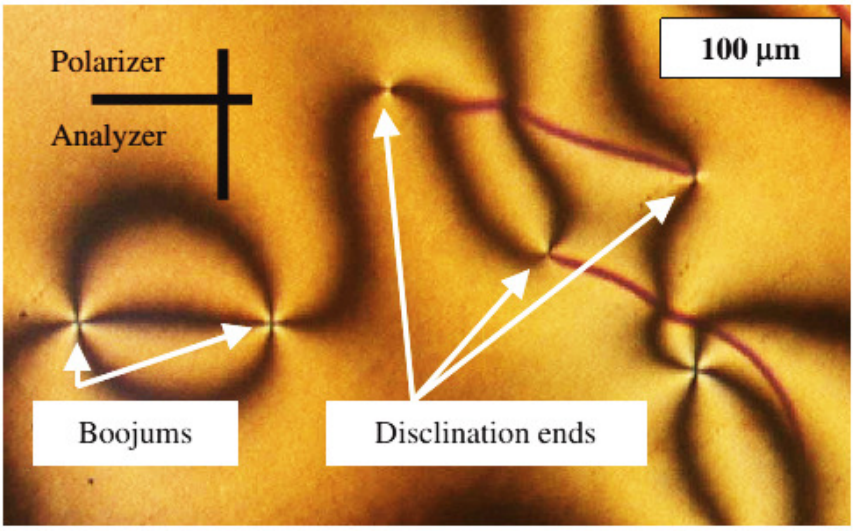

Figure 2. 31. Schlieren texture observed between crossed polars with two black brushes associated with the $k = \pm 1/2$ lines and four brushes associated with the $k = \pm 1$ lines. "Reprinted from *Philosophical Magazine*, 86, M. Kleman.; O. D. Lavrentovich, Topological point defects in nematic liquid crystals, 4117 - 4137, Copyright (2006), with permission from Taylor and Francis."

Nematic or cholesteric and smectic phases are shown by a number of many materials. Larger extent of crystalline order normally shows at lower temperature phases. That means that the nematic phase mostly appears at higher temperature in comparison to smectic phase and the smectic phases appear in the order of A → C → B as the temperature decreases. A number of compounds experience transition from a crystalline to a nematic phase with no proof of any smectic properties.[74]

2.3.4 Examples of β-diketonato complexes showing mesogenic behaviour

2.3.4.1 Mesogenic behaviour of β-diketones and other ester moieties

Different organic systems have been incorporated into liquid crystals in both low and high molecular materials.[90] Calmitic liquid crystal phases are secured by generally the presence of at least two ring structures in relation to the structure-phase affinities in liquid crystals, but work done by Belfield *et al.*[74] show that even a single benzene ring in a structure qualifies a liquid crystalline material. Among other things, the thermal behaviour and a mesomorphic

study of 4-(4-pentenyloxy)benzoic acid were undertaken. The results of the thermal behaviour are shown in the thermogram and table below (see **Figure 2.32b**).[74]

Heating		
Phase Transition	**Temperature °C**	**Δ H kJmol^{-1}**
Cr-SmX1	99	1.14
SmX1-SmX2	117	1.43
SmX2-N	126	14.2
N-I	154	2.9
Cooling		
Phase Transition	**Temperature °C**	**Δ H kJmol^{-1}**
I-N	150	-2.80
N-SmX1	117	-15.0
SmX1-SmX2	103	Very small
SmX2-Cr	89.0	-0.40

I: isotropic, N:nematic, SmX1: smectic X1, SmX2: smectic X2, Cr: crystalline.

(a)

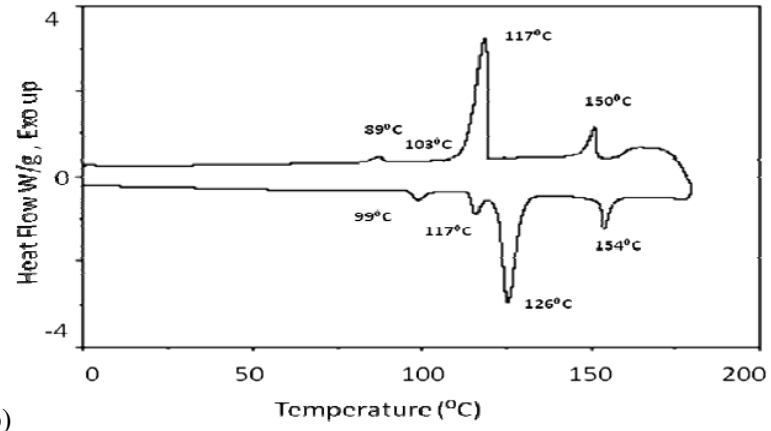

(b)

Figure 2.32. (a) Phase transition temperatures and enthalpy changes and (b) DSC thermograms for 4-(4-pentenyloxy) benzoic acid. Open access journal: Qaddoura, M.A.; Belfield, K.D. Probing the Texture of the Calamitic Liquid Crystalline Dimer of 4-(4-Pentenyloxy)benzoic Acid. *Materials* 2010, *3*, 827-840.

A minor disturbance on the packing order of the liquid crystal is indicated by only 1.14 kJmol^{-1} released at 99 °C, because of translational and rotational activity around the long access of the molecule. A small amount of only 1.4 kJ mol^{-1} was again given off at 117 °C. This indicated a smectic-smectic transition; in addition, a significantly larger amount of 14.2 kJ mol^{-1} was released, adhering to considerable disturbances in the molecular packing order.[74] At 154 °C, any kind of order is lost by molecules and become an isotropic liquid (see **Figure 2.32** and **Figure 2.34**). Phase transitions are observed in 4-(4-pentenyloxy)benzoic acid while having only one benzene ring because it dimerizes *via* hydrogen bonds (**Figure 2.33**).

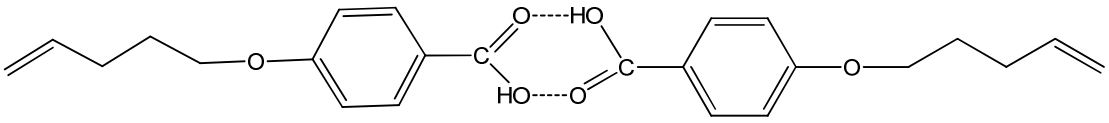

Figure 2.33. The proposed dimeric structure of 4-(4-pentenyloxy) benzoic acid.

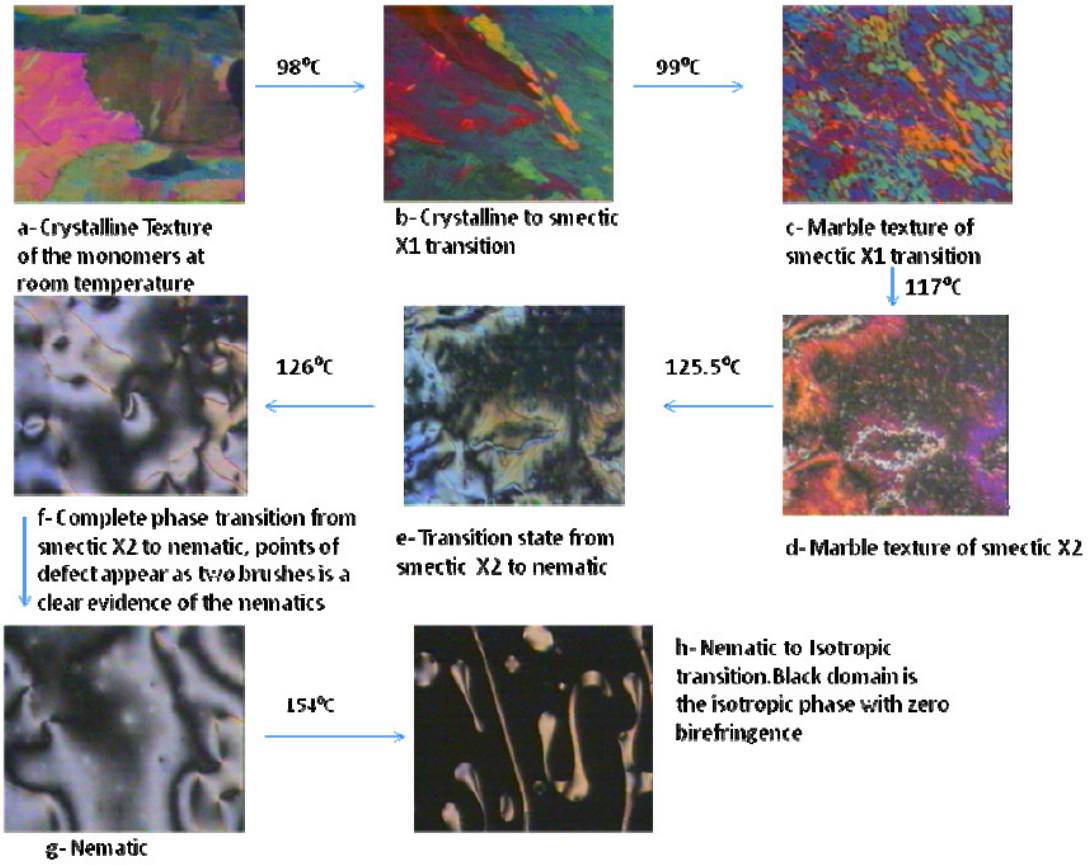

Figure 2.34. Liquid crystalline transitions for the compound 4-(4-pentenyloxy)benzoic acid as observed under light polarized microscopy, crossed polarizer, magnification ×150. Open access journal: Qaddoura, M.A.; Belfield, K.D. Probing the Texture of the Calamitic Liquid Crystalline Dimer of 4-(4-Pentenyloxy)benzoic Acid. *Materials* 2010, *3*, 827-840.

The β-diketone group absorb a substantial dipole moment that increases the anisotropy of the molecular polarizability and consequently favours mesogenic behaviour.[91] Cativiela *et al.*[13] have studied mesogenic characterization on a series of β-diketones (see **Scheme 2. 3 complexes 3 - 8**) and find that β-diketones **7b** and **8b** both exhibit two monotropic phases (thermodynamically unstable mesophases, and is observed in the cooling process only). They are nematic and smectic A respectively. When cooling of the isotropic liquid is done, a

Schlieren texture permits a nematic phase to be identified. After further cooling, focal-conic texture become visible in the smectic A phase and this final texture is simply changed into a homeotropic texture by utilizing mechanical stress.[13]

It is only in the presence of a group that joins the mesogenic core to the β-diketone that liquid crystal phases will appear permitting an extension of conjugation in the two groups. Among those β-diketones which could show mesogenic properties, were only by-product where the primary unit is connected to the β-diketone unit *via* a carboxyl group.[13] Electronic conjugation is disturbed by the linking groups CH_2 and CH_2CH_2 and, yet the phenyl group is directly attached to the β-diketone, conjugation is inhibited because of steric influences as shown in **Figure 2.35**. β-diketones in the series (linking group CH_2, CH_2CH_2 or phenyl) could not give any mesogenic phases.[13]

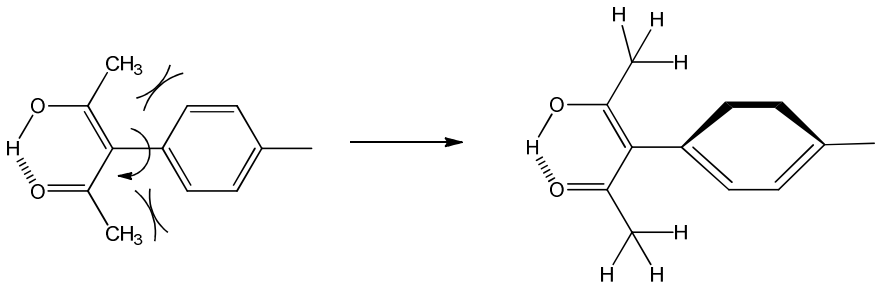

Figure 2.35. Steric hindrance shown when a phenyl group is directly attached to the β-diketone.

The phenyl 4-(*n*-decy1oxy) benzoate group induces mesogenic properties in the series. Mesophase formation is possible if there is a side-by-side arrangement of molecules while a voluminous terminal unit of the β-diketone greatly hinders this possibility.[13] However, when the group connecting the two is an ester, the aromatic conjugation can be extended to the β-diketone. Molecular planarity is therefore favoured while increasing the anisotropy of the electronic polarizability, liquid crystal behaviour is advanced as a result by a consequent expansion of molecular communication (van der Waal's forces).[13]

On the other hand, Wan's *et al.*[14] mesogenic characterisation on a β-diketone **8b** (**Scheme 2. 3**) finds no mesomorphic properties displayed. However, Barbera *et al*[19], who did similar work (**Figure 2.36**), disagree with Wan *et al's*[14] results.

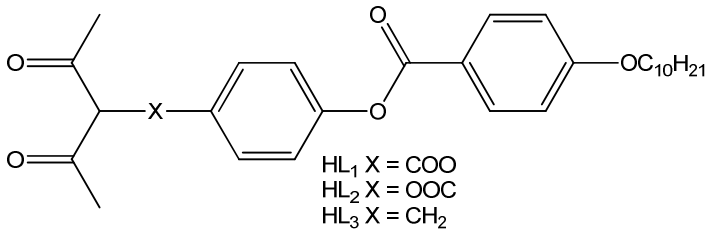

Figure 2.36. A series of β-diketones characterised by Barbera *et al.*[19]

The charge transfer is observed to be from the *n*-decyloxy group to the β-diketone *via* X = OOC, since the oxygen atom in the molecular axis acts as a π-donor and transferring charge to the main acceptor (**Figure 2.37**).[19]

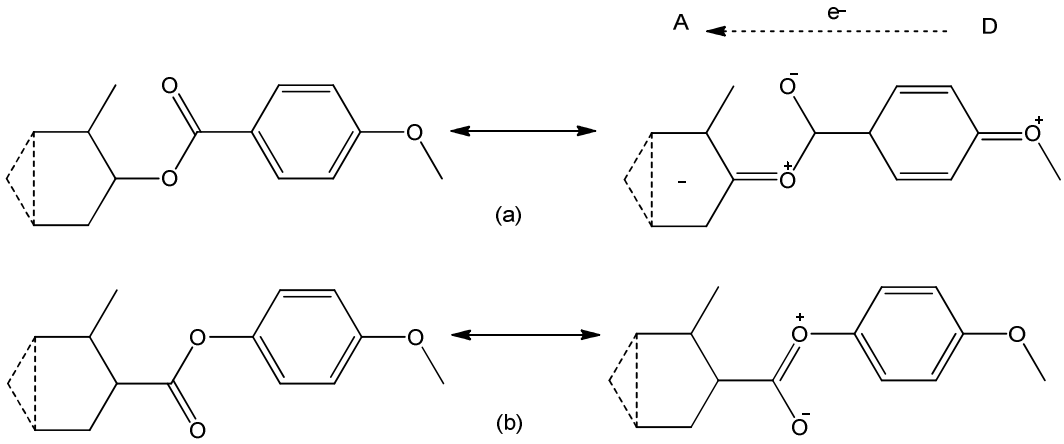

Figure 2.37. Charge transfer for molecules with (a) X=OOC and for molecules with (b) X =COO. A is the acceptor group, and D is the donor group.[19]

The charge transfer is to a degree hindered when X= COO where the π-acceptor C atom of the ester group is connected directly to the main acceptor group (**Figure 2.37b**). Yet when X= CH_2, there is limited – if any – charge transfer since the CH_2 group disrupts molecular conjugation.[19]

Recent work was done by Han *et al.*[18] on another series of β-diketones as shown by the **Figure 2.38**.

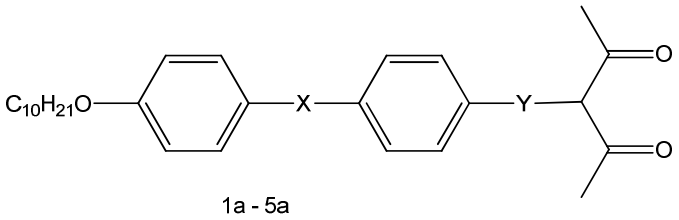

Figure 2.38. A series of β-diketones by Han *et al*[18] in which series 1a: X=-CH=CHCOO- and Y=COO-; series 2a: X=-CH=CHCOO- and Y= CH=CHCOO- ; series 3a: X=-COO- and Y=-CH=CHCOO- ; series 4a: X=-CH_2O- and Y=-COO- , series 5a: X=- N=N-and Y=-COO-.

A single monotropic phase (N) at a small temperature range of about 20^o C was observed for β-diketones **1a** and **3a** (**Figure 2.38**), monotropic phases N and Sc were displayed by **2a** at a temperature range of about 40^o C, and two enantiotropic phases (N and Sc) were observed for **5a** at a temperature range of 78.5–184.5 ^{o}C, a vast range in compounds **1a**, **2a**, **3a** and **5a** (**Figure 2.38**), while **4a** does not display mesomorphism because CH_2O in **4a** as a linking group disturbs electronic conjugation and unable to produce sufficient mesogenic core, as a fundamental element for mesomorphic phases to emerge.[18] Dissimilar liquid crystal behaviours of the β-diketones **1a**, **2a**, **3a** and **5a** (**Figure 2.38**) are due to the conjugation of the linking groups which increase according to the order: -CO_2-<-CH=$CHCO_2$-<-N=N-. Molecular rigidity and planarity, the intermolecular communication – and as a result an organized ordering of molecules – may be increased by the conjugation of the linking groups. The azo group in **5a** has an excellent mesomorphism in contrast to **1a**, **2a** and **3a** (**Figure 2.38**). Compared to the ester group in **1a** and **3a,** bridging groups X and Y in compound **2a** are two acrylic ester groups, and are more adequate for a conjugation structure production. That is why compound **2a** does not only have a broader mesogenic temperature ranges but additional mesogenic phases than **1a** and **3a** (**Figure 2.38**).[18]

2.3.4.2 Mesogenic behaviour of Rh β-diketonato complexes

Metallomesogen is a term that refers to metal complexes with liquid crystalline ligands. Among many potentialities given by metallomesoges they are utilised in colourful display devices, anisotropic polymerization catalysts, and advanced materials the exhibit peculiar physiochemical properties, for example mixed-valence states.[92] An advanced field of research has been made possible by the synthesis of metal-containing mesogenic compounds with much prospective possibility.[93] Liquid crystals exhibit improved properties such as colour,

paramagnetism, electric conductivity, etc., by incorporating a metal atom in an organic molecule.[94] Polarizability or hyper-polarizability is intensified by the presence of metals.[93(a),95]

1,3-Disubstituted propane-1,3-diones have been proven to be typical standards of precursors for the production of mesogenic heterocycles or metallomesogenic derivatives.[13] β-diketones were broadly utilised as organic ligands in mesogenic coordination complexes of few transition metals like Cu(II), Tl(I), Cr(III), V(IV), and Pd(1I).[96,94(a),97,98,99] Transition metal complexes have d-electron configuration, are responsive to ligand field environment, spin structures and their properties also critically rely on geometrical structures.[92] Some instances of mesogenic 3-substituted pentane-2,4-diones have been reported.[100] A strong dipole moment is incorporated by a β-diketone in heterocyclic derivatives or, in most instances, in the metal complex derivatives which raises the anisotropy of the molecular polarizability and consequently favour mesogenic behaviour.[91] G. Piao *et al.*[92] complexed liquid crystalline β-diketones to Ni, thus giving complexes which did not exhibit any mesophase but non-planar structures with high-spin states; such properties are improper for initiation of liquid crystal mesophase. The implication is that the geometrical structures of these Ni complexes are improper for the initiation of liquid crystal phase although coordinated to liquid crystalline ligands. On the other hand, the chelating ability of the β-diketone on the metal (except Ni) could result in converting the non-mesomorphic β-diketone ligand into the mesomorphic metal chelates.[97]

Mostly the metal atom is at the centre of the liquid crystalline complex,[93] but this disadvantage causes a further enhancement of an electro-optic property of the complex. However, rod-like γ-substituted β-diketones are reported with a terminal metal atom (dicarbonylrhodium(I) β-diketonate complexes), where Rh is the metal atom. The d-π and π-π^* interaction between the metal and carbon monoxides (CO), where the CO ligand accepts π-back donation from Rh(I), is expected to give these complexes a good conjugation due to the formation of a six-membered metallocycle structure and a great dipole moment – properties which enhance mesomorphism. A terminal polar group is provided by $[M(CO)_2]$ or $[RhCl(CO)_2]$ while, on the other hand, the decyloxy group, attached at the γ position of the β-diketonates plays the role of an electron-donor group. This also enhances mesomorphism. A series of dicarbonylrhodium(I) β-diketonate complexes characterised earlier (**Figure 2.39**).[19]

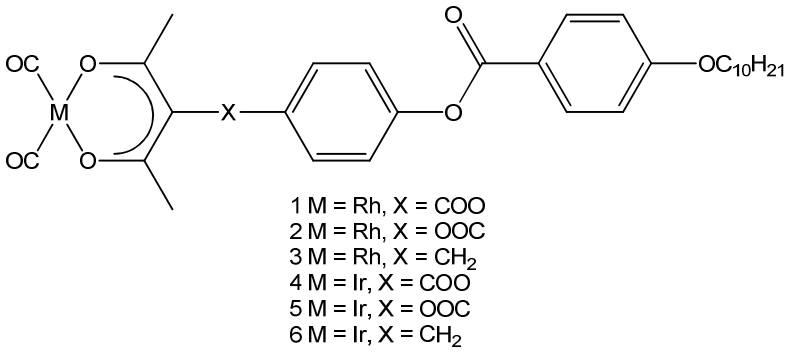

Figure 2.39. A series of dicarbonylrhodium(I) β-diketonate complexes characterised by Barbera *et al.*[19]

POM showed fan-shaped textures with homeotropic regions for complexes 1 and 4 (where M = Rh, X= COO and M = Ir, X = COO respectively) which have a monotropic smectic A phase.[19] On DSC, a mesophase emerges at 93.8 ^{o}C and stays over 20 ^{o}C when the isotropic liquid of compound 1 is cooled at 10 ^{o}C min^{-1}, , while for compound 4, mesophase appearance and crystallisation are simultaneous: this is shown by a partial overlap of peaks on a DSC thermogram. Owing to this overlap, the isotropic liquid-mesophase transition enthalpies were not calculated. No liquid crystal properties were observed for all other complexes (2, 3, 5, and 6) and the melting point was in the range of 111 to 145 ^{o}C for complexes. Because of the higher melting points of the complexes, the mesophases were observed on the ligands where X = COO or OOC disappeared when [M(CO)$_2$] was introduced. Introduction of [M(CO)$_2$] elongates the molecule without any significant change in the molecular width and this benefits the mesomorphic state. However, the high melting point of the complexes stabilises the crystalline phase to the disadvantage of the mesomorphic phases. Earlier work by Wan *et al.*[14] shows no mesophase observed for the ligand X = OOC except after the introduction of [M(CO)$_2$] where M = Rh. However, this is contrary to the findings of Barbera *et al.*[19] It is possible to have non-mesogenic ligands of β-diketones forming liquid crystalline phases by direct coordination to a metal.[97] Liquid crystalline β-diketones were observed only when the number of carbon atoms in the alkoxy-group is 12 and beyond, and when all the complexes have higher transition temperatures than the corresponding ligands.[14]

References

[1] Mehrotra, R. C., Bohra, R., Gaur, D. P. *Metal β-diketonates and allied derivatives*, **1978**, Academic Press, London.

[2] Bertolasi, V., Gilli, P., Ferretti, V., Gilli, G. *J. Am. Chem. Soc.* **1991**, 113, 4917.

[3] Iglesias, E. *Langmuir* **2000**, 16, 8438.

[4] du Plessis, W. C., Davis, W. L., Cronje, S. J., Swarts, J. C. *Inorg. Chim. Acta* **2001**, 314, 97.

[5] Conradie M. M., Muller, A. J., Conradie J. *S. Afr. J. Chem*. **2008**, 61, 13.

[6] Iglesias, E. *J. Phys. Chem.* **1996**, 100, 12592.

[7] Lukehart, C. M. *Acc. Chem. Res*. **1981**, 14, 109.

[8] Jiang, J. Q., Shen, Z. R., Lu, J., Fu, P. F., Lin, Y., Tang, H. D., Gu, H. W., Sun, J., Xie, P., Zhang, R. B. *Adv. Mater.* **2004**, 16, 1534.

[9] Trzaska, S. T., Swager, T. M. *Chem. Mater.* **1998**, 10, 438.

[10] Trzaska, S. T., Zheng, H., Swager, T. M. *Chem. Mater.* **1999**, 11, 130.

[11] (a) Diana, G. D., Salvador, U. J., Zalay, E. S., Johnson, R. E., Collins, J. C., Johnson, D., Hinshaw, W**.** B., Lorenz, R. R., Thielking, W**.** H., Pancic, F. *J. Med. Chem.* **1977**, 20, 6, 750 (b) Diana, G. D., Salvador, U. J., Zalay, E. S., Carabateas, P. M., Willians, G. L., Collins, J. C., Pancic, F. *J. Med. Chem.* **1977**, 20, 6, 757.

[12] Hauser, C. R., Manyik, R. M. *J. Org. Chem*. **1953**, 18, 588.

[13] Cativiela, C., Serrano, J. L., Zurbano, M. M. *J. Org. Chem*. **1995**, 60*,* 3074.

[14] Wan, W., Guang, W.J., Zhao, K. Q., Zheng, W. Z., Zhang, L. F. *J. Organomet. Chem.* **1998**, 557, 157.

[15] (a) Brieger, G., Pelletier, W. M. *Tetrahedron Lett.* **1965**, 3555. (b) Chatterjee, A., Banerjee, D., Banerjee, S. *Tetrahedron Lett.* **1965**, 3851. (c) Bottom, F. H., McQuillin, F. J. *Tetrahedron Lett*. **1967**, 1975. (d) Kurz, A. L., Beletskaya, I. P., Macias, A., Reutov, O. A. *Tetrahedron Lett.* **1968**, 3675.

[16] Classon, B., Liu, Z., Samuelsson, B. *J. Org. Chem.* **1988**, 53**,** 6126.

[17] Clemens, R. J., Hyatt, J. A. *J. Org. Chem.* **1985**, 50*,* 2431.

[18] Han, J., Zhang, L. F., Wan, W. *Journal of Organometallic Chemistry* **2003**, 672, 86.

[19] Barberá, J., Elduque, A., Giménez, R., Lahoz, F. J., López, J. A., Oro, L. A., Serrano, J. L., Villacampa, B., Villalba. J. *Inorg. Chem.* **1999**, 38, 3085.

[20] Mabbott, G. A. *J. Chem. Ed*., **1983**, 60, 697.

[21] Kissinger, P. T., Heineman, W. R. *J. Chem. Ed*. **1983**, 60, 702.

[22] Kissinger, P. T., Heineman, W. R. *Laboratory techniques in elcetroanalytical Chemistry* **1984**, 297, pp. 86, Marcel Dekker, Inc., New York.

[23] Erasmus, E. *Synthesis, substitution kinetics and electrochemistry of betadiketonato titanium and titanocene complexes with biomedical applications* **2003**, M.Sc. Thesis, University of the Free State.

[24] Gericke, H. J., Barnard, N. I., Erasmus, E., Swarts, J. C., Cook, M. J., Aquino, M. A. S. *Inorg. Chim. Acta* **2010,** 363, 2222.

[25] Bard, A. J., Faulkner, L. R. *Electrochemical Methods: Fundamentals and Applications* **1980**, pp. 213, Wiley, New York.

[26] Nicholson, R. S., Shain, I. *Anal. Chem*. **1964**, 36, 706.

[27] Christensen, P. A., Hamnett, A. *Techniques and Mechanisms in Electrochemistry*, **1994**, pp. 55, 170, Blackie Acadenic & Professional, London.

[28] Molina, A., Gonza´lez, J., Laborda, E., Wang, Y., Compton, R. G. *Phys. Chem. Chem. Phys* **2011**, 13, 16748.

[29] Mirceski, V., Komorsky-Lovric, S., Lovric, M. *Monographs in Electrochemistry (Square-Wave Voltammetry)*: *Theory and Application* **2007**, Introduction, pp 1, Springer-Verlag Berlin Heidelberg.

[30] Bard, A. J., *Electroanalytical chemistry: A series of advances* **1996**, 14, 57. Marcel Dekker, Inc., New York.

[31] Levich, V. *Acta Physicochim. URSS* **1942**, 17, 257.

[32] Newman, J., *J. Phys. Chem.* **1966**, 70, 4, 1327.

[33] Wang J. *Analytical Chemistry* **2006**, 3rd ed., pp. 117, John Wiley and sons.

[34] Kissinger, P. J., Heineman, W. R. *Laboratory Techniques in Electroanalytical Chemistry* **1984**, Dekker, New York.

[35] Conradie, J., Cameron, T. S., Aquino, M. A. S., Lamprecht, G. J., Swarts, J. C. *Inorg. Chim. Acta* **2005**, 358, 2530.

[36] Mann, C. K. *Electroanalytical Chemistry* **1969**, 3, 57, A. J. Bard, ed., Marcel Dekker, New York.

[37] Silva, S., Bond, A. M. *Anal. Chim. Acta,* **2003,** 500, 307.

[38] Le Seur, R. J., Geiger, W. E. *Angew. Chem., Int. Ed. Engl.* **2000,** 39, 248.

[39] Moore W. J. *Physical Chemistry* **1972**, pp. 333, 4th Ed, Longman Group Limited.

[40] Koepp, H. M., Wendt, H., Stehlow, H. Z. *Electrochem.* **1960,** 64, 483.

[41] Gagné, R. R., Koval, C. A., Lisenky, G. C. *Inorg. Chem.* **1980,** 19, 2855.

[42] Gritzner, G., Kuta, J. *Pure and Apl. Chem.* **1984,** 56, 461.

[43] (a) Weinberg, N. L., Weinberg, H. R. *Chem. Rev.* **1968,** 68, 449, (b) Nyberg, K. *Organic Electrochemistry* **1973**, pp 718, Baizer, M. M. ed., Marcl Dekker, New York, N. Y.

[44] Kemp, K. C., Fourie, E., Conradie, J., Swarts, J.C. *Organometallics* **2008**, 27, 353.

[45] du Plessis, W. C., Erasmus, J. C., Lamprecht, G. J., Conradie, J., Cameron, T. S., Aquino, M. A. S., Swarts, J. C. *Can. J. Chem.* **1999**, 77, 378.

[46] Buchta, R. C., Evans, D. H. *J. Electrochem. Soc.: Electrochemical Science* **1970**, 117, 1494.

[47] Evans, D. H., Woodbury, E. C. *J. Org. Chem.* **1967**, 32, 2158.

[48] Buchta, R. C., Evans, D. H. *Anal. Chem.* **1968**, 40, 2181.

[49] (a) Semerano, G., Chisini, A. *Gazz. Chim. Ital*. **1963**, 66, 504. (b) Winkel, A., Proske, G. *Ber*. **1936**, 69, 1917. (c) Tachi, I. *Mem. Coll. Agr.* **1938**, 42, 1.

[50] Neal, T. E., Murray, R. W. *Anal. Chem.* **1970**, 42, 1654.

[51] Kuhn, A., von Eschwege, K., Conradie, J. *Electrochim. Acta* **2011**, 56, 6211.

[52] Buchta, R. C., Evans, D. H. *J. Org. Chem.* **1970**, 35, 2844.

[53] Fourie, E., Swarts, J. C., Lorcy, D., Bellec, N. *Inorg. Chem.* **2010**, 49, 952.

[54].te Velde, G., Bickelhaupt, F. M., Baerends, E. J., Fonseca Guerra, C., van Gisbergen, S. J. A., Snijders, J. G., Ziegler, T. Chemistry with ADF. *J. Comput. Chem.* **2001**, 22, 931.

[55] Kudo, S., Iwase, A., Tanaka, N. Inorg. Chem. 1985, 24, 2388.

[56] Vosloo, T. G., du Plessis, W. C., Swarts, J. C. *Inorg. Chim. Acta* **2002**, 331, 188.

[57] Conradie, J., Swarts, J. C. *Eur. J. Inorg. Chem.* **2011**, 2439.

[58] (a) Basson, S. S., Leipoldt, J. G., Nel, J. T. *Inorg. Chim. Acta* **1984**, 84, 167. (b) Thompos, W. H., Sears, C. T. *Inorg. Chem.*, **1977**, 16, 769. (c) Hart-Davis, A. J., Graham, W. A. G. *Inorg. Chem.* **1970**, 9, 2658.

[59] Sarapu, A. C., Fenske, R. F. *Inorg. Chem.* **1975**, 14, 247.

[60] Kovacik, I., Gevert, O., Werner, H., Schmittel, M., Sollner, R. *Inorg. Chim. Acta*, **1998**, 275, 435.

[61] Erasmus, J. J. C., Conradie, J. *Electro. Chim. Acta* **2011**, 56, 9287.

[62] Lamprecht, D., Lamprecht, G. J. *Inorg. Chim. Acta* **2000**, 309, 72.

[63] Guedes da Silva, M. F. C., Trzeciak, A. M., Ziólkowski, J. J., Pomberiro, A. J. L. *J. Organomet. Chem.* **2001**, 620, 174.

[64] Lever, A. B. P., *Inorg. Chem.* **1990**, 29, 1271.

[65] a) Barriere, F., Kirss, R. U., Geiger, W. E. *Organometallics* **2005**, 24, 48 and references therein, b) Trupia, S., Nafady, A., Geiger, W. E. *Inorg. Chem.* **2003**, 42, 5480, c) Barriere, F., Camire, N., Geiger, W. E., Mueller-Westerhoff, U. T., Sanders, R. *J. Am. Chem. Soc.*, **2002**, 124, 7262, d) Barriere, F., Geiger, W. E. *J. Am. Chem. Soc.*, **2006**, 128, 3980, e) Nafady, A., Chin, T. T., Geiger, W. E. *Organometallics* **2006**, 25, 1654, f) Chong, D. S., Slote, J., Geiger, W. E. *J. Electroanal. Chem.* **2009**, 630, 28.

[66] a) Swarts, J. C., Nafady, A., Roudebush, J. H., Trupia, S., Geiger, W. E. *Inorg. Chem.* **2009**, 48, 2156, b) Fourie, E., Swarts, J. C., Chambrier, I., Cook, M. J. *Dalton Trans*. **2009**, 1145, c) Chambrier, I., Hughes, D. L., Swarts, J. C., Isara, B., Cook, M. J. *J. Chem. Soc. Chem. Commun.* **2006**, 3504.

[67] Fourie, E. *A structural, electrochemical and kinetic Investigation of fluorinated and metallocene-containing phosphines and their Rhodium complexes* **2008**, PhD thesis, University of Free State.

[68] Conradie, J., Lamprecht, G. J., Roodt, A., Swarts, J. C. *Polyhedron*, **2007**, *26*, 5075.

[69] Brown, G. H., Shaw, W.G. *Chem. Rev*., **1957**, 57, 1049.

[70] Gray. G.W. *Molecular Structure and the Properties of Liquid Crystals* **1962**, Academic Press, New York, N.Y.

[71] Schroeder, D. C., Schroeder, J. P. *J. Org. Chem.* **1976**, 41, 15, 2566.

[72] Hussein, M. A., Abdel-Rahman, M. A., Asir, A. M., Alamry, K. A., Aly, K. I. *Designed Monomers and Polymers* (review) **2012**, 15, 431.

[73] Lemieux, P. *Chirality Transfer in Ferroelectric Liquid Crystals*. *Acc. Chem. Res.* **2001**, *34*, 845.

[74] Qaddoura, M. A., Belfield, K. D. *Materials*, **2010**, 3, 827.

[75] Andrienko, D. *Introduction to liquid crystals: Modelling of soft matter* **2006**, International Max Planck Research School.

[76] Qaddoura, M. A., Belfield, K. D. *Int. J. Mol. Sci.*, **2009**, 10, 4772.

[77] Ros, M. B., Serrano, J. L., de la Fuenteb, M. R., Folcia, C. L. *J. Mater. Chem.,* **2005**, 15, 5093.

[78] Holgate, G. A., Ward, W. H. J. *Drug Discovery Today*, **2005**, 10, 1543.

[79] Barnard, N. I. *The influence of ligand chain length and central metal on the thermal and structural properties of metal carboxylates* **2010**, PhD thesis, University of Free State.

[80] Skoog, D. A. Holler, J. F. Nieman, T. *Principles of Instrumental Analysis* **1998**, 905, 5th Ed. New York.

[81] O'Neill, M. J. *Anal. Chem*., **1964**, 1238, 36**,** 7.

[82] Cowie, J. M. G. *Polymers: Chemistry & Physics of modern materials* **2007**.pp13, CRC press, 3rd ed.

[83] Verdonck, E., Schaap, K. Thomas, L. C. A discussion of the principles and application of modulated temperature DSC. *Int. J. Pharm*. **1999**, 192, 3.

[84] Diekring, I. *Textures of liquid crystals* **2003**, Chapter 3, 33. Wiley-VCH.

[85] Barron, A. R. (collection editor) *Physical Methods in Inorganic and Nano Chemistry* **2011**, Chapter 6, 412.

[86] Braun, D., Cherdron, H., Rehahn, M., Ritter, H., Voit, B. *Polymer Synthesis Theory and Practice,* **2005**, Chapter 2, page 129, Springer.

[87] Thomas, M. S. *Complexes of thiophene derivatives as potential metallomesogens* **2006**, PhD thesis, University of Pretoria, RSA.

[88] Dierking, I. *Liquid Crystals Today* **2012**, 21, 54.

[89] Kleman, M., Lavrentovich, O. D. *Philosophical Magazine* **2006**, 86, 4117.

[90] (a) Ringsdorf, H., Schlarb, B., Venzmer, J. *Angew. Chem. Int. Ed. Engl.*, **1988**, 27, 113. (b) Noel, C., Navard, P. *Prog. Polym. Sci*. **1991**, 16, 55.

[91] Gray, G. W., Winsor, P. A. *Liquid Crystals & Plastic Crystals* **1974**, 1, Chapter 4, Ellis Horwood Limited: Chichester, U.K.

[92] Piao, G., Akagi, K., Shirakawa. H. *Synthetic Metals* **1997**, 85, 1669.

[93] (a) Espinet, P., Esteruelas, M. A., Oro, L. A., Serrano, J. L., Sola, E. *Coord. Chem. Rev.*, **1992**, 117, 215. (b) Hudson, S. A., Maitlis, P. M. *Chem. Rev.* **1993**, 93, 861.

[94] (a) Barbera, J., Cativiela, C., Serrano, J. L., Zurbano, M. M. *Adv. Mater*. **1991**, 3, 602. (b) Atencio, R., Barbera, J., Cativiela, C., Lahoz, F. J., Serrano, J. L., Zurbano, M. M. *J. Am. Chem. Soc*. **1994**, 116, 11558. (c) Barbera, J., Elduque, A., Gimenez, R., Oro, L. A., Serrano, J. L. *Angew. Chem., Int. Ed. Engl*. **1996**, 35, 2832. (d) Barbera, J., Elduque, A., Gimenez, R., Lahoz, F. J., Lopez, J. A., Oro, L. A., Serrano, J. L. *Inorg. Chem.* **1998**, 37, 2961.

[95] Bruce, D. W. *J. Chem. Soc., Dalton Trans.* **1993**, 2984.

[96] (a) Ohta, K., Muroki, H., Takagi, A., Hatada, I.C.I., Ema, H., Yamamoto, I., Matsuzaki, K. *Mol. Cryst. Liq. Cryst.* **1988**, 140, 131. (b) Giroud-Godquin, A. M., Gauthier, M. M., Sigaud, G., Hardouin, F., Achard, M. F. *Mol. Cryst. Liq. Cyst.* **1986**, 132, 35. (c) Hanabusa, K., Isogai, T., Koyamata, T., Shirai, H. *Makromol. Chem.* **1993**, 194, 197.

[97] Zhaohui, Z., Youzhi, W., Fuzhou, W., Ping, X. , Rongben, Z. *Polymers for Advanced Technologies* **1996**, 7, 662.

[98] Zheng, H., Swager, T. M. *J. Am. Chem. Soc.* **1994**, 116, 761.

[99] (a) Zheng, H., Carroll, P. J., Swager, T. M. *Liq. Cryst.* **1993**, 14, 1421. (b) Zheng, H**.,** Lai,C. K., Swager, T. M. *Chem. Mater.* **1994**, 6, 101.

[100] Blake, A. B., Chipperfield, J. R., Clark, S., Nelson, P. G. *J. Chem. SOC. Dalton Trans.* **1991**, 1159.

3

Results and discussion

3.1 Synthesis

In this study, synthesis, the characterisation, electrochemistry, density functional theory calculations and the mesomorphic properties of selected γ-substituted β-diketones, their rhodium(I) dicarbonyl complexes and their rhodium(I) monocarbonyl triphenylphosphine complexes are investigated. In addition, synthetic, structural and computational studies on a series of four β-substituted-β-diketonato-rhodium complexes are also presented.

The following five gamma substituted β-diketones were synthesised, characterised and then coordinated to a rhodium(I) metal ion:

- 2,4-dioxo-3-pentyl-4-hydroxybenzoate ($CH_3COCH(\mathbf{HOC_6H_4COO})COCH_3$), **1a**;
- 2,4-dioxo-3-pentyl-4-hydroxycinnamate ($CH_3COCH(\mathbf{HOC_6H_4C_2H_2COO})COCH_3$), **2a**;
- 2,4-dioxo-3-pentyl-4-decanyloxybenzoate ($CH_3COCH(\mathbf{C_{10}H_{21}OC_6H_4COO})COCH_3$), **3a**;
- 2,4-dioxo-3-pentyl-4-[[4-(n-decanyloxy)benzoyl]oxy]benzoate ($CH_3COCH(\mathbf{C_{10}H_{21}OC_6H_4COOC_6H_4COO})COCH_3$), **4a**; and
- 2,4-dioxo-3-pentyl-4-[[4-(n-decanyloxy)cinnamoyl]oxy]benzoate ($CH_3COCH(\mathbf{C_{10}H_{21}OC_6H_4C_2H_2COOC_6H_4COO})COCH_3$), **5a**.

A different synthetic route from what was reported earlier[1,2] for β-diketones **1a**; **2a**; **4a** and **5a** was explored in this study to optimise the yield of the reaction to a range of 79 – 85%. Optimisation was achieved by utilising calmer and more affordable reaction conditions as compared to the use of transfer catalyst[2] and protection of functional groups[3] reported in literature with a yield range of ±61%, while no report was found for the synthesis of **3a**.

Rhodium dicarbonyl complexes (which are referred to as **1b – 5b** in this study) that were found reported in literature[1] are only those shown in **4b** and **5b** while no reports were found for the synthesis of all the rhodium mono phosphine complexes (referred to as **1c – 5c**) done in this study.

The systematic variation of the gamma substituent allowed the characterisation of these β-diketones with their complexes by means of spectroscopic (^{1}H NMR), spectrophotometric (IR), liquid crystal study (POM, DSC), computational calculations (DFT) and electrochemical (CV, OSWV, LSV) methods. No liquid crystal studies were done on the β-substituted-β-diketones and their complexes, since they do not have the correct design to exhibit liquid crystal properties.

3.1.1 Gamma-substituted β-diketones

4-hydroxybenzoate for β-diketone **1a**, 4-hydroxycinnamic acid for β-diketone **2a**, and 4-decyloxybenzoate for β-diketone **3a** (see **Scheme 3. 1** below) in tetrahydrofuran (THF) were added drop-wise to a stirred suspension of sodium hydride (NaH) in THF. Dimethylformamide (DMF) was added to the product, followed by the addition of 3-chloropentane-2,4-dione. Stirring was continued for twenty-four hours under reflux. After cooling to room temperature, the product was extracted with chloroform and it was dried over sodium sulphate. Purification was done by column chromatography with hexane and ethylacetate as eluents and crystallization was done in ethanol.

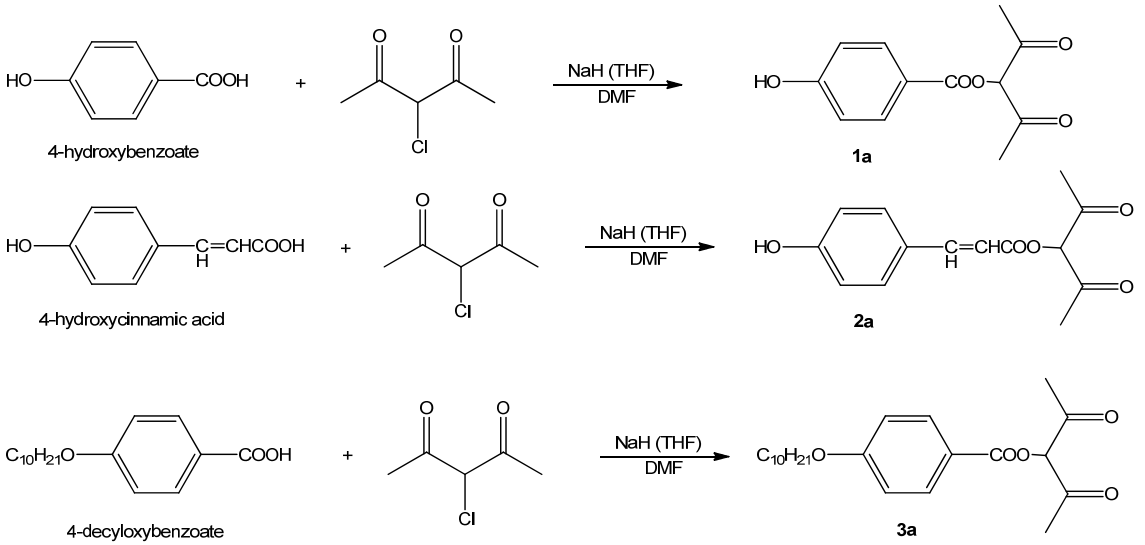

Scheme 3. 1. Synthetic route for the synthesis of γ-substituted β-diketone 2,4-dioxo-3-pentyl-4-hydroxybenzoate ($CH_3COCH(HOC_6H_4COO)COCH_3$)1a;2,4-dioxo-3-pentyl-4-hydroxycinnamate ($CH_3COCH(HOC_6H_4C_2H_2COO)COCH_3$) 2a; and 2,4-dioxo-3-pentyl-4-decanyloxybenzoate ($CH_3COCH(C_{10}H_{21}OC_6H_4COO)COCH_3$) 3a.

β-diketone **4a** (**Scheme 3. 2**) was synthesised by reacting 4-decyloxybenzoate with thionyl chloride ($SOCl_2$) in benzene over reflux overnight to give an appropriate chloride salt. To this salt was added 4-hydroxybenzoate in pyridine to give an appropriate acid for the synthesis of β-diketone **4a**. This product was subjected to the procedure used for the synthesis of **1a**, **2a** and **3a**. In this procedure, potassium hydroxide in DMF was used instead of NaH to give β-diketone **4a**.

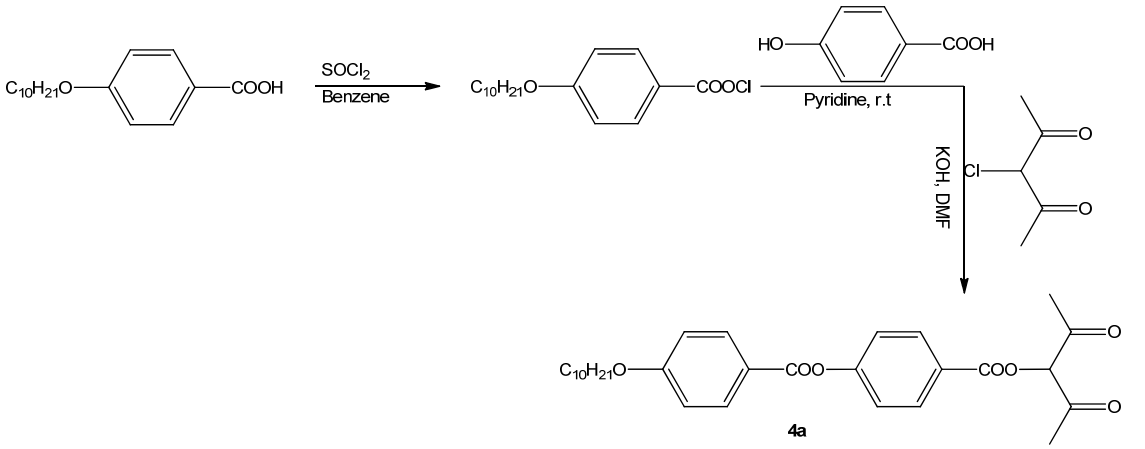

Scheme 3. 2. Synthetic route for the synthesis of γ-substituted β-diketone 2,4-dioxo-3-pentyl-4-[[4-(n-decanyloxy)benzoyl]oxy]benzoate ($CH_3COCH(C_{10}H_{21}OC_6H_4COOC_6H_4COO)COCH_3$) 4a.

In contrast, β-diketone **5a** (**Scheme 3. 2**) was first synthesised by a synthesis of 4-decyloxycinnamic acid. This was achieved by *p*-hydroxycinnamic acid and KOH dissolved in an ethanol water solution. A small amount of potassium iodide was added to catalyse the reaction before the slow addition of 1-bromodecane. To the product (4-decyloxycinnamic acid), $SOCl_2$ was added and refluxed for 18 hours. 2,4-dioxo-3-pentyl 4-hydroxybenzoate (β-diketone **1**) in benzene was added and refluxed for 24 h to afford the desired product **5a**.

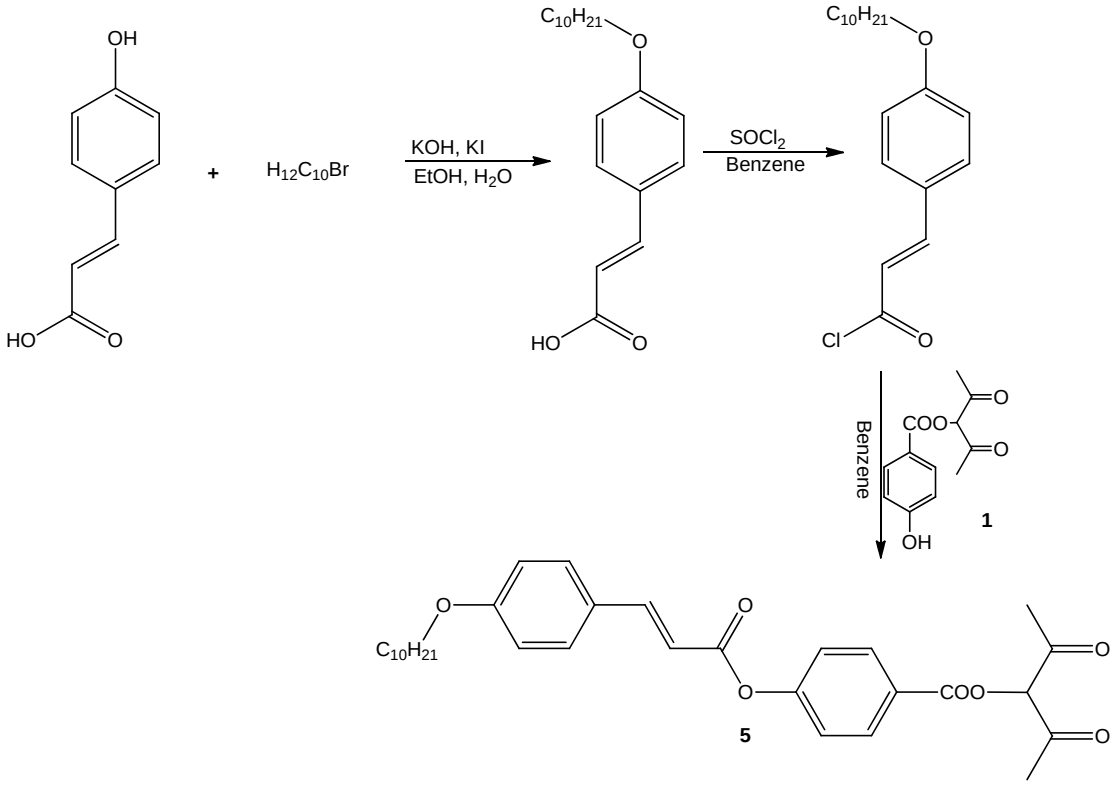

Scheme 3. 3. Synthetic route for the synthesis of γ-substituted β-diketone 2,4-dioxo-3-pentyl-4-[[4-(n-decanyloxy)cinnamoyl]oxy]benzoate ($CH_3COCH(C_{10}H_{21}OC_6H_4C_2H_2COOC_6H_4COO)COCH_3$) [5a].

A comparative view of the ^{1}H NMR of β-diketones **1a – 5a** is given in **Figure 3. 1**. A short discussion follows below. In Appendix A, the ^{1}H NMR with a detailed assignment of the peaks is given.

Signals representing H on the β-diketone backbone: From the ^{1}H NMR of β-diketones **1a – 5a,** it is clear that all ^{1}H NMR of β-diketones exist in the keto and in the enol form. For example, for β-diketone **3a,** the signal at ca 14.50 ppm is due to the enolic proton and a signal at 2.0 ppm for the two methyl groups (6H, 2xCH_3) in the enol form. The signals that correspond to the keto form are at ca 5.7 and 2.35 ppm (1H and 6H) respectively.

The signal presenting the keto methine H on the β-diketone backbone does not shift more than 0.07 ppm when it goes from β-diketone **1a** to **5a**. The two signals representing the methyl groups (6H, 2xCH_3) of the keto and the enol forms respectively on the β-diketone is 0.3 – 0.7 ppm apart.

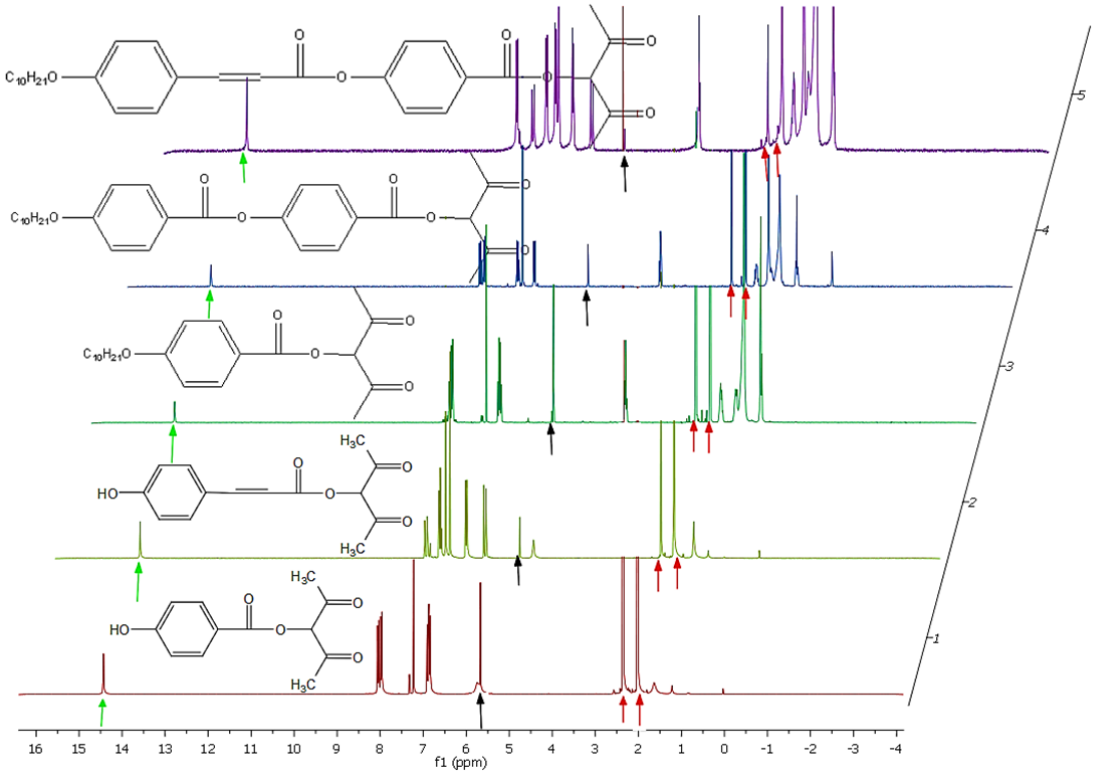

Figure 3. 1. ^{1}H NMR for β-diketones 1a, 2a, 3a, 4a and 5a. The signal of the methine H on the β-diketone backbone is indicated with a black arrow at *ca* 5.7 ppm. The two singlet peaks presenting the methyl groups CH_3 on the β-diketone is indicated with red arrows at ca 2 ppm and the enol OH peak at ca 14.5 ppm with a green arrow.

Signals representing H on the γ-substituent: The signals of protons of the phenyl groups for β-diketone **1a-3a** are two doublets, with J^1 = 8.0 ppm and 6.9 ppm. For β-diketones 4a and 5a, that each have two phenyl groups, there are four doublets for each. They are generally found at 6.9, 7.3, 8.2 and 8.5 ppm respectively. The signals of protons of the carbine-H (-CH=CH-) of β-diketones **2a** and **5a** are two singlets, one for each H, at 6.4 and 7.7 ppm respectively. The $C_{10}H_{21}$ chain β-diketones **3a** to **5a** generally give the following signals: CH_3 (3H, triplet at ca. 0.8 ppm), $(CH_2)_7$ (14H, multiplet at ca. 1.3 ppm), CH_2 (2H, multiplet at ca. 1.8 ppm),

CH_2 (2H next to O, multiplet at ca. 4 ppm). The signal for the OH of the enol form of the β-diketones is found at ca 14.5 ppm – which overlaps with the OH signal found in the γ-substituent of Hβ**1a** and Hβ**2a**.

3.1.2 Rh(I)-dicarbonyl complexes

All Rh(I)-dicarbonyl complexes were synthesized by procedures which were adapted from the available literature.[1,4] $[Rh(CH_3COCHCOCH_3)(CO)_2]$ was synthesized according to published methods for comparative reasons.[5]

3.1.2.1 Gamma-substituted β-diketonato-Rh(I)-dicarbonyl complexes

β-diketonato-Rh(I)-dicarbonyl complexes of β-diketones **1a; 2a** and **3a** {2,4-dioxo-3-pentyl-4-hydroxybenzoate ($CH_3COCH(\mathbf{HOC_6H_4COO})COCH_3$) ; 2,4-dioxo-3-pentyl-4-hydroxycinnamate ($CH_3COCH(\mathbf{HOC_6H_4C_2H_2COO})COCH_3$) and 2,4-dioxo-3-pentyl-4-decanyloxybenzoate ($CH_3COCH(\mathbf{C_{10}H_{21}OC_6H_4COO})COCH_3$) respectively} were synthesised by dissolving sodium acetate in methanol and adding an equivalent amount of an appropriate β-diketone into this sodium acetate solution. Half the amount of the dimer $[Rh_2Cl_2(CO)_4]$ was added, giving a clear yellow solution. The reaction mixture was stirred at room temperature for one hour. The resulting precipitate was separated by filtration, washed with methanol and vacuum-dried, giving the product.

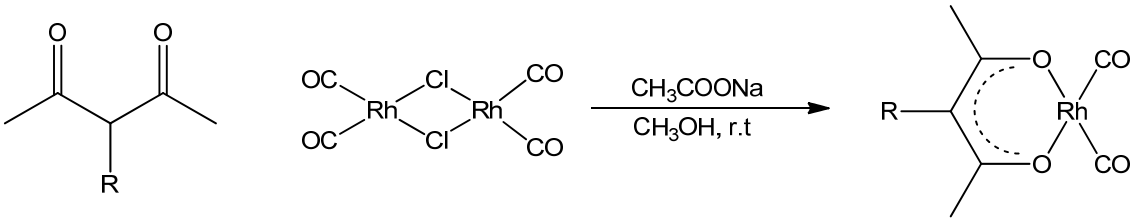

R = $HOC_6H_4COO^-$ (Rh-dicarbonyl **1b**)
R = $HOC_6H_4C_2H_2COO^-$ (Rh-dicarbonyl **2b**)
R = $C_{10}H_{21}OC_6H_4COO^-$ (Rh-dicarbonyl **3b**)

Scheme 3. 4. Synthetic route for the synthesis of the [Rh(β-diketonato)$(CO)_2$] complexes of gamma-substituted β-diketonato-Rh(I)-dicarbonyl complexes from β-diketones 1a; 2a and 3a, referred to as Rh-dicarbonyl 1b; 2b and 3b respectively.

Infrared spectroscopy, in addition to NMR and other methods, was used to characterise the rhodium carbonyl complexes. Two sharp peaks at ca 2000 cm^{-1} are expected due to the symmetric and anti-symmetric stretching of the two CO-groups. Rh-dicarbonyl **1b** and **2b** gave similar spectra and displayed two distinctive peaks for the two carbonyl moieties (C=O) and one distinctive peak for the hydroxyl moiety (O-H) stretching (see **Table 3. 1** and **Figure 3. 2**).

Table 3. 1. CO, OH and CH stretching frequencies of rhodium dicarbonyl complexes 1b - 5b.

Rh-dicarbonyl complex	**ν (CO) / cm^{-1}**	**ν / cm^{-1}**
Rh-dicarbonyl **1b**	2071; 2011	3396 **(OH)**
Rh-dicarbonyl **2b**	2071; 2003	3417 **(OH)**
Rh-dicarbonyl **3b**	2079; 2005	2925; 2854 **(C-H)**
Rh-dicarbonyl **4b**	2079; 2005	2925; 2854 **(C-H)**
Rh-dicarbonyl **5b**	2079; 2005	2925; 2854 **(C-H)**

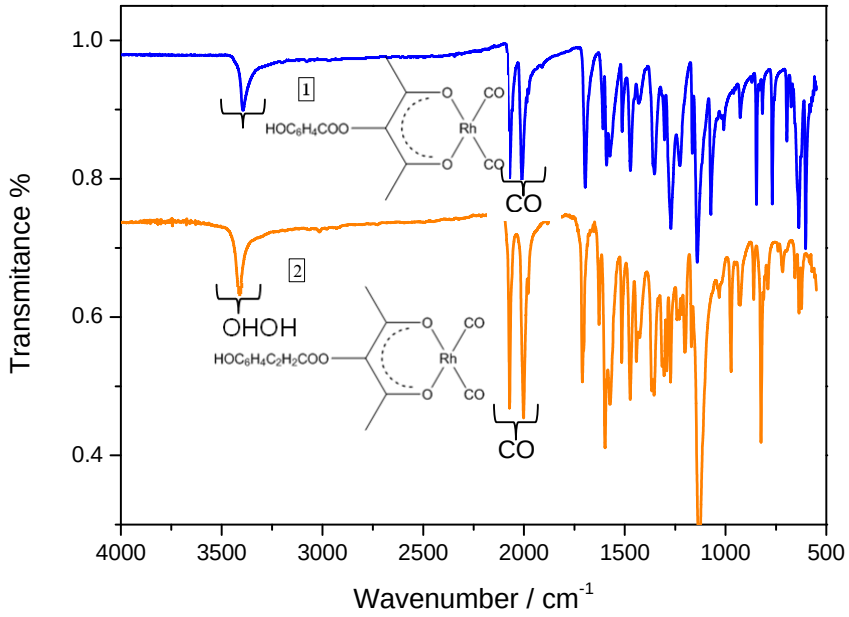

Figure 3. 2. Infrared spectra for the [Rh(β-diketonato)$(CO)_2$] complexes 1b and 2b. The gamma-substituted β-diketonato-Rh(I)-dicarbonyl complexes synthesized from β-diketones 1a and 2a.

β-diketonato-Rh(I)-dicarbonyl complex **4b** of β-diketone **4a** {2,4-dioxo-3-pentyl-4-[[4-(n-decanyloxy)benzoyl]oxy]benzoate ($CH_3COCH(\mathbf{C_{10}H_{21}OC_6H_4COOC_6H_4COO})COCH_3$) } was synthesised by dissolving the dimer $[Rh_2Cl_2(CO)_4]$ in acetone. Twice the amount of an appropriate β-diketone was dissolved in acetone. The solutions were mixed together in an excess of barium carbonate ($BaCO_3$) at room temperature. The reaction mixture was stirred under argon for 2h. The resulting precipitate was filtered off and evaporated under reduced pressure, giving a yellow precipitate.

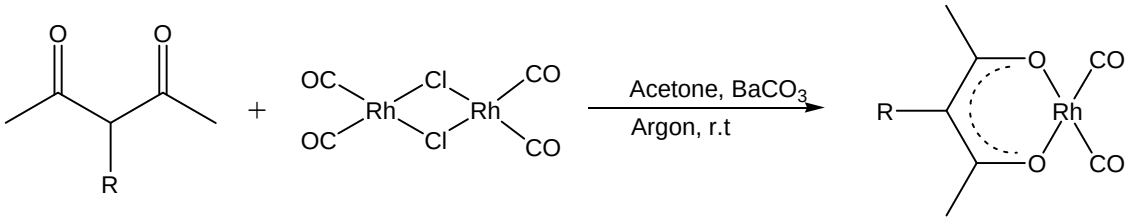

R = $C_{10}H_{21}OC_6H_4COOC_6H_4COO^-$ (Rh-dicarbonyl **4b**)

Scheme 3. 5. Synthetic route for the synthesis of the [Rh(β-diketonato)$(CO)_2$] complex of gamma-substituted β-diketonato-Rh(I)-dicarbonyl complex from β-diketone 4a .

β-diketonato-Rh(I)-dicarbonyl complex **5b** of β-diketones **5a** {2,4-dioxo-3-pentyl-4-[[4-(n-decanyloxy)cinnamoyl]oxy]benzoate($CH_3COCH(C_{10}H_{21}OC_6H_4C_2H_2COOC_6H_4COO)COCH_3$) } was prepared by dissolving rhodiumchlorohydrate ($RhCl_3.H_2O$) in eight to ten drops of water and a small amount of DMF. The dark red mixture was stirred under reflux until a yellow-orange colour was observed. After cooling the reaction mixture to room temperature, β-diketone **5a** was added slowly and stirring was continued for an hour at room temperature. The product precipitated after having been quenched with ice and stirred further for another hour. The precipitate was washed with excess water, dried and recrystallized with hot hexane.

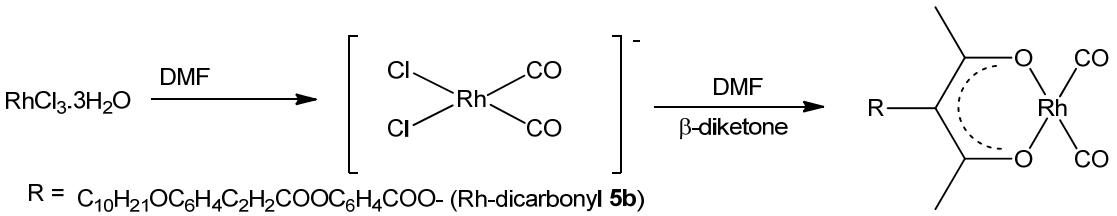

R = $C_{10}H_{21}OC_6H_4C_2H_2COOC_6H_4COO$- (Rh-dicarbonyl **5b**)

Scheme 3. 6. Synthetic route for the synthesis of the [Rh(β-diketonato)$(CO)_2$] complexes of gamma-substituted β-diketonato-Rh(I)-dicarbonyl complexes from β-diketones 5a.

^{1}H-NMR of these rhodium dicarbonyl complexes **3b**; **4b** and **5b** neither the enolic nor the keto form peaks observed on the corresponding β-diketones. **Figure 3. 3** is ^{1}H NMR for rhodium dicarbonyl complex **5b.** This example indicates the positions where the enolic and the keto peaks are found in the corresponding β-diketone **5a** respectively. The signals which represent protons on the γ-substituent of rhodium dicarbonyl complex **5b** show no significant shift when compared to the position of the signals of free β-diketone **5a**.

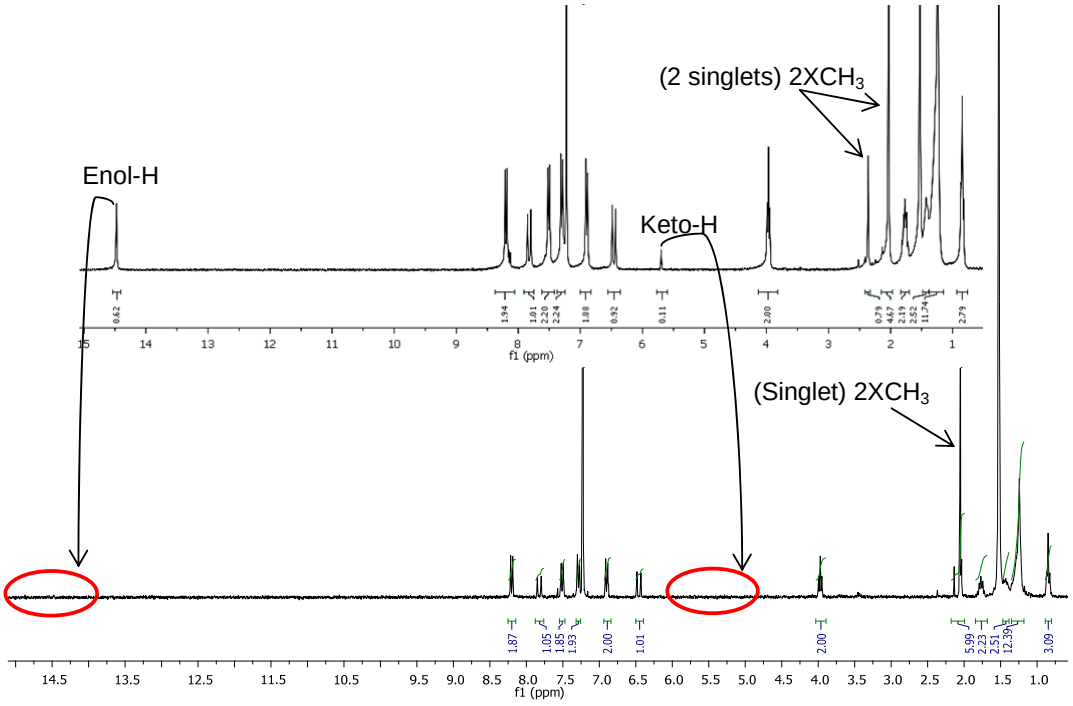

Figure 3. 3. ^{1}H NMR for rhodium dicarbonyl complex 5b. The red circles indicate the positions where the enolic and the keto peaks are found in the corresponding β-diketone 5a respectively.

Figure 3. 4 shows the infrared spectra of dicarbonyl complexes **3b**, **4b** and **5b**. We observe that the IR of rhodium dicarbonyl complexes **3b**; **4b** and **5b** are very similar, with two distinctive peaks of the two C=O moieties at 2079 cm^{-1} and 2005 cm^{-1}, while at 2925 cm^{-1} and 2854 cm^{-1} we find C-H stretching of the alkyl chain.

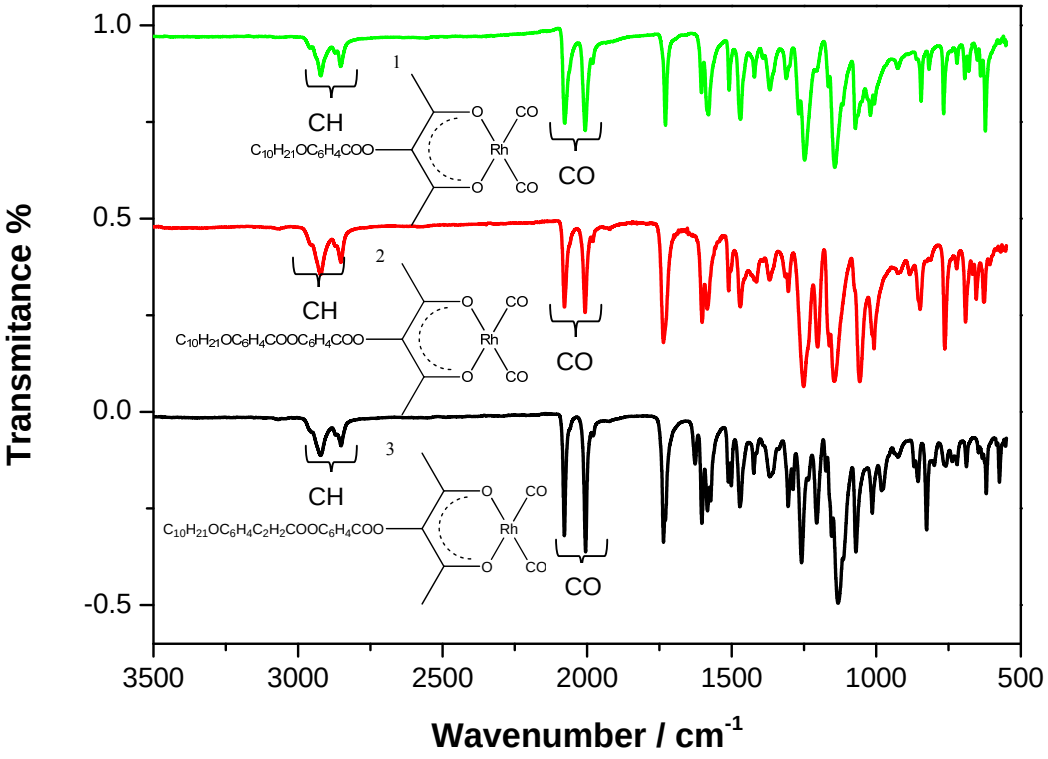

Figure 3. 4. Infrared spectra for the [Rh(β-diketonato)(CO)$_2$] complexes 3b, 4b and 5b. The gamma-substituted β-diketonato-Rh(I)-dicarbonyl complexes synthesized from β-diketones 3a, 4a and 5a.

3.1.2.2 Beta-substituted β-diketonato-Rh(I)-dicarbonyl complexes

The yellow-orange complexes of [Rh(β-diketonato)(CO)$_2$] with β-diketonato = ba (95% yield), bap (27% yield), bab (17% yield), and bav (18%) were synthesized by a reaction pathway shown in **Scheme 3. 7.**[4] The abbreviations used are defined in **Scheme 3. 7**.

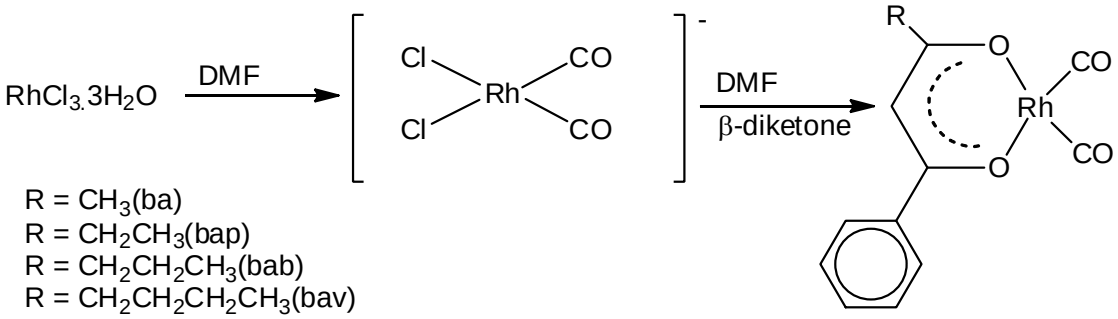

Scheme 3. 7. Synthetic route for the synthesis of the [Rh(β-diketonato)(CO)$_2$] complexes.

Heating a DMF solution of $RhCl_3.xH_2O$ leads to the formation of the salt $[NH_2(CH_3)_2]^+[Rh(CO)_2Cl_2]^-$.[6] An equivalent amount of the appropriate β-diketone added into the reaction mixture while stirring yielded the desired products. The obtained products were precipitated by ice water. Silica gel column chromatography was employed to clean the products. The pure products were obtained by recrystallization from hot hexane. The longer the chain on the R-group, the more difficult it is to crystallise the product. It was possible to solve the crystal structure of $[Rh(bap)(CO)_2]$,[7] $[Rh(bab)(CO)_2]$[8] by X-ray.

3.1.3 Rh(I)-monocarbonyl-PPh_3 complexes

3.1.3.1 Gamma-substituted β-diketonato-Rh(I)-monocarbonyl-PPh_3 complexes

An appropriate rhodium dicarbonyl complex was dissolved in hot hexane and put to boil in a water bath. Triphenylphosphine (PPh_3) was also dissolved in hot hexane then added to the boiling rhodium dicarbonyl complex solution. The reaction mixture was stirred for thirty minutes in a water bath until all the CO gas had bubbled off. On cooling, a light yellow product precipitated out.

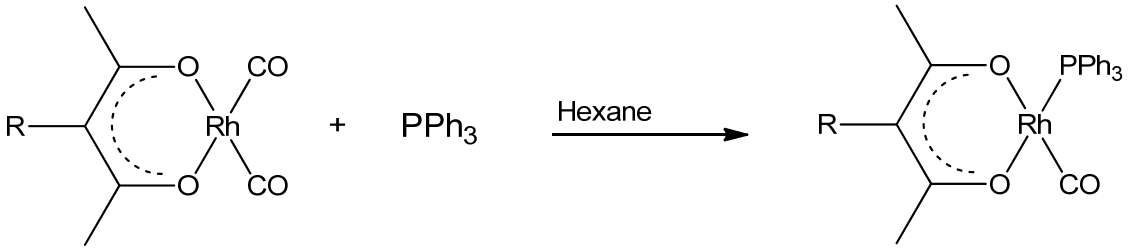

Scheme 3. 8. Synthetic route for the synthesis of the [Rh(β-diketonato)(CO) PPh_3] complexes of gamma-substituted β-diketonato-Rh(I)-dicarbonyl complexes from β-diketones.

^1H NMR and ^{31}P NMR were used for the analysis of all the γ-substituted β-diketonato-Rh(I)-monocarbonyl-PPh_3 complexes synthesised. **Figure 3. 5** shows ^1H NMR of one (**2c**) of the Rh(β-diketonato-**2a**)(CO)PPh_3 complexes with its ^{31}P NMR. On the ^{31}P NMR, a doublet for the ^{31}P signal is observed due to coupling to rhodium. The signal of P coupled to Rh(I) are all at ca 50 ppm. On the ^1H NMR signals, representing protons of the three phenyl groups of triphenylphosphine and protons of the phenyl group of the γ-substituent are found as multiplets at ca 7.4 ppm to 7.8 ppm.

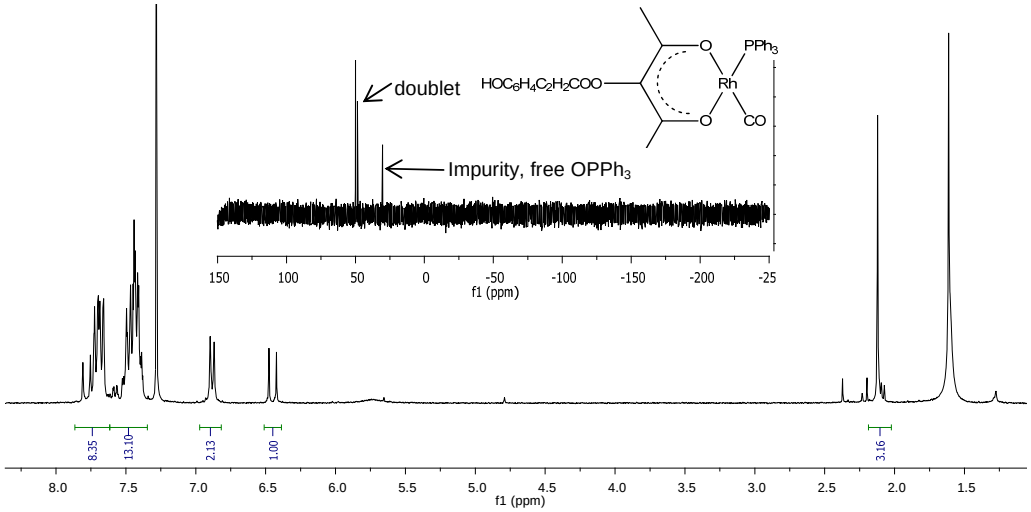

Figure 3. 5. ^{1}H NMR and ^{31}P NMR (insert) of [Rh(2a)(CO)(PPh$_3$)].

3.1.3.2 Beta-substituted β-diketonato-Rh(I)-monocarbonyl-PPh$_3$ complexes

The light yellow [Rh(β-diketonato)(CO)(PPh$_3$)] complexes with β-diketonato = bap (16% yield), bab (13% yield) and bav (14% yield) were obtained by adding an equivalent amount of PPh$_3$ dissolved in hot hexane, to a hot [Rh(β-diketonato)(CO)$_2$] *n*-hexane orange solution.[4] The reaction is immediate, turning the yellow solution to orange, with the displacement of one CO ligand and the precipitation of the monocarbonyl product [Rh(β-diketonato)(CO)(PPh$_3$)][9] (see **Scheme 3. 9**). Two possible product isomers are possible when the coordinated β-diketonato is asymmetric as will be the case for the products containing (ba)$^-$, (bap)$^-$, (bab)$^-$ or (bav)$^-$.

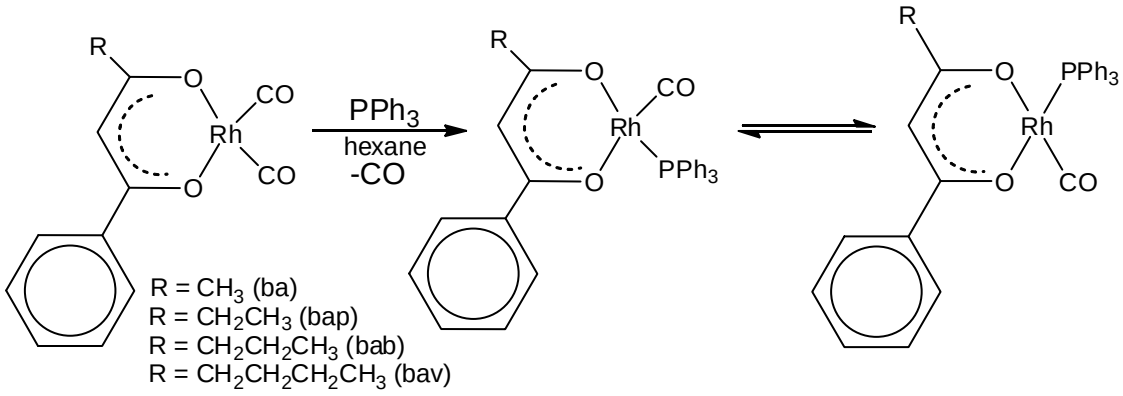

Scheme 3. 9. Synthesis of [Rh(β-diketonato)(CO)(PPh$_3$)] complexes from the corresponding [Rh(β-diketonato)(CO)$_2$] complexes.

The ^{1}H NMR spectra show that, for each of the [Rh(β-diketonato)(CO)(PPh_3)] complexes synthesised, two isomers exist in solution.[4] The difference between the two isomers can be seen in the large difference between the positions, δ_H in ppm, of the signals of the protons of the alkyl group ($(CH_2)_nCH_3$, n = 0-3) of the β-diketonato ligand[4] – see **Figure 3. 6** for [Rh(bap)(CO)(PPh_3)]. The two different isomers of the [Rh(β-diketonato)(CO)(PPh_3)] complexes have been labelled isomer A (IUPAC *SP*-4-2[10]) and isomer B (IUPAC *SP*-4-3,[10] **Scheme 3. 10**). We do not know whether both isomers formed directly from the substitution reaction or through a subsequent isomerisation reaction. X-ray crystal structures of the mono-phosphine product complexes [Rh(RCOCHCOR')(CO)(PPh_3)] typically display only one of two possible geometric isomers,[11,12,13,14] which was interpreted that only one isomer was formed in the substitution reaction. However, the presence of only one of the [Rh(RCOCHCOR')(CO)(PPh_3)] product isomers in the solid state can also be a consequence of the crystallization conditions.[15,16] In solution it was found that the isomers are in a fast equilibrium with each other, with a resulting equilibrium constant (K_c) that depends *inter alia* on the polarity of the solvent and the effects of the temperature.[4,15, 16,17,18]

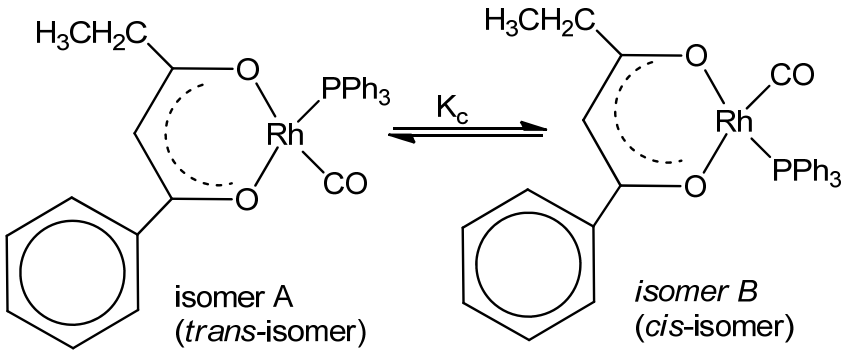

Scheme 3. 10: The equilibrium between the two isomers of the complex [Rh(bap)(CO)(PPh_3)]. Polarization theory and the σ-trans effect predict that isomer A should be dominant.

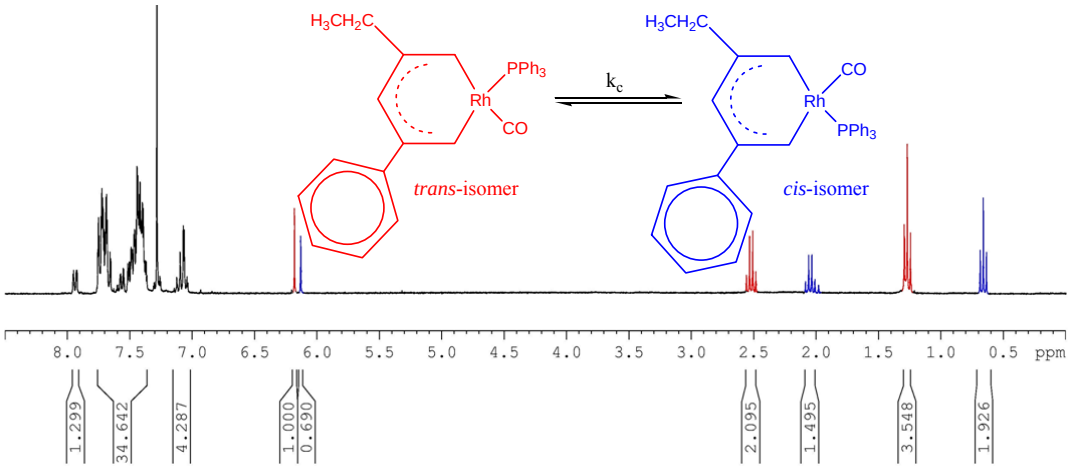

Figure 3. 6: ^{1}H NMR of isomer mixture of [Rh(bap)(CO)(PPh$_3$)]. δ_H (300 MHz, CDCl$_3$) ISOMER A (red): 1.27 (3H, t, CH$_3$), 2.52 (2H, q, CH$_2$), 6.21 (1H, s, CH), 7.02-7.99 (20H, m, aromatic). δ_H (300 MHz, CDCl$_3$) ISOMER B (blue): 0.66 (3H, t, CH$_3$), 2.01 (2H, q, CH$_2$), 6.10 (1H, s, CH), 7.02-7.99 (20H, m, aromatic).

The equilibrium constant, K_c = [isomer B]/[isomer A] = 0.69/1.00 of [Rh(bap)(CO)(PPh$_3$)] isomers, is calculated from the peak integrals of the methine proton of the coordinated β-diketonato ligand bap. The two isomers are the isomer with PPh$_3$ *trans* to the oxygen nearest to the more electron-donating phenyl group of the chelate ring, the expected isomer labelled as isomer A (red), and the isomer with PPh$_3$ *cis* to the oxygen nearest to the phenyl group as defined in **Scheme 3. 10** is labelled isomer B (blue). Isomer A is the main isomer due to the *trans*-influence where PPh$_3$ is *trans* to the oxygen near an electron-donating group (Ph) which has a larger *trans*-influence compared to an alkyl group; it will be referred to as the *trans* isomer. This is in agreement with the polarization theory because the oxygen atom nearest to an alkyl group will be least polarisable since the alkyl group is electron attracting.[4,19,20,21,22,23]

Only in two cases did both the geometrical isomers crystallize at independent positions in the same crystal lattice, *i.e.* at a 50:50 ratio, for [Rh(PhCOCHCOCH$_3$)(CO)(PPh$_3$)][24] and [Rh(PhCOCHCOCH$_2$CH$_3$)(CO)(PPh$_3$)]7 (bab = PhCOCHCOCH$_2$CH$_3$). The crystal structure of [Rh(PhCOCHCOCH$_2$CH$_3$)(CO)(PPh$_3$)] will be presented in paragraph **3.1.3.3** of this study. In the case of [Rh(PhCOCHCO(CH$_2$)$_3$CH$_3$)(CO)(PPh$_3$)],[9] (bav = PhCOCHCO(CH$_2$)$_3$CH$_3$), both geometrical isomers crystallized in the same space in the unit cell at an 89.7:10.3 ratio.[9] The β-diketonato substituents of these three complexes have similar Gordy group electronegativities, χ_{Ph} = 2.21,[25] $\chi_{(CH2)CH3}$ = 2.31,[4] $\chi_{(CH2)3CH3}$ = 2.22[4] and χ_{CH3} = 2.34[26], and

this might have contributed to the fact that it was possible to isolate both isomers in the solid state.

3.1.3.3 Crystal Structure of [Rh(PhCOCHCOCH$_2$CH$_3$)(CO)(PPh$_3$)][a]

The crystal data, the details of the data collection and the refinement, as well as a discussion on the bond lengths and angles, are given in reference 4. In the previous section it was mentioned that, since the Gordy group electronegativities of χ_{Ph} = 2.21,[25] and $\chi_{(CH2)CH3}$ = 2.31,[4] are very similar, the formation of a specific product isomer of [Rh(PhCOCHCOCH$_2$CH$_3$)(CO)(PPh$_3$)] was not favoured by *trans*-influence arguments, *i.e.* both product isomers should form on grounds of *trans*-influence arguments. The discussion in this section shows that the steric influence of Ph and CH$_2$CH$_3$ in [Rh(PhCOCHCOCH$_2$CH$_3$)(CO)(PPh$_3$)] is similar and should not play a role in the substitution reaction of PPh$_3$ for CO in [Rh(PhCOCHCOCH$_2$CH$_3$)(CO)$_2$], *i.e.* on the grounds of arguments about steric influence, both product isomers should form experimentally.

First, one may observe that the PPh$_3$ ligands of the two isomers of [Rh(PhCOCHCOCH$_2$CH$_3$)(CO)(PPh$_3$)] adopt similar spatial orientations. Superimposing the 'backbone' Rh(CCOCHCOC)(CO)(PPh$_3$) moieties of the two isomers shows remarkable similarities, see **Figure 3. 7** for a graphical representation.

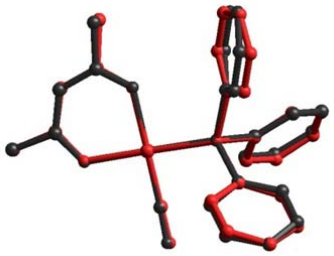

Figure 3. 7. An overlay of the Rh(CCOCHCOC)(CO)(PPh$_3$) moieties of the two isomers of [Rh(PhCOCHCOCH$_2$CH$_3$)(CO)(PPh$_3$)]. (Reprinted with permission from Hopmann, K.H.; Stuurman, N.F.; Muller, A. and Conradie, J. *Organometallics*, Vol. 29, No. 11, 2010. Copyright 2010 American Chemical Society.)

[a] The crystal structure of this section was solved by Alfred Muller from the Department of Chemistry, University of Johannesburg (APK Campus), PO Box 524, Aucklandpark, Johannesburg 2006, South Africa. Parts of the work is published, see references 7 and 9.

The above observation is in agreement with the DFT (density functional theory) calculated conformation analysis of PPh_3 coordinated to square planar metal centres.[9,27] DFT results, in agreement with the experimental structures, showed that the favoured degenerate conformations of coordinated PPh_3 in square planar [Rh(β-diketonato)(CO)(PPh_3)] complexes possess specific features and can be described as the orientation of PPh_3 relative to the plane incorporating all points of minimum steric compression, called the *plane of nadir energy*.[28] The energy of the plane of nadir for square planar complexes is shown in **Figure 3. 8 (a)**. In this case, the plane of nadir energy is perpendicular to the square plane. The favoured degenerate conformations of coordinated PPh_3 in square planar [Rh(β-diketonato)(CO)(PPh_3)] complexes can be obtained by applying the following principles (clockwise or P helicity of PPh_3, view along P-Rh axis, Ph rings are numbered A, B, and C (see **Figure 3. 8 (a)**). They are applied in the steps described below:[9,27]

(i) Superimpose C_{ortho} of the vertical Ph ring **A** onto the nadir plane that lies perpendicular to the square plane, then allow Ph ring **A** to tilt towards the smallest ligand.

(ii) Allow Ph ring **B** to tilt in the space below the smallest ligand in the quadrant between the nadir plane, below the complex and a horizontal plane that lies through the SQP of the complex.

(iii) Tilt Ph ring **C** over the largest ligand.

(iv) Allow correlated tilting of Ph rings **A**, **B** and **C** to minimize inter ring-ligand and inter ring-ring interactions.

DFT calculations, in agreement with the experimental crystal structures, also show that the steric influence of $O_{\beta\text{-diketonato}}$ and CO is similar on the preferred orientation of the vertical phenyl ring A of PPh_3 in [Rh(β-diketonato)(CO)(PPh_3)] complexes.[9] The fact that both isomers of [Rh($PhCOCHCOCH_2CH_3$)(CO)(PPh_3)] crystallized in the solid state, with a similar orientation of PPh_3, further shows that the size of the side groups Ph and CH_2CH_3 on the β-diketonato ligand $(PhCOCHCOCH_2CH_3)^-$ does not influence the preferred conformation of coordinated PPh_3 in [Rh($PhCOCHCOCH_2CH_3$)(CO)(PPh_3)] in this case.[9]

Secondly, the steric parameters of the two ligands, Ph and CH_2CH_3, of [Rh($PhCOCHCOCH_2CH_3$)(CO)(PPh_3)], as measured by cone and solid angles, are similar: Cone angles = 156.7 and 158.5°;[29] solid angles = 26.41 and 26.36%[30] for P in isomer A and P in isomer B respectively).[31] A solid angle projection[30] of the ligand shows two comparable lobes for the substituents of the β-diketonato ligand of

[Rh(PhCOCHCOCH$_2$CH$_3$)(CO)(PPh$_3$)], see **Figure 3. 9 (a)**. Separation of these, **Figure 3. 9 (b),** shows that Ph and CH$_2$CH$_3$ shield 12.48 and 12.43% of the sphere, indicating similar steric properties.

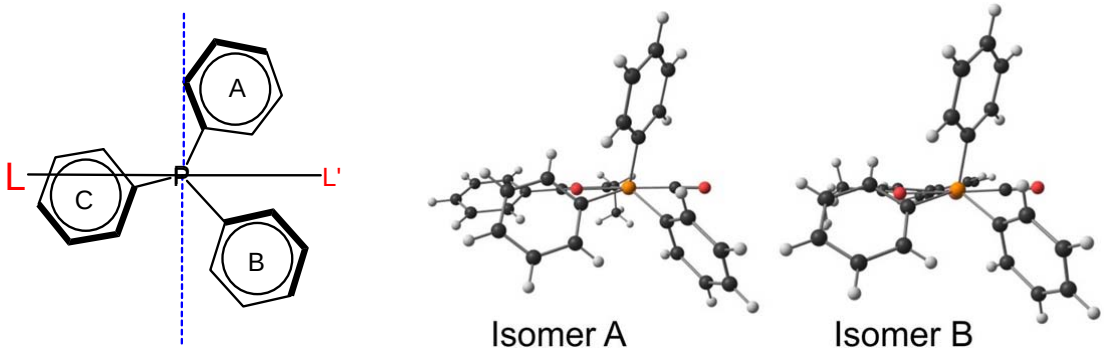

(a) (b)

Figure 3. 8. (a) The preferred conformation minimum energy orientation of PPh$_3$ (as viewed along the P–Metal bond axis), within square planar complexes relative to the plane incorporating all points of minimum steric compression, called the *plane of nadir energy* (plane perpendicular to paper, indicated by the dotted blue lines) .[28] L is more bulky than L′.

(b). View along the P–Rh bond axis showing the PPh$_3$ orientation of the two isomers of [Rh(PhCOCHCOCH$_2$CH$_3$)(CO)(PPh$_3$)]. For comparative reasons, *P* helicities are shown.

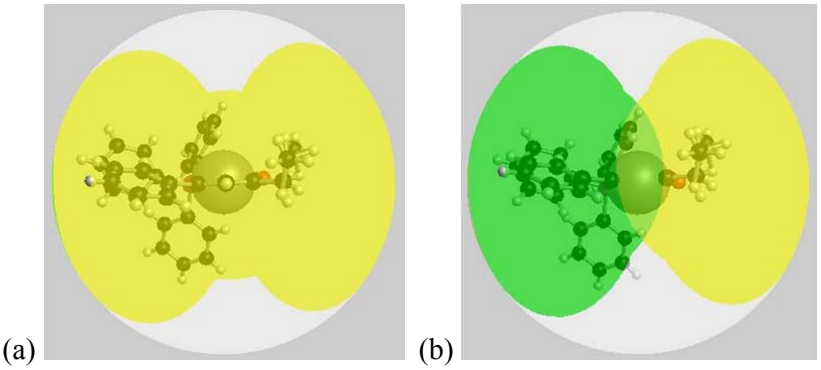

(a) (b)

Figure 3. 9. Solid angle projections on isomer B of [Rh(PhCOCHCOCH$_2$CH$_3$)(CO)(PPh$_3$)].

a) Solid angle projection of the (PhCOCHCOCH$_2$CH$_3$)$^-$ ligand.

b) A solid angle projection of the Ph and CH$_2$CH$_3$ substituents on the (PhCOCHCOCH$_2$CH$_3$)$^-$ ligand. (Reprinted with permission from Hopmann, K.H.; Stuurman, N.F.; Muller, A. and Conradie, J. *Organometallics*, Vol. 29, No. 11, 2010. Copyright 2010 American Chemical Society.)

From the above we observe that both isomers of [Rh(PhCOCHCOCH$_2$CH$_3$)(CO)(PPh$_3$)] were obtained experimentally and that electronic or steric reasons did not prefer one of the isomers. It has also been shown by computational chemical study of the substitution reaction of PPh$_3$ for CO in [Rh(PhCOCHCOCH$_2$CH$_3$)(CO)(PPh$_3$)] that both isomers can form directly from the substitution reaction or from the subsequent isomerisation.[7]

3.2 CV and DFT

Cyclic voltammetry (CV), Oster Young square wave voltammetry (SW) and linear sweep voltammetry (LSV) were performed on all synthesized gamma substituted compounds. The formal reduction potentials, $E^{0'}$, of the redox active species were determined in acetonitrile containing 0.1 mol.dm^{-1} tetrabutylammonium tetrakis[pentafluorophenyl]borate ([NBu$_4$][PF$_6$]) as the supporting electrolyte in order to limit interaction of the solvent or electrolyte to a minimum, either by means of solvation or ion-paring interactions.

Although electrochemically reversible one-electron redox couples are theoretically characterized by $\Delta E_p = E_{pa} - E_{pc} = 59$ mV[32], in this study an *experimentally* determined value of $\Delta E_p < 90$ mV will be considered small enough to imply electrochemical reversibility. Quasi-reversible processes will be assigned to any process showing 90 mV $< \Delta E_p <$ 150 mV, while irreversible electrochemistry will be assigned to a process showing $\Delta E_p > 150$ mV. Peak current ratios were always calculated as i_{pa}/i_{pc} for reduction processes and i_{pc}/i_{pa} for oxidation processes. Formal redox potentials ($E^{o'}$), anodic peak potential (E_{pa}) and cathodic peak potentials (E_{pc}) were measured experimentally *vs* an in-house constructed Ag/Ag$^+$ reference electrode. For this study, Fc/Fc$^+$ = 0.073 V *vs*, Ag/Ag$^+$.

3.2.1 Gamma-substituted β-diketones.

The electrochemical behaviour of gamma substituted β-diketones has been investigated in this study. The cyclic voltammograms of the following gamma substituted β-diketones are recorded in [NBu$_4$][PF$_6$] / CH$_3$CN:

i) CH$_3$COCH(**HOC$_6$H$_4$COO**)COCH$_3$, (Hβ1a)

ii) CH$_3$COCH(**HOC$_6$H$_4$C$_2$H$_2$COO**)COCH$_3$, (Hβ2a)

iii) CH$_3$COCH(**C$_{10}$H$_{21}$OC$_6$H$_4$COO**)COCH$_3$, (Hβ3a)

iv) $CH_3COCH(\mathbf{C_{10}H_{21}OC_6H_4COOC_6H_4COO})COCH_3$ (Hβ4a); and
v) $CH_3COCH(\mathbf{C_{10}H_{21}OC_6H_4C_2H_2COOC_6H_4COO})COCH_3$ (Hβ5a).

Their ability to gain an electron to form a corresponding anion radical makes neutral organic β-diketone molecules interesting. This is possible due to their delocalized π-electron system. Cyclic voltammetry was first done on pentane-2,4-dione (Hacac) to investigate the reduction of the β-diketone backbone. The CV showed an irreversible process of a one electron reduction at *ca* -2500 mV, which formed a chemically unstable anion radical (see **Figure 3. 10**). Due to the instability of this anionic radical, no re-oxidation peak was observed in the voltammogram. It is the enol form of the β-diketone that is reduced. In aprotic solvents an enol form is dominant by more than 85%. Due to the fast keto-enol isomerization, isomerization to the enol form occurs faster than the time-scale of the CV. Therefore, all the β-diketone in the vicinity of the working electrode is conversed to the enol form during the CV.

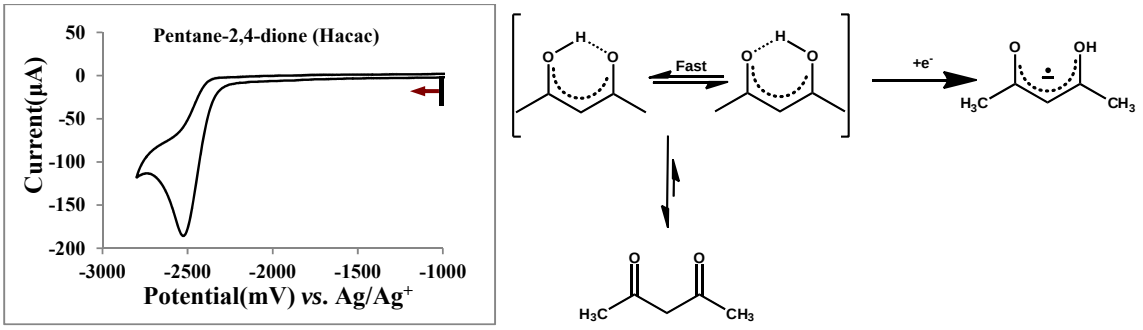

Figure 3. 10. Cyclic voltammogram (*vs.* Ag/Ag^+) for pentane-2,4-dione (Hacac) at scan rate of 100 mV s^{-1}. Scans initiated in the direction of the arrow. Measured in 0.1 mol dm^{-3} $[NBu_4][PF_6]$ /CH_3CN on a glassy carbon working electrode at 25 °C. [Hacac] = 1 mmol dm^{-3}.

A similar irreversible reduction process was observed for all the gamma-substituted β-diketones of this study. No re-oxidation peak is observed – only the reduction peak. This is due to the formation of chemically unstable anionic radicals.

Hβ**1a**, 2,4-dioxo-3-pentyl-4-hydroxybenzoate ($CH_3COCH(\mathbf{HOC_6H_4COO})COCH_3$) has two redox centres, the acid moiety of 4-hydroxybenzoic acid and the β-diketone moiety of Hacac. As a consequence, two reduction peaks were expected: at the region of the acid (-2000 mV) and of β-diketone Hacac (-2500 mV). The two electro-active centres give a two times one

electron reduction reaction which is confirmed by linear sweep voltammograms (**Figure 3. 11**). For Hβ**1a,** it is observed that, when attached to Hβ**1a**, the reduction of the acid moiety shifts ca200 mV more negative to the reduction of the free acid.

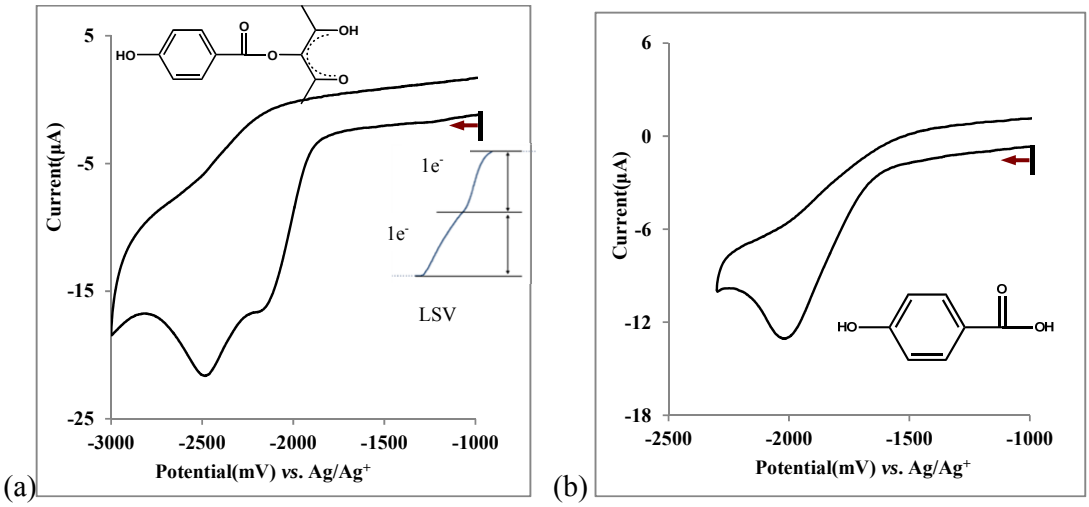

Figure 3. 11. Cyclic voltammograms (*vs*Ag/Ag$^+$) for (a) Hβ1a and (b) 4-hydroxybenzoic acid at scan rates of 100 mVs^{-1}. Scans initiated in the direction of the arrow. Measured in 0.1 mol dm^{-3} [NBu$_4$][PF$_6$] /CH$_3$CN on a glassy carbon working electrode at 25 °C. [Hβ1a] = 1 mmol dm^{-3}. Insert in a): Linear Sweep Voltammogram (LSV).

Similar to what was observed for Hβ**1a**, Hβ**2a** 2,4-dioxo-3-pentyl-4-hydroxycinnamate (CH$_3$COCH(**HOC$_6$H$_4$C$_2$H$_2$COO**)COCH$_3$) has the acid moiety and 4-hydroxycinnamic acid and the β-diketone moiety of Hacac. Two reduction peaks were observed for Hβ**2a**, in the region of the acid and of the Hacac reduction peaks respectively (-2000 mV and -2300 mV). The two electro-active centres each give a two times one electron reduction reaction which is confirmed by linear sweep voltammograms (see **Figure 3. 12**). No shift of the acid moiety reduction was observed when it was attached to the β-diketone but a shift of *ca* 200 mV to less negative potentials of the β-diketone moiety was observed relative to Hacac.

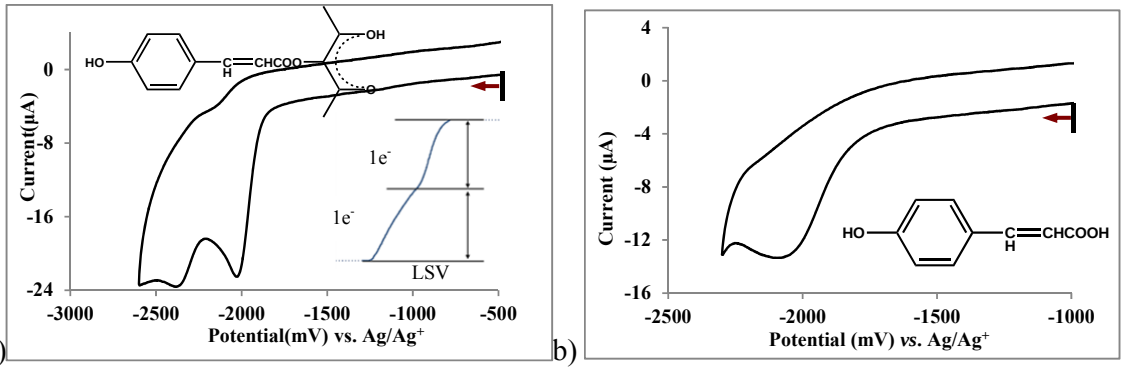

Figure 3. 12. Cyclic voltammograms (*vs* Ag/Ag^+) for (a) Hβ2a and (b) 4-hydroxycinnamic acid at scan rates of 100 mVs^{-1}. Scans were initiated in the direction of the arrow. Measured in 0.1 mol dm^{-3} $[NBu_4][PF_6]$ /CH_3CN on a glassy carbon working electrode at 25 °C. [Hβ2a] = 1 mmol dm^{-3}. Insert in a): Linear Sweep Voltammogram (LSV).

Hβ**3a** 2,4-dioxo-3-pentyl-4-decanyloxybenzoate ($CH_3COCH(\mathbf{C_{10}H_{21}OC_6H_4COO})COCH_3$), which differs from Hβ**1a** by having a long alkyl chain on the gamma substituent, showed a similar CV result to that for Hβ**1a** (see Figure 3. 13). The free acid moiety of Hβ**3a** reduces at *ca* -2300mV (Figure 3. 13**b**). This peak shifts by 100 mV to *ca* -2400 mV when attached to the β-diketone backbone (**Figure 3. 13a**). This reduction of the gamma substituent is at a lower potential (more negative) than that of the gamma substituent of Hβ**1a.** This is possibly caused by stabilization due to the conjugation of a long alkyl-chain substituent. Reduction of the β-diketonato backbone of β-diketones seems to be in the same region of -2500 mV as Hacac and Hβ**1a**. SWV was used to better resolve the two reduction peaks of Hβ**3a**, see **Figure 3. 13a** (insert).

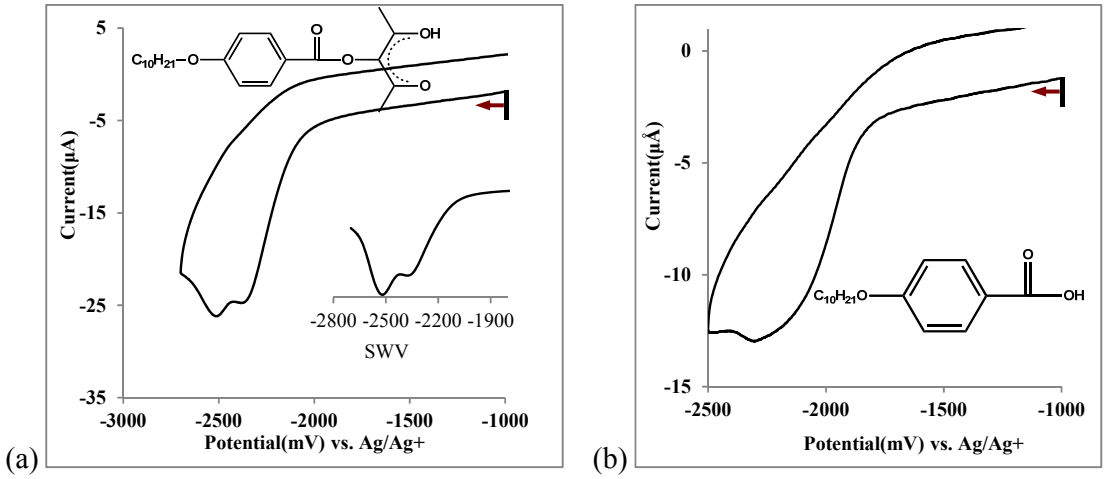

Figure 3. 13. Cyclic voltammograms (*vs* Ag/Ag^{+}) for (a) Hβ3a and (b) gamma substituent at scan rates of 100 mVs^{-1}. Scans initiated in the direction of the arrow. Measured in 0.1 mol dm^{-3} $[NBu_4][PF_6]$ /CH_3CN on a glassy carbon working electrode at 25 °C. [Hβ3a] = 1 mmol dm^{-3}. Insert in a): Square Wave Voltammogram (SWV).

In Hβ**1a**; Hβ**2a** and Hβ**3a,** the reduction of the gamma substituent is at a higher potential (less the negative potential) than that of the β-diketonato backbone (more negative). However, in comparing Hβ**1a** and Hβ**3a,** we observe that the reduction of the gamma substituent with the increased chain of Hβ**3a** is at a lower (more negative) potential than that of Hβ**1a**. There is no significant effect on the redox behaviour of the β-diketone backbone, as shown by an increased alkyl chain on the gamma substituent.

Hβ**4a** ($CH_3COCH($**$C_{10}H_{21}OC_6H_4COOC_6H_4COO$**$)COCH_3$) has three electro-active centres: two from its acid gamma substituent precursor and one on the β-diketone backbone. The CV of the acid gamma substituent precursor and Hβ**4a** are displayed in **Figure 3. 14**. The LSV clearly show three one electron reduction processes. The first reduction of the acid gamma substituent precursor is at *ca* -2100 mV, the same region as the first reduction observed for Hβ**4a**. The second and third reduction processes of Hβ**4a** are very near to each other and it is not clear from experimental observation which occurs on the β-diketone backbone of Hβ**4a** and which at the gamma substituent fragment.

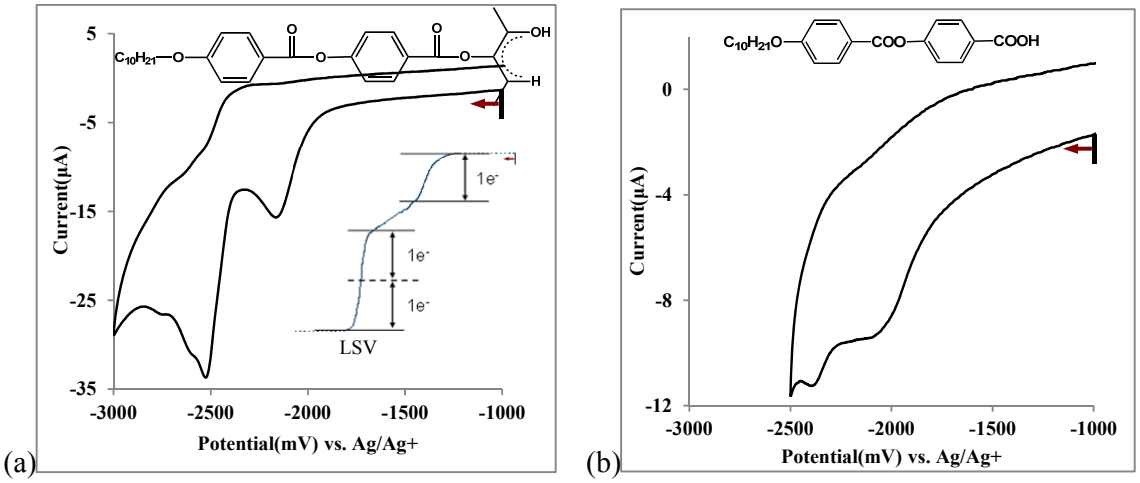

Figure 3. 14. Cyclic voltammograms (*vs.* Ag/Ag^{+}) for (a) Hβ4a and (b) gamma substituent at scan rates of 100 mVs^{-1}. Scans initiated in the direction of the arrow. Measured in 0.1 mol dm^{-3} $[NBu_4][PF_6]$ /CH_3CN on a glassy carbon working electrode at 25 °C. [Hβ4a] = 1 mmol dm^{-3}. Insert in a): Linear Sweep Voltammogram (LSV).

Hβ5a ($CH_3COCH(C_{10}H_{21}OC_6H_4C_2H_2COOC_6H_4COO)COCH_3$) has three electro-active centres: two from its acid gamma substituent precursor and one on the β-diketone backbone (see **Figure 3. 15 b**). The first reduction of the acid gamma substituent precursor is at *ca* -2100 mV, the same region as the first reduction observed for the acid moiety. The second and third reduction processes of Hβ**5a** are at *ca* -2100 mV and -2700 mV. It is not clear from experimental observation which processes occur on the β-diketone backbone of Hβ**5a** and which at the gamma substituent fragment.

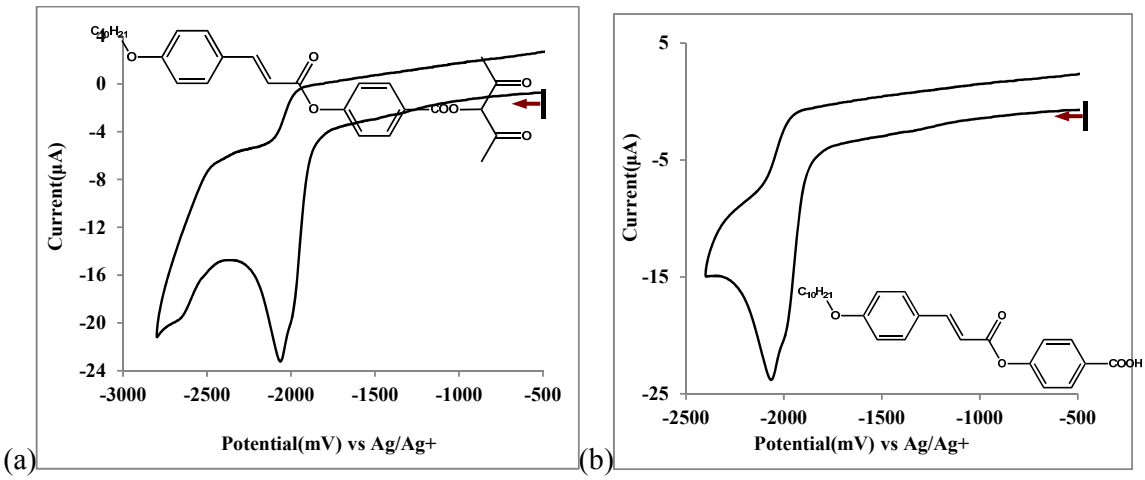

Figure 3. 15. Cyclic voltammograms (*vs.* Ag/Ag^{+}) for (a) Hβ5a and (b) gamma substituent at scan rates of 100 mVs^{-1}. Scans initiated in the direction of the arrow. Measured in 0.1 mol dm^{-3} $[NBu_4][PF_6]$ /CH_3CN on a glassy carbon working electrode at 25 °C. [Hβ5a] = 1 mmol dm^{-3}.

3.2.2 DFT calculations as a tool to understand the CV of γ substituted β-diketones

To validate the reduction processes of the gamma substituted β-diketones further, a DFT computational study was done. The neutral β-diketones, the reduced, doubly and triply reduced β-diketones, as applicable, were optimized. Because the reduction of a complex involves the addition of an electron to the lowest unoccupied molecular orbital (LUMO) of the complex, the location of the LUMO will show where the reduction process take place. By the same way of reasoning, the highest occupied molecular orbital (HOMO) of the species that is reduced, will show where the reduction took place.

Experimentally, Hβ**1a** ($CH_3COCH(\mathbf{HOC_6H_4COO})COCH_3$) showed two one-electron reduction peak processes at *ca* -2000 mV and -2500 mV. The first reduction peak was described as the reduction of the acid moeity in Hβ**1a**, because the free acid reduced at *ca* -2000 mV. The second reduction peak was described as the reduction of the β-diketonato ligand in Hβ**1a**, since Hacac reduced at *ca* -2500 mV. The reduction process can thus be described as:

$$H\beta\mathbf{1a}^{-2} \xleftarrow{+e^-} H\beta\mathbf{1a}^{-} \xleftarrow{+e^-} H\beta\mathbf{1a}$$

During reduction of Hβ**1a**, an electron an electron is added to its LUMO. Thus, either the LUMO of Hβ**1a** or the HOMO of the reduced species $H\beta\mathbf{1a}^-$ will show where the first reduction took place. Similarly the LUMO of the reduced species $H\beta\mathbf{1a}^-$ or the HOMO of the double reduced species $H\beta\mathbf{1a}^{2-}$ will show where the second reduction took place. **Figure 3. 11** shows that the first reduction mainly took place on the acid moeity of Hβ**1a,** while the second reduction clearly took place on the β-diketonato backbone of Hβ**1a**. (The triplet $H\beta\mathbf{1a}^{2-}$ is 0.52 eV more stable than the singlet $H\beta\mathbf{1a}^{2-}$)

An additional argument in favour of the first reducion taking place on the acid moeity of Hβ**1a** is that the calculated electron affinity (EA) of the acid (-0.23 V) > EA for Hacac (-0.43 V), thus the acid chain, will be reduced first, at higher (less negative) potential than the β-diketonato backbone of Hβ**1a**.

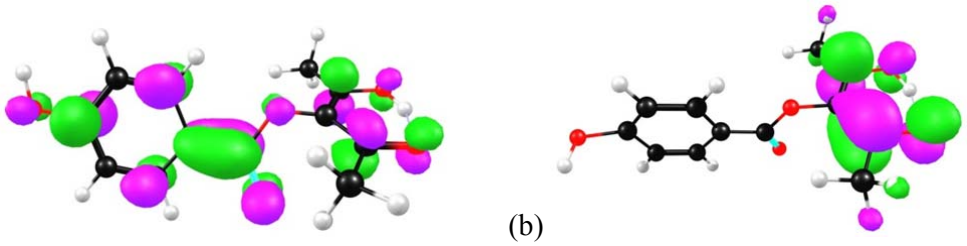

(a) (b)

Figure 3. 16. Visualisation of the HOMO of (a) the reduced species Hβ1a^{-} (first reduction) and (b) the double reduced species Hβ1a^{2-} (second reduction).

Two reduction processes were experimentally observed for Hβ**2a** according to:

$$H\beta\mathbf{2a}^{-2} \xleftarrow{+e^-} H\beta\mathbf{2a}^{-} \xleftarrow{+e^-} H\beta\mathbf{2a}$$

Experimentally, the first reduction peak was described as the reduction of the acid moeity in Hβ**2a**, because the free acid reduced at *ca* -2000 mV. The second reduction peak was described as the reduction of the β-diketonato ligand in Hβ**2a**, because Hacac reduced at *ca* -2500 mV. In agreement with the experiment, the HOMO of Hβ**2a**$^{-}$ is mainly on the acid moeity (first reduction) and that of Hβ**2a**$^{2-}$ on the β-diketonato backbone of Hβ**2a** (second reduction), see **Figure 3. 17**. (The triplet Hβ**2a**$^{2-}$ is 0.16 eV more stable than the singlet Hβ**2a**$^{2-}$). The calculated electron affinity (EA) of the acid (+0.40 V) > EA for Hacac (-0.43 V), *i.e.* the acid chain, will be reduced first, at higher (less negative) potential than the β-diketonato backbone of Hβ**2a**.

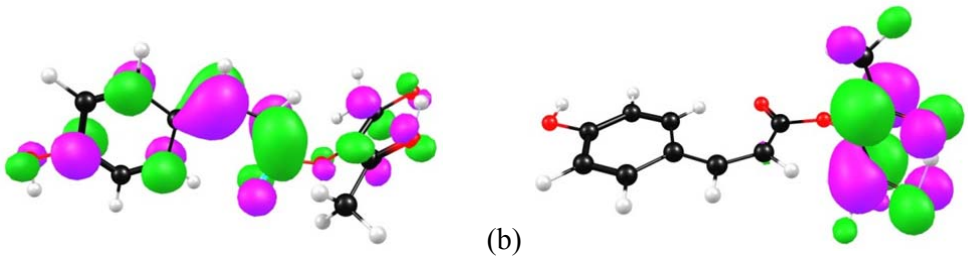

(a) (b)

Figure 3. 17. Visualisation of the HOMO of: (a) the reduced species Hβ2a^{-} (first reduction) and (b) the double reduced species Hβ2a^{2-} (second reduction).

In going from Hβ**1a** to Hβ**3a**, the only structural difference is the $C_{10}H_{21}$ alkyl chain on Hβ**3a**. As for Hβ**1a**, the two reduction processes were also experimentally observed for Hβ**3a.** According to $H\beta\mathbf{3a}^{-2} \xleftarrow{+e^-} H\beta\mathbf{3a}^{-} \xleftarrow{+e^-} H\beta\mathbf{3a}$, the first reduction process experimentally observed in the region is that of the reduction of the free acid of Hβ**3a**. DFT calculations on a simplified model of Hβ**3a**, with a reduced C_5H_{11} alkyl chain again show that the HOMO of

Hβ**3a**$^{-}$ is mainly on the acid moeity (first reduction) and that of Hβ**3a**$^{2-}$ on the β-diketonato backbone of Hβ**3a** (second reduction), see **Figure 3. 17**. (The triplet of the simplified Hβ**3a**$^{2-}$ is 0.28 eV more stable than the singlet Hβ**3a**$^{2-}$).

The calculated electron affinity is (EA) of Hβ**1a** (+0.67 V) > EA of simplified Hβ**3a** (0.39 V); thus the first reduction of Hβ**1a,** will occur at a higher (less negative) potential than that the first reduction of Hβ**3a**. This agrees well with the experiment in which the first reduction process of Hβ**1a** was observed at *ca* -2000 mV and that of Hβ**3a** was observed at *ca* -2300 mV.

(a) (b)

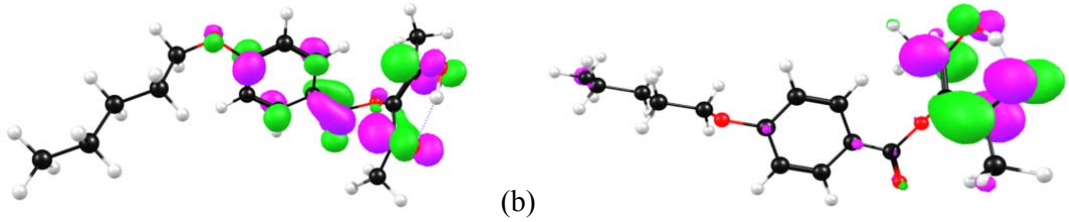

Figure 3. 18. Visualisation of the HOMO of a simplified version of (a) the reduced species Hβ3a^{-} (first reduction) and (b) the double reduced species Hβ3a^{2-} (second reduction).

Hβ**4a** contains two of the acid precursor moeities of Hβ**1a,** as well as the $C_{10}H_{21}$ alkyl chain. Three reduction processes were experimentally observed for Hβ**4a** according to:

$$H\beta\mathbf{4a}^{-3} \xleftarrow{+e^-} H\beta\mathbf{4a}^{-2} \xleftarrow{+e^-} H\beta\mathbf{4a}^{-} \xleftarrow{+e^-} H\beta\mathbf{4a}$$

The first reduction process experimentally observed for Hβ**4a** is in the region of the reduction of the free acid precursor of Hβ**1a**. The second and third reduction precesses were very near to each other and it is not clear from experimental observation which occurs on the β-diketone backbone of Hβ**4a** and which at the gamma substituent fragment. DFT calculations on a simplified version of Hβ**4a,** in which the $C_{10}H_{21}$ chain was replaced by H, give the following results. The LUMOs of Hβ**4a**, Hβ**4a**$^{-}$ and Hβ**4a**$^{2-}$ and the HOMOs of Hβ**4a**$^{-}$, Hβ**4a**$^{2-}$ and Hβ**4a**$^{3-}$ are displayed in **Figure 3. 19**. The LUMO shows where the reduction process will take place, while the HOMO of the reduced species of the complex shows where the reduction took place. It is clear from **Figure 3. 19** that the LUMO of a species corresponds to the HOMO in its reduced form. The MOs of **Figure 3. 19** also indicate that the first reduction takes place mainly on the acid moeity of Hβ**4a**, the second reduction on the β-diketonato backbone of Hβ**4a** and the third reduction on the acid moeity of Hβ**4a**.

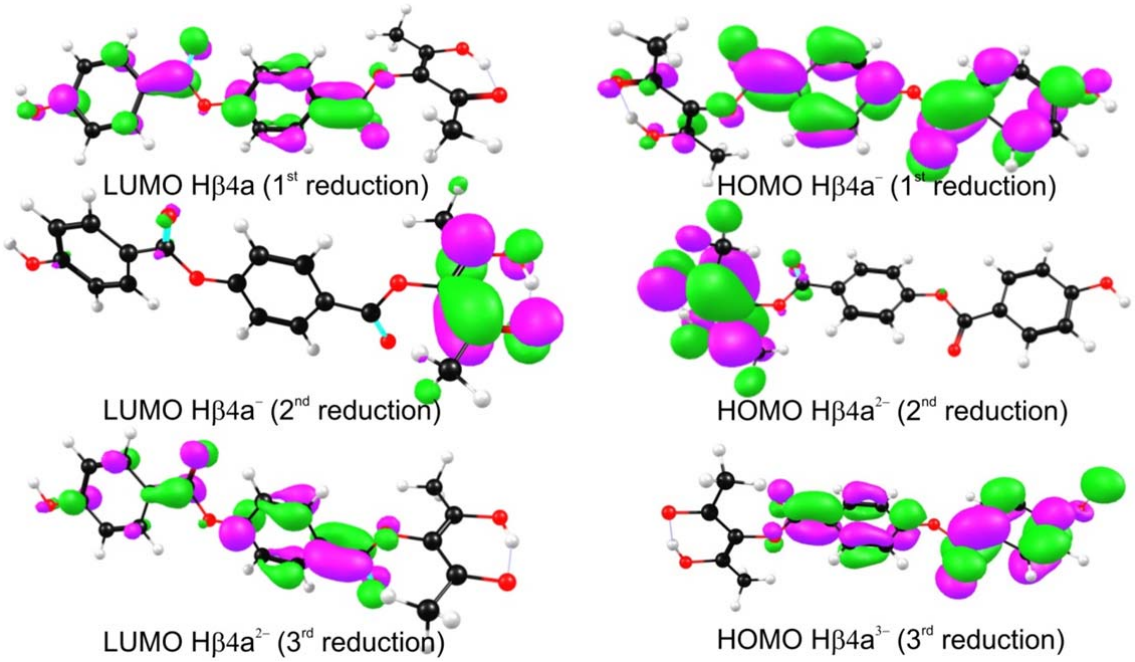

Figure 3. 19. Visualisation of the HOMOs and LUMOs of a simplified version of Hβ4a and its reduced species.

In calculating the optimized geometry of the different reduced species, it is important to determine the lowest energy spin state (ie. the amount of unpaired electrons) of each reduced species. The MO energy level diagram in **Figure 3. 20** visualize the reduction process of Hβ**4a**. The neutral Hβ**4a** is a singlet (no unpaired electrons), see the MO energy level diagram left in **Figure 3. 20**. Upon reduction, one electron is added to the LUMO of Hβ**4a.** The reduced Hβ**4a**$^{-}$ is thus a doublet with one unpaired electron (S = ½). Another reduction involves a second electron to be added to the complex to form the Hβ**4a**$^{2-}$ species. The Hβ**4a**$^{2-}$ species can either be a singlet with no unpaired electrons (S = 0) or a triplet (S = 1) with two unpaired electrons. The triplet (S = 1) of the simplified Hβ**4a**$^{2-}$ is 0.41 eV more stable than the singlet (S = 0) Hβ**4a**$^{2-}$, implying that Hβ**4a**$^{2-}$ is a triplet. After the third reduction, three electrons have been added to the complex (one upon each reduction). The Hβ**4a**$^{3-}$ species could thus be a doublet (S = ½ i.e. one unpaired electron) or a quartet (S = 3/2, i.e. three unpaired electrons). The doublet (S = ½) of the simplified Hβ**4a**$^{3-}$ is 0.77 eV more stable than the quartet Hβ**4a**$^{3-}$ (S = 3/2), implying Hβ**4a**$^{3-}$ is a doublet.

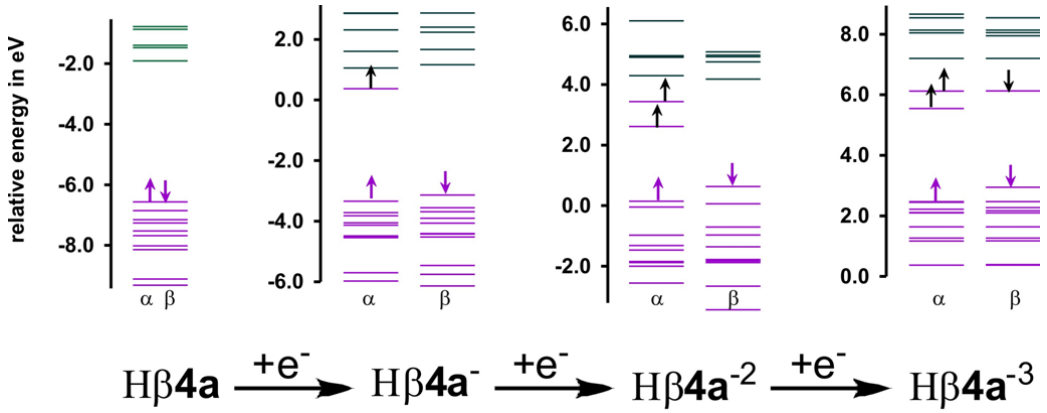

Figure 3. 20. MO energy level diagram of Hβ4a and its reduced species. The purple lines represent the frontier occupied energy levels. Each of these energy levels contain 2 electrons, only the two electrons in the HOMO of the neutral Hβ4a are shown for simplicity (purple arrows). The up arrows indicate α electrons (spin up) and the down arrows β (spin down) electrons. The green lines represent the frontier unoccupied energy levels. The black arrows represent the electrons added upon each reduction.

Hβ**5a** contains the acid precursor moeity of Hβ**1a**, the acid precursor moeity of Hβ**2a,** as well as the $C_{10}H_{21}$ alkyl chain. Three reduction processes are thus expected for Hβ**5a** according to:

$$H\beta\mathbf{5a}^{-3} \xleftarrow{+e^-} H\beta\mathbf{5a}^{-2} \xleftarrow{+e^-} H\beta\mathbf{5a}^{-} \xleftarrow{+e^-} H\beta\mathbf{5a}$$

Experimentally, it is not clear where the processes take place. The HOMOs of Hβ**5a**$^{-}$, Hβ**5a**$^{2-}$ and Hβ**5a**$^{3-}$ displayed in **Figure 3. 21**, predict that the first reduction takes place on the acid moeity of Hβ**5a**, the second reduction on the β-diketonato backbone of Hβ**5a** and the third reduction on the acid moeity of Hβ**5a**.

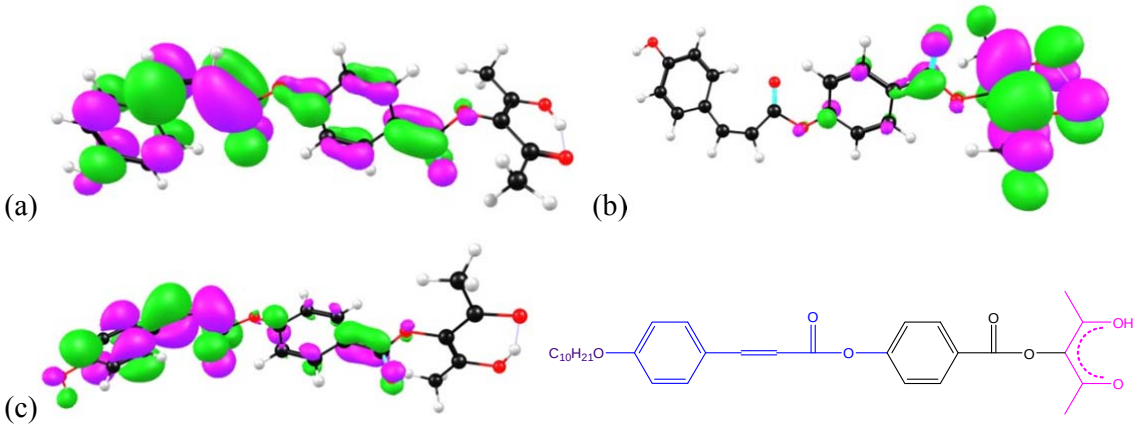

Figure 3. 21. Visualisation of the HOMO of a simplified version of (a) the reduced species Hβ5a^{-} (first reduction); (b) the double reduced species Hβ5a^{2-} (second reduction) and (c) the triply reduced species Hβ5a^{3-} (third reduction).

3.2.3 Rh(I)-dicarbonyl complexes

Yellow [Rh(β-diketonato)$(CO)_2$] complexes from the synthesised γ-substituted β-diketones (Hβ**1a-5a**) were obtained and CV experiments were performed in acetonitrile as the solvent. Similar work done by Conradie *et al.*[33] suggests that [Rh(RCOCHCOR′)$(CO)_2$] (R= Fc and R′ = CF_3; CH_3; Ph; Fc) in a solvent like acetonitrile, the rhodium nucleus undergoes a two-electron transfer process in which a slow dynamic equilibrium of rhodium(I) to rhodium(III) is generated. It is further suggested that there are two oxidation waves per rhodium complex due to the presence of another rhodium complex [Rh(RCOCHCOR′)$(CO)_2$solvent] in which the solvent coordinates with the rhodium metal which is in equilibrium with the solvent-free complex [Rh(RCOCHCOR′)$(CO)_2$]. Two anodic peaks per rhodium nucleus are therefore observed where the peak that is at lower potential is assigned to the solvent-free rhodium complex while, at higher potentials, a peak for the solvated rhodium complex is assigned.[33] It is expected that the solvent-free complex will be oxidized more easily than the complex that has been stabilized with solvent molecules. In this study, complex [Rh(acac)$(CO)_2$] has two redox centres: the oxidation of Rh and a reduction centre for the β-diketonato ligand. A solvent free rhodium(I) which is in equilibrium with a solvated rhodium(I) is assumed. The irreversible oxidation of rhodium(I) to rhodium(III), as well as the reduction of the β-diketonato ligand was observed for both the solvent free rhodium complex and the solvated rhodium complex each(see **Figure 3. 22**). No reduction peak coupled to the rhodium(I) oxidation was observed during the negative scans, only the reduction of the β-diketonato ligand. This indicates that there is no Rh(III) present in the analyte solution and that the observed reduction of the rhodium(III) species can only be generated by the oxidation of the Rh(I) (**Figure 3. 22** insert).

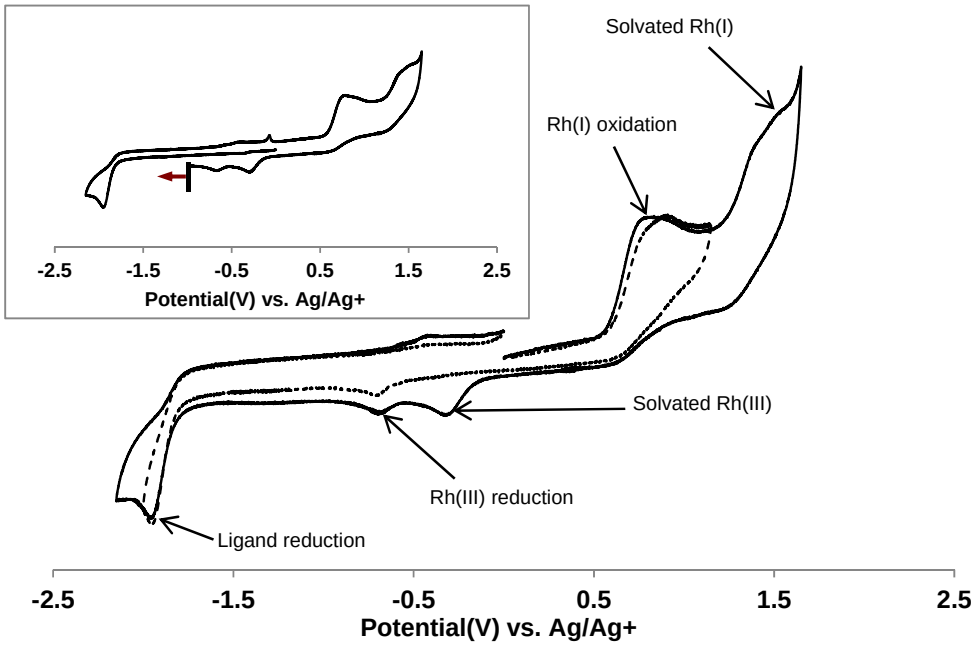

Figure 3. 22. Cyclic voltammetry of 1mmol dm^{-3} solution of [Rh(acac)(CO)$_2$] in acetonitrile at 25°C, utilising a glassy carbon working electrode. Positive scan rate = 100mVs^{-1}, supporting electrolyte = 0.1 mol dm^{-3} [NBu$_4$][PF$_6$]. Insert: Negative scan showing first reduction of only the ligand.

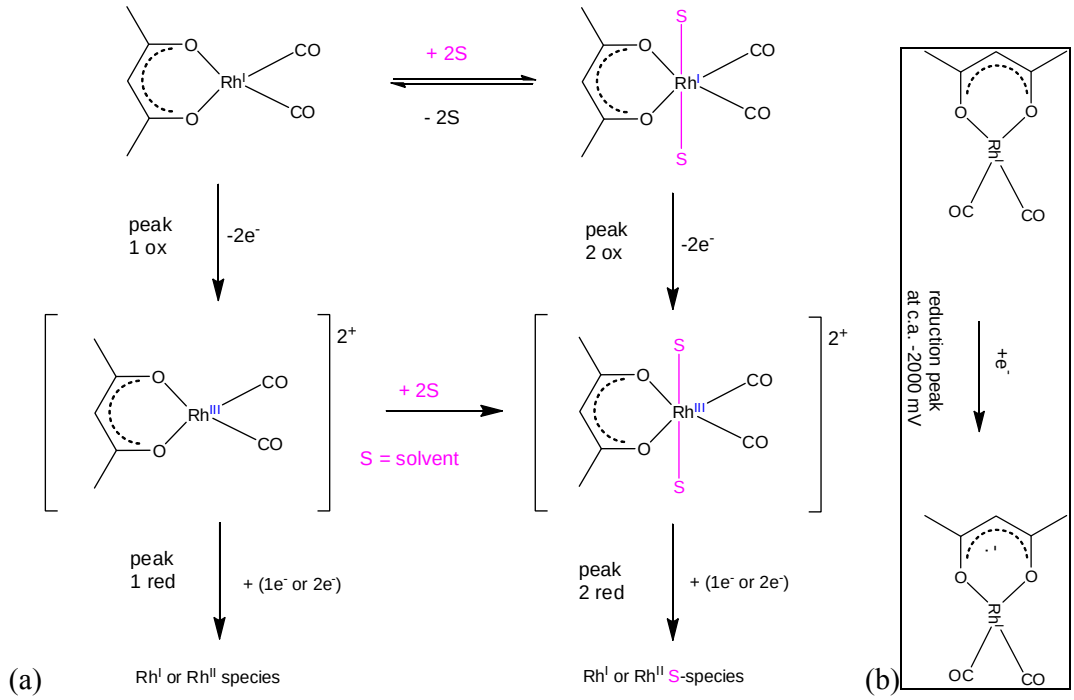

Scheme 3. 11. (a) Redox process for the solvent-free and the solvated rhodium complexes [Rh(acac)(CO)$_2$] and [Rh(acac)(CO)$_2$ solvent]; (b) Reduction of the ligand.

Electrochemical results are therefore consistent with the general electrochemical scheme proposed in **Scheme 3. 11**.

Although the redox behaviour of [Rh(**β1a**)$(CO)_2$] is similar to that of [Rh(**acac**)$(CO)_2$] (**Figure 3. 23**), it is evident that, at lower scan rates (100 mV and lower), there is no reduction of Rh(III) from either the solvated and the solvent free rhodium complexes; there is only ligand reduction for the forward and the reverse scans (see insert of **Figure 3. 23**). At low scan rates, the oxidized species diffuses away from the electrode before it can be reduced.

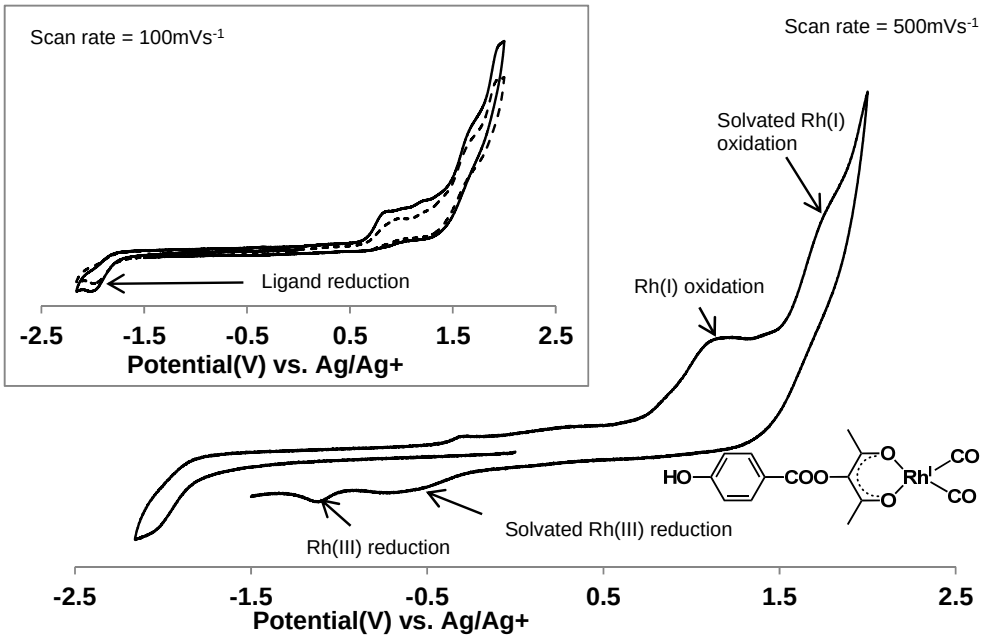

Figure 3. 23. Cyclic voltammetry of 1mmol dm^{-3} solution of [Rh(β1a)$(CO)_2$] in acetonitrile at 25 °C utilising a glassy carbon working electrode at 500mVs^{-1}, supporting electrolyte = 0.1 mol dm^{-3} [NBu_4][PF_6]. Insert: Solid line indicative of a negative scan and dotted line indicative of a positive scan, both showing no reduction of Rh(III) but of only the ligand at 100 mVs^{-1}.

For the [Rh(**β2a**)$(CO)_2$] complex, there seems to be only one rhodium redox process which stabilizes – because no such formation of a solvated rhodium complex is observed. Only the oxidation of rhodium(I) is observed at slow scan rates, but both the oxidation and reduction processes of rhodium are observed at higher scan rates (see **Figure 3. 24**).

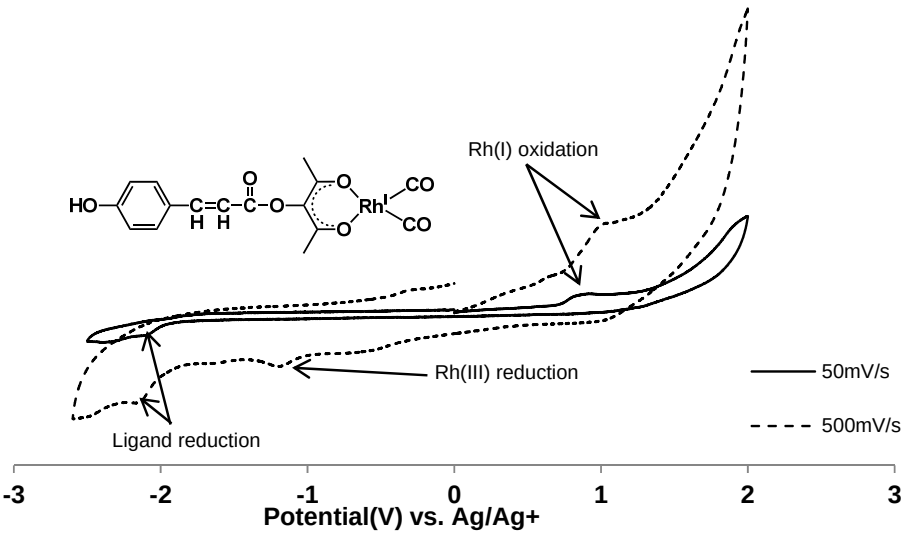

Figure 3. 24. Cyclic voltammetry of 1mmol dm^{-3} solution of [Rh(β2a)$(CO)_2$] in acetonitrile at 25°C utilising a glassy carbon working electrode at 50mVs^{-1} and 500mVs^{-1}, supporting electrolyte = 0.1 mol dm^{-3} [NBu_4][PF_6].

Both the solvent-free and solvated rhodium complexes undergo oxidation and reduction processes in [Rh(**β3a**)$(CO)_2$] (**Figure 3. 25**). An increase in the scan rate and, after the redox process, rhodium complexes shift the ligand reduction from -1900 mV to higher potentials (less negative values) -1500 mV. This was clearly observed when a negative scan was run at 200 mVs^{-1} (see insert: **Figure 3. 25**). Unidentified species resulted to oxidation peaks that were observed after the oxidation of the rhodium centre.

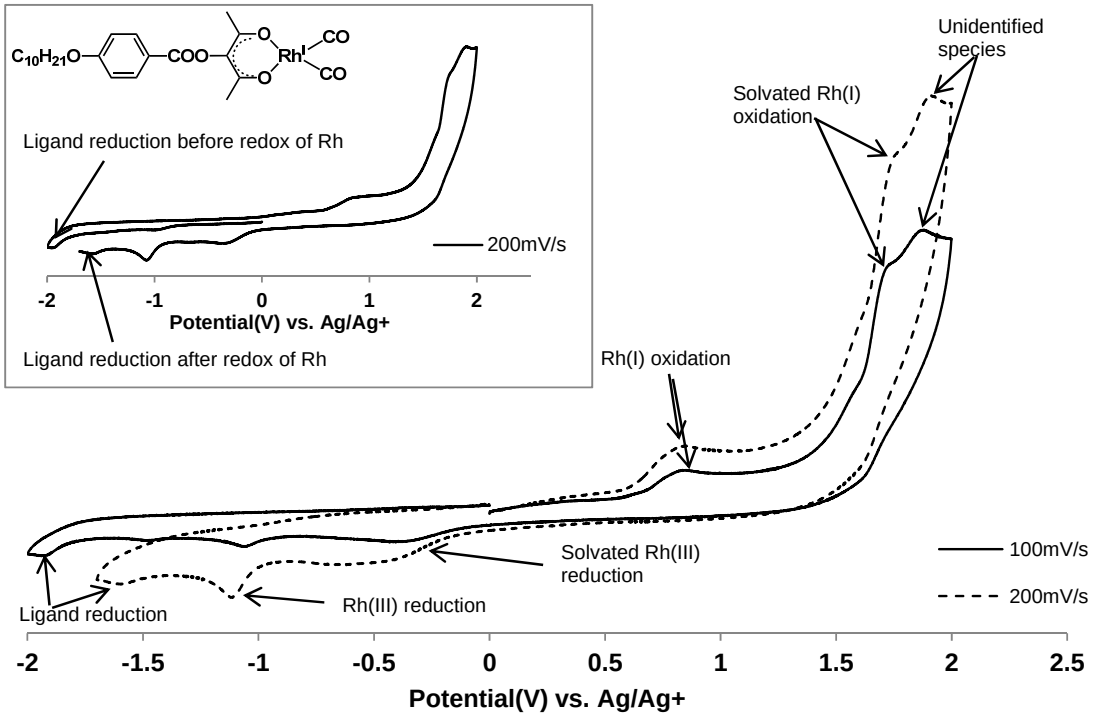

Figure 3. 25. Cyclic voltammetry of 1mmol dm^{-3} solution of [Rh(β3a)$(CO)_2$] in acetonitrile at 25 °C, utilising a glassy carbon working electrode at 100mVs^{-1} and 200mVs^{-1}, supporting electrolyte = 0.1 mol dm^{-3} [NBu_4][PF_6].

Insert: CV of [Rh(β3a)$(CO)_2$]. A negative scan at 200mVs^{-1} shows ligand reduction before and after the redox of rhodium complexes.

For [Rh(β**4a**)$(CO)_2$], reduction of the ligand is observed at -2000 mV, while no reduction of any of the rhodium complexes is witness at low scan rates of 50 mV/s (see insert in **Figure 3. 26**). Multiple oxidation peaks are observed in [Rh(**β4a**)$(CO)_2$] after Rh(I) oxidation was caused by the formation of unidentified species (see **Figure 3. 26**).

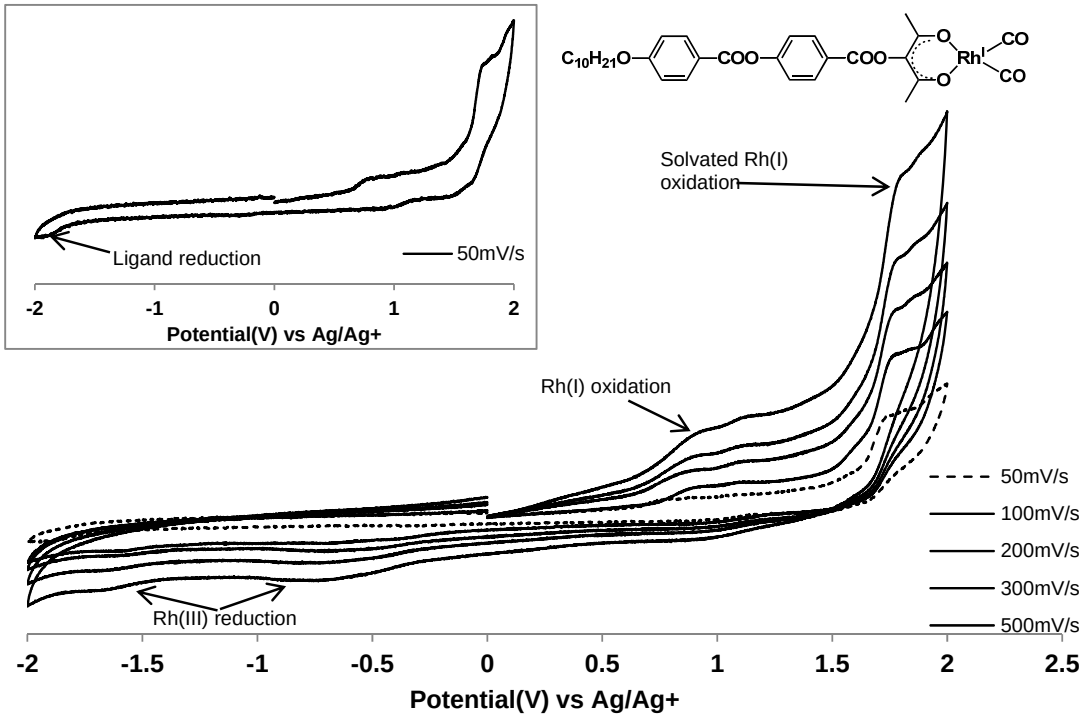

Figure 3. 26. Cyclic voltammetry of 1mmol dm^{-3} solution of [Rh(β4a)$(CO)_2$] in acetonitrile at 25 ˚C utilising a glassy carbon working electrode at 50mVs^{-1},100mVs^{-1}, 200mVs^{-1}, 300mVs^{-1} and 500mVs^{-1}, supporting electrolyte = 0.1 mol dm^{-3} [NBu_4][PF_6].

Insert: CV of [Rh(β4a)$(CO)_2$] a scan at 50mVs^{-1} showing the ligand reduction peak.

Multiple oxidation peaks are also observed in [Rh(**β5a**)$(CO)_2$] after Rh(I) oxidation was caused by the formation of unidentified species (see **Figure 3. 27**). A broad peak at -400 mV is observed for the reduction of both solvent-free and solvated rhodium complexes. No reduction of the rhodium complex is observed at low scan rates (50 and 100 mVs^{-1}). The ligand reduction remains at -2000 mV.

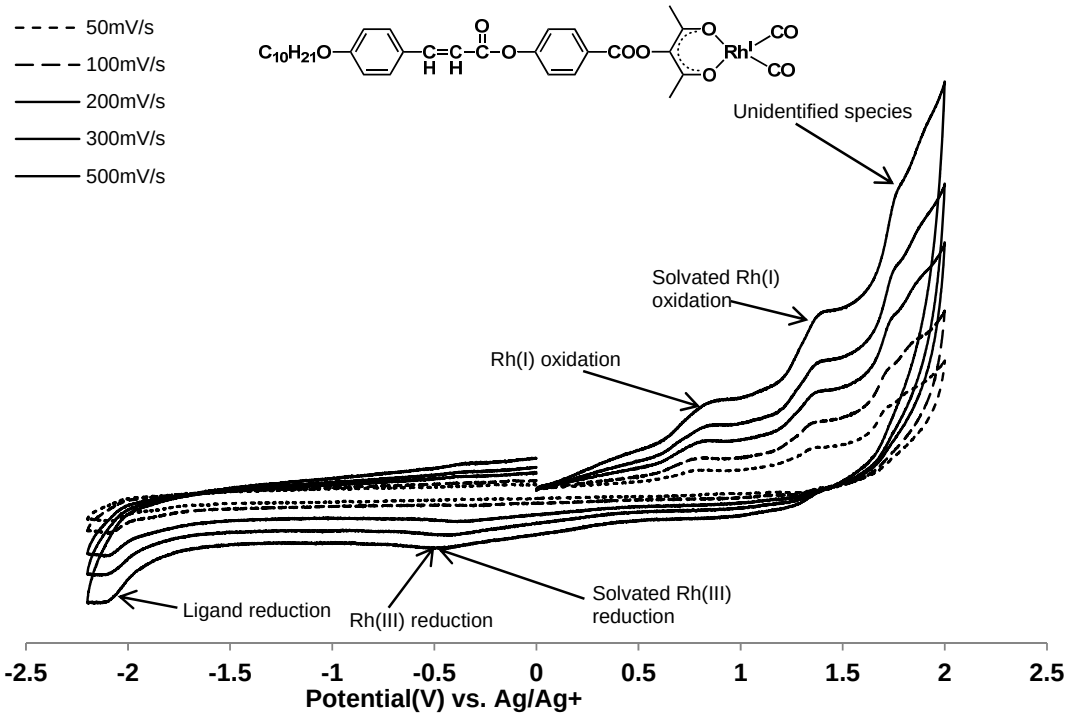

Figure 3. 27. Cyclic voltammetry of 1mmol dm^{-3} solution of [Rh(β5a)(CO)$_2$] in acetonitrile at 25 °C, utilising a glassy carbon working electrode at 50mVs^{-1},100mVs^{-1}, 200mVs^{-1}, 300mVs^{-1} and 500mVs^{-1}, supporting electrolyte = 0.1 mol dm^{-3} [NBu$_4$][PF$_6$].

3.2.4 Rh(I)-monocarbonyl-PPh$_3$ complexes.

The electrochemical behaviour of [Rh(β-diketonato)(CO)(PPh$_3$)] complexes was studied in acetonitrile containing 0.1 mol dm^{-3} tetra-*n*-butylammonium hexafluorophosphate {[N(nBu$_4$)][PF$_6$]}, utilizing a glassy carbon working electrode. The choice of acetonitrile as the solvent ensures that there is a two-electron oxidation process on the rhodium(I) centre which is analogous with the oxidation of rhodium(I) during oxidative addition with methyliodide.[33, 34] Anodic peak potential (E_{pa}) and cathodic peak potentials (E_{pc}) are reported *vs* FcH/FcH$^+$ as internal standard.

The focus of this part of the study is the oxidation potential of the different [Rh(β-diketonato)(CO)(PPh$_3$)] complexes and not on the reduction processes. The ease of oxidation of Rh(I) to Rh(III) is related to the kinetic rate constant of oxidative addition of CH$_3$I to Rh(I) in [Rh(β-diketonato)(CO)(PPh$_3$)] complexes.[35] The rate oxidative addition of CH$_3$I to Rh(I) has important application in catalysis, for example in the Monsanto process.[36] **Table 3. 2**

gives the oxidation potential of rhodium(I) to rhodium(III) for [Rh(acac)(CO)(PPh3)], [Rh(β2a)(CO)(PPh3)], Rh(β3a)(CO)(PPh3)] and [Rh(β4a)(CO)(PPh3)] complexes.

Table 3. 2. Cyclic voltammetry data of [Rh(acac)(CO)(PPh_3)], [Rh(Hβ2a)(CO)(PPh_3)], Rh(Hβ3a)(CO)(PPh_3)] and [Rh(Hβ4a)(CO)(PPh_3)] complexes in acetonitrile containing 0.1 mol dm^{-3} [$N(nBu_4)$][PF_6] at 25°C and a scan rate of 100 mV/s

Complex	E_{pa} (mV)	E_{pc} (mV)	ΔE_p
[Rh(acac)(CO)(PPh_3)]	321	1245	-923
[Rh(β2a)(CO)(PPh_3)]	412	1307	-1038
[Rh(β3a)(CO)(PPh_3)]	299	1000	-701
[Rh(β4a)(CO)(PPh_3)]	353	1167	-814

For the [Rh(β-diketonato)(CO)(PPh_3)] complexes considered in this study, ferrocene was used as the internal standard and potentials are reported as opposed to FcH/FcH^+. Oxidation of the internal standard ferrocene occurs at lower potentials than the rhodium centre. In all the complexes studied, ΔE_p is far larger than 100 mV. This indicates that all the complexes give a definite electrochemically irreversible system. In [Rh(acac)(CO)(PPh_3)] (see **Figure 3. 28(a)**) at various scan rates, there is a sharp oxidation peak of Rh(I) at about 380 mV during the positive scan. This peak increases with increasing scan rates. The reduction peak of Rh(III)-species is observed at -800 mV and the reduction of the ligand at -2500 mV also increases with an increase in the scan rate.

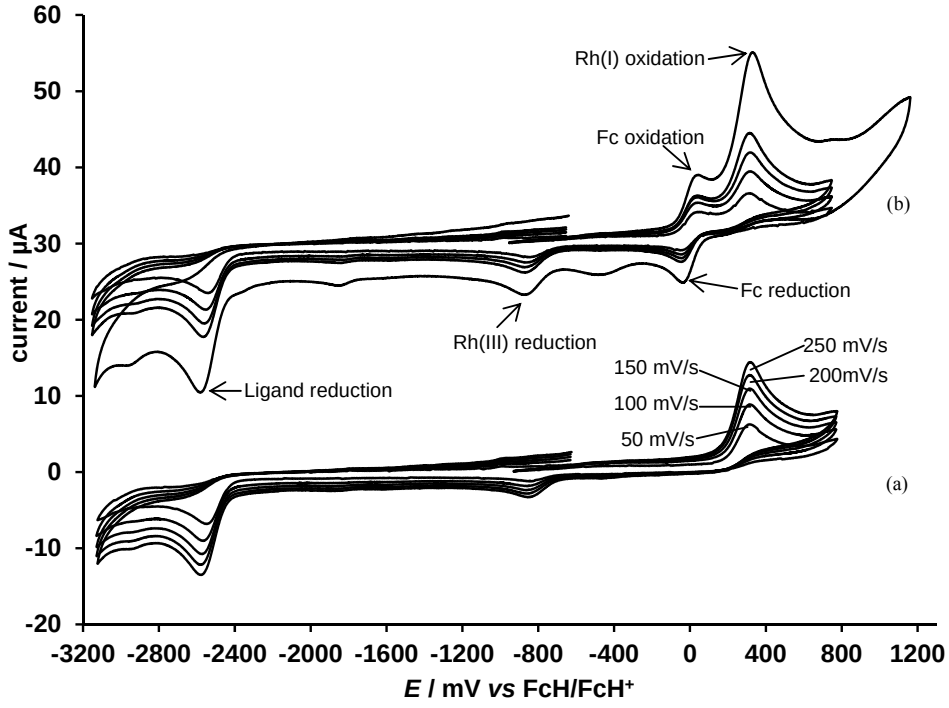

Figure 3. 28(a) Cyclic voltammograms of 0.5 mmol dm^{-3} solution of [Rh(acac)(CO)(PPh_3)]; (b) [Rh(acac)(CO)(PPh_3)] with ferrocene all measured in 0.1 mol dm^{-3} [N(nBu_4)][PF_6]/CH_3CN at varied scan rates on a glassy carbon working electrode at 25 ˚C.

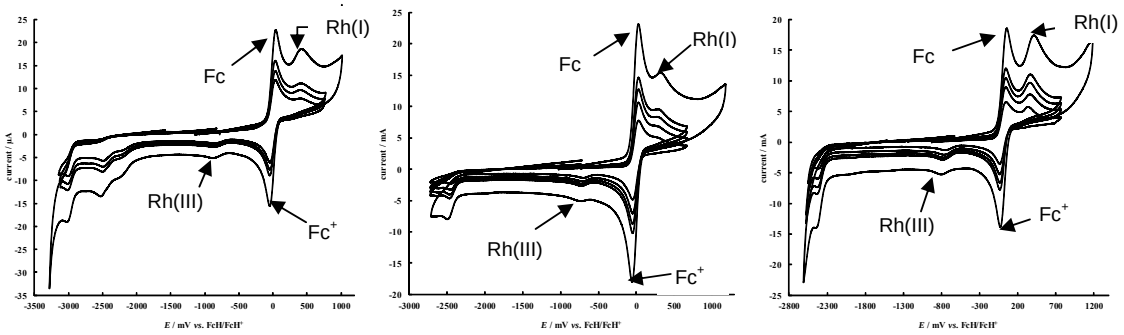

Figure 3. 29. Cyclic voltammograms of 0.5 mmol dm^{-3} solution of [Rh(Hβ2)(CO)(PPh_3)] (left), [Rh(β3)(CO)(PPh_3)], (middle) and [Rh(β4)(CO)(PPh_3)] (right). Ferrocene were used as internal standard and all CVs were measured in 0.1 mol dm^{-3} [N(nBu_4)][PF_6]/CH_3CN at varied scan rates on a glassy carbon working electrode at 25 ˚C.

Oxidation of Rh(I) to Rh(III)) involves the removal of $2e^-$ from the HOMO, d-orbital which is mainly of dz^2 character of the complex. The Rh(III) complex with an empty dz^2 orbital is very unstable and it is proposed that solvent co-ordination to Rh(III) take place, similar to what

was found for related [Rh(β-diketonato)(CO)(PPh_3)] complexes.[34] The following electrochemical scheme is thus proposed for the [Rh(β-diketonato)(CO)(PPh_3)] complexes of this study.

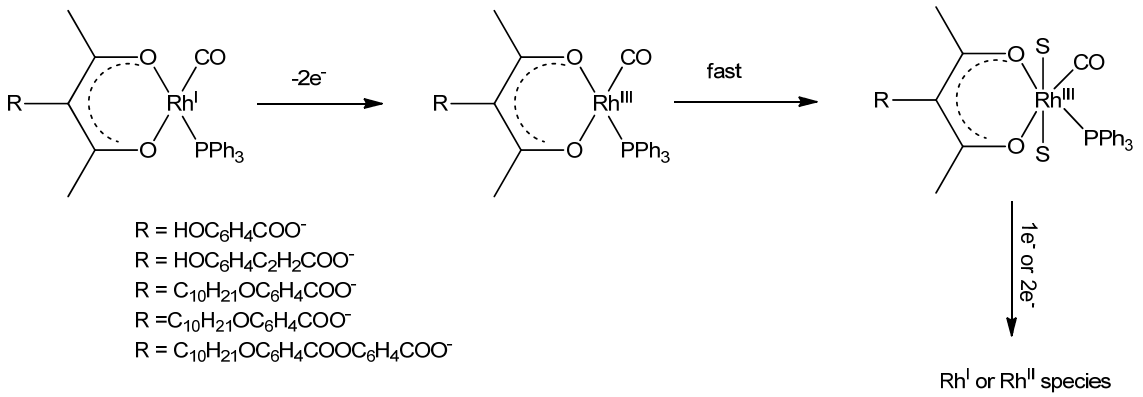

Scheme 3. 12. Electrochemical scheme highlighting the chemical and electrochemical irreversible rhodium electron transfer process for the [Rh(β-diketonato)(CO)(PPh_3)] complexes of this study. S = solvent molecule.

3.3 DSC and POM

The mesomorphic properties observed for β-diketones **3a-5a** were found to be drastically dependent on the presence of an aliphatic chain in the phenyl ring of the gamma substituent. No mesomorphic properties were observed for β-diketones **1a** and **2a,** with no aliphatic chain in the phenyl ring. The group joining the γ-substituent group to the β-diketone group should allow for the extended conjugation between the two groups for the mesomorphic properties to be observed.[2]

In this study, the phenyl 4-(*n*-decy1oxy) benzoate group acts as a classic pro-mesogenic unit. The β-diketone is considered as a voluminous terminal group which can strongly impedes the parallel molecular arrangement that is necessary for the mesophase formation. With an ester-linking group, the aromatic conjugation can be extended to the β-diketone.

3.3.1 Gamma-substituted β-diketones

3.3.1.1 β-diketone 3a

The DSC thermogram of β-diketone **3a**, measured at a heating and cooling rate of 10 °C min^{-1}, is displayed in **Figure 3. 30(a)**. Several mesophase changes were observed on both the heating and the cooling cycles. The presence of transitions (labelled iii, iv and v on the heating cycle) indicated the presence of several mesophases which were very weak and not detectable during the cooling cycle because either the heat involved in the phase transition was too low to measure, or due to the slow kinetic rate of phase transitions. A significantly larger amount of energy, 18.63 Jg^{-1}, was released during the first thermal event: that of melting (transition C1-C2-S1; C1-C2) was unresolved from event C2-S1, and Transition C1-C2 is consistent with a transition in the solid state from a crystalline solid state (C1) to the crystalline solid state (C2). The transition C2-S1 consists of a transition from the crystalline solid state (C2) to a smectic mesophase state, labelled S1. Different mesophases began forming. At 102.5 °C (transition S1-S2) and 115.0°C (transition S2-N) were then detected, where S2 denotes a second smectic mesophase and N a nematic mesophase. At 127.5 °C, the all types of order between the molecules is lost and it becomes an isotropic (I) liquid. This phase transition is represented by the transition N-I.

Only three main events were detected during the cooling cycle: the isotropic liquid to a nematic liquid crystalline mesophase transition at 132.0 °C (I-N), followed by the crystallization of the sample during a S1-C2 transition at 66.1 °C. A further DSC-observed crystalline solid- crystalline solid phase transition at -4.39 °C is consistent with a C2-C1 transition.

From the DSC results, it is not possible to identify the different types of mesomorphous liquid crystalline states, but polarized light optical microscopy (POM) studies allowed the assignment of smectic, or nematic mesophases S1, S2 and N, as well as the crystalline solid phases C1 and C2 and isotropic liquid phase I. The polarized light microphotographs at the indicated temperatures for β-diketone **3a** are shown by **Figure 3. 31** and are also superimposed on the DCS thermogram in **Figure 3. 30(b)**. It is important to realize that not all detectable thermal events observed by the DSC are necessarily associated with a strong spectroscopic change and vice versa. The energies associated with each transition and the

temperature at which they occur, summarized in **Table 3. 3 ,** are insights that were obtained from the simultaneous evaluation of DSC and POM results.

A closer look at the POM results that highlight the optical appearance of each phase may be found in **Figure 3. 31. Figure 3. 31a** shows the optical appearance of crystalline solid phase C1 of β-diketone **3a** at room temperature (27.9 °C). **Figure 3. 31b** at 67.3 °C shows it as a second crystalline solid phase C2. We conclude that the broad exothermic event between 40 and 90 °C on the DSC curves of **Figure 3. 30** includes two transitions: the first small shoulder (indicated by 'i' in the heating cycle) started at 61.6 °C, and represented the solid phase transition from C1 to C2. The main peak (ii) of the broad exothermic event between 40 and 90 °C corresponds with the C2 to smectic (S1) phase transition, see **Figure 3. 31c** for a photo of the schlieren texture of the S1 mesophase. A smectic 1 to smectic 2 transition is observed at peak (iii) at 102.5 °C; the smectic 2 photo at 105.5 °C with clear batonnets lines is shown by **Figure 3. 31d**. The peak at (iv) (115.0 °C) in **Figure 3. 30(a)** presents a smectic 2 to the nematic mesophase transition. The nematic phase is identified by the presence of fan-shaped nematic schlieren brushes of four and two, see **Figure 3. 31e**. Upon further heating, nematic phase islands form (**Figure 3. 31f**), and a phase transition to a isotropic liquid results in higher temperatures after the peak at (v) at 127.5 °C.

On cooling, the reverse of the heating cycle is observed, although the N-S2 and S2-S1 mesophase transitions were not observed on the DSC (**Figure 3. 30a). Figure 3. 32** shows the polarizing microphotographs for β-diketone **3a** which were taken during the cooling cycle. During cooling of the isotropic phase of the β-diketone **3a** (**Figure 3. 32a**), nematic islands start to form from the isotropic phase, see **Figure 3. 32b** and event (v') on **Figure 3. 30a.** The nematic state at the clearing point starts appearing as round islands. When a system from the homogenous high temperature phase is quenched across a phase transition at the transition temperature, a situation of non-equilibrium is created. At this stage crystalline germs of the low-temperature phase start forming nuclei that grow spontaneously, forming round droplets. When these droplets come close enough to each other, they start to coalesce to form the nematic texture. This can be clearly seen in **Figure 3. 32b** and **Figure 3. 32c**. The N-S2 phase transition was observed with POM (peak (iv') on **Figure 3. 30a**), but is not measurable on the DSC. At 103.4 °C (**Figure 3. 32d**), the smectic mesophase S2 is observed on the POM. Similarly, the S2-S1 phase transition was observed with POM at peak (iii') on **Figure 3. 30a**, but it is not measurable on the DSC. At 92.2 °C and 80.8 °C (**Figure 3. 32e** and **f**), S1 is

observed on the POM. At 70.0 °C, the crystalline solid phase C2 become observable, see **Figure 3. 32g – i.**

Table 3. 3. A summary of DSC at 10°C min^{-1} results of 2,4-dioxo-3-pentyl-4-decanyloxybenzoate ($CH_3COCH(C_{10}H_{21}OC_6H_4COO)COCH_3$) 3a with POM temperature.

Heating			
Phase Transition	**DSC Onset (peak) temperature, °C**	**ΔH / Jg^{-1}**	**POM temperature, °C**
C1 – C2	61.6 (79.4)	{-18.63}	67.3
C2 – S1			96.8
S1 – S2	95.8 (102.5)	-0.62	105.5
S2 – N	111.6 (115.0)	-0.27	112.8
N – I	122.1 (127.5)	-1.50	129.6
Cooling			
I – N	138.6 (132.0)	0.59	131.0
N – S2			103.4
S2 – S1			92.2
S1 – C2	72.4 (66.1)	17.84	70.0
C2 – C1	1.07 (-4.4)	5.06	-3.9

I = isotropic liquid, N = nematic mesophase, S1 = smectic mesophase 1, S2 = smectic mesophase 2, C1 = crystalline solid phase 1, C2 = crystalline solid phase 2. DSC = Differential Scanning Calorimetry, POM = polarized light optical microscopy.

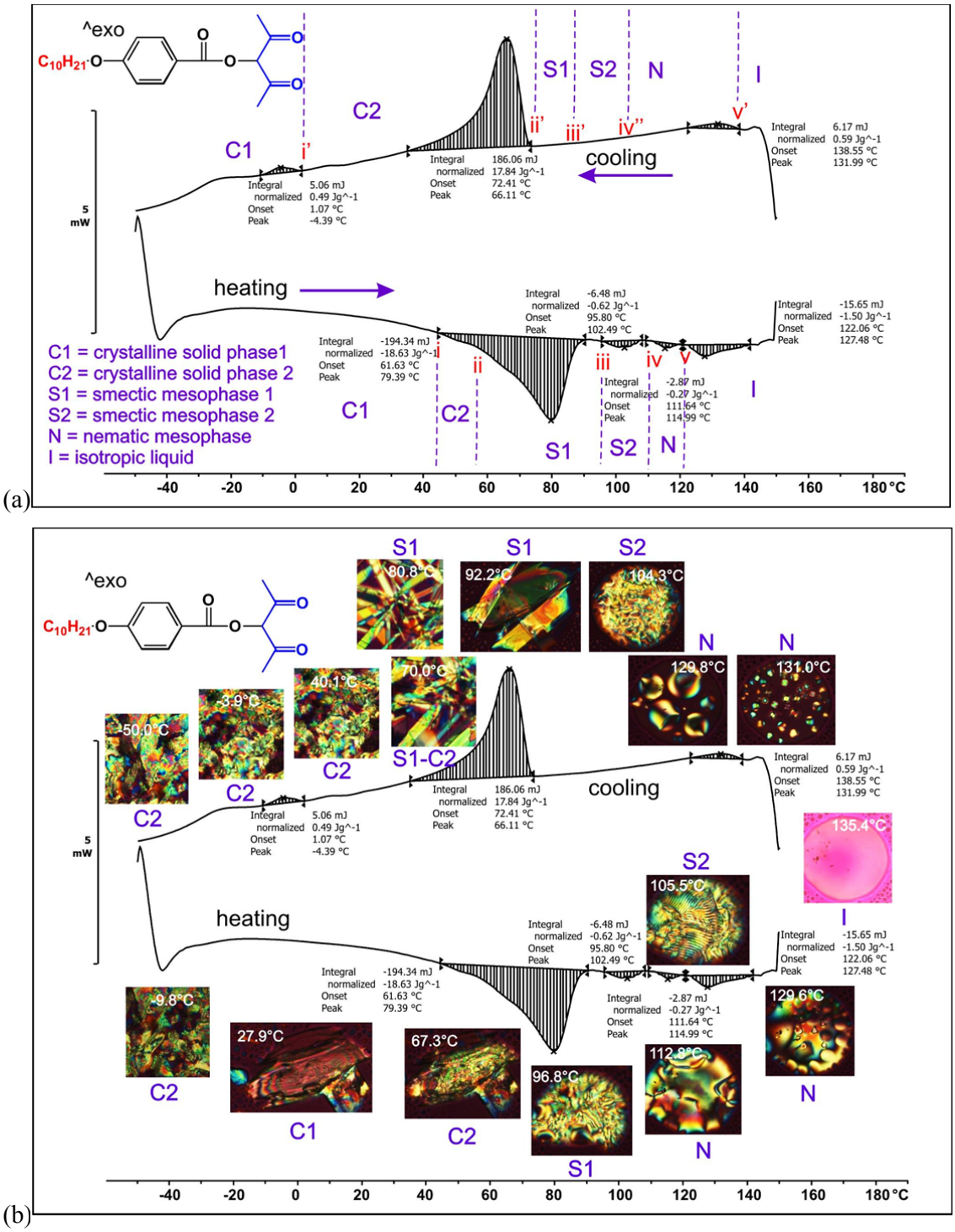

Figure 3. 30(a): Phase transition temperatures, enthalpy changes and DSC thermogram at heating and cooling rates of 10°C min^{-1} for 2,4-dioxo-3-pentyl-4-decanyloxybenzoate ($CH_3COCH(C_{10}H_{21}OC_6H_4COO)COCH_3$) 3a. (b) DSC thermogram with POM photos of the different phases observed. DSC sample mass = 10.45 mg. Events i – v are associated with the heating cycle and events v' – i' are associated with the cooling curve. (The roman numbers with the dashed line indicate the onset of the events).

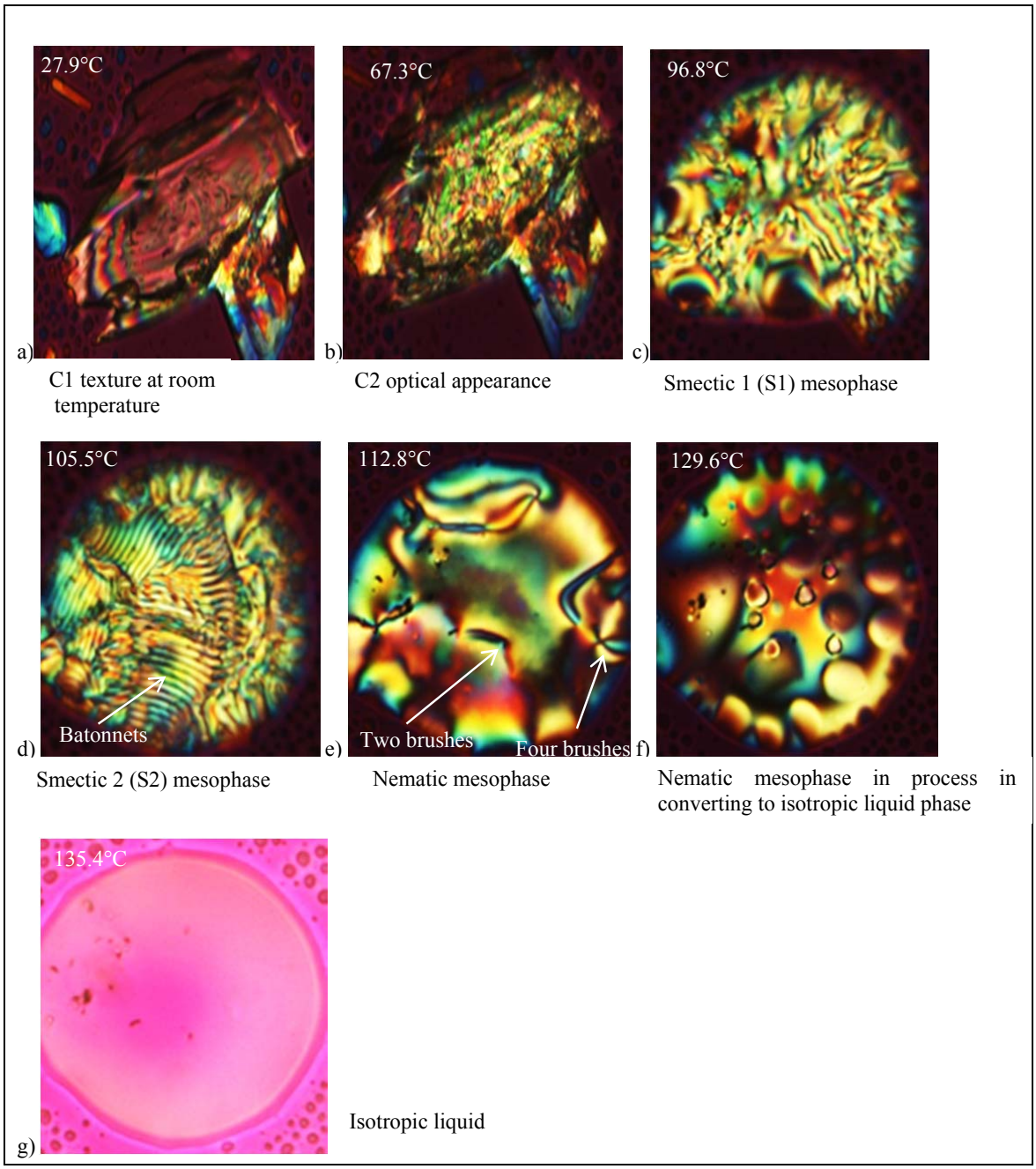

Figure 3. 31. Liquid crystalline transitions for the β-diketone 3 during heating cycle as observed under polarized light optical microscopy, magnification ×100. 2,4-dioxo-3-pentyl-4-decanyloxybenzoate ($CH_3COCH(C_{10}H_{21}OC_6H_4COO)COCH_3$) 3.

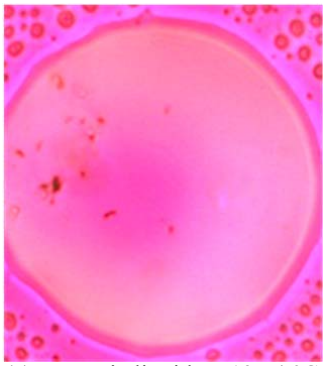

(a) Isotropic liquid at 135.4 °C

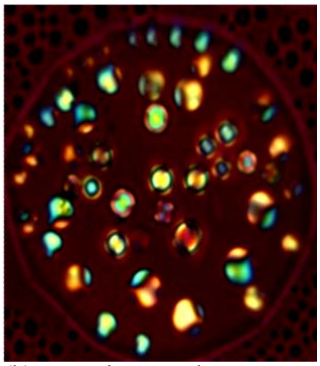

(b) Nematic mesophase at 131.0 °C

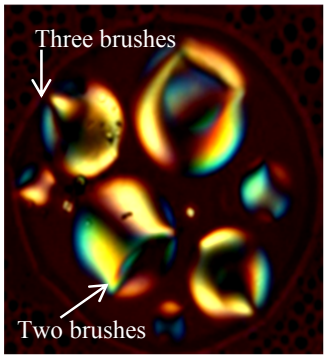

(c) Larger nematic mesophase at 129.8 °C

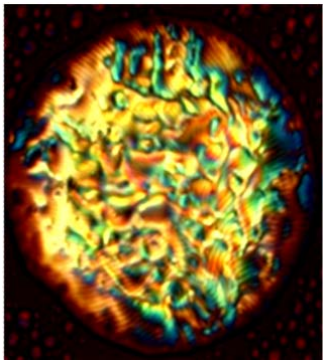

(d) Smectic mesophase S2 at 103.4 °C

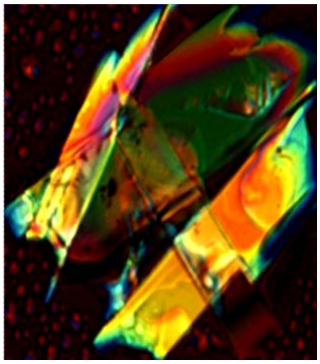

(e) Smectic mesophase S1 at 92.2 °C

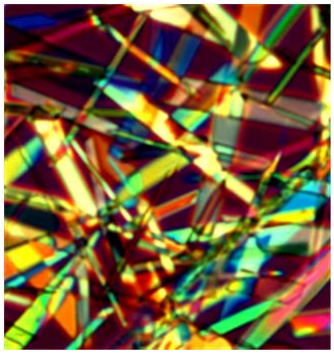

(f) Smectic mesophase S1 at 80.8 °C

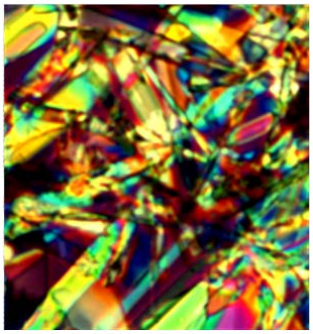

(g) Crystalline solid phase C2 at 70.0 °C now clearly becomes observable

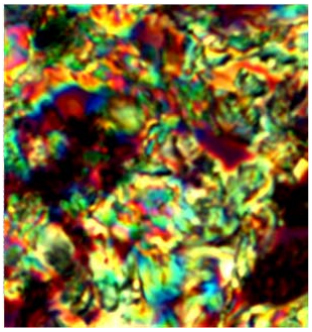

(h) Crystalline solid phase C2 at 40.1 °C

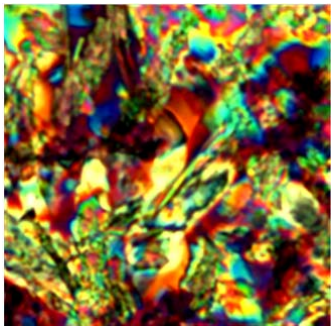

(i) Crystalline solid phase C2 at -3.9 °C. This is a super cooled state of C2.

Figure 3. 32. Liquid crystalline transitions for the β-diketone 3 during the cooling cycle as observed under polarized light optical microscopy, magnification ×100. 2,4-dioxo-3-pentyl-4-decanyloxybenzoate ($CH_3COCH(C_{10}H_{21}OC_6H_4COO)COCH_3$).

3.3.1.2 β-diketone 4a

The DSC thermogram of β-diketone **4a**, measured at a heating and cooling rate of at 10 °C min^{-1}, is displayed in **Figure 3. 33** and the polarized light optical microphotographs during heating and cooling cycles are observed under polarized light optical microscopy, in **Figure 3. 35** and **Figure 3. 34.** The DSC and POM results of β-diketone **4a** indicate the following: after running the sample through 3 heating and 2 cooling, the sample exists as an isotropic liquid at high temperatures. On cooling, two overlapping peaks could be observed at 23.98 ^{o}C and 28.17 ^{o}C, indicating that there are two thermodynamically unstable liquid crystal LC1 and LC2 mesophases very close to each other. The POM microphotograph at 28.6 °C and 27.6 °C shows that it has two nematic liquid crystalline phases. The first nematic phase starts to appear at 28.6 °C (**Figure 3. 34a**) and the second, with dark, fan-shaped four brushes, at 27.6 °C (**Figure 3. 34b**). Upon further cooling, crystals are formed (**Figure 3. 34c**). At -17.16 °C, a weak glass transition is observed.

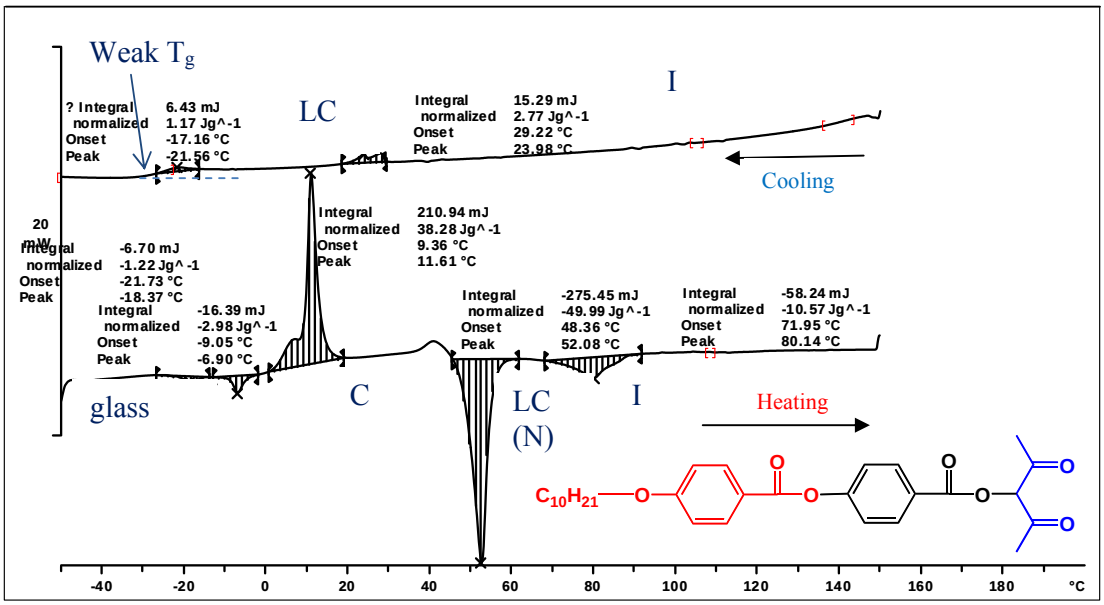

Figure 3. 33. Phase transition temperatures, enthalpy changes and DSC thermogram at heating and cooling rates of 10°C min^{-1} for 2,4-dioxo-3-pentyl-4-[[4-(n-decanyloxy)benzoyl]oxy]benzoate ($CH_3COCH(C_{10}H_{21}OC_6H_4COOC_6H_4COO)COCH_3$) 4.

During the heating cycle, DSC analyses for β-diketone **4a** insignificant C-C transitions of minority crystalline that might exist in the sample are observed. Cold crystallization of glass into a crystalline solid C is observed at -6.90 °C. Melting of C occurs at 48.36 °C and this is

confirmed by a great release of energy -49.99 Jg^{-1}. A liquid crystal phase is formed (**Figure 3. 35b**). The sample molecules begin to lose all types of order and become an isotropic liquid at 80.14 ^{o}C.

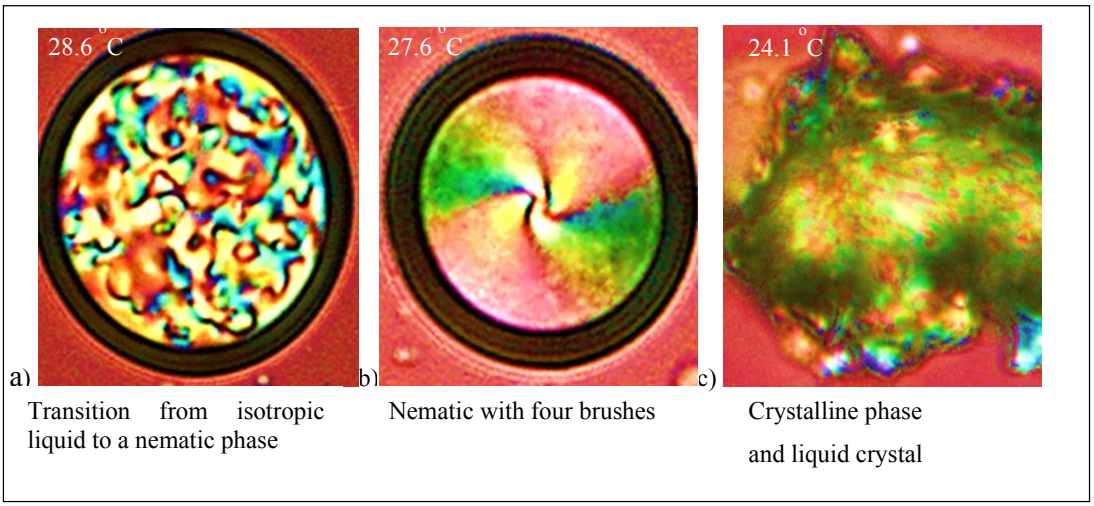

Figure 3. 34. Liquid crystalline transitions for the β-diketone 4 during cooling observed under polarized light optical microscopy, magnification ×100, 2,4-dioxo-3-pentyl-4-[[4-(n-decanyloxy)benzoyl]oxy]benzoate ($CH_3COCH(C_{10}H_{21}OC_6H_4COOC_6H_4COO)COCH_3$).

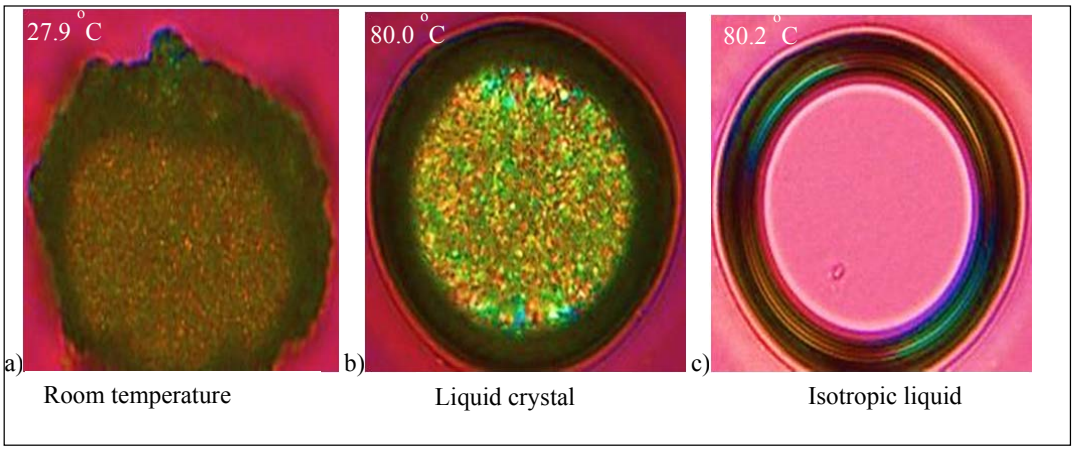

Figure 3. 35. Liquid crystalline transitions for the β-diketone 4 during heating observed under polarized light optical microscopy, magnification ×100. 2,4-dioxo-3-pentyl-4-[[4-(n-decanyloxy)benzoyl]oxy]benzoate ($CH_3COCH(C_{10}H_{21}OC_6H_4COOC_6H_4COO)COCH_3$).

3.3.1.3 β-Diketone 5a

The DSC thermogram of β-diketone **5a**, measured at a heating and cooling rate of at 10 °C min^{-1}, is displayed in **Figure 3. 36(a)** and the polarized light optical microphotographs at the

indicated temperatures for β-diketone **5a** are superimposed on the DCS thermogram in **Figure 3. 36(b)**.

(a)

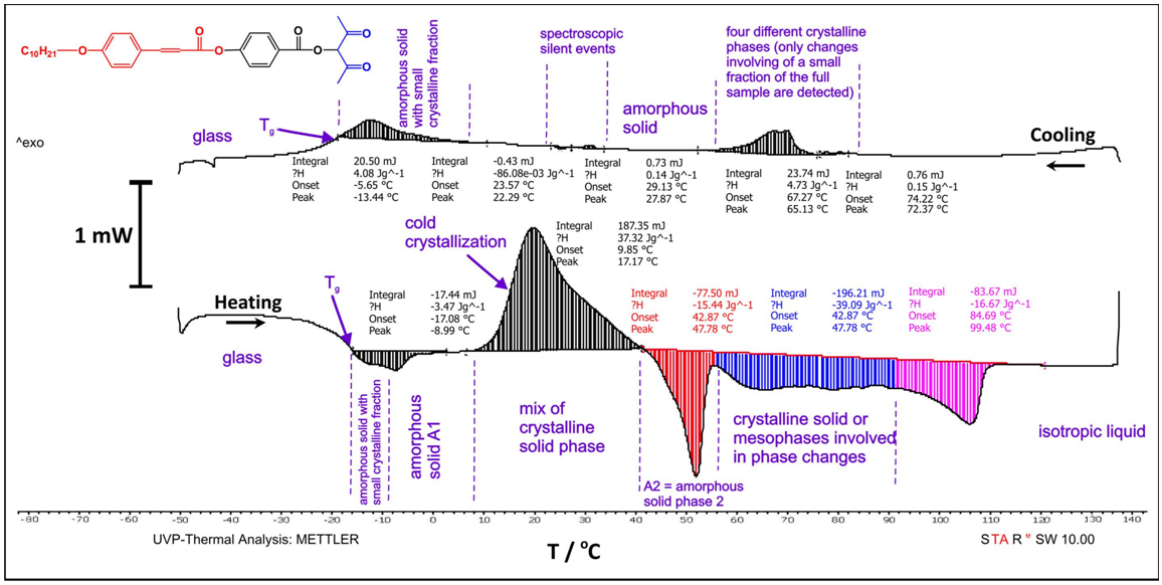

(b)

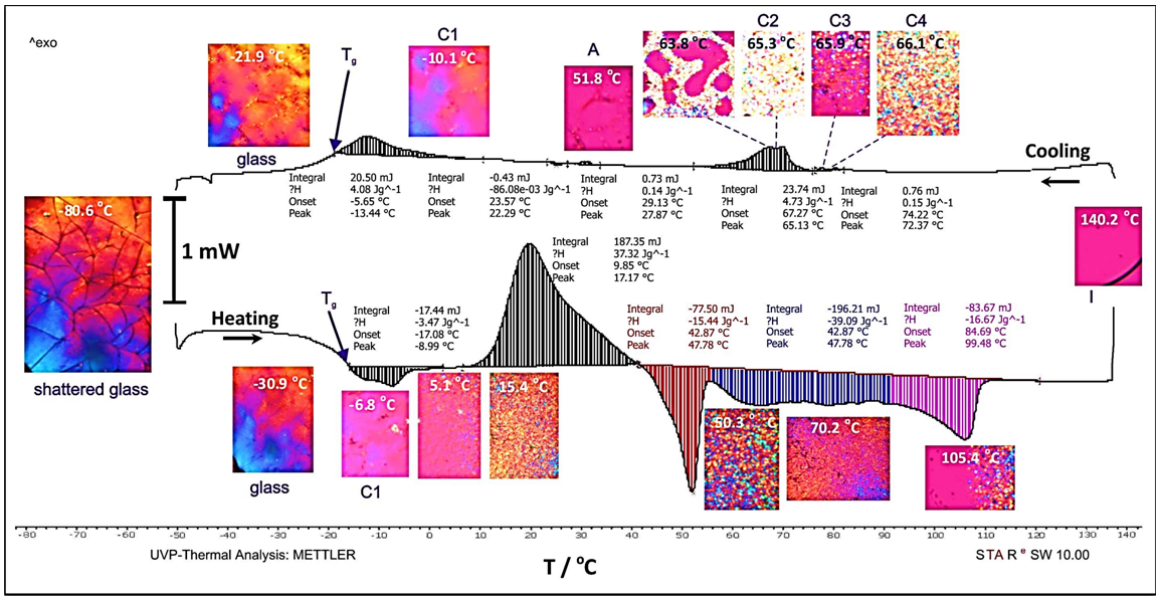

Figure 3. 36(a): Phase transition temperatures, enthalpy changes and DSC thermogram at heating and cooling rates of 5 °C min^{-1} for 2,4-dioxo-3-pentyl-4-[[4-(n-decanyloxy)cinnamoyl]oxy]benzoate, β-diketone 5, ($CH_3COCH(C_{10}H_{21}OC_6H_4C_2H_2COOC_6H_4COO)COCH_3$).

(b) DSC thermogram with POM photos of the different phases observed. DSC sample mass = 5.02 mg.

The DSC and POM results of β-diketone **5a** indicate the following: at low temperatures (below *ca* -20 °C) the complex exists as a glass. The POM photo at -80.6 °C shows the cracks of a very cold sample of the glass. As the temperature increases on the heating cycle, at T_g = *ca* -18.0 °C, a glass transition is observed in which the glass converts to an amorphous solid containing a small fraction of crystals. Melting of the small fraction of crystalline solids in the largely amorphous sample probably occurs at -14 to -8 °C. (Alternatively, the peaks between -14 and -8 °C may be a small fraction of crystalline material mixed into the largely amorphous solid that undergo a solid state transition.) The resulting amorphous solid with other phases are observed at 5.1 °C. Cold crystallization of the amorphous solid occur at between 9.85 and 42.87 °C to create a broth of different crystalline solids consisting of different phases of enol and keto isomers, all mixed together. This broth of phases begins to melt at 42.87 °C in several distinctly different steps until a clear isotropic liquid has formed at 100 °C. No clear indication of a liquid crystalline mesophase that can be assigned as a smectic, nematic or columnar mesophase, could be detected in this entire temperature region.

On the cooling curve, four phase transitions involving a small fraction of the sample are observed within a few degrees between 66.1 and 63.8 °C on the POM and 81 – 55 °C on the DSC:

- at 81 °C, phase transition from isotropic liquid to a small amount of crystalline solid phase 4 is observed (I-C4);
- at 78 °C, this phase converts to crystalline solid phase 2 (C4-C3);
- at 70 °C, another phase transition C3 to yet another solid phase C2 is observed (C3-C2); and
- at 68°C, the C2 phase apparently becomes unstable and the entire sample becomes amorphous. This conversion is completed at 55°C (C2-A).

Further cooling leads to small events observed at 31 and 27 °C on the DSC but they are optically silent, which was not observed by POM. Crystallization of a small fraction of the amorphous solid starts at ca 0 °C on the cooling curve. Finally, the remainder of the sample, which is an amorphous solid, converts to a glass at T_g = -15.4 °C.

In summary, no smectic, nematic or columnar liquid crystalline mesophase could unambiguously be identified for β-diketone **5a**; only a series of different phases which included glassy, amorphous solids and several crystalline solids could be detected.

3.3.2 Rh(I)-dicarbonyl complexes.

In this study, it was observed that Rh complexes which have been prepared from gamma-substituted β-diketones are not suitable for the generation of mesomorphic phases in spite of their having been coordinated to mesomorphic ligands. Comparing the complexes with their respective ligands, coordination of $[M(CO)_2]$ with β-diketones **3a, 4a** and **5a** elongates the molecule without any significant change in the molecular width and this benefits the mesomorphic state. However, stronger intermolecular forces between molecules of **3b, 4b** and **5b** stabilise the crystalline phase to the detriment of the formation of the mesomorphic phase.

DSC thermograms measured at a heating and cooling rate of 10 °C min^{-1}, as well as optical images observed under polarized light optical microscopy (POM), are shown below for the [Rh(β-diketonato)$(CO)_2$] complexes of β-diketone **3a, 4a** and **5a** (**Figure 3. 37-Figure 3. 39**).

The DSC thermograms of all three [Rh(β-diketonato)$(CO)_2$] complexes (**3b – 5b)** look very similar. Each shows a clear crystalline solid-isotropic liquid transition on (C-I) the heating curve (melting). On the cooling curve, the isotropic liquid-crystalline solid phase transition (crystallization) occurs at a lower temperature due to super cooling. For [Rh(β-diketonato-5a)$(CO)_2$], complex **5b**, a solid phase transition is observed on the heating cycle at 57.8 °C.

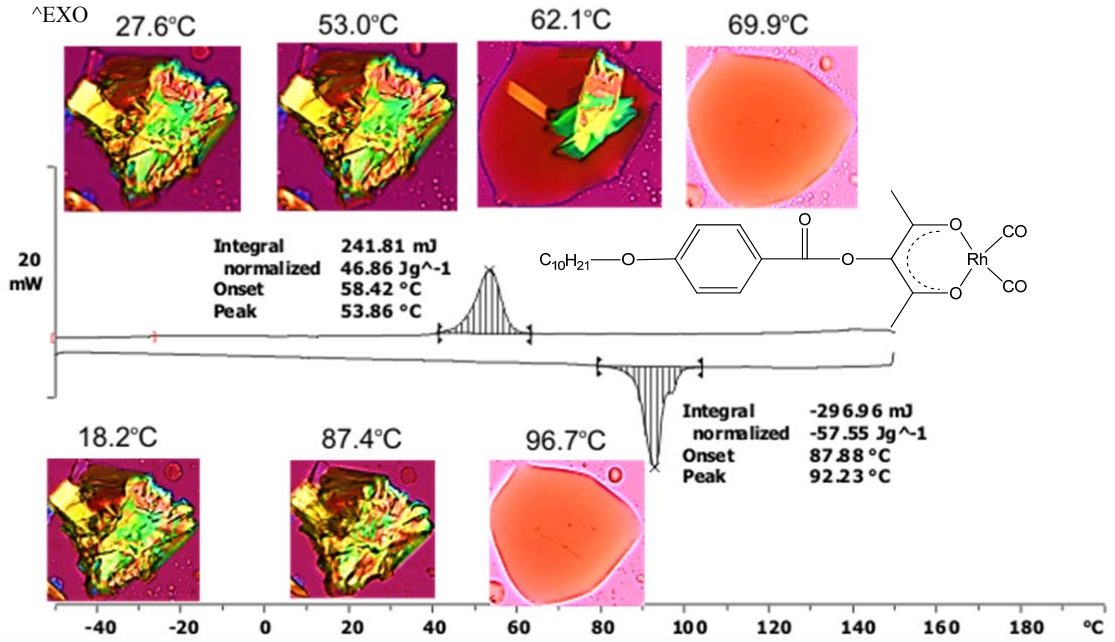

Figure 3. 37. DSC thermograms at 10 °C min^{-1} heating and cooling rates as well as images observed under polarized light optical microscopy, magnification ×100 for [Rh(β-diketonato-3)(CO)$_2$]. (Heating cycle no 3 and cooling cycle no 3 shown, mass of sample = 5.71 mg.)

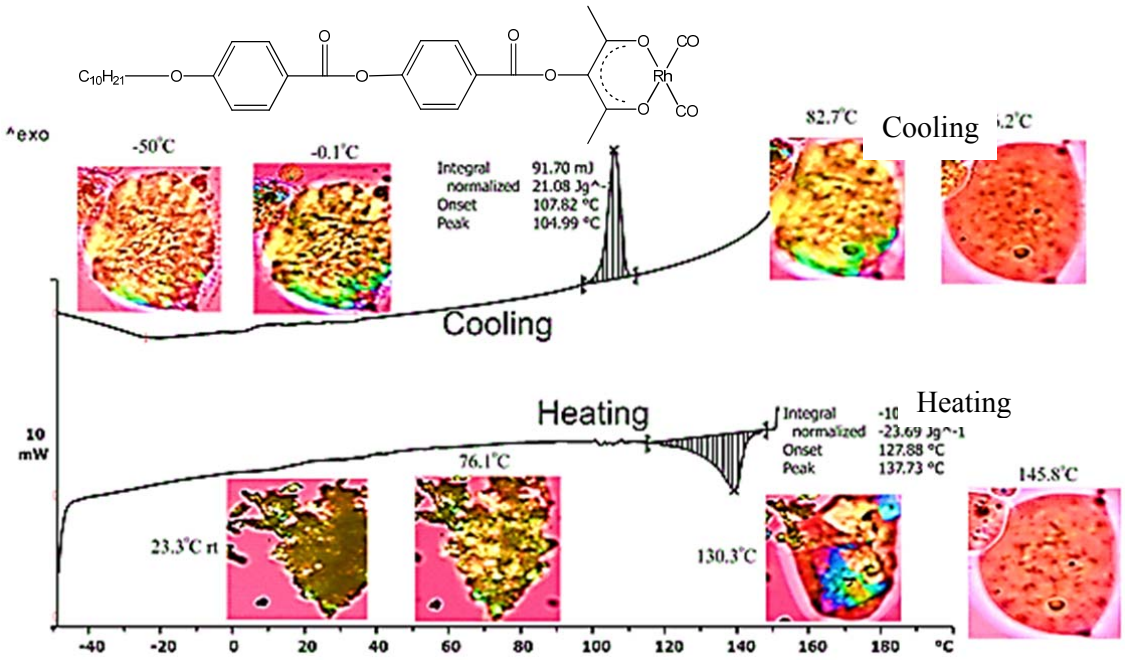

Figure 3. 38. DSC thermograms at 10 °C min^{-1} heating and cooling rates as well as images observed under polarized light optical microscopy, magnification ×100 for [Rh(β-diketonato-4)(CO)$_2$]. (Heating cycle no 3 and cooling cycle no 3 shown, mass of sample = 5.88 mg.)

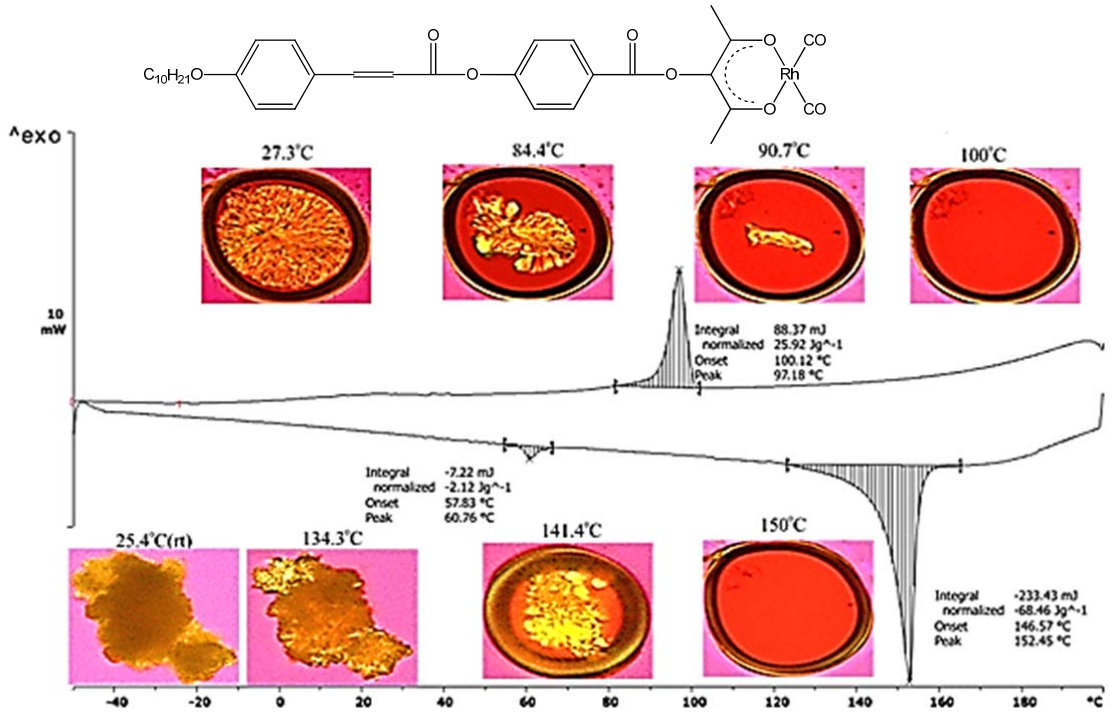

Figure 3. 39. DSC thermograms at 10 °C min^{-1} heating and cooling rates as well as images observed under polarized light optical microscopy, magnification ×100 for [Rh(β-diketonato-5)(CO)$_2$]. (Heating cycle no 3 and cooling cycle no 3 shown, mass of sample = 5.60 mg.)

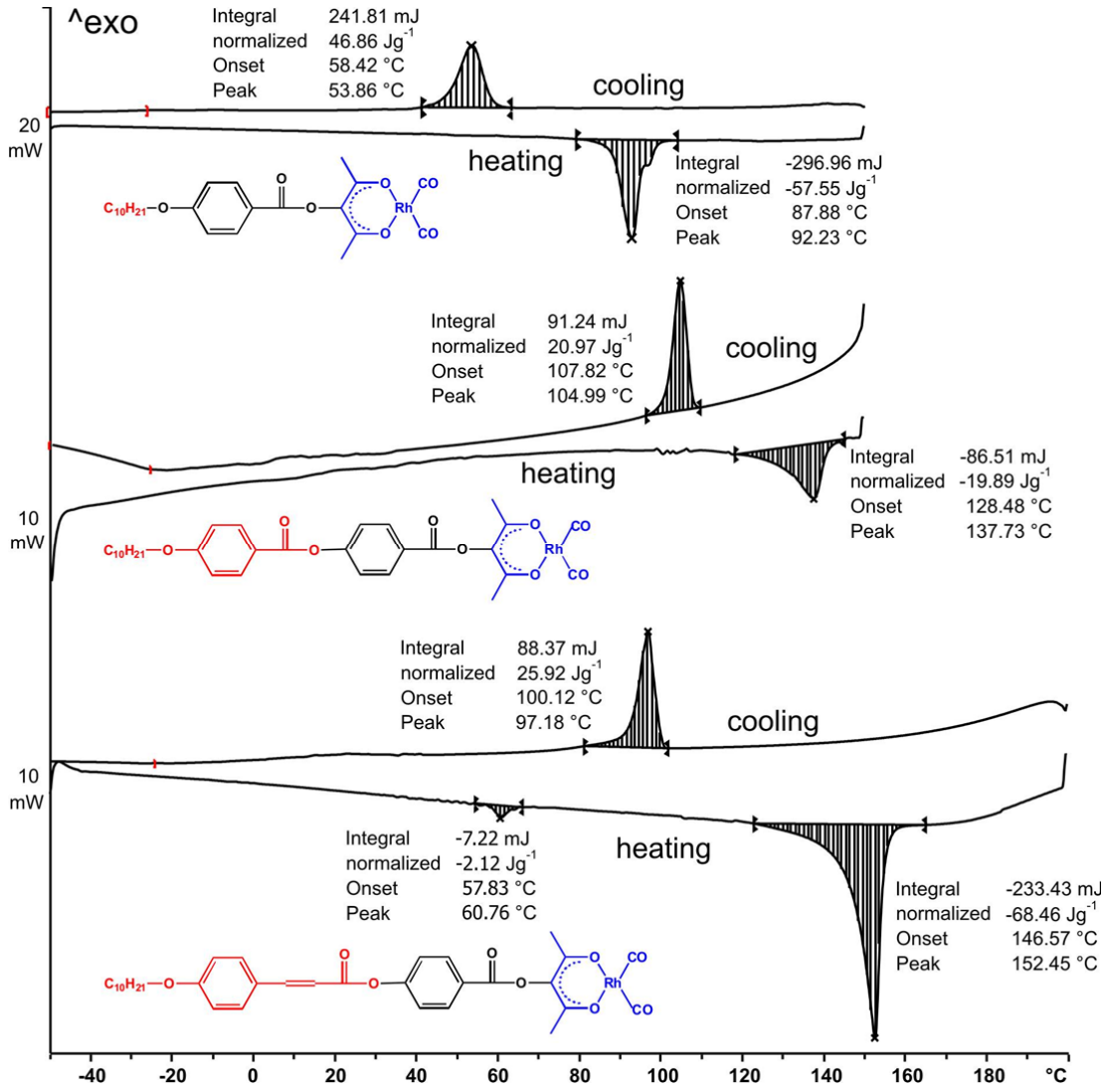

Figure 3. 40. DSC thermograms at 10 °C min^{-1} heating and cooling rates for [Rh(β-diketonato-3)(CO)$_2$] (top), [Rh(β-diketonato-4)(CO)$_2$] (middle) and [Rh(β-diketonato-5)(CO)$_2$] (bottom).

Figure 3. 40 gives a comparative DSC thermogram for the [Rh(β-diketonato)(CO)$_2$] complexes of β-diketones **3a**, **4a** and **5a**. We observe that, the longer the chain on the γ-position of the β-diketonato ligand, the higher the melting point of the [Rh(β-diketonato)(CO)$_2$] complex, see **Table 3. 4.**

Table 3. 4. Melting point (°C) of the γ-substituted β-diketones and their [Rh(β-diketonato)(CO)$_2$] complexes.

no	β-diketone	[Rh(β-diketonato)(CO)$_2$]
3	61.63	87.9
4	80.1	127.9
5	99.5	146.6

3.3.3 Rh(I)-monocarbonyl-PPh$_3$ complexes.

DSC thermograms at 10 °C min^{-1} heating and cooling rates, as well as optical images observed under light polarized microscopy, are shown below for the [Rh(β-diketonato)(CO)(PPh$_3$)] complexes of β-diketone **3a, 4a** and **5a** (see **Figure 3. 41–Figure 3. 43**). The DSC thermograms are all similar, showing that the [Rh(β-diketonato)(CO)(PPh$_3$)] complexes **3c**–**5c** exist as amorphous solids prior to their conversion to an isotropic liquid. No clear melting point can be identified on the DSC as such conversions do not register energy changes. However, on POM 'melting' could be seen. For [Rh(β-diketonato-3)(CO)(PPh$_3$)] complex, anhealing sets in at 90.5 °C and, at 130 °C it is a true isotropic liquid. With cooling, the isotropic liquid changes to an amorphous solid – again without any thermal event on the DSC. Solidification sets in at 120.3 °C on the cooling cycle. (Note the term is *solidification* and not *crystallization* because a crystalline solid is not formed).

In summary, when considering the phase transition properties of the gamma-substituted β-diketones **3a** – **5a**, as well as their dicarbonyl and phosphine complexes, we observe that the free gamma-substituted β-diketones can crystallize, and that they exhibit different liquid crystalline mesophases before melting to an isotropic liquid. The [Rh(β-diketonato)(CO)$_2$] complexes **3b**–**5b** exhibit clear crystalline solid and isotropic liquid phases. In contrast, the [Rh(β-diketonato)(CO)(PPh$_3$)] **3c**–**5c** are amorphous solids (without any crystal packing) that liquefy without showing any crystalline behaviour.

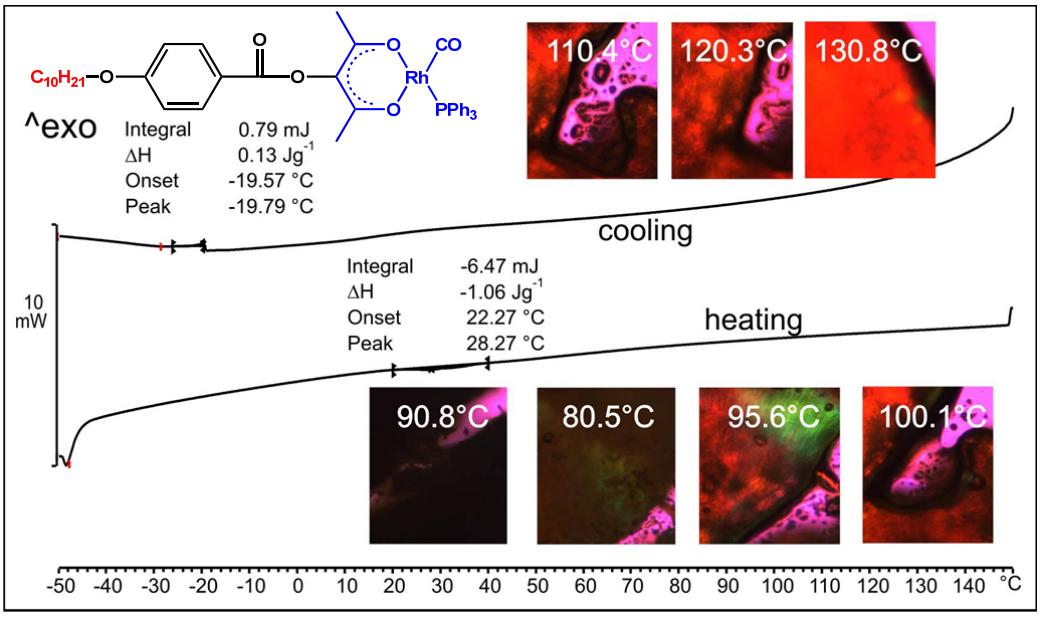

Figure 3. 41. DSC thermograms at 10 °C min^{-1} heating and cooling rates as well as images observed under polarized light optical microscopy, magnification ×100 for [Rh(β-diketonato-3)(CO)(PPh$_3$)]. (Heating cycle no 3 and cooling cycle no 3 shown, mass of sample = 6.10 mg.)

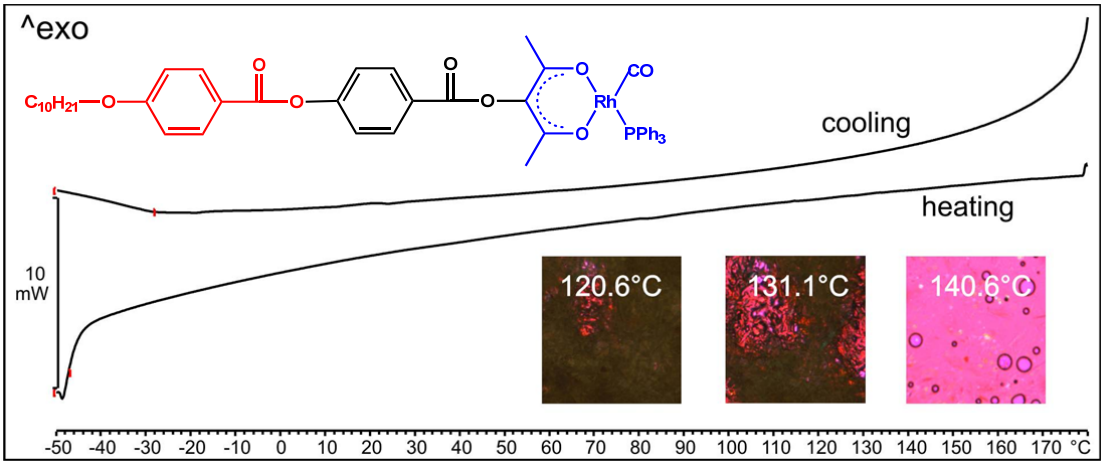

Figure 3. 42. DSC thermograms at 10 °C min^{-1} heating and cooling rates, as well as images observed under polarized light optical microscopy, magnification ×100 for [Rh(β-diketonato-4)(CO)(PPh$_3$)]. (Heating cycle no 3 and cooling cycle no 3 shown, mass of sample = 1.38 mg.)

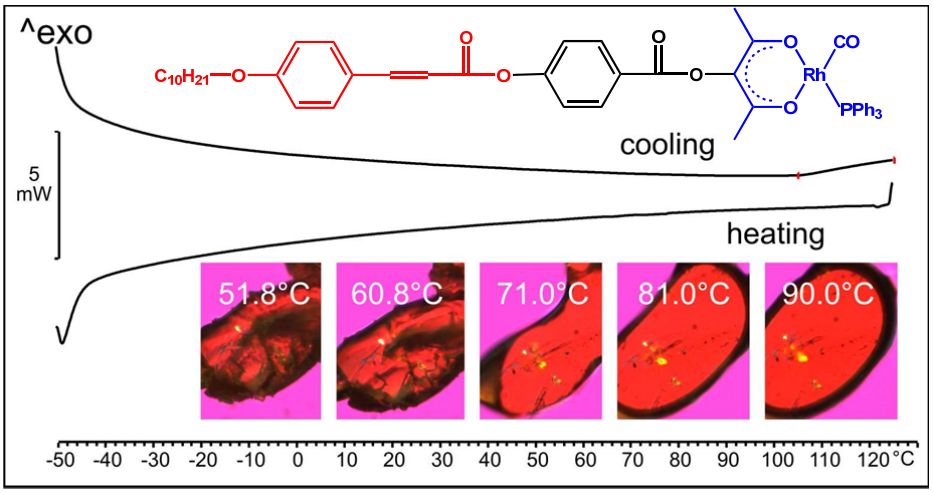

Figure 3. 43. DSC thermograms at 10 °C min^{-1} heating and cooling rates, as well as images observed under polarized light optical microscopy, magnification ×100 for [Rh(β-diketonato-5)(CO)(PPh_3)]. (Heating cycle no 3 and cooling cycle no 3 shown, mass of sample = 0.28 mg.)

References

[1] Han, J., Zhang, L. F., Wan, W. *J. Organomet. Chem*. **2003**, 672, 86.

[2] Cativiela, C., Serrano, J. L., Zurbano, M. M. *J. Org. Chem*. **1995**, 60, 3074.

[3] Classon, B., Liu, Z., Samuelsson, B. *J. Org. Chem.* **1988**, 53**,** 6126.

[4] Stuurman, N. F., Conradie, J. *J. Organomet. Chem*., **2009**, 694, 259.

[5] Adams, J. T., Hauser, C. R. *J. Am. Chem. Soc.* **1944**, 66, 1220.

[6] (a) Serp, P. H., Hernandez, M., Richard, B., Kalck, P. H. *Eur. J. Inorg. Chem*. **2001**, 9, 2327; (b) Varshavsky, Y. S., Cherkasova, T. G. *J. Organomet. Chem*. **2007**, 692, 887.

[7] Hopmann, K. H., Stuurman, N. F., Muller, A., Conradie, J. *Organometallics* **2010**, 29, 2446.

[8] Stuurman, N. F., Meijboom, R., Conradie, J. *Polyhedron* **2011**, 30, 660.

[9] Stuurman, N. F., Muller, A., Conradie, J. *Inorg. Chim. Acta* **2013**, 395, 237.

[10] http://www.iupac.org/publications/books/rbook/Red_Book_2005.pdf, p. 180. SQP complexes are designated *SP*-4, followed by a single digit referring to the priority number of the ligating atom *trans* to the ligating atom of priority number 1.

[11] Leipoldt, J. G., Basson, S. S., Potgieter, J. H. *Inorg. Chim. Acta* **1986,** 117, L3.

[12] Steynberg, E. C., Lamprecht, G. J., Leipoldt, J. G. *Inorg. Chim. Acta* **1987,** 133, 33.

[13] Leipolt, J. G., Basson, S. S., Nel, J. T. *Inorg. Chim. Acta* **1983**, 74, 85.

[14] Leipoldt, J. G., Bok, L. D. C., van Vollenhoven, J. S., Pieterse, A. I. *J Inorg. Nucl. Chem*. **1978**, 40, 61.

[15] Trzeciak, A. M., Zió1kowski, J. J. *Inorg. Chim. Acta* **1985,** *96,* 15.

[16] Conradie, J., Lamprecht, G. J., Otto, S., Swarts, J. C. *Inorg. Chim. Acta* **2002**, *328*, 191.

[17] Conradie, M. M., Conradie, J. *Inorg. Chim. Acta* **2008**, 361, 208.

[18] Conradie, M. M., Conradie, J. *Inorg. Chim. Acta* **2008**, 361, 2285.

[19] Leipolt, J. G., Bok, L. D. C., Van Vollenhoven, J. S., Pieterse, A. I. *J. Inorg. Nucl. Chem*. **1978**, 40, 61.

[20] Leipolt, J. G., Bok, L. D. C., Basson, S. S., Gerber, T. I. A. *Inorg. Chim. Acta* **1979**, 34, L293.

[21] Langford, C. H., Gray, H. B. *Ligand Substitution Processes* **1966**, Benjamin, New York.

[22] Huq, F.; Skapski, A. C. *J. Cryst. Mol. Struct.*, **1974**, 4, 411.

[23] Tolman, C. A. *Electron Donor-Acceptor Properties of Phosphorus Ligands* **1969**, No. 1577 from the Central Research Department, Experimental station., E.I. du Pont de Nemours and Company, Welmington, Delaware.

[24] Purcell, W., Basson, S. S., Leipoldt, J. G., Roodt, A., Preston, H. *Inorg Chim Acta* **1995**, 234, 153.

[25] Du Plessis, W. C., Vosloo, T. G., Swarts, J. C. *J. Chem. Soc., Dalton Trans.* **1998**, 2507.

[26] Kagarise, R. E. *J. Am. Chem. Soc.* **1955**, 77, 1377.

[27] Conradie, J. *Dalton Trans.* **2012**, 41, 10633.

[28] Costello, J. F., Davies, S. G., McNally, D. *J Chem Soc, Perkin Trans*. **1999**, 2, 465.

[29] For calculation of cone angles: Taverner, B. C. *Steric v1.12B*, available at http://www.gh.wits.ac.za

[30] Solid angle calculations: Guzei, I.A., Wendt, M. Program Solid-G, UW-Madison, WI, USA, **2004**.

[31] Calculations were performed with the Rh-P distance fixed to 2.28 Å to eliminate deviations incorporated by differences in bond distances.

[32] Bard, A. J., Faulkner, L. R. *Electrochemical Methods: Fundamentals and Applications*, **1980**, Chapter 6, pp 213, Wiley, New York.

[33] Conradie, J., Cameron, T. S., Aquino, M. A. S., Lamprecht, G. J., Swarts, J. C. *Inorg. Chim. Acta* **2005**, 2530.

[34] Lamprecht, D., Lamprecht, G. J. *Inorg. Chim. Acta* **2000**, 72.

[35] Conradie, J., Swarts, J. C. *Eur. J. Inorg. Chem.* **2011**, 13, 2439.

[36] Maitlis, P. M., Haynes, A., Sunley, G. J., Howard, M. J. *J. Chem. Soc. Dalton Trans.* **1996**, 2187.

4

Experimental

4.1 Materials.

Solid and liquid materials (Merck, Aldrich) were used without further purification. The solvents were distilled before use and water was double distilled. Flash chromatograph was performed on Silica gel 60 (Merck, grain size 0.040 – 0.063 mm), utilizing an overpressure that did not exceeded 100 Torr (1 Torr = 1 mmHg = 133.32 Pa).

4.2 Techniques and apparatus

4.2.1 Melting point (m.p.) and liquid crystal determination

Melting points (m.p.), liquid crystal transition temperatures and mesophase morphologies were determined with polarised optical microscopy (POM) using an Olympus BX51 microscope, with a LINKAM, TMS 600 hot stage. The melting points given are the onset temperature of melting and are uncorrected for standard pressure (P ≈ 650 Torr during measurements, not 760 Torr). Polarised optical micrographs were obtained with a colour camera in conjunction with Mettler Studio Capture software and polarised microscopy setup.

4.2.2 Spectroscopic measurements

NMR spectra were measured at 298 K on a Bruker Avance DPX 300 NMR spectrometer. The chemical shifts were reported relative to tetramethylsilane $Si(CH_3)_4$ at 0.00 ppm. The CDCl3 ^1H NMR signal and traces of water were at 7.27 ppm and 1.60 ppm respectively, under the conditions mentioned above. Selective spectra have been provided in the appendix.

FTIR measurements were determined with a Bruker Tensor 27 IR spectrometer and Pike MIRacle ATR, running OPUS software (Version 1.1).

4.2.3 Electrochemistry

Cyclic voltammetry (CV), linear sweep voltammetry (LSV) and square wave voltammetry (SWV) were determined with a Princeton Applied Research PARSTAT 2273 voltammograph. Data was recorded using Power Suite (version 2.28) and BAS 100B electrochemical analyser, recording data with BAS100W (Version 2.3).

Complex solutions of 0.001 M were dissolved in CH_3CN as solvent containing 0.1 M tetrabutylammonium hexafluorophosphate (TBAHFP, $[NBu_4][PF_6]$) as supporting electrolyte. Measurements were conducted under a blanket of argon at room temperature. A three-electrode cell, consisting of a Pt auxiliary electrode, a glassy carbon (surface area 0.0707 cm^2) working electrode and a reference electrode Ag/Ag^+ (0.01mM $AgNO_3$ in CH_3CN) mounted on a Luggin capillary was used. The working electrode was polished on a Buhler polishing mat with a 1 micron and a ¼ micron diamond paste respectively. Ferrocene was used as an internal standard.

4.2.4 Phase studies

Liquid crystal transitions and melting points were confirmed by Differential Scanning Calorimetry (DSC) and all temperatures quoted are onset values from the transitions. DSC results were obtained using Mettler TOLEDO DSC 822e/700 with STARe DB software (version 9.00). Measurements were conducted under a nitrogen atmosphere at room temperature with a N_2 flow of 3.5 $mlmin^{-1}$. Samples were mounted in aluminium crucibles of 40 microliter.

4.2.5 Purification and reaction progress

Thin layer chromatography (TLC) and Column chromatography using silica gel were used to purify and monitor the reaction progress of many materials. The TLC plate used consisted of fluorescent silica gel 60 F_{254} (Merk) on aluminium oxide 60 F_{254} (Fluka) on PET foil and all plates were inspected using ultraviolet light.

4.2.6 DFT calculations

Density functional theory (DFT) calculations of this study were performed with the B3LYP hybrid functional [1,2] (for the radical cations and anions uB3LYP was used) as implemented in the Gaussian 09 program package.[3] Geometries of the neutral and charged complexes were optimized in gas phase using the triple-ζ basis set 6-311G(d,p).

4.3 Synthesis and identification of compounds.

β-diketones Hβ1a, Hβ2a and Hβ2a were synthesized by adapting a published method by Han *et. al*[4] while Hβ4a was synthesized by adapting a published method by Wan *et. al*[5] and Hβ5a was synthesized by adapting a published method.[5,6]

4.3.1 Synthesis of γ-substituted β-diketones.

4.3.1.1 Synthesis of 2,4-dioxo-3-pentyl 4-hydroxybenzoate $CH_3COCH(COOC_6H_4OH)COCH_3$ (Hβ1a)

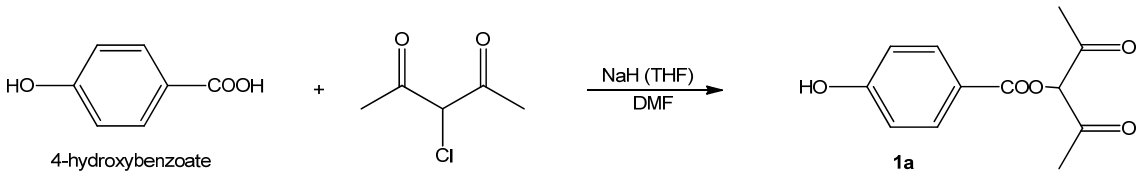

Sodium salt of 4-hydroxybenzoate was synthesised by 4- hydroxybenzoate (0.02mol., 2.7624g) in THF (15.0 ml pre-dried overnight) slowly added to a stirred suspension of sodium hydride (0.02 mol., 0.480g) in THF (20.0 ml pre-dried overnight). The reaction mixture was stirred overnight at room temperature. To the product, anhydrous DMF (25.0 ml) was added and stirred under argon for 30 minutes followed by 3-chloropentane-2,4-dione (0.02mol., 2.692g) in 10.0 ml of anhydrous DMF. Argon was passed through the light orange reaction mixture for another 30 minutes after which the reaction was stirred at 50-60^{0}C for 24hours under reflux. A light yellow reaction mixture was cooled at room temperature. Water (200.0

ml) was added and the product was extracted twice with 50.0 ml $CHCl_3$. Extracts were dried over sodium sulphate and the solvent was evaporated under reduced pressure. The product was purified by column chromatography with hexane: ethyl ether (2:3) solution as eluent which was evaporated under reduced pressure. A white precipitate produced was further purified by re-crystallisation in benzene two to three times. This gave a pale pink solid with a yield of 2.5404g (79%). δ_H (300 MHz, $CDCl_3$)/ppm: 2.0 (s, 6H, enol and keto overlap 2x CH_3), 5.5 (s, 1H, keto CH), 7.0 (d, 2H, C_6H_4), 8.0 (d, 2H, C_6H_4), 14.5 (s, 1H, overlap between enol CH and OH of γ-substituent).

4.3.1.2 Synthesis of 2,4-dioxo-3-pentyl 4-hydroxycinnamate $CH_3COCH(HOC_6H_4C_2H_2COO)COCH_3$ (Hβ2a)

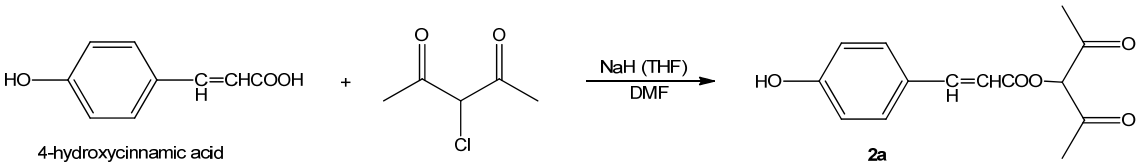

Sodium salt of 4-hydroxycinnmate was synthesised by 4- hydroxycinnamic acid (*p*-cuomeric acid 0.02 mol., 3.283g) in THF (15.0 ml pre-dried overnight) slowly added to a stirred suspension of sodium hydride (0.02 mol., 0.480g) in THF (20.0 ml pre-dried overnight). The reaction mixture was stirred overnight at room temperature. To the product anhydrous DMF (25.0 ml) was added and stirred under argon for 30 minutes followed by 3-chloropentane-2,4-dione (0.02 mol., 2.692g).in 10.0 ml of anhydrous DMF. Argon was passed through the light orange reaction mixture for another 30 minutes after which the reaction was stirred at 50-60^{0}C for 24hours under reflux. A light yellow reaction mixture was cooled at room temperature. Water (200.0 ml) was added and the product was extracted twice with 50.0 ml $CHCl_3$. Extracts were dried over sodium sulfate and the solvent was evaporated under reduced pressure. The product was purified by column chromatography with hexane: ethylacetate (1:3) solution as eluent. It was further purified by re-crystallisation in benzene. This gave a pale pink solid with a yield of 1.8401g (35%). δ_H (300 MHz, $CDCl_3$)/ppm: 2.3 (s, 6H, enol and keto overlap 2xCH_3), 5.6 (s, 1H, keto CH), 6.35, 6.4 (2s, 2x1H, -CH=CH), 6.8 (d, 2H, C_6H_4), 7.4 (d, 2H, C_6H_4), 7.65, 7.7 (2s, 2x1H, -CH=CH), 14.5 (s, 1H, overlap between enol CH and OH of γ-substituent).

4.3.1.3 Synthesis of 2,4-dioxo-3-pentyl 4- decanyloxybenzoate $CH_3COCH(C_{10}H_{21}OC_6H_4COO)COCH_3$ (Hβ3a).

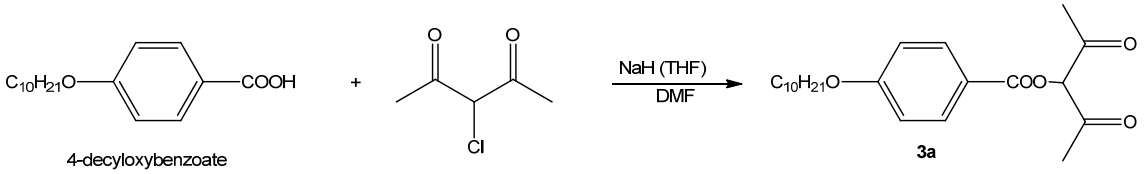

Sodium salt of 4-decyloxybenzoate was synthesised by 4- decyloxybenzoic acid (0.02mol., 5.688g) in THF (15.0 ml pre-dried overnight) slowly added to a stirred suspension of sodium hydride (0.02 mol., 0.480g) in THF (20.0 ml pre-dried overnight). The reaction mixture was stirred overnight at room temperature. To the product anhydrous DMF (25.0 ml) was added and stirred under argon for 30 minutes followed by 3-chloropentane-2,4-dione (0.02 mol., 2.692g) in 10.0 ml of anhydrous DMF. Argon was passed through the light orange reaction mixture for another 30 minutes after which the reaction was stirred at 50-60^{0}C for 24hours under reflux. A light yellow reaction mixture was cooled at room temperature. Water (200ml) was added and the product was extracted twice with 50.0 ml $CHCl_3$. Extracts were dried over sodium sulfate and the solvent was evaporated under reduced pressure. The product was purified by column chromatography with hexane: ethylacetate (1:3) solution as eluant. It was further purified by re-crystallisation in benzene. This gave a pale pink solid with a yield of 4.8348g (85 %). δ_H (300 MHz, $CDCl_3$)/ppm: 0.9 (t, 3H, CH_3), 1.2-1.5 (m, 14H, 7xCH_2), 1.75 (m, 2H, CH_2), 2.0, 2.3 (2s, 6H, keto and enol 2xCH_3), 4.0 (m, 2H, RCH_2OAr), 5.6 (s, 1H, keto CH), 6.9 (d, 2H, C_6H_4), 8.0 (d, 2H, C_6H_4), 14.5 (s, 1H, enol CH). m.p. 61.63 ˚C.

4.3.1.4 Synthesis of 2,4-dioxo-3-pentyl 4-[[4-(n-decanyloxy)benzoyl]oxy]benzoate $CH_3COCH(C_{10}H_{21}OC_6H_4COOC_6H_4COO)COCH_3$ (Hβ4a)

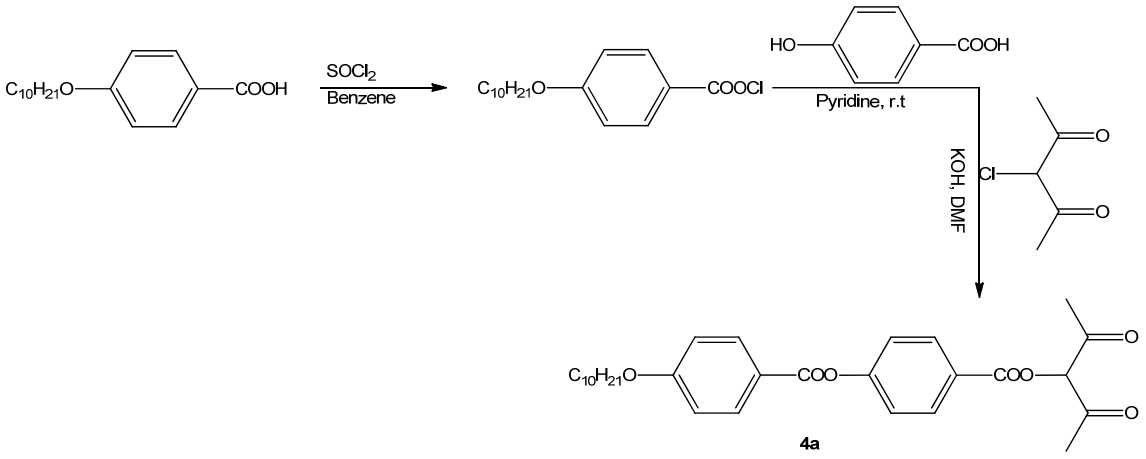

An acid 4-decyloxybenzoate (10 mmol, 2.7839g) was dissolved in 30.0 ml benzene. Thionyl chloride $SOCl_2$ (5.0 ml) was slowly added and the reaction mixture was refluxed overnight giving an appropriate chloride salt. Benzene was evaporated and to this salt 4-hydroxybenzoate (10 mmol, 1.3812g) in 30.0 ml pyridine was added and refluxed for 24 hours. The product 4-[[4-(n-decanyloxy)benzoyl]oxy]benzoic acid was extracted with CH_3Cl which was evaporated under reduced pressure and recrystallized in ethanol.

Grinded potassium hydroxide (0.003 mmol., 0.168g) was dissolved in 30.0 ml of DMF and stirred for thirty minutes. Pre-synthesized 4-[[4-(n-decanyloxy)benzoyl]oxy]benzoic acid (0.0015 mol., 0.50g) was added followed by the addition of 3-chloropentane-2,4-dione (0.0015 mol., 0.2018g) and the reaction mixture was stirred overnight under argon atmosphere. An orange reaction mixture was cooled at room temperature. Water (200ml) was added and the product was extracted three times with 100.0 ml $CHCl_3$. Extracts were dried over sodium sulfate and the solvent was evaporated under reduced pressure. The product was purified by column chromatography with hexane: ethylether (2:1) solution as eluent. It was further purified by re-crystallisation in ethanol. This gave a white solid with a yield of 0.160g (79%). δ_H (300 MHz, $CDCl_3$)/ppm: 0.8 (t, 3H, CH_3), 1.15-1.5 (m, 14H, 7xCH_2),1.75 (m, 2H, CH_2), 2.0, 2.4 (2s, 6H, keto and enol 2xCH_3), 4.0 (m, 2H, RCH_2OAr), 5.6 (s, 1H, keto CH), 6.9 (d, 2H, C_6H_4), 7.4 (d, 2H, C_6H_4), 8.1 (2d, 2x2H, 2x C_6H_4), 14.5 (s, 1H, enol CH). m.p. 80.1 ˚C.

4.3.1.5 Synthesis of 2,4-dioxo-3-pentyl-4-[[4-(n-decanyloxy)cinnamoyl]oxy]benzoate ($CH_3COCH(C_{10}H_{21}OC_6H_4C_2H_2COOC_6H_4COO)COCH_3$) (Hβ5a).

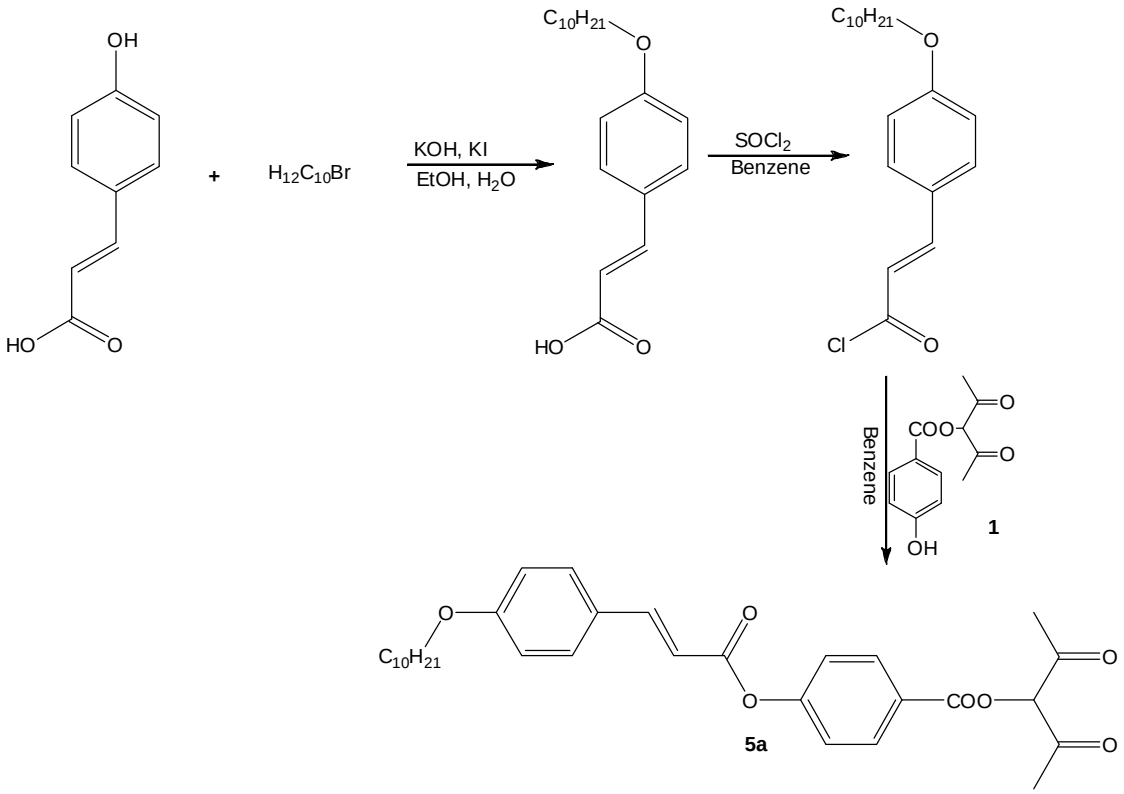

p-Hydroxcinnamic acid (0.03mol.,4.4962g) and KOH (0.06mol., 3.5569g) were dissolved in 150ml of ethanol and 50 ml of distilled water with a small amount of KI (0.5595g) as a catalyst. The solution was refluxed for an hour before a slow addition of 1-bromodecane (0.035mol., 7.7734g). Subsequently, the reaction mixture was refluxed for an additional 16 hours and cooled to room temperature after which the solvent was evaporated under reduced pressure. The residue was diluted with 80.0 ml of distilled water, washed with diethyl ether to remove unreacted bromodecane and acidified with 6M HCl. A precipitate, 4-(*n*-decyloxy)cinnamic acid was collected and washed several times with water and re-crystallised in ethanol. Yield: 3.0771g (68%).

To a solution of 4-(n-decyloxy)cinnamic acid (2 mmol., 0.5640g) in 20.0 ml of anhydrous benzene was added 2.5 ml of thionyl chloride under stirring. The reaction mixture was refluxed for 18 hours, cooled to room temperature and concentrated under reduced pressure. The residue was diluted with 30.0 ml of anhydrous benzene. To this solution was added 2,4-

dioxo-3-pentyl 4-hydroxybenzoate (2 mmol., 0.4720g) and refluxed for 24 hours. The solvent was evaporated under reduced pressure and the product was re-crystallised twice in ethanol. Yield: 0.320g (80%). δ_H (300 MHz, $CDCl_3$)/ppm: 0.9 (t, 3H, CH_3), 1.15-1.5 (m, 14H, 7xCH_2),1.75 (m, 2H, CH_2), 2.0, 2.4 (2s, 6H, keto and enol 2xCH_3), 4.0 (m, 2H, RCH_2OAr), 5.6 (s, 1H, keto CH), 6.4 (2s, 2x1H, -CH=CH), 6.9 (d, 2H, C_6H_4), 7.3 (d, 2H, C_6H_4), 7.5 (d, 2H, 2 C_6H_4), 7.7 (2s, 2x1H, -CH=CH), 8.1(d, 2H, C_6H_4),14.5 (s, 1H, enol CH). m.p. 99.5 ˚C.

4.3.2 Synthesis of γ-substituted [Rh(β-diketonato)dicarbonyl] complexes.

All [Rh(β-diketonato)$(CO)_2$] complexes were synthesized by adapting and optimizing published methods.[4,5,7]

4.3.2.1 Synthesis of 2,4-dioxo-3-pentyl-rhodium(I)-dicarbonyl

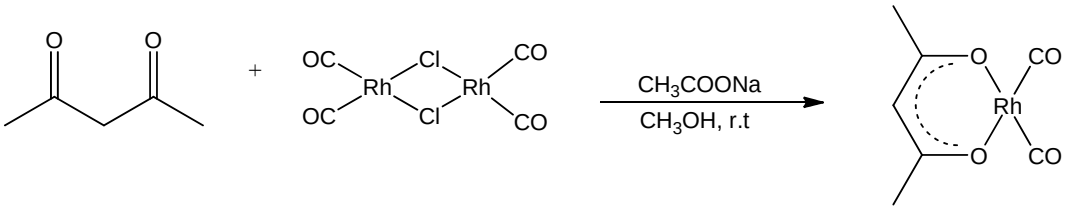

β-diketone (Hacac) (0.536 mmol., 53.6 mg) and sodium acetate (0.536 mmol., 44.0 mg) were dissolved in few drops of methanol. A saturated solution of rhodium dimer [$Rh_2(\mu\text{-}Cl)_2(CO)_4$] (0.268 mmol., 104 mg) in methanol was slowly added into the β-diketone-sodium acetate solution. The vials were washed with more ethanol and the washings were added into the reaction mixture. A dark green precipitate formed and the reaction mixture was stirred at room temperature for an hour. The resulting precipitate was separated by filtration, washed with methanol and left open to dry. Shiny dark green crystals gave a yield of 0.0723g (74%). δ_H (300 MHz, $CDCl_3$)/ppm: 2.0 (s, 6H, 2xCH_3), 5.51 (s, 1H). IR peaks: 1995; 2062 ν (CO) / cm^{-1}

4.3.2.2 Synthesis of 2,4-dioxo-3-pentyl-4-hydroxybenzoate rhodium(I)-dicarbonyl

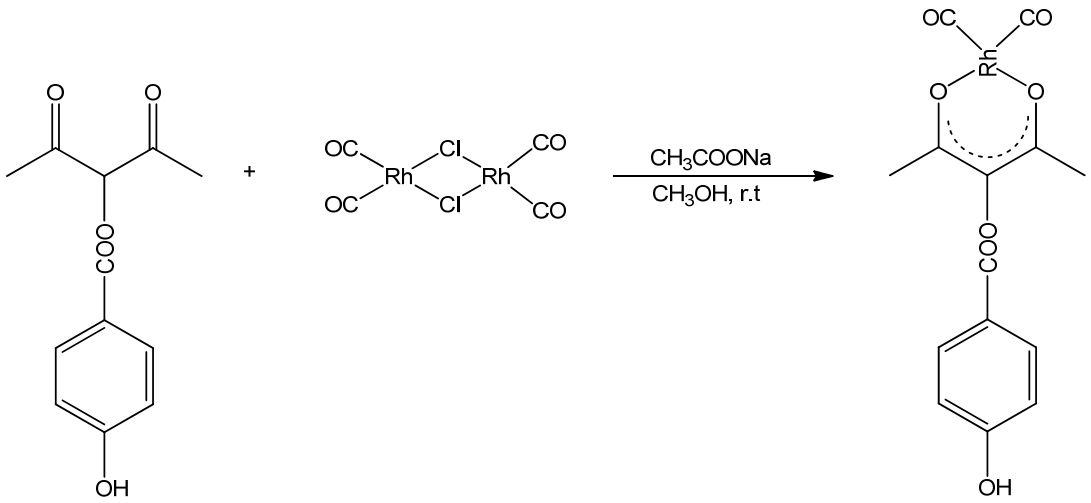

β-diketone (2,4-dioxo-3-pentyl-4-hydroxybenzoate) (0.536 mmol., 0.127g) and sodium acetate (0.536 mmol., 44.0 mg) were dissolved in few drops of methanol. A saturated solution of rhodium dimer $[Rh_2(\mu\text{-}Cl)_2(CO)_4]$ (0.268 mmol. 104 mg) in methanol was slowly added into the β-diketone-sodium acetate solution. The vials were washed with more ethanol and the washings were added into the reaction mixture. A yellow precipitate formed and the reaction mixture was stirred at room temperature for an hour. The resulting precipitate was separated by filtration, washed with methanol and left open to dry. A yellow precipitate gave a yield of 0.0651g (51.3%). δ_H (300 MHz, $CDCl_3$)/ppm: 2.0 (s, 6H, 2x CH_3), 6.9 (d, 2H, C_6H_4), 8.1 (d, 2H, C_6H_4). IR peaks: 2071; 2011 ν (CO) / cm^{-1}, 3396 ν (OH) / cm^{-1}

4.3.2.3 Synthesis of 2,4-dioxo-3-pentyl-4-hydroxycinnamate rhodium(I)-dicarbonyl

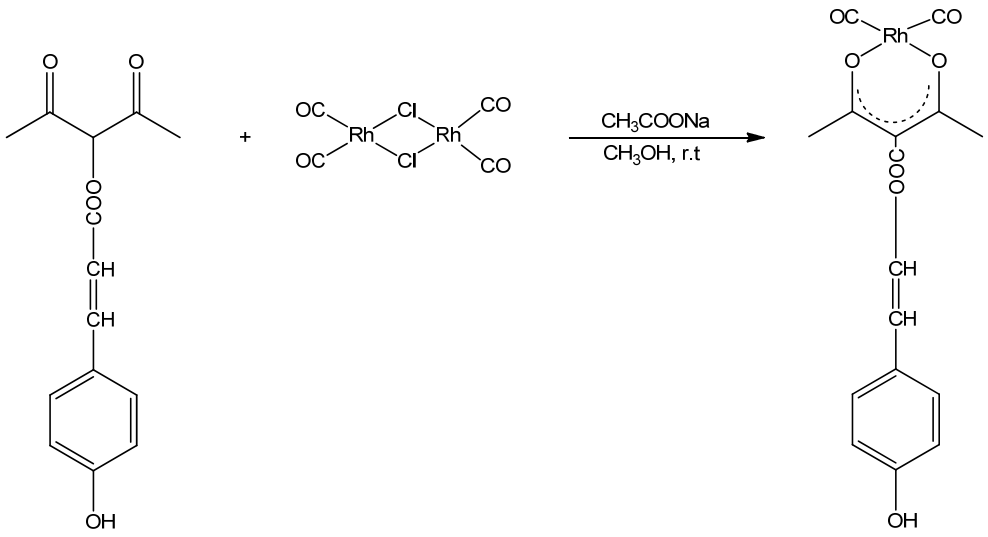

β-diketone (2,4-dioxo-3-pentyl-4-hydroxycinnamate) (0.536 mmol., 0.15g) and sodium acetate (0.536 mmol., 44.0 mg) were dissolved in few drops of methanol. A saturated solution of rhodium dimer $[Rh_2(\mu\text{-}Cl)_2(CO)_4]$ (0.268 mmol. 104 mg) in methanol was slowly added into the β-diketone-sodium acetate solution. The vials were washed with more ethanol and the washings were added into the reaction mixture. Ice was added to force precipitation of a yellow-orange product and the reaction mixture was stirred at room temperature for an hour. The resulting precipitate was recrystallized from hexane giving the expected product with a yield of 0.1214 g (81%). δ_H (300 MHz, $CDCl_3$)/ppm: 2.3 (s, 6H, 2xCH_3), 6.35, 6.4 (2s, 2x1H, -CH=CH), 6.8 (d, 2H, C_6H_4), 7.4 (d, 2H, C_6H_4), 7.65, 7.7 (2s, 2x1H, -CH=CH), 14.5 (s, 1H, OH of γ-substituent). IR peaks: 2071; 2003 ν (CO) / cm^{-1}, 3417 ν (OH) / cm^{-1}.

4.3.2.4 Synthesis of 2,4-dioxo-3-pentyl-4-decanyloxybenzoate rhodium(I)-dicarbonyl

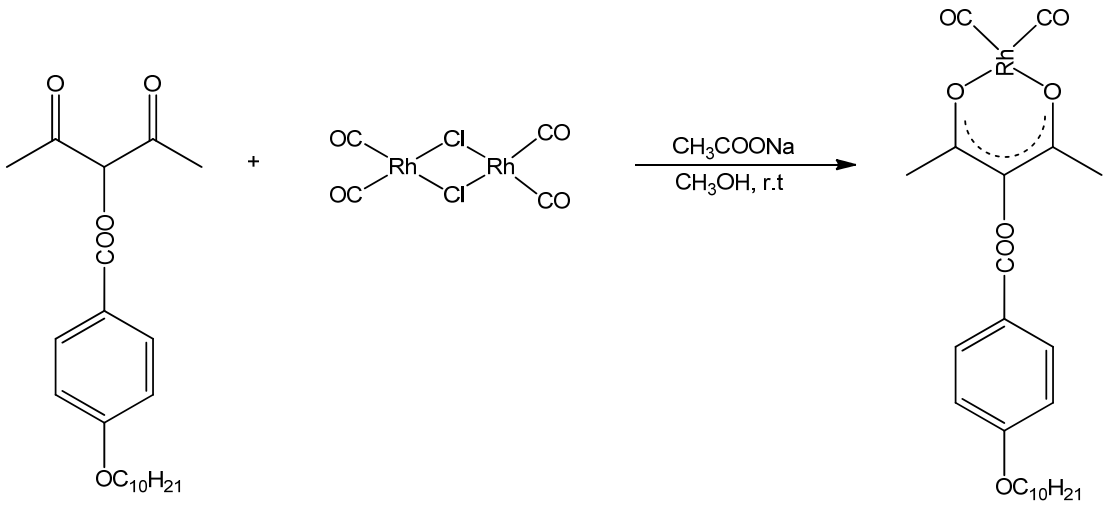

β-diketone (2,4-dioxo-3-pentyl-4-decanyloxybenzoate) (0.536 mmol., 0.14g) and sodium acetate (0.536 mmol., 44.0 mg) were dissolved in few drops of methanol. A saturated solution of rhodium dimer $[Rh_2(\mu\text{-}Cl)_2(CO)_4]$ (0.268 mmol. 104 mg) in methanol was slowly added into the β-diketone-sodium acetate solution. The vials were washed with more ethanol and the washings were added into the reaction mixture. Ice was added to force precipitation of a yellow-orange product and the reaction mixture was stirred at room temperature for an hour. The resulting precipitate was recrystallized from hexane giving the expected product with a yield of 0.1029 g (74%). δ_H (300 MHz, $CDCl_3$)/ppm: 0.9 (t, 3H, CH_3), 1.2-1.5 (m, 14H, $7xCH_2$),1.75 (m, 2H, CH_2), 2.2 (s, 6H, $2xCH_3$), 4.0 (m, 2H, RCH_2OAr), 6.9 (d, 2H, C_6H_4), 8.1 (d, 2H, C_6H_4). IR peaks: 2079; 2005 ν (CO) / cm^{-1}, 2925; 2854 ν (CH) / cm^{-1}. m.p. 87.9 °C.

4.3.2.5 Synthesis of 2,4-dioxo-3-pentyl-4-[[4-(n-decanyloxy)benzoyl]oxy]benzoate rhodium(I)-dicarbonyl

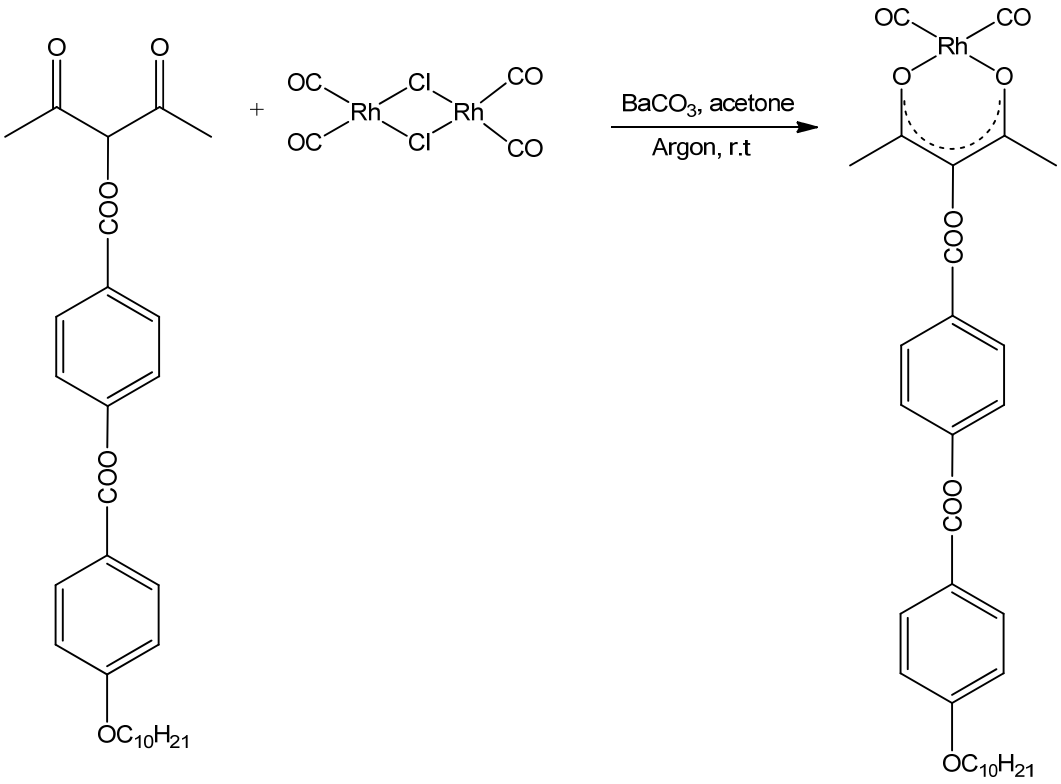

The dimer $[Rh_2Cl_2(CO)_4]$ (0.05mmol.;0.0195g) was dissolved in 10.0ml of acetone. β-diketone 2,4-dioxo-3-pentyl-4-[[4-(n-decanyloxy)benzoyl]oxy]benzoate (0.1mmol.;0.0516g) was dissolved in 5.0ml of acetone. The two acetone solutions were mixed in a round bottom flask where barium carbonate ($BaCO_3$) (10mmol, 1.9671g) was added. The reaction mixture was stirred under argon atmosphere at room temperature for two hours. The resulting precipitate was filtered off and evaporated under reduced pressure, giving a yellow precipitate of 0.045g yield (90%). δ_H (300 MHz, $CDCl_3$)/ppm: 0.9 (t, 3H, CH_3), 1.2-1.5 (m, 14H, 7xCH_2),1.75 (m, 2H, CH_2), 2.05 (s, 6H, 2xCH_3), 4.0 (m, 2H, RCH_2OAr), 6.9 (d, 2H, C_6H_4), 7.4 (d, 2H, C_6H_4), 8.1 (d, 2H, C_6H_4), 8.2 (d, 2H, C_6H_4). IR peaks: 2079; 2005 ν (CO) / cm^{-1}, 2925; 2854 ν (CH) / cm^{-1}. m.p. 127.9 ˚C.

4.3.2.6 Synthesis of 2,4-dioxo-3-pentyl-4-[[4-(n-decanyloxy)cinnamoyl]oxy]benzoate rhodium(I)-dicarbonyl

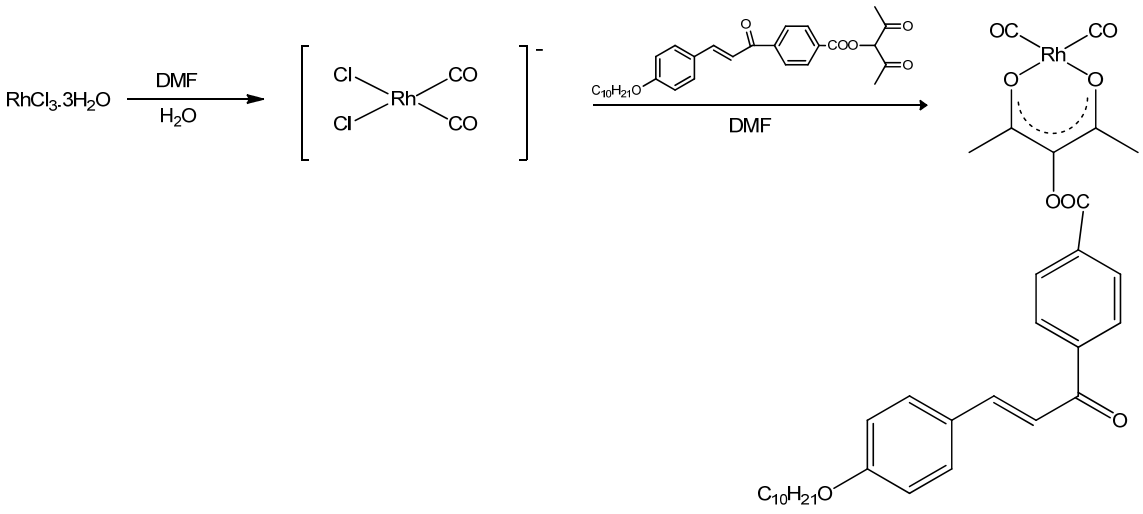

The reaction flask was washed by refluxing DMF for three hours and poured out. The flask was allowed to cool and rhodiumchlorohydrate ($RhCl_3.H_2O$) (0.38mmol., 0.1g) was put in, dissolved with eight drops of water and ca 4.0ml of DMF. The dark red mixture was stirred under reflux for one hour until a yellow-orange colour was observed. The reaction mixture was cooled to room temperature then β-diketone 2,4-dioxo-3-pentyl-4-[[4-(n-decanyloxy)cinnamoyl]oxy]benzoate (0.3mol., 0.2919g) was slowly added and further stirred for one hour at room temperature. Ice was added while stirring for another hour to enhance precipitation. The yellow product was filtered off, washed with water, dried and recrystallized in hot hexane giving a yield of 0.0586g (58.6%). δ_H (300 MHz, $CDCl_3$)/ppm: 0.9 (t, 3H, CH_3), 1.15-1.5 (m, 14H, 7xCH_2),1.75 (m, 2H, CH_2), 2.1 (s, 6H, 2xCH_3), 4.0 (m, 2H, RCH_2OAr), 6.4 (2s, 2x1H, -CH=CH), 6.9 (d, 2H, C_6H_4), 7.3 (d, 2H, C_6H_4), 7.5 (d, 2H, 2 C_6H_4), 7.7 (2s, 2x1H, -CH=CH), 8.3(d, 2H, C_6H_4). IR peaks: 2079; 2005 ν (CO) / cm^{-1}, 2925; 2854 ν (CH) / cm^{-1}. m.p. 146.6 ˚C.

4.3.3 Synthesis of γ-substituted β-diketonato-Rh(I)-monocarbonyl-PPh_3 complexes

All γ-substituted β-diketonato-Rh(I)-monocarbonyl-PPh_3 complexes were synthesized by adapting published methods.[7]

4.3.3.1 Synthesis of 2,4-dioxo-3-pentyl-rhodium(I)-monocarbonyl-PPh_3

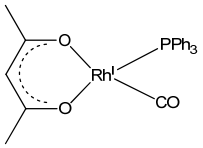

To a solution of [Rh(Hacac)$(CO)_2$] (0.1mmol, 0.0259g) in 30.0 ml *n*-hexane was added a solution of PPh_3 (0.1mmol, 0.0262g) in warm 15.0ml *n*-hexane which resulted in bubbling off of CO gas. The resulting reaction mixture was stirred for 5min. in a boiling water bath until no more CO gas was released and filtered while still warm. Pure crystals of the desired complex were obtained by slowly cooling the filtered reaction mixture overnight at room temperature. Yield 0.0322g (80.4)%. δ_H (300 MHz, $CDCl_3$)/ppm: 1.25 (s, 3H, CH_3), 2.4 (s, 3H, CH_3), 4.7 (s, 1H, CH), 7.3 – 7.7 (m, 15H, 3xC_6H_5).

4.3.3.2 Synthesis of 2,4-dioxo-3-pentyl-4-hydroxybenzoate rhodium(I)-monocarbonyl-PPh_3

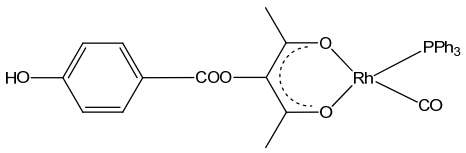

To a solution of [Rh(Hβ1a)$(CO)_2$] (0.1mmol, 0.0402g) in 30.0 ml n-hexane was added a solution of PPh_3 (0.1mmol, 0.0269g) in warm 15.0ml n-hexane which resulted in bubbling off of CO gas. The resulting reaction mixture was stirred for 5min. in a boiling water bath until no more CO gas was released and filtered while still warm. Pure crystals of the desired complex were obtained by slowly cooling the filtered reaction mixture overnight at room temperature. Yield 0.0352g (87.6%). ^{31}P NMR (CH_2Cl_2): δ (ppm) 50.0 (d, $^1J_{Rh\text{-}P}$ = 180.02 Hz).

4.3.3.3 Synthesis of 2,4-dioxo-3-pentyl-4-hydroxycinnamate rhodium(I)-monocarbonyl-PPh_3

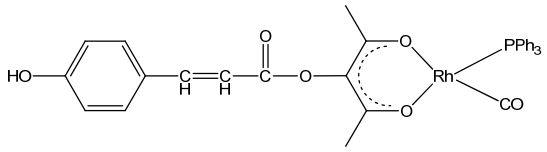

To a solution of $[Rh(H\beta 2a)(CO)_2]$ (0.1mmol, 0.0426g) in 30.0 ml n-hexane was added a solution of PPh_3 (0.1mmol, 0.0262g) in warm 15.0ml n-hexane which resulted in bubbling off of CO gas. The resulting reaction mixture was stirred for 5min. in a boiling water bath until no more CO gas was released and filtered while still warm. Pure crystals of the desired complex were obtained by slowly cooling the filtered reaction mixture overnight at room temperature. Yield 0.0496g (84.9%). δ_H (300 MHz, $CDCl_3$)/ppm: 2.3 (s, 6H, $2xCH_3$), 6.4, 6.5 (2s, 2x1H, -CH=CH), 6.8 (d, 2H, C_6H_4), 7.4 (m, 9H, C_6H_5) 7.5 (d, 2H, C_6H_4), 7.65 (m, 6H, C_6H_5), 7.7, 7.8 (2s, 2xH, -CH=CH).

4.3.3.4 Synthesis of 2,4-dioxo-3-pentyl-4-decanyloxybenzoate rhodium(I)-monocarbonyl-PPh_3

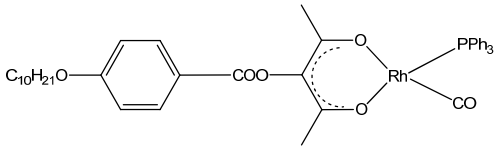

To a solution of $[Rh(H\beta 3a)(CO)_2]$ (0.1mmol, 0.0544g) in 30.0 ml n-hexane was added a solution of PPh_3 (0.1mmol, 0.0262g) in warm 15.0ml n-hexane which resulted in bubbling off of CO gas. The resulting reaction mixture was stirred for 5min. in a boiling water bath until no more CO gas was released and filtered while still warm. Pure crystals of the desired complex were obtained by slowly cooling the filtered reaction mixture overnight at room temperature. Yield 0.0429g (79.8%). δ_H (300 MHz, $CDCl_3$)/ppm: 0.9 (t, 3H, CH_3), 1.2-1.5 (m, 16H, $7xCH_2$, one of $2xCH_3$), 1.75 (m, 2H, CH_2), 2.2 (s, 3H, one of $2xCH_3$), 4.0 (m, 2H, RCH_2OAr), 6.9 (d, 2H, C_6H_4), 7.3-7.5 (m, 9H, C_6H_5), 7.6 (m, 6H, C_6H_5), 8.1 (d, 2H, C_6H_4).

4.3.3.5 Synthesis of 2,4-dioxo-3-pentyl-4-[[4-(n-decanyloxy)benzoyl]oxy]benzoate rhodium(I)-monocarbonyl-PPh_3

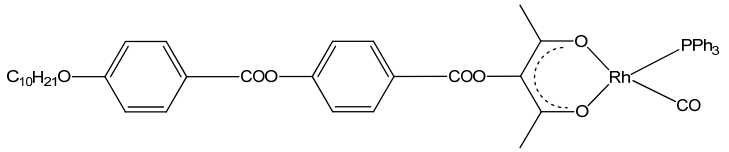

To a solution of [Rh(Hβ4a)$(CO)_2$] (0.1mmol, 0.0259g) in 30.0 ml n-hexane was added a solution of PPh_3 (0.1mmol, 0.0262g) in warm 15.0ml n-hexane which resulted in bubbling off of CO gas. The resulting reaction mixture was stirred for 5min. in a boiling water bath until no more CO gas was released and filtered while still warm. Pure crystals of the desired complex were obtained by slowly cooling the filtered reaction mixture overnight at room temperature. Yield 0.0322g (80.4%). %. δ_H (300 MHz, $CDCl_3$)/ppm: 0.9 (t, 3H, CH_3), 1.2-1.4 (m, 14H, 7xCH_2), 1.6 (s, 3H, one of 2xCH_3), 1.75 (m, 2H, CH_2), 2.05 (s, 3H, one of 2xCH_3), 4.0 (m, 2H, RCH_2OAr), 6.9 (d, 2H, C_6H_4), 7.3-7.5 (m, 10H, C_6H_5), 7.6 (m, 5H, C_6H_5), 8.1 (d, 2H, C_6H_4), 8.2 (d, 2H, C_6H_4). IR peaks: 2079; 2005 ν (CO) / cm^{-1}, 2925; 2854 ν (CH) / cm^{-1}.

4.3.3.6 Synthesis of 2,4-dioxo-3-pentyl-4-[[4-(n-decanyloxy)cinnamoyl]oxy]benzoate rhodium(I)-monocarbonyl-PPh_3

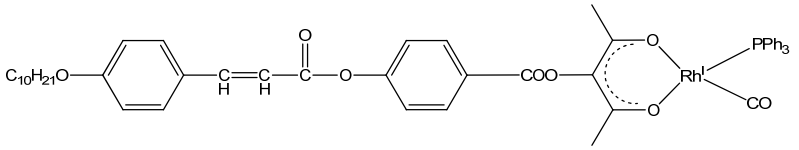

To a solution of [Rh(Hβ5a)$(CO)_2$] (0.1mmol, 0.0259g) in 30.0 ml n-hexane was added a solution of PPh_3 (0.1mmol, 0.0262g) in warm 15.0ml n-hexane which resulted in bubbling off of CO gas. The resulting reaction mixture was stirred for 5min. in a boiling water bath until no more CO gas was released and filtered while still warm. Pure crystals of the desired complex were obtained by slowly cooling the filtered reaction mixture overnight at room temperature. Yield 0.0322g (80.4%). δ_H (300 MHz, $CDCl_3$)/ppm: 0.9 (t, 3H, CH_3), 1.15-1.5 (m, 14H, 7xCH_2), 1.6 (s, 3H, one of 2xCH_3), 1.75 (m, 2H, CH_2), 2.1 (s, 3H, one of 2xCH_3), 4.0 (m, 2H, RCH_2OAr), 6.4 (2s, 2x1H, -CH=CH), 6.9 (d, 2H, C_6H_4), 7.1 (d, 2H, C_6H_4), 7.2-7.4 (m, 10H, C_6H_5), 7.5 (m, 5H, C_6H_5), 7.6 (d, 2H, 2 C_6H_4), 7.7 (2s, 2x1H, -CH=CH), 8.3(d, 2H, C_6H_4). ^{31}P NMR (CH_2Cl_2): δ (ppm) 50.0 (d, $^1J_{Rh\text{-}P}$ = 180.02 Hz).

References

[1] Becke, A. D. *Density-functional exchange-energy approximation with correct asymptotic behavior*, *Physical Review A*, **1988**, 38, 3098.

[2] Lee, C. T. Yang, W.T. Parr, R.G. *Development of the Colle-Salvetti correlation-energy formula into a functional of the electron-density, Physical Review B* **1988**, 37, 785.

[3] M.J. Frisch, G.W. Trucks, H.B. Schlegel, G.E. Scuseria, M.A. Robb, J.R. Cheeseman, G. Scalmani, V. Barone, B. Mennucci, G.A. Petersson, H. Nakatsuji, M. Caricato, X. Li, H.P. Hratchian, A.F. Izmaylov, J. Bloino, G. Zheng, J.L. Sonnenberg, M. Hada, M. Ehara, K. Toyota, R. Fukuda, J. Hasegawa, M. Ishida, T. Nakajima, Y. Honda, O. Kitao, H. Nakai, T. Vreven, J.A. Montgomery (Jr), J.E. Peralta, F. Ogliaro, M. Bearpark, J.J. Heyd, E. Brothers, K.N. Kudin, V.N. Staroverov, T. Keith, R. Kobayashi, J. Normand, K. Raghavachari, A. Rendell, J.C. Burant, S.S. Iyengar, J. Tomasi, M. Cossi, N. Rega, J.M. Millam, M. Klene, J.E. Knox, J.B. Cross, V. Bakken, C. Adamo, J. Jaramillo, R. Gomperts, R.E. Stratmann, O. Yazyev, A.J. Austin, R. Cammi, C. Pomelli, J.W. Ochterski, R.L. Martin, K. Morokuma, V.G. Zakrzewski, G.A. Voth, P. Salvador, J.J. Dannenberg, S. Dapprich, A.D. Daniels, O. Farkas, J.B. Foresman, J.V. Ortiz, J. Cioslowski, D.J. Fox, *Gaussian 09, Revision C.01*, Gaussian Inc., Wallingford CT, **2010**.

[4] Han, J., Zhang, L. F., Wan, W. *Journal of Organometallic Chemistry* **2003**, 672, 86.

[5] Wan, W., Guang, W.J., Zhao, K. Q., Zheng, W. Z., Zhang, L. F. *J. Organomet. Chem.* **1998**, 557, 157.

[6] Zheng, W. Y., Hammond, P. T. *Macromol. Rapid Comm*. **1996**, 17, 813

[7] (a) Conradie, M. M., Conradie, J. *Inorg. Chim. Acta* **2008**, 361, 2285. (b) Erasmus, J. J. C., Conradie, J. Dalton Trans., 2013, 42, 8. (c) Stuurman, N. F., Conradie, J. J. Organomet. Chem. **2009**, 694, 259. (d) Bonati, F., Wilkinson, G. J. Chem. Soc. **1964**, 3156. (e) Graham, D. E., Lamprecht, G. J., Potgieter, I. M., Roodt, A., Leipoldt, J. G. Transition Met. Chem. **1991**, 16, 193. (f) Leipoldt, J. G., Basson, S. S., Nel, J. T. Inorg. Chim. Acta **1983**, 74, 85. (g) Conradie, J., Lamprecht, G. J., Otto, S., Swarts, J. C. *Inorg. Chim. Acta* **2002**, 328, 191.

5

Concluding remarks

In this study new and selected, known beta- and gamma-substituted beta-diketones, as well as their rhodium complexes were synthesised. Known synthetic protocols were optimised to enhance synthetic yields. These complexes were characterised spectroscopically with ^{1}H NMR, ^{31}P NMR and IR spectroscopy. Electrochemical (voltammetry) and phase (DSC and POM) studies were used to investigate physical properties.

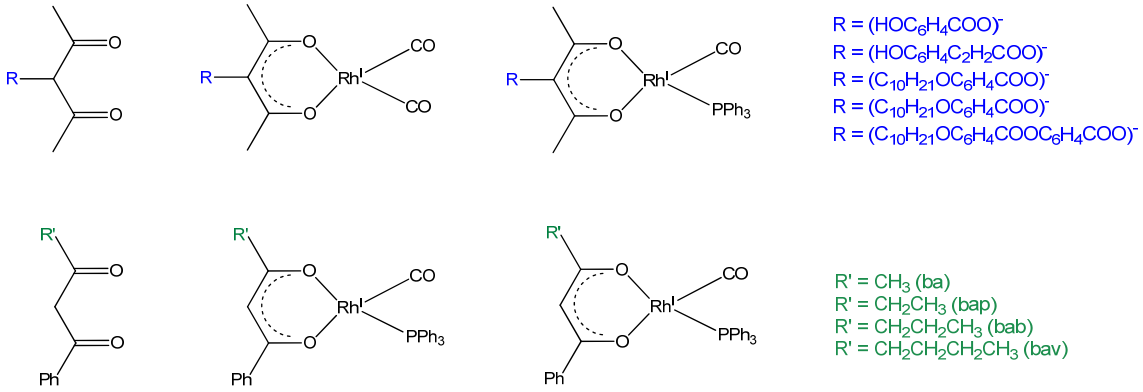

The electrochemical reduction of the different gamma-substituted beta-diketones showed that the first reduction of the gamma-substituted beta-diketones occurs at the acid substituent moiety while the second reduction occurs at the beta-diketone backbone. A third reduction, where possible, occurs again at the acid moiety. DFT calculations were used as a tool to understand the electrochemical results of gamma-substituted beta-diketones. These calculations confirmed the assignment of the reductions.

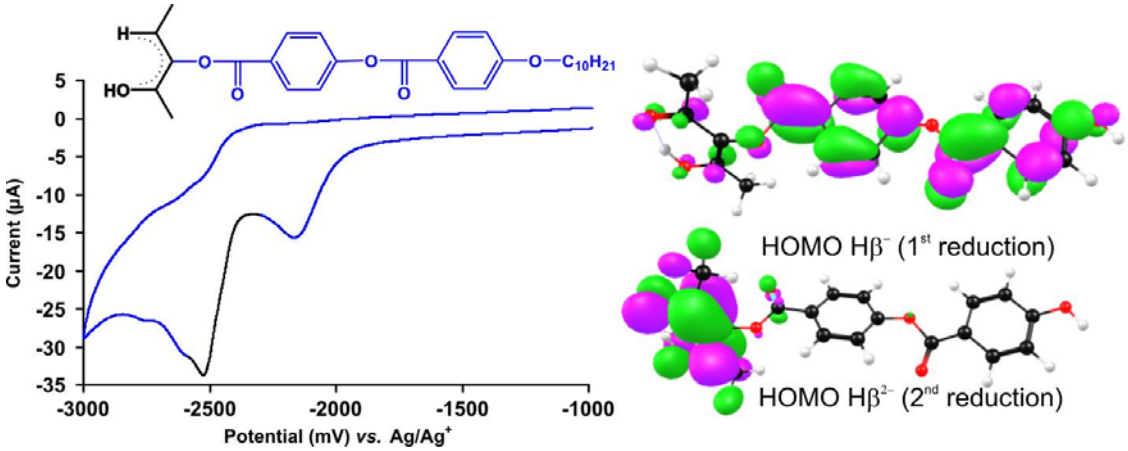

Cyclic voltammogram of 1 mmol dm^{-3} Hβ4a at a scan rate of 100 mVs^{-1}, measured in 0.1 mol dm^{-3} $[NBu_4][PF_6]$ /CH_3CN on a glassy carbon working electrode at 25 °C. The location of the added electron after the first and second reduction can be visualized by the HOMOs of $Hβ4a^-$ and $Hβ4a^{2-}$ respectively.

Electrochemical oxidation of Rh(I) to Rh(III) of both [Rh(β-diketonato)$(CO)_2$] and [Rh(β-diketonato)$(CO)(PPh_3)$] involves the removal of $2e^-$ from the HOMO, which is mainly of d_{z2}, character of the complex. The Rh(III) complex with an empty dz^2 orbital is very unstable and it is proposed that solvent co-ordination to Rh(III) takes place.

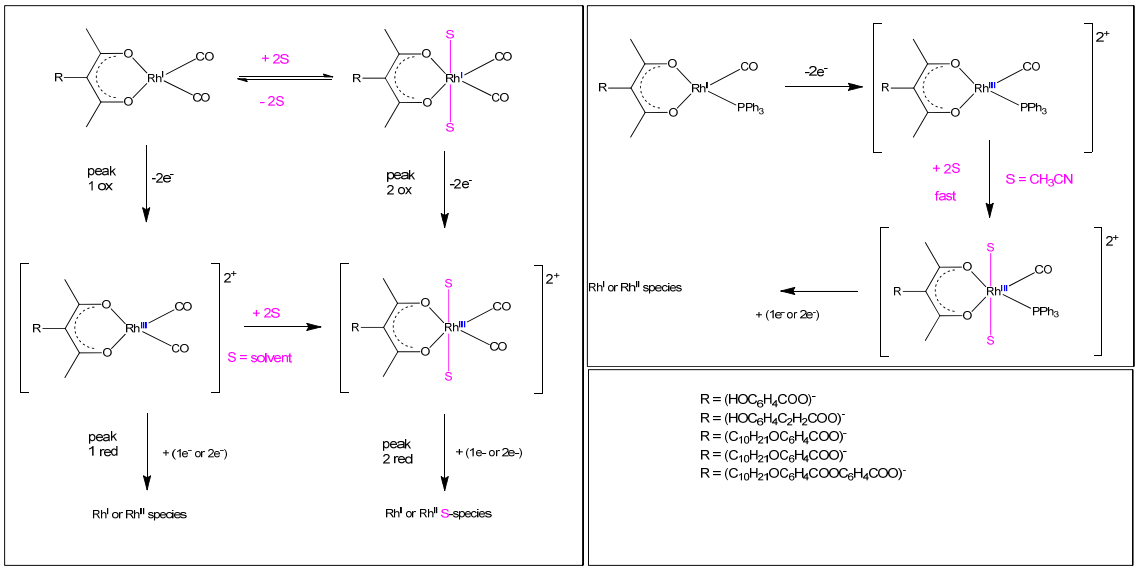

In considering the phase transition properties of the gamma-substituted β-diketones **3a** – **5a**, as well as their dicarbonyl and phosphine complexes, we observe that the solid crystalline free gamma-substituted β-diketones exhibit different liquid crystalline mesophases before melting to an isotropic liquid. The [Rh(β-diketonato)$(CO)_2$] complexes **3b** – **5b** exhibit clear crystalline solid and isotropic liquid phases. In contrast, the [Rh(β-diketonato)$(CO)(PPh_3)$] **3c** – **5c** are amorphous solids (without any crystal packing) that liquefy without showing crystalline behaviour.

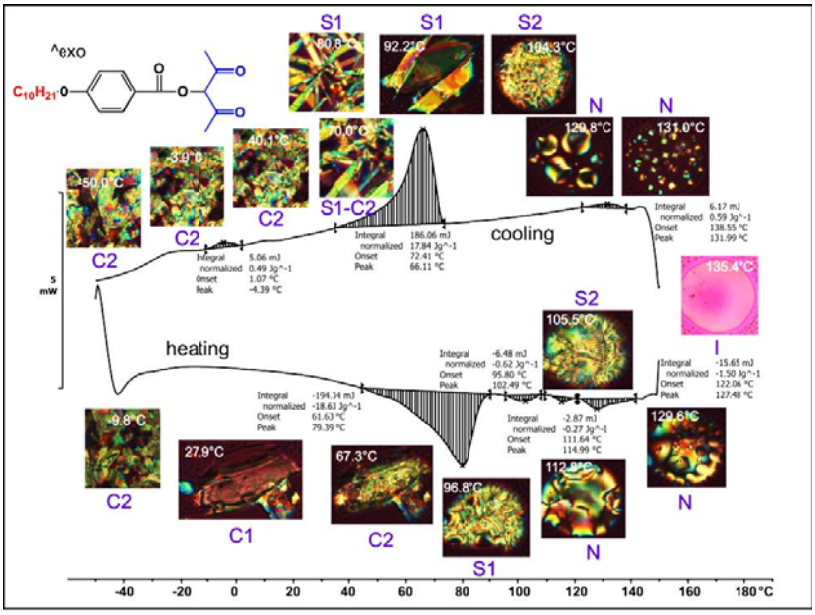

DSC thermogram with POM photos of the different phases observed during heating and cooling at a rate of 10°C min^{-1} for 2,4-dioxo-3-pentyl-4-decanyloxybenzoate ($CH_3COCH(C_{10}H_{21}OC_6H_4COO)COCH_3$) Hβ3a. DSC sample mass = 10.45 mg. Events i – v are associated with the heating cycle and events v' – i' are associated with the cooling curve. (The roman numbers with the dashed line indicate the onset of the events).

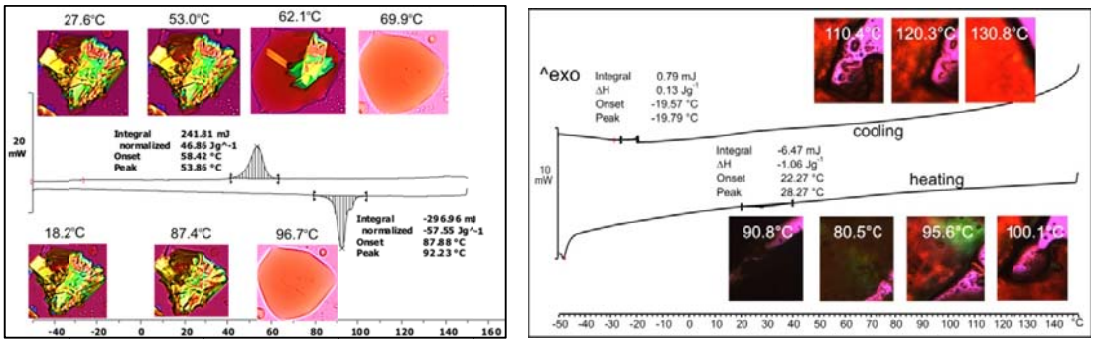

DSC thermograms at 10 °C min^{-1} heating and cooling rates as well as images observed under polarized light optical microscopy, magnification ×100 for [Rh(β3a)$(CO)_2$] (left) and [Rh(β3a)$(CO)(PPh_3)$] (right).

Abstract

Synthetic routes to prepare β-substituted and γ-substituted β-diketones, rhodium(I)dicarbonyl and rhodium(I)monocarbonyltriphosphine complexes were developed and optimised. All complexes were characterised with ^{1}H NMR, ^{31}P NMR, and IR. Further characterisation of the complexes was done by means of the electrochemical techniques, DSC and POM.

Cyclic voltammetry of the studied complexes shows irreversible chemical and electrochemical behaviour for both the reduction of the ligands and the oxidation of Rh(I). DFT calculations were used to optimise the neutral, the reduced, doubly reduced and triply reduced β-diketones, as applicable.

Phase study of the synthesized compounds was done by means of a differential scanning calorimeter and a polarizing optical microscope. It was found that β-diketones exhibit different liquid crystalline mesophases before melting to an isotropic liquid. Rhodium(I)dicarbonyl complexes exhibit clear crystalline solid and isotropic liquid phases, while [Rh(β-diketonato)(CO)(PPh_3)] has no crystal packing.

Key words

β-substituted β-diketones, γ-substituted β-diketones, rhodium(I)dicarbonyl, rhodium(I)monocarbonyltriphosphine, DFT, Cyclic voltammetry, DSC Phase study.

Opsomming

Sintetiese roetes vir β- en γ-gesubstieerde β-diketone, rodium(I)dikarboniel en rodium(I)monokarbonieltrifosfien komplekse was ontwikkel en geoptimaliseer. Alle komplekse is deur middel van ^{1}H KMR, ^{31}P KMR en IR gekarakteriseer. Verdere karakterisering van die komplekse is deur middel van elektrochemiese tegnieke, DSC en POM gedoen.

Sikliese voltammetrie van die bestudeerde komplekse toon chemiese en elektrochemiese onomkeerbare prosesse vir beide die reduksie van die ligand en die oksidasie van Rh(I). DFT berekeninge is gebruik om, waar van toepassing, die neutrale, die gereduseerde, die dubbel gereduseerde en die trippel gereduseerde β-diketone te optimiseer.

'n Fasestudie van die gesintetiseerde komplekse is gedoen met behulp van 'n DSC ("differential scanning calorimeter") en 'n POM (polariserings optiese mikroskoop). Dit is gevind dat β-diketone verskillende kristallyne meso-fases toon voordat dit in 'n isotropiese vloeistof in smelt. Rodium(I)dikarboniel komplekse toon duidelike kristallyn vaste- en isotropiese vloeistof fases, terwyl [Rh(β-diketonato)(CO)(PPh_3)] geen kristalpakking toon nie.

Sleutelwoorde

β-gesubstieerde β-diketone, γ-gesubstieerde β-diketone, rodium(I)dikarboniel, rodium(I)monokarbonieltrifosfien, DFT, sikliese voltammetrie, DSC fasestudie.

A ^{1}H NMR and ^{31}P NMR

1. β-diketones

1.1. ^{1}H NMR

Spectrum 1: ***2,4-dioxo-3-pentyl 4-hydroxybenzoate*** **[$CH_3COCH(COOC_6H_4OH)COCH_3$] (Hβ1a)**

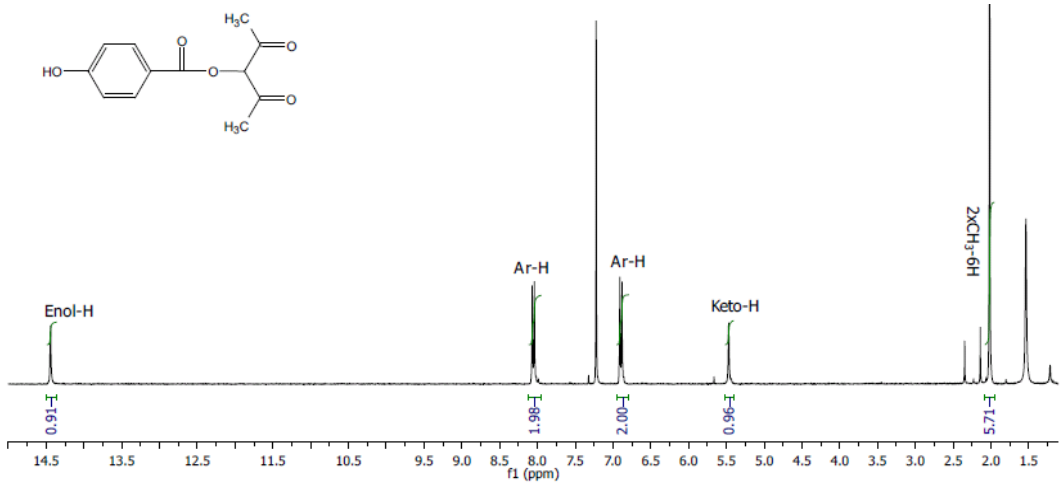

Spectrum 2. ***2,4-dioxo-3-pentyl 4-hydroxycinnamate*** **[($CH_3COCH(HOC_6H_4C_2H_2COO)COCH_3$)] (Hβ2a).**

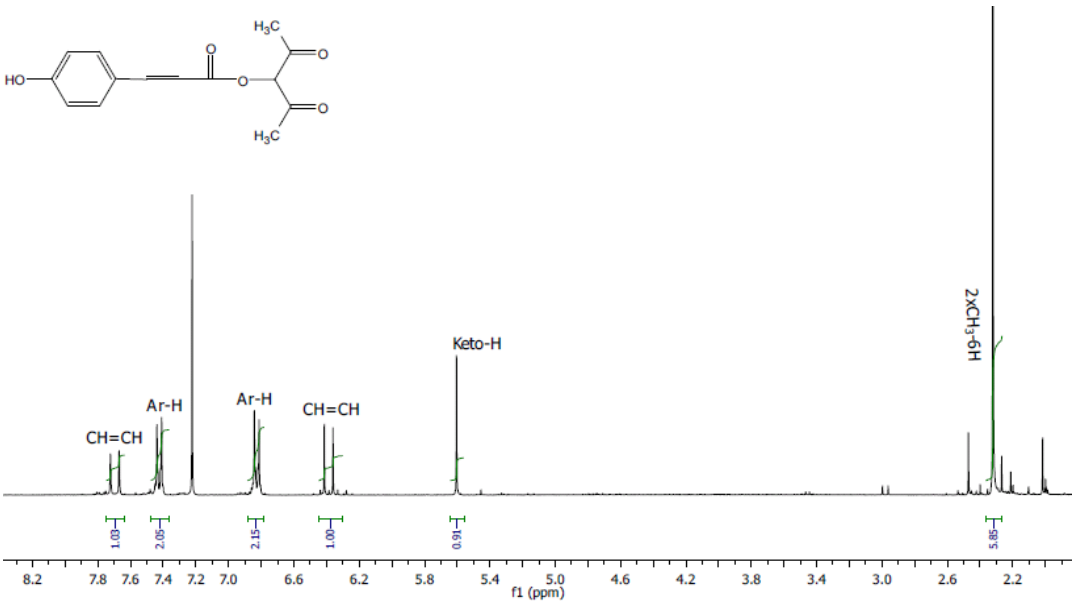

Spectrum 3. ***2,4-dioxo-3-pentyl 4- decanyloxybenzoate*** **[$CH_3COCH(C_{10}H_{21}OC_6H_4COO)COCH_3$] (Hβ3a).**

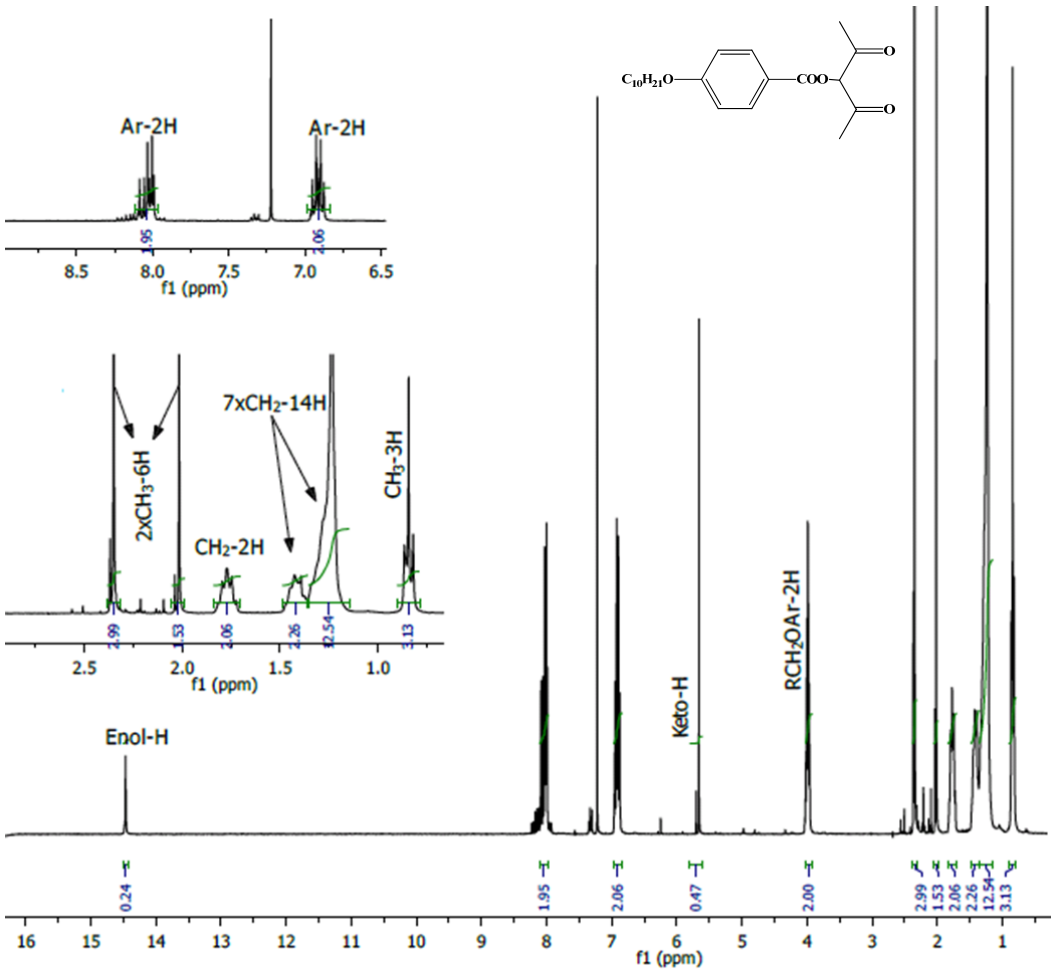

Spectrum 4: ***2,4-dioxo-3-pentyl 4-[[4-(n-decanyloxy)benzoyl]oxy]benzoate***
$[CH_3COCH(C_{10}H_{21}OC_6H_4COOC_6H_4COO)COCH_3]$ (Hβ4a).

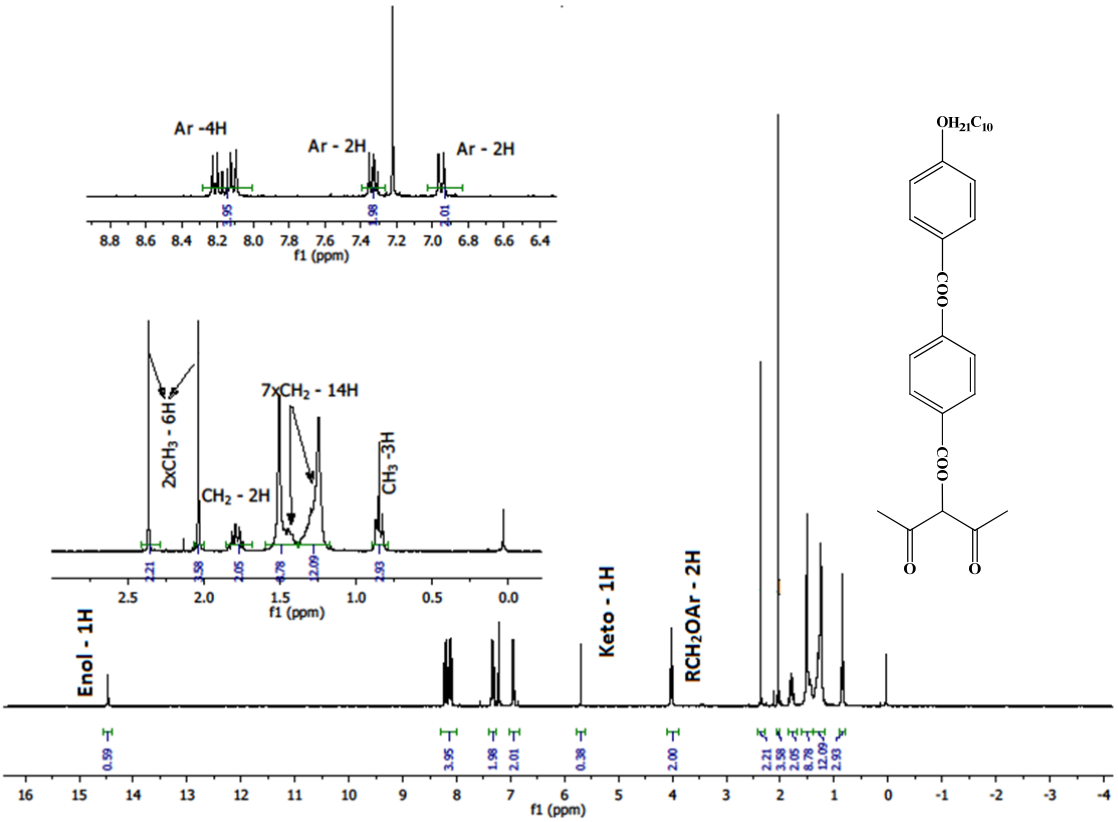

Spectrum 5: ***2,4-dioxo-3-pentyl-4-[[4-(n-decanyloxy)cinnamoyl]oxy]benzoate*** **$[CH_3COCH(C_{10}H_{21}OC_6H_4C_2H_2COOC_6H_4COO)COCH_3]$ (Hβ5a).**

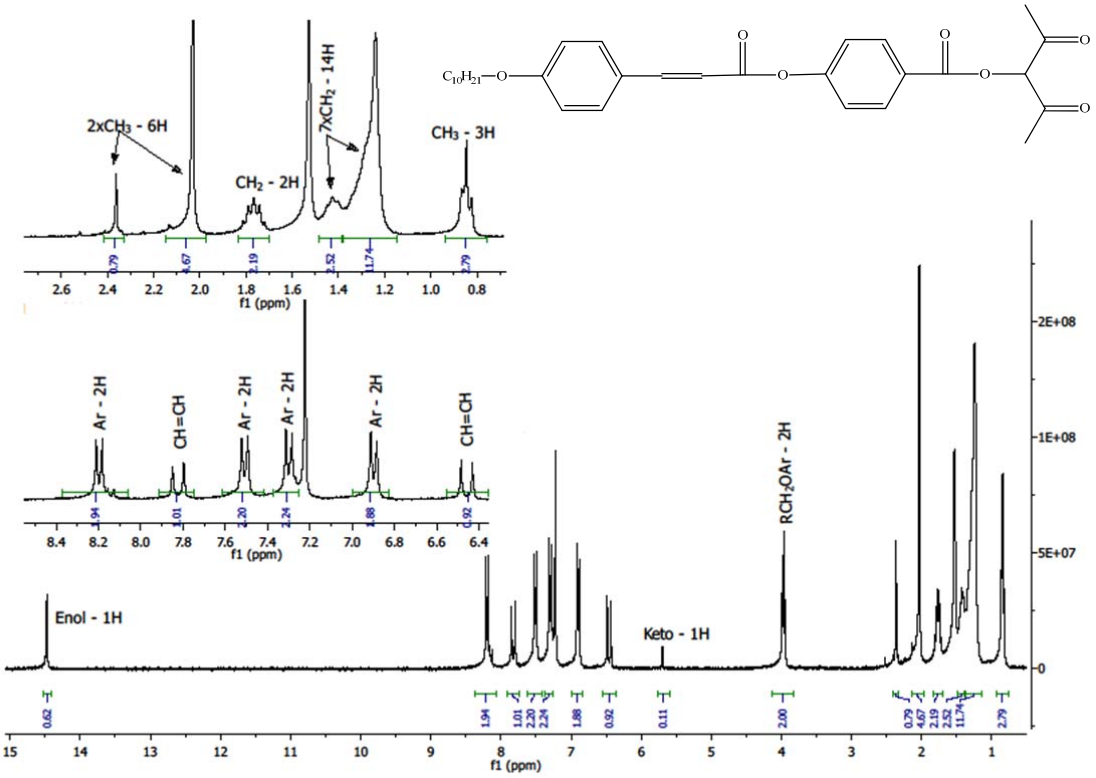

2. Rh(I)-dicarbonyls

2.1. ^{1}H NMR

Spectrum 6: ***2,4-dioxo-3-pentyl-4-hydroxybenzoate rhodium(I)-dicarbonyl*** **$[Rh(\beta 1a)(CO)_2]$**

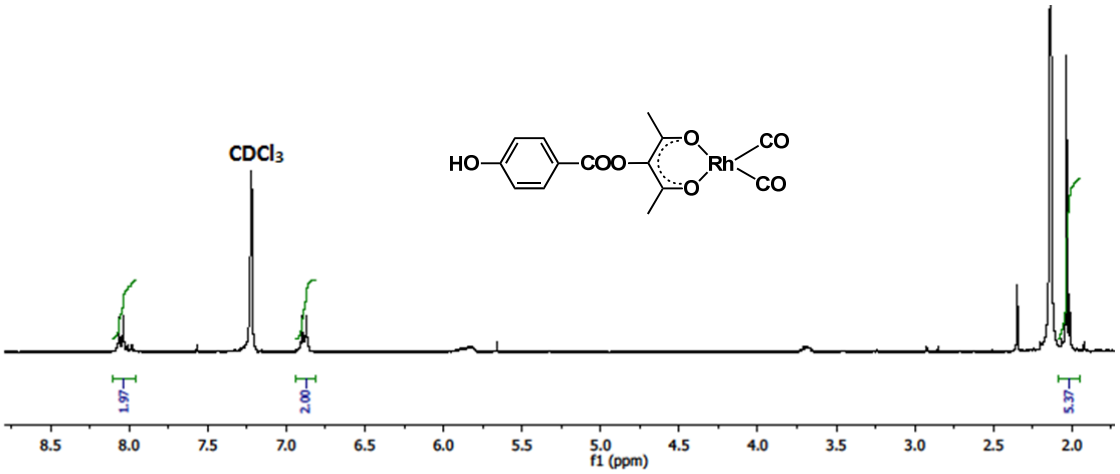

Spectrum 7: ***2,4-dioxo-3-pentyl-4-decanyloxybenzoate rhodium(I)-dicarbonyl*** **[Rh(β2a)$(CO)_2$]**

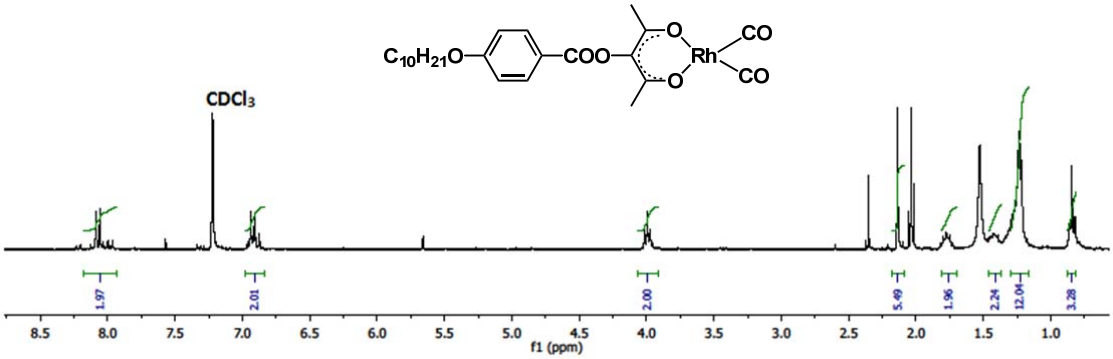

Spectrum 8: ***2,4-dioxo-3-pentyl-4-[[4-(n-decanyloxy)benzoyl]oxy]benzoate rhodium(I)-dicarbonyl*** **[Rh(β2a)$(CO)_2$]**

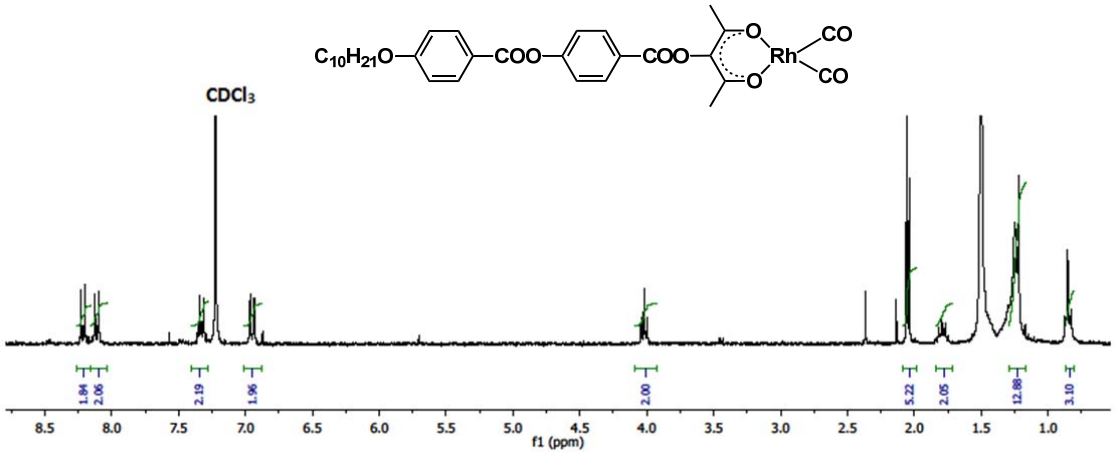

Spectrum 9: ***2,4-dioxo-3-pentyl-4-[[4-(n-decanyloxy)cinnamoyl]oxy]benzoate rhodium(I)-dicarbonyl*** **[Rh(β2a)(CO)$_2$]**

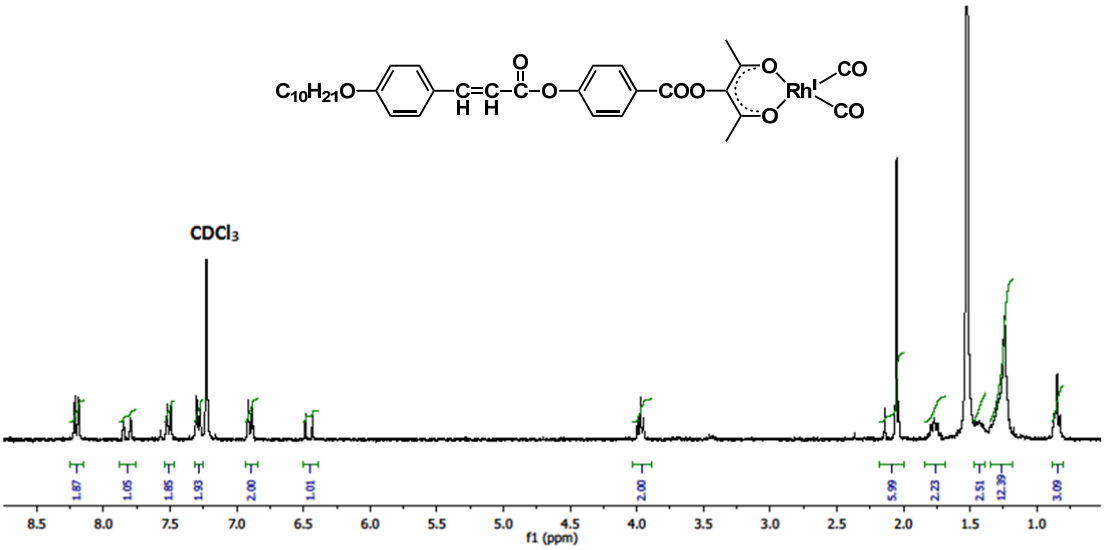

3. Rh(I)-monocarbonyl-PPh3 complexes

3.1. ^{1}H NMR

Spectrum 10: ***2,4-dioxo-3-pentyl-4-hydroxycinnamate rhodium(I)-monocarbonyl-PPh3*** **[Rh(β2a)(CO)(PPh$_3$)]**

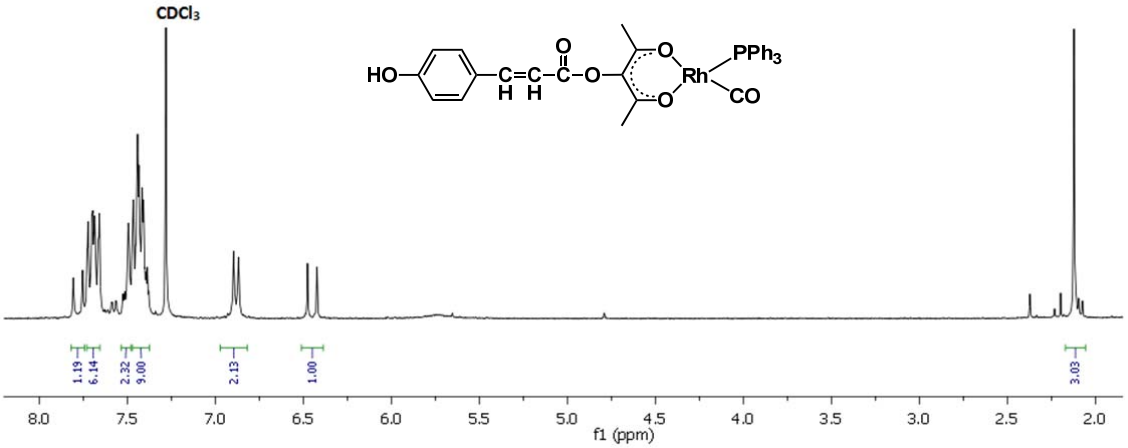

Spectrum 11: ***2,4-dioxo-3-pentyl-4-decanyloxybenzoate rhodium(I)-monocarbonyl-PPh$_3$***
[Rh(β3a)(CO)(PPh$_3$)]

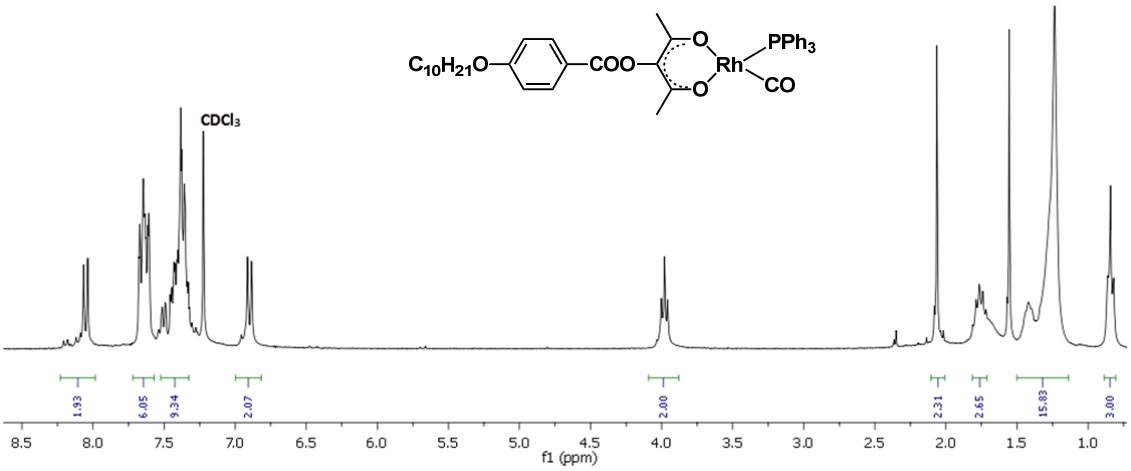

Spectrum 12: ***2,4-dioxo-3-pentyl-4-[[4-(n-decanyloxy)benzoyl]oxy]benzoate rhodium(I)-monocarbonyl-PPh$_3$***
[Rh(β4a)(CO)(PPh$_3$)]

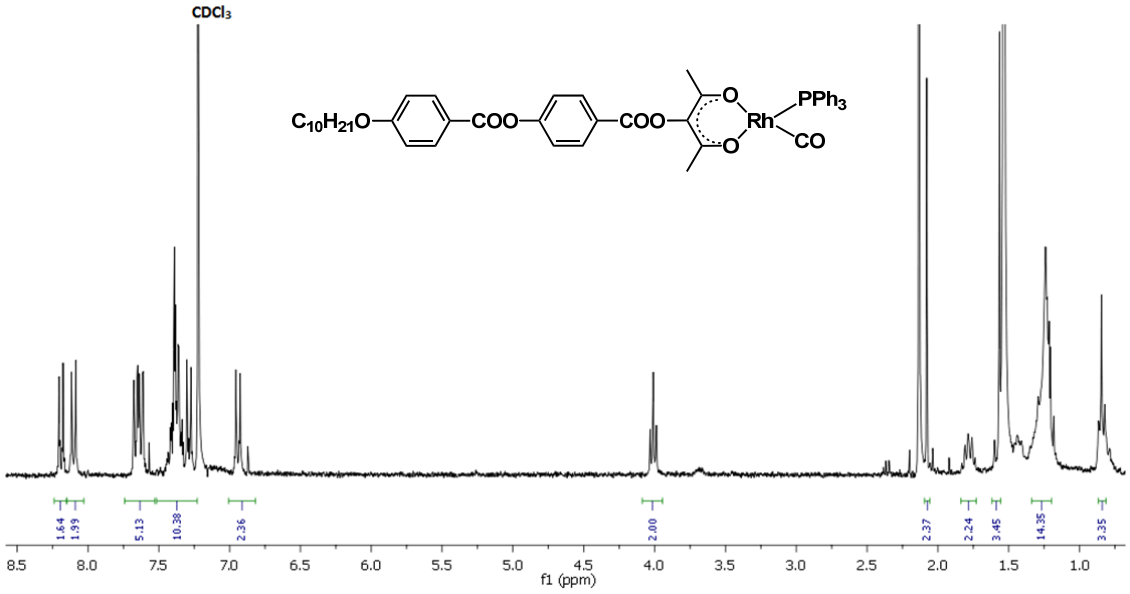

3.2. ^{31}P NMR

Spectrum 13: ***2,4-dioxo-3-pentyl-4-hydroxycinnamate rhodium(I)-monocarbonyl-PPh3*** **[Rh(β2a)(CO)(PPh_3)]**

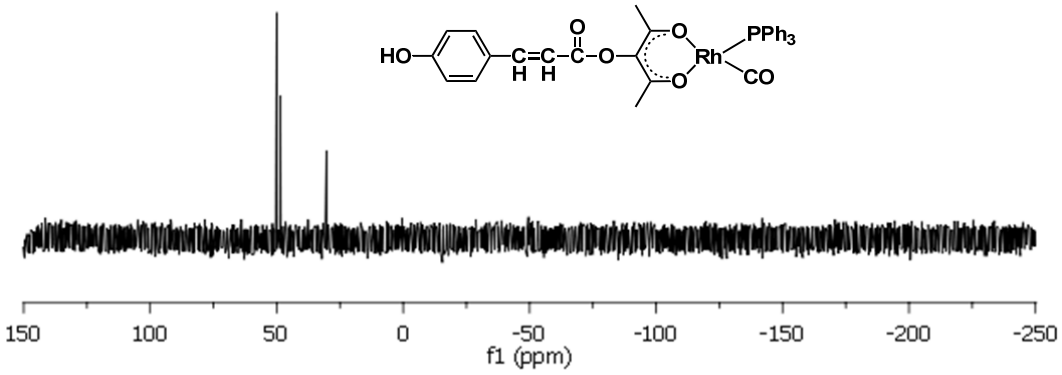

Spectrum 14: ***2,4-dioxo-3-pentyl-4-decanyloxybenzoate rhodium(I)-monocarbonyl-PPh$_3$*** **[Rh(β3a)(CO)(PPh_3)]**